Investigating the Northeast Pacific Ocean Carbon Sink using a Machine Learning Approach

by

Patrick James Duke
B.Sc. (First Class Honours), University of Calgary, 2016
M.Sc. University of Calgary, 2019

A Dissertation Submitted in Partial Fulfillment
of the Requirements for the Degree of

DOCTOR OF PHILOSOPHY

in the School of Earth and Ocean Sciences

We acknowledge and respect the Lək̓ʷəŋən (Songhees and Esquimalt) Peoples on whose territory the university stands, and the Lək̓ʷəŋən and W̱SÁNEĆ Peoples whose historical relationships with the land continue to this day.

Supervisory committee

Investigating the Northeast Pacific Ocean Carbon Sink using a Machine Learning Approach

by

Patrick James Duke
B.Sc. (First Class Honours), University of Calgary, 2016
M.Sc. University of Calgary, 2019

Supervisory Committee

Dr. Roberta Hamme, School of Earth and Ocean Sciences, University of Victoria
Co-supervisor

Dr. Debby Ianson, School of Earth and Ocean Sciences, University of Victoria
Co-supervisor

Dr. Neil Swart, School of Earth and Ocean Sciences, University of Victoria
Member

Dr. Peter Landschützer, Flanders Marine Institute (VLIZ)
Outside Member

Abstract

Improving our understanding of how the ocean absorbs carbon dioxide (CO_2) is critical to climate change mitigation efforts. The global ocean takes up nearly a quarter of anthropogenic CO_2 emissions annually, but the variability of this uptake at regional scales remains poorly understood. In this dissertation I compiled an extensive collection of reported surface ocean air-sea CO_2 exchange values within each of Canada's three adjacent ocean basins. I go on to summarize current research and identify steps forward to improve our understanding of the marine carbon sink in Canadian national and offshore waters. I then developed advanced techniques for quantifying air-sea CO_2 fluxes in the Northeast Pacific Ocean to improve our understanding of processes driving seasonal, interannual, decadal, and long-term variability, aiding in monitoring, reporting, and verification of future marine carbon dioxide removal, and helping inform carbon and climate policies. Utilizing a neural network approach to interpolate sparse observations, I created monthly gridded seawater partial pressure of CO_2 (pCO_2) data products from January 1998 to December 2019, at 1/12°x1/12° spatial resolution, in the Northeast Pacific Ocean. The two data products, encompassing the open ocean and the coastal ocean, were created using non-linear relationships between pCO_2 observations and a range of predictor variables representing processes affecting pCO_2, at a spatial resolution four times greater than leading global products. Using an ensemble approach, I was able to produce robust pCO_2 estimates, evaluated against independently withheld data, that represent regional variability with better overall performance compared to global products. I conducted a novel sensitivity analysis which identified that the parameters responsible for the neural network's ability to capture regional pCO_2 variability agrees with mechanistic processes. The regional open ocean and coastal products also reproduced pCO_2 estimates well within the overlapping domain, with differences influenced by scarcity of observations. Using wind speed and atmospheric CO_2, I calculated air-sea CO_2 fluxes. In the open ocean, on sub-decadal to decadal timescales, I found that the upwelling strength of the subpolar Alaskan Gyre, driven by large-scale atmospheric forcing, acts as the primary control on air-sea CO_2 flux variability. In the coastal ocean, I report an anticorrelation between annual air-sea CO_2 flux and its seasonal amplitude with the relationship driven by regional processes. I estimate long-term surface ocean pCO_2 increase at a rate below the atmospheric trend. The slowest rate of increase occurs where there is strong interaction with subsurface waters in the Alaskan Gyre and the West Coast upwelling zone. Basin-wide, my results suggest that the region is a net sink for atmospheric CO_2 with trends indicating increasing oceanic uptake.

Table of Contents

List of Tables

List of Figures

Acknowledgements

So much love for my family for everything. Thanks to Dr. Roberta Hamme and Dr. Debby Ianson for the mentorship and guidance they provided during my doctorate experience. Heartfelt thanks to Canada's Marine Carbon Cohort comprised of Johanna Länger, Parsa Gooya, Matthew Miller, Mohamed Ahmed, Christina Braybrook, Gina Nickoloff, Benjamin Richaud, Ricardo Arruda, Kitty Kam, Romina Piunno, Katrina Schuler, Yayla Sezginer, Ana Franco, Robert Izett, Tereza Jarníková, and Samantha Jones for their dedication to team, peer support, and scientific inquiry from the first connection. Special thanks to fellow founding members of the International Carbon Ocean Network for Early Career (ICONEC) Austin Pugh, Mary Margaret Stoll, Sarah Cryer, Anna Hughes, Amanda Kirkland, Kalina Grabb, and Gabby Kitch for elevating early career voices and connecting community. This work would not have been possible without the guidance from collaborators and committee members Dr. Peter Landschützer and Dr. Neil Swart, as well as contributions from co-authors Dr. Mohamed Ahmed and Dr. Paul Covert. Very special thanks to the warm host institutes, generous staff, and incredible friends across visiting researcher stays at Flanders Marine Institute (Ostend, Belgium) with Dr. Peter Landschützer, Max Planck Institute for Meteorology (Hamburg, Germany) with Dr. Tatiana Ilyina, University of Exeter (Cornwall, UK) with Dr. Jamie Shutler, University of Tasmania (Hobart, Australia) with Dr. Elizabeth Shadwick, and University of Hawai'i at Mānoa (Honolulu, USA) with Dr. Seth Bushinsky. Thanks to the crew and staff on the CSIRO Marine National Facility 2023 Southern Ocean Time Series cruise aboard the RV Investigator. Lastly, thanks to pals Maximilian Lauch, Kurtis Anstey, Joe Crowther, and Joseph Martin for sports, late nights, and early surfs.

Funding for this project was provided by the Natural Sciences and Engineering Research Council of Canada (NSERC) through the Advancing Climate Change Science in Canada program grant to Dr. Roberta Hamme, as well as financial support from NSERC Doctoral Postgraduate Scholarship and the joint Fisheries and Oceans Canada (DFO) and National Oceanic and Atmospheric Administration (NOAA) Ocean Acidification Collaborative Funding Initiative.

Chapter 1. Introduction

Contains text that has been submitted to a scientific journal as: Kitch, G. D., Duke, P. J., Grabb, K. C., Simancas-Giraldo, S., Adekunbi, F. O., Addey, C. I., Arbilla, L. A., Carvalho, A. C. O., Chu, S. N., Green, R. A., Hamnca, S., Ghosh, A., Kirkland, A., Lowder, K. B., Meléndez, M., Fontela, M., Robache, K., Ringham, M. C., Rønning, J., Schockman, K. M., Stoll, M. M., Oliveira, R. R., and Wright-Fairbanks, E. K.: Early Career Recommendations for Scaling an Equitable Marine Carbon Dioxide Removal Sector, Perspectives of Earth and Space Scientists, under review, submitted April 30, 2024, Manuscript ID: 2024CN000246.

1.1 Motivation

Greenhouse gas emissions from human activities are driving adverse changes to Earth's climate at an unprecedented rate, including biodiversity loss, food and water insecurity, and extreme weather events (IPCC, 2023b). Countries around the world must meet carbon emission reduction targets to retain diverse ecosystems and support equitable human development (UNFCCC, 2015). Doing so requires careful accounting of carbon stocks and fluxes (Peters et al., 2017). If global carbon sinks are shifting under climate change, climate actions and emission reduction goals need to be adjusted accordingly, while considering the social equity of the resulting policies (Boyce, 2018; Carley and Konisky, 2020; Peng, 2020). At present, there still exists a global carbon budget imbalance (i.e., a mismatch between estimated total emissions and changes in the nearly independent estimated atmosphere, land, and ocean reservoirs) of 0.3 Gt C yr^{-1} (Friedlingstein et al., 2023). While the 2023 imbalance is small, there is substantial variability ($\pm$1 Gt C yr^{-1}) over semi-decadal timescales resulting in a cumulative imbalance of 15 GT from 1850-2023 (i.e., approximately half of Canada's cumulative emissions over the same time; Friedlingstein et al., 2023). Imbalance variability is attributed to uncertainty in global land and ocean sinks. Emissions have tripled in the past 60 years (Friedlingstein et al., 2023), but do not display a sub-decadal signal.

The global ocean takes up approximately one quarter of the total anthropogenic (i.e., human-caused) carbon emissions annually (Friedlingstein et al., 2023). However, temporal and spatial variability of the marine sink are still not well constrained, particularly on interannual to decadal timescales (Fay and McKinley, 2013a; McKinley et al., 2011a; Wanninkhof et al., 2013a). Both global ocean biogeochemistry models and observation-based data products show the same patterns of decadal variability, yet the primary driver remains a matter of debate (Friedlingstein et al., 2023). Previous studies point to changes in the Southern Ocean (Landschützer et al., 2015; Le Quéré et al., 2007), contributions from the North Atlantic and North Pacific (DeVries et al., 2019; Landschützer et al., 2016), or a global signal (McKinley et al., 2020). In recent years, ocean carbon sink estimates from global ocean biogeochemistry models and

observation-based data products have increasingly diverged with a mean offset of 0.61 Gt C yr^{-1} in 2022 (Friedlingstein et al., 2023), leaving potential future changes in the marine sink associated with climate change unclear (O'Neill et al., 2016).

The ocean's absorption of anthropogenic carbon dioxide (CO_2) from the atmosphere is driving a decrease in ocean pH, a process known as ocean acidification, which endangers marine ecosystems and human communities that depend upon them (Doney et al., 2012, 2020; IPCC, 2013; Orr et al., 2005). Increased acidity negatively impacts marine organisms that build calcium carbonate shells or skeletons (e.g., corals, bivalves, coccolithophores, pteropods; Azetsu-Scott et al., 2010; Haigh et al., 2015), which may have consequences for marine food webs (Fabry et al., 2008; Haigh et al., 2015), including culturally and economically relevant species (Armstrong et al., 2005; Boldt and Haldorson, 2003). A greater understanding of the spatial heterogeneity of ocean acidification is needed to better inform stakeholders from government, industry, and communities on potential threats and actions such as carbon dioxide removal (CDR) approaches that offer associated ocean acidification mitigation co-benefits (e.g., ocean alkalinity enhancement; Bach et al., 2019).

Immediate and substantial emission reductions remain the highest priority action to mitigate adverse climate change impacts (Ho, 2023a; Shutler, 2020). However, almost all pathways to limit warming to 1.5-2 °C globally over the coming century will also require CDR from the atmosphere (Cross et al., 2023; IPCC, 2023b). CDR draws down legacy carbon pollution from the atmosphere and durably stores it in geological, land, or ocean reservoirs (IPCC, 2023b). Marine CDR (mCDR) is experiencing a surge in research, development, and proposed deployments. The momentum for mCDR is driven by the ocean's natural storage of 50 times more inorganic carbon compared to the preindustrial atmosphere (Siegenthaler and Sarmiento, 1993), the ocean's vast surface area for air-sea CO_2 equilibration, its absorption of a quarter of anthropogenic CO_2 emissions to date (Friedlingstein et al., 2023), and finally the limits of other CDR strategies (e.g., land use). Proposed mCDR interventions include stimulation of biological carbon drawdown through ecosystem restoration, nutrient fertilization, and macroalgae cultivation, direct stripping of CO_2 from seawater, artificial upwelling and/or downwelling of seawater, and the manipulation of seawater alkalinity to enhance absorption of atmospheric CO_2 (GESAMP, 2019; NASEM, 2022). Achieving Paris Agreement climate goals will require scaling up CDR capacity to remove 10-15 Gt CO_2 per year from the atmosphere by the middle of the century (Rogelj et al., 2018). Sustainable land-based CDR methods can only remove up to 2-5 Gt per year if they are to pose little risk to ecosystems and other Sustainable Development Goals (Deprez et al., 2024). Whereas mCDR

approaches are estimated to offer immense mitigation potential (e.g., ocean alkalinity enhancement: 1-100 Gt per year; Smith et al., 2023) as part of the global CDR portfolio.

Demonstrating additionality of mCDR interventions above a counterfactual baseline represents one of the largest challenges in mCDR monitoring, reporting, and verification (Ho et al., 2023; Novick et al., 2022). Differentiating signals of mCDR from natural variability and anthropogenic climate change requires extensive baseline assessments over sufficiently long-time frames and a firm understanding of driving processes (GESAMP, 2019; Oschlies et al., 2023). Marine systems, particularly coastal systems, experience considerable natural variability over seasonal, interannual, decadal, and long-term timescales (e.g., Gruber et al., 2023; Resplandy et al., 2024; Takahashi et al., 2002). The need to design, maintain, and grow regional scale ocean carbon observations, synthesis tools, and high-resolution process-based models is essential in establishing mCDR baseline understanding for assessing additionality as well as ecosystem impacts and response (Cross et al., 2022).

1.2 Research approach

Improved spatial and temporal coverage of marine carbon flux estimates can help improve our understanding of the ocean's role in the global carbon cycle (Aricò et al., 2021). Gap-filling approaches interpolating sparse observations to basin-wide estimates help inform global carbon budget accounting, describe flux variability over multiple scales, map ocean acidification hotspots and trends, potential to aid in establishing baselines for mCDR, and build a deeper understanding of drivers (Shutler et al., 2024). Early continuous partial pressure of CO_2 (pCO_2) products were limited by fewer observations used to inform estimates, coarse spatial resolution (i.e., 4°x5°; Takahashi et al., 2002, 2009), and used a space–time interpolation method (i.e., lateral 2-dimensional advection–diffusion transport equation for surface-ocean water; Takahashi et al., 1995, 1997) to create monthly climatologies for a single reference year. Evolving methods shifted to empirical approaches that considered high-order dependencies on predictors (e.g., remotely sensed sea surface temperature, chlorophyll, etc.) to more robustly generate the large dynamic range of observed pCO_2 distributions (Hales et al., 2012). Multiple linear regressions have proven sufficient in describing mathematical relationships between predictor variables and other marine carbonate system parameters (e.g., alkalinity, pH, aragonite saturation state) to produce robust subsurface estimates (e.g., Carter et al., 2014, 2016, 2018; Espinosa, 2012; Evans et al., 2013a; Juranek et al., 2011; Lee et al., 2006; Takatani et al., 2014). However, multiple linear regressions have been shown to be less capable at estimating surface ocean pCO_2 (e.g., Hales et al., 2012). Previous methods included labelling self-organizing map output (Friedrich and Oschlies, 2009; Nakaoka et al., 2013; Telszewski et al.,

2009), adapting an atmospheric tracer transport model trained on mixing ratio observations (Rödenbeck et al., 2013), and two-step methods, for example using a self-organizing map and mechanistic nonlinear relationships (Hales et al., 2012).

Benefitting from the increasing abundance of pCO_2 measurements at sea and community synthesis efforts (e.g., through the Surface Ocean CO_2 Atlas (SOCAT); Bakker et al., 2016), a variety of artificial neural network (ANN) methods have since evolved to create observation-based pCO_2 data products (Bittig et al., 2018; Chen et al., 2019; Denvil-Sommer et al., 2019; Fay et al., 2021; Landschützer et al., 2013; Laruelle et al., 2017; Ritter et al., 2017; Zhong et al., 2022). ANN approaches are empirical statistical models designed to describe the nonlinear and often discontinuous relationships between pCO_2 targets and a set of predictor variables without any a priori assumptions. These data products, combined with wind speed and atmospheric pCO_2, have informed regional to global air-sea CO_2 flux estimates of multiyear variability in the open ocean (Hauck et al., 2020; Landschützer et al., 2015, 2016, 2019; Wang et al., 2021), as well as the coastal ocean (Chen et al., 2016; Laruelle et al., 2017; Parard et al., 2015, 2016; Roobaert et al., 2019; Xu et al., 2019).

In this dissertation, I investigate drivers of air-sea CO_2 flux variability over multiple scales in the Northeast Pacific Ocean using a novel regional high-resolution ANN approach. I created continuous, monthly, gridded seawater pCO_2 data products from January 1998 to December 2019, at an unprecedented 1/12°x1/12° spatial resolution, in the Northeast Pacific open ocean and coastal ocean. I adapted the ANN self-organizing-map-feed-forward-network (SOM-FFN) approach developed by Landschützer et al. (2013, 2014) to interpolate sparse pCO_2 observations to continuous basin-wide estimates (Figure 1.1).

In a first step, the method divides the study area into biogeochemical provinces with similar environmental characteristics, using a self-organizing map (SOM) approach. The unsupervised machine learning SOM approach uses a predefined number of neurons (i.e., processing unit consisting of a weight vector where each element of the weight vector corresponds to one predictor variable such as sea surface temperature), for the same number of biogeochemical provinces, arranged on a 2-dimentional grid. The elements of each weight vector represent its coordinates and the Euclidean distance between neurons is calculated. The algorithm iteratively adjusts the neuron positions to minimize the sum of Euclidean distances between all input vectors (i.e., individual grid cells) and the closest neurons. Each input vector is assigned the value of the closest neuron, representing the province the grid cell belongs

to, then the vectors are converted back to a multidimensional array representative of dynamic biogeochemical provinces in space and time.

In the second step, within each biogeochemical province, a feed-forward neural network (FFN) was used to create non-linear functional relationships between pCO_2 observations and independent predictor variables that are known to influence surface ocean CO_2 (i.e., sea surface temperature, chlorophyll, etc.). The supervised machine learning FFN approach creates non-linear relationships between predictor data co-located with target data by connecting them through two layers of artificial neurons. The first layer, called the hidden layer, has neurons (equivalent to the number of degrees of freedom; number of neurons based on the ratio of training sample size to number of predictors; Amari et al., 1997) with random weights and biases (i.e., acting like coefficients) that act on the predictors using a hyperbolic tangent sigmoid transfer function that computes elements in the range of -1 to +1. The output vector of the hidden layer serves as the input for the second layer of neurons, the linear output layer, to produce one scalar pCO_2 estimate. Weights and biases are assigned an initial guess, then the output layer estimate is compared to the internal training and evaluation target data, computing the mean squared error (MSE). The Levenberg-Marquardt backpropagation training algorithm then iteratively adjusts the weights and biases of the hidden layer neurons to minimize the MSE. With each iteration the FFN reduces the MSE between the estimate and the internal pCO_2 targets. Once the MSE reaches a minimum acceptable level, the training process stops, and the approximated non-linear relationships can be applied to the gridded predictor data to fill space and time gaps to create continuous sea surface pCO_2 maps.

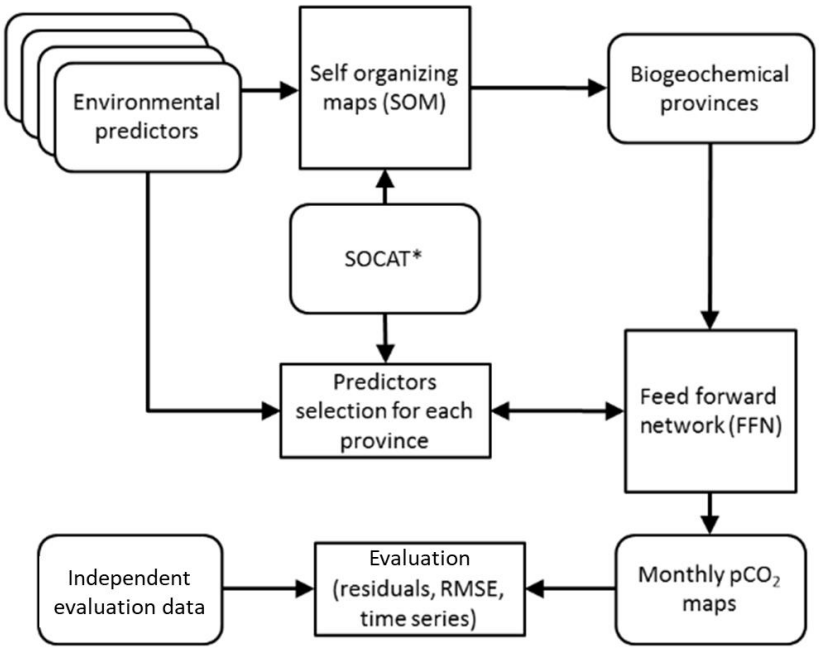

Figure 1.1 Schematic of steps involved in the SOM-FFN artificial neural network method. Adapted from Laruelle et al. (2017).

Using the estimated pCO_2, wind speed, and atmospheric CO_2, I calculated the associated air-sea CO_2 fluxes (Wanninkhof, 2014). I go on to report integrated regional carbon drawdown, describe temporal and spatial flux variability over seasonal, interannual, decadal, and long-term timescales, and uncover drivers of variability. The created data products and insight mined in this dissertation provide foundational knowledge for proposed mCDR in the region, and could be used to investigate ocean acidification in surface waters if combined with another marine carbonate system parameter (e.g., alkalinity; Carter et al., 2018).

1.3 Study region

No high-resolution observation-based air-sea CO_2 flux estimate existed previously for the Northeast Pacific Ocean. The open ocean Northeast Pacific has been characterized as a net annual sink for atmospheric CO_2 (Franco et al., 2021; Sutton et al., 2017; Wong et al., 2010). While large heterogeneity in air-sea CO_2 fluxes exist in the coastal Northeast Pacific (Fennel et al., 2019; Laruelle et al., 2018), substantial stretches of the coast completely lack observations (Bakker et al., 2016; Benway et al., 2016; Jiang et al., 2021; Lauvset et al., 2022). Large discrepancies exist between previous air-sea CO_2 flux estimates within this region, with disagreement over the net annual flux magnitude and direction (i.e., as a net sink or source for atmospheric CO_2; Fennel et al., 2019).

Ocean acidification is expected to progress faster and more severely in the Northeast Pacific compared to lower latitude waters (Fabry et al., 2009; Mathis et al., 2015). Cooler water temperatures can hold more CO_2, plus high baseline carbon concentrations due to global circulation patterns make waters in the region more naturally acidic (Feely et al., 2004, 2012). Ocean acidification in the Gulf of Alaska may be even further accelerated due to changes in glacial melt runoff, precipitation, and snow pack patterns (Ballinger et al., 2023), as freshwater dilutes the buffering capacity of seawater (Evans et al., 2014). Along the West Coast of Vancouver Island, shelf marine ecosystems are particularly vulnerable to ocean acidification as upwelled waters have relatively low pH, and organic matter produced by upwelling remineralizes to further lower pH (Feely et al., 2008).

The region is increasingly gaining attention as an mCDR pilot project hotspot while still lacking established comprehensive baselines and process understanding. The British Columbia Ocean Acidification and Hypoxia Action Plan identifies scientific and socio-cultural steps forward to evaluate mCDR efficacy, potential remediation benefits for ocean acidification, and permanency of carbon storage (British Columbia Ocean Acidification and Hypoxia Action Plan Advisory Committee, 2023). Characterizing spatial and temporal air-sea CO_2 flux variability in British Columbia coastal waters was identified as a priority action. Companies like Running Tide in collaboration with Ocean Networks Canada, Ebb Carbon, and Planetary, currently have, or are proposing, mCDR field trials in the basin (Geoengineering Map, 2023). The region has already been the location of geoengineered biological carbon drawdown experiments (Boyd et al., 2005, 2007; Ianson et al., 2012; Wong and Johnson, 2002), in some cases propagating colonialism with promises of mCDR and ecosystem co-benefits (e.g., Haida Gwaii 2012 ocean iron fertilization; Gannon and Hulme, 2018).

The geographic focus of this dissertation is the Northeast Pacific Ocean between latitudes 45°N and 62°N and longitudes 120°W and 155°W (Figure 1.2). The coastal–open-oceanic boundary is defined as 300 km offshore following Laruelle et al. (2017), corresponding roughly to the global average outer edge of territorial waters (Crossland et al., 2005). The region is characterized as seasonally stratified and experiences both subtropical and subarctic gyre influences (Whitney and Freeland, 1999). Two dominant oceanographic features divide the region, the Alaskan Gyre system to the north, and the North Pacific Current to the south (Figure 1.2; Franco et al., 2021). At approximately the latitude of Vancouver Island, the North Pacific Current bifurcates to form the northward Alaska Current and the southward California Current (Tabata, 1975). The Alaskan Gyre lies below the cyclonic winds of the Aleutian low pressure system driving strong circulation and subsurface connection, with stratified summer conditions allowing

eddies and irregular meanders along the coast to persist (Thomson, 1981). Along the Alaskan Southwestern coast, a strong narrow boundary current called the Alaskan Stream drives circulation out of the region (Royer, 1979). The North Pacific open ocean has been typically characterized as a high-nutrient, low-chlorophyll region. The designation is due to the inability of phytoplankton to use all available macro-nutrients in surface waters in summer, because of the low influx of iron to the surface ocean (Aumont et al., 2003; Dugdale and Wilkerson, 1991; Hamme et al., 2010; Martin et al., 1994).

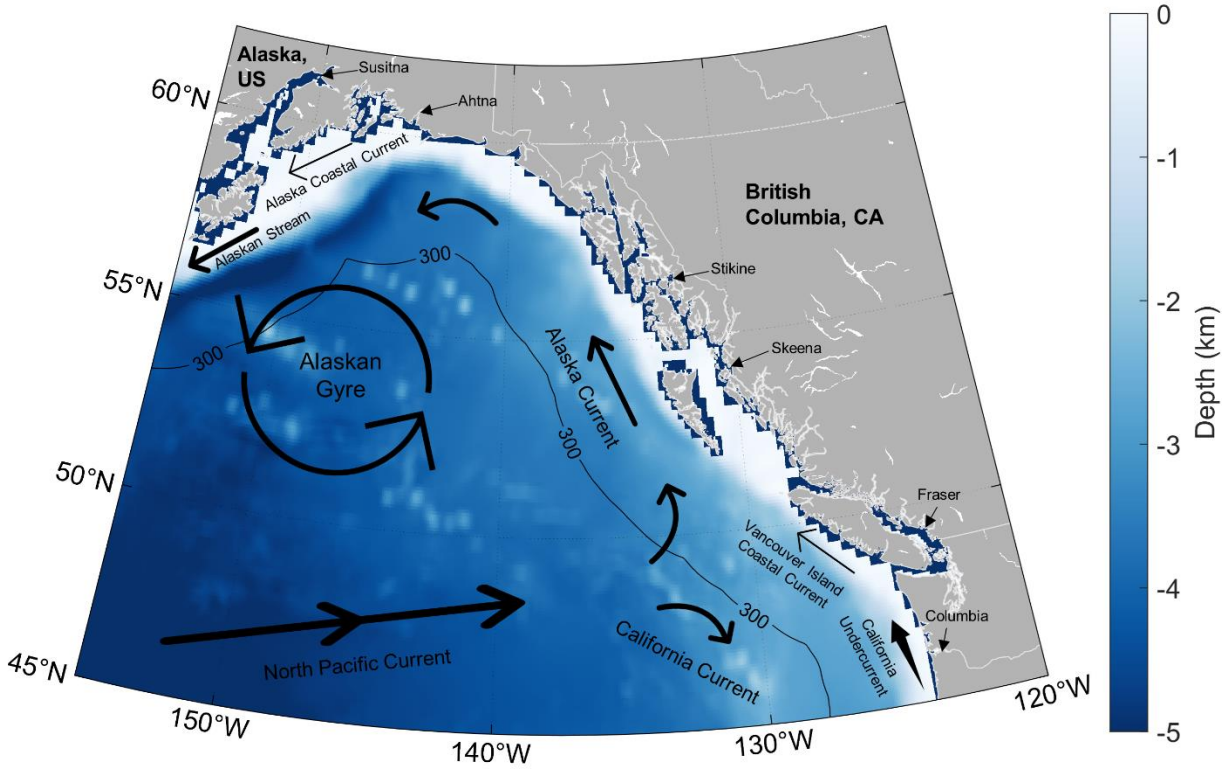

Figure 1.2 Geographical features in the Northeast Pacific Ocean and dominant surface currents (artistic representation). Major freshwater inputs are labeled (> 40 km^3 y^{-1}). Bold straight arrows represent major surface currents, thin straight arrows show coastal currents, and bold tapered arrows are subsurface currents. Interpretation comes from (Freeland et al., 1984; Stabeno et al., 2004; Thomson, 1981; Weingartner et al., 2002). The coastal–open-oceanic boundary at 300 km offshore is shown, as well as the nearshore region outside of the Laruelle et al. (2017) global coastal pCO_2 estimate (dark pixelated squares nearshore).

The coastal ocean is heavily impacted by upwelling, terrestrial freshwater discharge, tidal mixing, and coastal currents occurring on spatial scales on the order of tens of kilometers or less (Liu et al., 2010; Nemcek et al., 2008). Wind induced upwelling dominates from late spring through early fall along the coast from 45°N to the northern tip of Vancouver Island, with downwelling conditions favored during the winter (Thomson, 1981; Ware and Thomson, 2005). Upwelling along the Pacific eastern boundary shelf acts as an important pathway for nutrient delivery to the euphotic zone (Bianucci et al., 2011; Hales et

al., 2005; Messié and Chavez, 2015), but also as an environmental stressor bringing CO_2-rich water to the surface (Chan et al., 2017; Feely et al., 2008; Hales et al., 2005; Ianson et al., 2003). Further north along the Southeastern Alaskan coast, downwelling dominates from early fall through late spring (Thomson and Ware, 1996; Weingartner et al., 2002). Large volume freshwater sources such as the Columbia and Fraser Rivers (Evans et al., 2013b; Morrison et al., 2012), glacial runoff along the southern coast of Alaska (Wang et al., 2004), and sea ice in Cook Inlet (Poole and Hufford, 1982), all exert freshwater controls over the coastal ocean in the region. Prominent buoyancy driven currents include the Vancouver Island Coastal Current running northward over the inner-shelf along the southeastern coast of Vancouver Island (Freeland et al., 1984), and the Alaska Coastal Current flowing westward along the Kenai Peninsula (Stabeno et al., 1995). The study area receives a mean annual terrestrial to marine runoff of approximately 1850 $km^3\ y^{-1}$ (Morrison et al., 2012; Wang et al., 2004).

1.4 Overview of chapters

There were three primary research questions explored in this dissertation.

(1) What is the present-day net annual air-sea CO_2 flux of Northeast Pacific Ocean?
(2) What drives variability over seasonal, interannual, decadal timescales?
(3) How has the air-sea CO_2 flux changed over the past decades?

Chapter 2 summarizes current research and identifies steps forward to improve our understanding of the marine carbon sink in Canadian national and offshore waters.

Chapter 3 investigates drivers of air-sea CO_2 flux variability in the Northeast Pacific open ocean using a novel regional high-resolution artificial neural network approach.

Chapter 4 investigates drivers of air-sea CO_2 flux variability in the Northeast Pacific coastal ocean adapting the neural network approach used in Chapter 3.

Chapter 5 compares the coastal–open-oceanic boundary between the two observation-based pCO_2 data products used in Chapter 3 and 4 and considers the impact of wind speed uncertainty on flux estimates.

Chapter 6 summarizes results and makes concluding recommendations for future work in the region and in advancing observation-based pCO_2 estimates.

Chapter 2. Canada's marine carbon sink: An early career perspective on the state of research and existing knowledge gaps

Key points

1. Canadian waters are a net sink for atmospheric CO_2.
2. Large heterogeneity and uncertainty attributed to observational and model estimates make it challenging to quantify a "policymaker relevant" value in terms of grams of CO_2 uptake per year.
3. Robust and transparent monitoring, reporting, and verification protocols are needed to ensure emerging ocean-based carbon dioxide removal techniques are real and durable.
4. Institutional barriers actively discourage collaboration with First Nations in marine science in Canada; however, existing collaborative frameworks and Indigenous-led programs offer potential pathways to align future work with truth and reconciliation calls to action.
5. Expanded support (e.g., financially, emotionally, and collaboratively) for graduate students and postdocs will enable a more innovative, equitable, and diverse marine carbon science and technology community in Canada.

This work has been published in a scientific journal as: Duke, P. J., Richaud, B., Arruda, R., Länger, J., Schuler, K., Gooya, P., Ahmed, M. M. M., Miller, M. R., Braybrook, C. A., Kam, K., Piunno, R., Sezginer, Y., Nickoloff, G., and Franco, A. C.: Canada's marine carbon sink: an early career perspective on the state of research and existing knowledge gaps, Facets, 8, 1–21, 2023, https://doi.org/10.1139/facets-2022-0214.

2.1 Abstract

Improving our understanding of how the ocean absorbs carbon dioxide is critical to climate change mitigation efforts. We, a group of early career ocean professionals working in Canada, summarize current research and identify steps forward to improve our understanding of the marine carbon sink in Canadian national and offshore waters. We have compiled an extensive collection of reported surface ocean air-sea carbon dioxide exchange values within each of Canada's three adjacent ocean basins. We review the current understanding of air-sea carbon fluxes and identify major challenges limiting our understanding in the Pacific, the Arctic, and the Atlantic Ocean. We focus on ways of reducing uncertainty to inform Canada's carbon stocktake, establish baselines for marine carbon dioxide removal projects, and support efforts to mitigate and adapt to ocean acidification. Future directions recommended by this group include investing in maturing and building capacity in the use of marine carbon sensors, improving ocean biogeochemical models fit-for-purpose in regional and ocean carbon dioxide removal applications, creating transparent and robust monitoring, verification, and reporting

protocols for marine carbon dioxide removal, tailoring community-specific approaches to co-generate knowledge with First Nations, and advancing training opportunities for early career ocean professionals in marine carbon science and technology.

2.2 Introduction

Increases in greenhouse gas emissions due to human activity are driving adverse changes to human systems and ecosystems, including increases in biodiversity loss, food and water insecurity, and extreme weather events (IPCC, 2023a). To mitigate climate change related risks, Canada must adhere to national and international greenhouse gas emission reduction strategies and environmental policies. Doing so requires careful accounting of Canada's carbon stocks and fluxes. To this end, we must improve our understanding of the ocean's role in the global carbon cycle. Understanding the variability of the marine carbon sink can better inform future scientific observational programs, climate forecasting, and net-zero emission pathways (Environment and Climate Change Canada, 2020). Current estimates suggest that the global ocean has taken up approximately one quarter of the total anthropogenic (i.e., human-caused) carbon dioxide (CO_2) emissions (Friedlingstein et al., 2022a; Lindoso, 2019). Yet, gaps in our knowledge of the spatial and temporal variability in the natural marine carbon sink limit our ability to assess potential future changes in this important process. Indeed, owing to a lack of continuous observations of surface ocean CO_2 and air-sea CO_2 fluxes, especially in high-latitude regions and during the winter season, the long-term variability of the physical and biological processes that contribute to the marine carbon sink remain poorly understood (Fay and McKinley, 2013a; McKinley et al., 2011a; Wanninkhof et al., 2013a). To address this knowledge gap, we must improve the spatial and temporal coverage of marine carbon flux observations (Aricò et al., 2021) and integrate new data with efforts to improve ocean biogeochemical modelling and climate projections. These tools should be used alongside other approaches from non-scientific viewpoints (e.g., traditional knowledge) to inform the co-development of climate change impact adaptation strategies and marine mitigation methods.

In Canada, current climate policy focuses on energy systems, infrastructure, transportation, and the terrestrial carbon sink. Presently, the marine carbon sink is excluded from climate policy considerations in the Pan-Canadian Framework on Clean Growth and Climate Change (Dion et al., 2021; Government of Canada, 2016). However, the Canadian coastline is the largest in the world, touching three major ocean basins: the Pacific, Arctic, and Atlantic (Figure 2.1). In these waters, both physics and biology cause the marine carbon sink to vary strongly over space and time (Fennel et al., 2019; Laruelle et al., 2018). As the data we have compiled will show, Canada's oceans are collectively considered a natural CO_2 sink with

large heterogeneity, making it difficult to incorporate the marine system into Canada's climate change mitigation plans, let alone the United Nations' Framework Convention on Climate Change emissions accounting system (Dion et al., 2021). In order to measure the success of the Paris Agreement as part of the global stocktake (Peters et al., 2017), climate action and emission reduction targets must be adjusted to reflect variability in the marine carbon sink, while considering the social equity of the resulting policies (Boyce, 2018; Carley and Konisky, 2020; Peng, 2020).

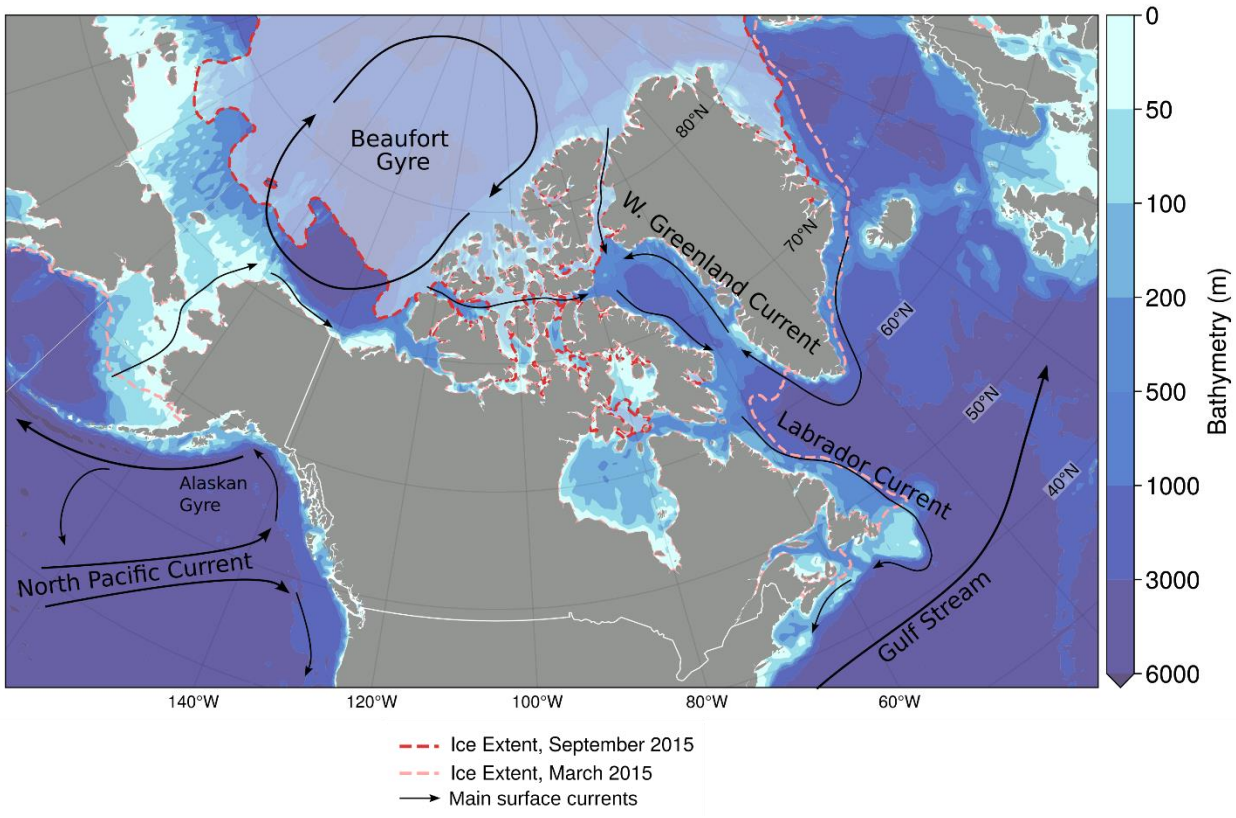

Figure 2.1 Schematic of major surface ocean currents in Canada's adjacent ocean basins and both seasonal minimum and maximum sea ice extent. Map uses a Lambert Conformal Conic projection.

In reaching net-zero emissions there is high demand from governments and businesses for Carbon Dioxide Removal (CDR) projects, with many proposed in marine settings (Cooley et al., 2023). Proposed projects include artificially stimulating biological carbon drawdown or manipulating seawater properties to enhance CO_2 absorption (GESAMP, 2019; NASEM, 2021). In western Canada, the Provincial Government of British Columbia has designated coastal blue carbon (i.e., carbon stored in marine systems) as a negative emissions "technology" aimed at meeting emission reduction goals (Government of British Columbia, 2021). Other Canadian jurisdictions will likely follow suit (Drever et al., 2021; Fong and MacDougall, 2023), with many start-up companies and carbon creditors rapidly moving into ocean

CDR (Hurd et al., 2022). However, many proposed CDR approaches focus on CO_2 removal from seawater (GESAMP, 2019), instead of direct uptake from the atmosphere. While the resulting deficit in oceanic CO_2 drives the transfer of CO_2 from the atmosphere to ocean, the timescale of re-equilibration varies from weeks to months, and depends heavily on various environmental factors (e.g., gas transfer velocity, mixed layer depth, ratio between marine carbonate system chemical species, water mass subduction; Wanninkhof *et al.*, 2009; Jones *et al.*, 2014). A firm understanding of processes driving carbon fluxes and establishing environmental baselines becomes critical to ensuring emerging ocean CDR techniques are robust, permanent, measurable, and verifiable. In the absence of such considerations, CDR approaches may simply be moving CO_2 between different oceanic carbon pools, which may help mitigate ocean acidification locally but does not lead to CO_2 removal from the atmosphere, the latter being required for climate change mitigation.

As a consequence of oceanic uptake of anthropogenic CO_2, ocean acidification is an increasingly prominent threat to both marine ecosystems and shellfish aquaculture (Doney et al., 2012, 2020; IPCC, 2013; Orr et al., 2005). For example, increased acidity negatively impacts marine organisms that build calcium carbonate shells or skeletons (Azetsu-Scott et al., 2010) (e.g., corals, bivalves, coccolithophores, pteropods), which may have consequences for marine food webs (Fabry et al., 2008; Haigh et al., 2015), including the culturally and economically relevant species that rely on them. Key commercial species such as oysters, mussels, and lobsters are particularly vulnerable to ocean acidification effects (Barton et al., 2012; Ekstrom et al., 2015; McLean et al., 2018), jeopardizing Canadian aquaculture revenues of approximately $115 million per year (Aquaculture Value Added, 2022) and fisheries revenues of $3.6 billion per year (Seafisheries Value Added, 2022). Coastal communities, especially First Nations that have constitutionally protected rights to traditional harvests, will likely incur unquantifiable social, cultural, and economic losses through the consequences of ocean acidification. Some ocean CDR approaches offer associated ocean acidification mitigation co-benefits (e.g., ocean alkalinity enhancement; Bach *et al.*, 2019). In Canada, the British Columbia Ocean Acidification and Hypoxia Action Plan will support commitments within the CleanBC Roadmap to 2030 to explore ocean CDR (Government of British Columbia, 2022).

Coastal Indigenous communities as rights and title holders will disproportionately require ocean acidification mitigation strategies and be faced with evaluating ocean CDR project proposals (Lezaun, 2021). Natural science research is not immune to or removed from the need for reconciliation to rebalance relationships with First Nations (Truth and Reconciliation Commission of Canada, 2015), which

can create a path forward based on trust and respect (Kovach, 2021; McGregor, 2018; Wong et al., 2020). Indigenous peoples have a deep understanding of the land and waterways that comprise their traditional territories and continue to require new information to adapt to climate change impacts. Collaborative efforts to bridge different knowledge systems (Indigenous and Western) can help solve complex climate adaptation and mitigation problems. However, there is no one-size fits all approach to integrating different knowledge systems (Rivers et al., 2023). These projects require meeting individual community needs in a tailored approach built on trust, and those needs vary between coasts and Nations (Rivers et al., 2023).

The next generation of oceanographers will need to evolve ocean science research to aid in climate change mitigation and adaptation action while addressing truth and reconciliation with First Nations in Canada. Against the backdrop of unprecedented rates of change in the marine environment (Pörtner et al., 2019), these early career researchers are playing (and will continue to play) a critical role in creating and regulating monitoring, reporting, and verification (MRV) protocols for ocean CDR. Differentiating the immense background noise of natural variability (i.e., seasonal, interannual, decadal), compounded with anthropogenic climate change impacts, to discern and monetize ocean CDR intervention requires complete marine carbon budgets (Legge et al., 2020). Following widespread public criticism over forestry-based carbon credits that did not lead to genuine carbon reductions (Greenfield, 2023), early career ocean scientists will face strong public scrutiny to ensure ocean CDR is real and durable.

In light of the challenges identified above, in this article, we provide an early career perspective on the state of research and necessary steps to improve our understanding of the marine carbon sink in Canadian national and offshore waters. First, we outline the current state of knowledge and major challenges to quantify air-sea CO_2 fluxes in each of Canada's three adjacent ocean basins (coastal and offshore) along with coast-specific Indigenous-led or co-led projects. In the Future Directions section, we present our recommendations for future research initiatives. We prescribe enhanced collaboration among the observational and modelling communities, and strongly advocate for the co-generation of knowledge by scientists and First Nations. As an interdisciplinary cohort of graduate students and postdoctoral fellows spanning five major Canadian universities and seven different nationalities, this article offers firsthand insight into the perspectives and direction for the upcoming generation of Canadian carbon-flux research scientists and ocean professionals.

2.3 Canadian marine CO_2 uptake

Here, we have compiled the most complete collection of reported air-sea CO_2 flux data in Canadian and adjacent open-ocean waters (Figure 2.2; Table A.1), drawn from 61 published studies (14 Pacific, 8 Atlantic, 29 Arctic, 10 global). This compilation of data will act as a reference for future work and as a timestamp for monitoring efforts as future climate change impacts the variability and intensity of the marine carbon sink. Figure 2.2 summarizes air-sea CO_2 flux density (i.e., the amount of CO_2 moving between the atmosphere and surface ocean in a given area and time) estimates complied in Table A.1 in Canadian waters from a range of observational studies, interpolation-based products, and biogeochemical models. Air-sea CO_2 flux estimates based on marine carbon state variables other than the partial pressure of CO_2 (i.e., dissolved inorganic carbon, alkalinity, and pH) have been excluded due to elevated uncertainty from such calculations (Orr et al., 2018). In general, Canadian waters are a net sink for atmospheric CO_2 (Figure 2.2 & Table A.1). However, given the current uncertainty attributed to each individual estimate, as well as the variability and time between estimates, we cannot yet quantify a "policymaker relevant" value in terms of grams of CO_2 uptake per year. The compiled estimates come from both inside Canada's exclusive economic zone (200-mile offshore limit) and beyond it including the offshore open ocean regions adjacent to Canada's shelf seas. Table A.1 also includes expanded Arctic coverage of air-sea CO_2 flux estimates. The offshore regions were included based on the transboundary nature of ocean processes and their potential influence on fluxes along Canada's continental margins (Figure 2.1), as well as Canada's proximity to monitoring for global stocktake efforts. This collection of air-sea CO_2 flux estimates only addresses one component of building complete marine carbon budgets (Legge et al., 2020). Carbon fluxes between other stocks, including the water column (pelagic), seafloor sediments (benthic), and at the terrestrial to marine interface (river input), as well as fluxes of non-CO_2 greenhouse gasses (e.g., methane, nitrous oxide), are not the focus of this article.

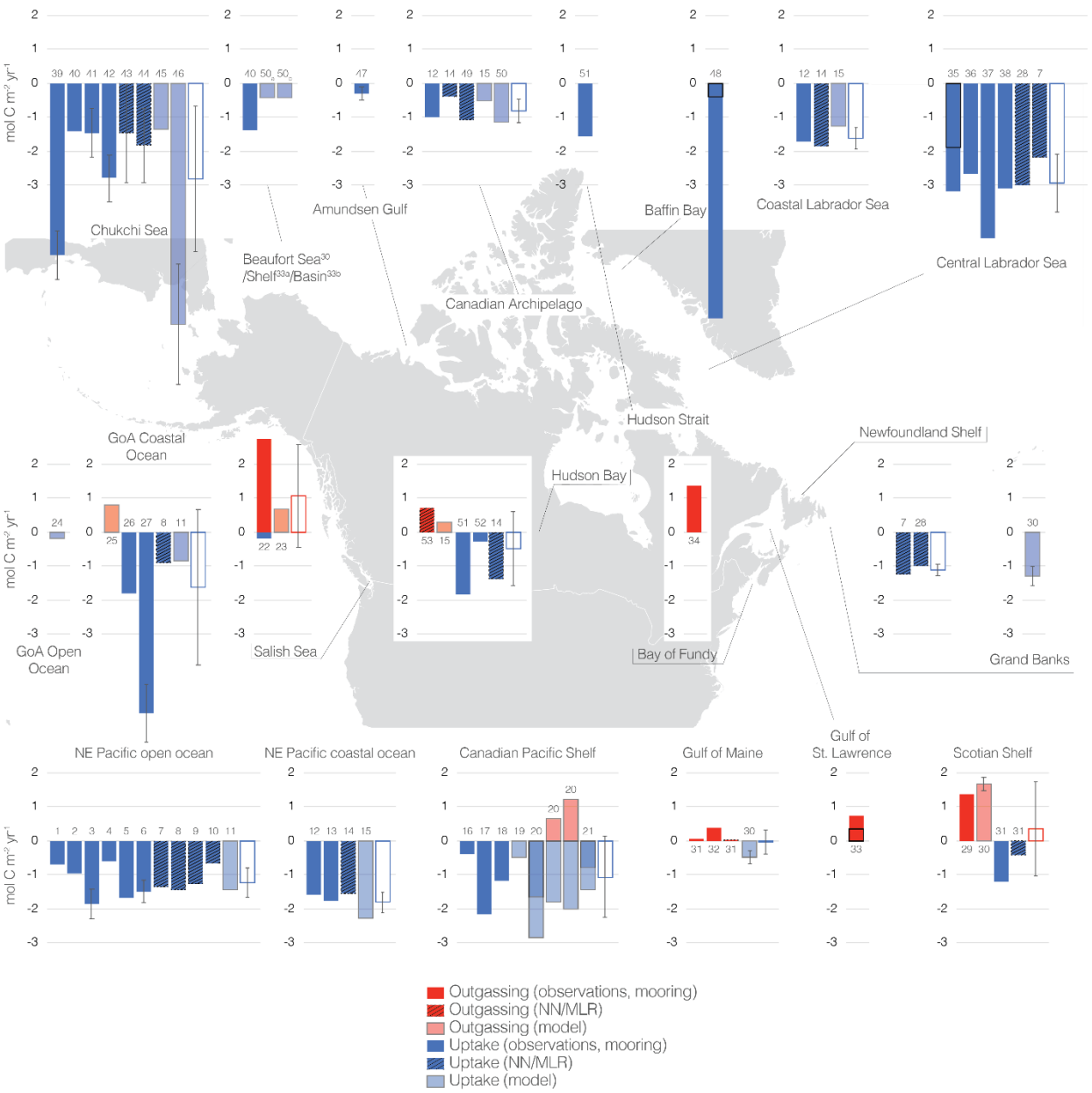

Figure 2.2 Air-sea CO_2 flux densities by region in mol C m^{-2} yr^{-1}. Negative flux (blue) indicates oceanic sink, positive flux (red) indicates oceanic outgassing. The estimation method is indicated as: direct observations (solid dark bars), observation-based interpolation products such as Neural Network (NN) and Multiple Linear Regression (MLR) (hatched bars), and regional ocean biogeochemical models (solid light bars). Bars with a maximum and a minimum for the same study have the minimum indicated on the same bar. The bars with a white filling are the average for the region. The error bars for the regional average indicate the standard deviation. The error bars in individual studies indicate the reported uncertainty. Numbers above or below the bars indicate the references: 1) Wong and Chan (1991), 2) Sutton et al. *(2017), 3) Palevsky* et al. *(2013), 4) Chierici, Fransson and Nojiri (2006), etc. Details in Table A.1. Expanded Arctic coverage in Table A.1. Modified and expanded on from Fennel* et al.*, (2019). Map uses a Lambert Conformal Conic projection.*

2.3.1 Canadian Pacific

The Subarctic Northeast Pacific appears to behave as a net sink for atmospheric CO_2 at present day (Figure 2.2). However, the Canadian Pacific comprises diverse oceanographic regions - open ocean, continental shelf, a marginal sea (i.e., Salish Sea), and numerous fjords - that contribute to large spatial variability in the magnitude and direction of the air-sea CO_2 flux.

Published results suggest an overall open ocean CO_2 sink of -1.1±0.6 mol C m^{-2} yr^{-1} (mean and standard deviation from Table A.1). While persistently undersaturated with respect to atmospheric CO_2, the seasonal amplitude in surface ocean CO_2 is also relatively small (approximately 20 μatm; Sutton *et al.*, 2017), mainly reflecting competing seasonal variability in sea surface temperature and dissolved inorganic carbon content (Sutton et al., 2017; Wong et al., 2010). Through the spring and summer, rising sea surface temperatures increase the partial pressure of surface ocean CO_2 while biology consumes carbon in the iron-limited high-nutrient low-chlorophyll region (Aumont et al., 2003; Dugdale and Wilkerson, 1991; Freeland et al., 1984; Martin et al., 1994; Wong et al., 2010). Over the fall and winter, sea surface cooling decreases the partial pressure of surface ocean CO_2 while mixed layer deepening mixes high-CO_2 water into the surface (Wong et al., 2010). Observed long-term changes in CO_2 fluxes show a clear increase in surface ocean CO_2 generally consistent with, or slightly weaker than the atmospheric CO_2 increase (Franco et al., 2021; Wong et al., 2010). Further north, the upwelling strength of the subpolar Alaskan Gyre has been shown to be the dominant control on surface carbonate chemistry seasonally (Figure 2.1; Chierici, Fransson and Nojiri, 2006; Palevsky *et al.* 2013; Brady *et al.* 2019) and on longer timescales (Hauri et al., 2021). Increased winter wind speeds drive stronger gyre upwelling bringing CO_2-rich subsurface waters to the surface leading to seasonal outgassing (Chierici et al., 2006). Over decadal timescales this upwelling strength can dampen or accelerate apparent ocean acidification rates (Hauri et al., 2021).

Along the continental margin, strongly varying estimates suggest a seasonal summer CO_2 source (Figure 2.2). The air-sea CO_2 flux of coastal waters are heavily impacted by upwelling (Figure 2.3), river plumes, and coastal currents (Evans et al., 2012, 2019; Evans and Mathis, 2013; Ianson et al., 2003; Nemcek et al., 2008). Upwelling along the Pacific eastern boundary shelf has contrasting impacts on the oceanic CO_2 sink (Figure 2.3). Upwelling stimulates biological CO_2 uptake by supplying nutrients for primary production (Messié and Chavez, 2015) leading to very strong atmospheric uptake values in bloom hotspots (Figure 2.3; Table A.1; Ribalet *et al.,* 2010). Upwelling also transports high-CO_2 water from depth to the surface, counteracting the biological uptake and temperature-driven CO_2 uptake (Figure 2.3;

Christensen, 1994; Ianson and Allen, 2002; Feely *et al.*, 2008; Chan *et al.*, 2017). The balance of upwelling to downwelling strength has been shown to be a dominant control on air-sea CO_2 flux along the Canadian Pacific continental slope and shelf (Ianson et al., 2009). In general, regions further north such as Queen Charlotte Sound, are expected to act as a stronger atmospheric CO_2 sink driven by stronger winter downwelling pushing high-CO_2 subsurface shelf waters offshore (Ianson et al., 2009). Within the Salish Sea, Alaska's Inside Passage, and coastal inland fjords, gas fluxes into and out of the ocean are highly episodic and spatially heterogeneous (Jarníková et al., 2022b), owing to seasonal freshwater input, high organic matter fluxes and longer residence times (i.e., nutrient trapping; Jarníková *et al.*, 2022), and the significant variability in tidal mixing throughout the coastal archipelago of British Columbia (Evans et al., 2022).

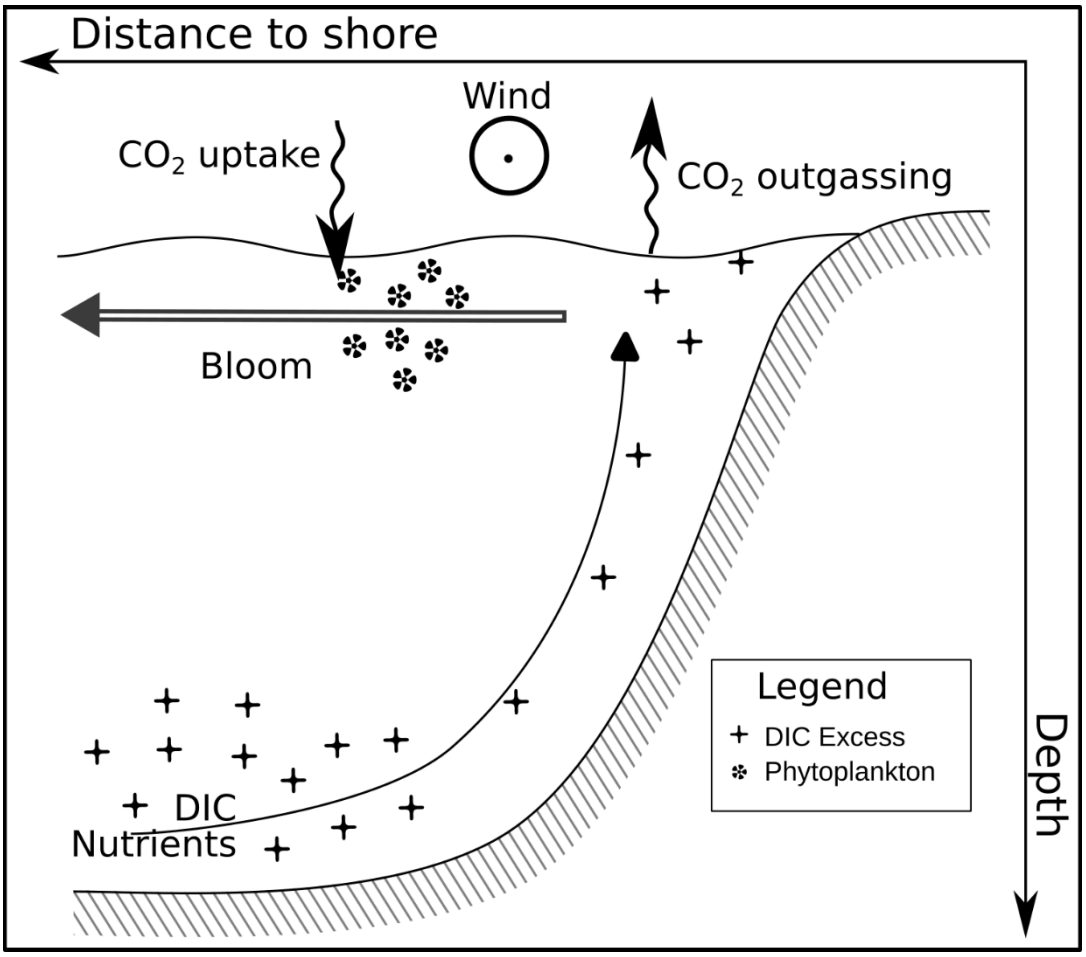

Figure 2.3 Conceptual model of wind-induced upwelling along the West Coast of North America. Equatorward winds combined with Coriolis force move nearshore surface waters offshore, forcing colder, nutrient, and dissolved inorganic carbon (DIC) rich subsurface waters to rise to the surface leading to outgassing. As the new stratified surface waters move offshore, rapid phytoplankton blooms deplete nutrients and lower CO_2, enhancing uptake.

Historically, the Subarctic Northeast Pacific has been relatively well-sampled for surface ocean CO_2 measurements (Bakker et al., 2016). The Line P program, operated by Fisheries and Oceans Canada, has contributed over 30 years of sustained inorganic carbon system observations. While the program constitutes one of the longest such time series in the global ocean (Franco et al., 2021; Freeland, 2007), samples are usually only collected three times a year. The Ocean Station Papa mooring operated by the US-based National Oceanic and Atmospheric Administration offers continuous ocean carbon measurements beginning in 2007 at the oceanic end of Line P (Sutton et al., 2017). Increased international Biogeochemical-Argo profiling float deployments in the region will also likely lead to improved air-sea CO_2 flux estimates (Bushinsky et al., 2019). Despite the large number of studies conducted in the Canadian Northeast Pacific (Table A.1), the mechanisms driving past, and potential future changes in the marine CO_2 sink remain unclear (O'Neill et al., 2016). Projected restrictions in upper ocean mixing due to increased seasonal stratification (Cummins and Ross, 2020; Durack et al., 2012; Freeland, 2013) and warming (Capotondi et al., 2012) will likely alter the seasonal CO_2 cycle (Fassbender et al., 2018a, b; Landschützer et al., 2018), and the net flux. The impact of interannual variability (e.g., El Niño-Southern Oscillation, Pacific Decadal Oscillation), and extreme events (e.g., marine heatwaves), on the air-sea CO_2 flux are just beginning to be understood (Mogen et al., 2022). Marine heatwaves have already become longer-lasting, more frequent, more extensive, and more intense (Frölicher et al., 2018), with the Northeast Pacific experiencing dramatic temperature anomalies during 2014 and 2019 (Bond et al., 2015; Ross et al., 2019).

Modelling and observation work suggest that the time required to distinguish changes in the magnitude of the ocean carbon sink due to anthropogenic climate change is longer in the Northeast Pacific than in other Canadian ocean basins (Gooya et al., 2023; McKinley et al., 2016; Sutton et al., 2019). The longer time to detection is due to surface ocean CO_2 in the region largely increasing at a rate similar to atmosphere CO_2. Similar growth rates cause the change in the carbon sink to remain small, while internal variability remains large relative to the anthropogenic signal (McKinley et al., 2016; Resplandy et al., 2015; Sutton et al., 2019). There is a glaring lack of continuous observations during winter months (entire region), and year-round in some regions (e.g., coastal waters and regions surrounding Haida Gwaii), which are required to describe this natural variability (Hunter et al., 2015). High spatial and temporal resolution regional biogeochemical models have been successful in describing the influence of terrestrial freshwater inputs, spatial heterogeneity in the upwelling zone, and submesoscale eddies (Table A.1). However, these modelling studies remain limited in their spatial extent and multiyear coverage required to characterize the entire Canadian West Coast over decadal timescales. Similarly,

observations of coastal waters have limited temporal coverage, with most coastal interpolation-based products only capable of producing seasonal climatologies (Table A.1).

Enhanced collaboration is needed in improving observational coverage in the Northeast Pacific, in communicating with stakeholders (e.g., commercial fishers, aquaculture farmers) and rightsholders (e.g., First Nations) on changing ocean acidification risk, and in developing community-first governance policies with respect to ocean CDR approaches. Priority should be placed on building relationships leading to knowledge sharing and knowledge co-production with Indigenous-led groups actively developing and updating marine use plans (Wong et al., 2020). The Marine Plan Partnership Initiative, developed by the province of British Columbia and 17 member First Nations, has already created guiding policy around the management of human activities in northern coastal territorial waters using an ecosystem-based management framework (Marine Planning Partnership Initiative, 2015d, b, a, c). The First Nations Health Authority's "We All Take Care of the Harvest" program aims to help coastal communities plan for and manage climate impacts that affect seafoods. The Government of Canada's "Salish Sea Initiative" offers funding for collaborative Indigenous marine ecosystem stewardship activities. The First Nations Fisheries Council of British Columbia's action plan is built around relationships and reconciliation, aquatic resource management, safeguarding habitat, and responding to threats like climate change (Atlas et al., 2019; Haggan et al., 2009). Enhanced observation of carbon fluxes and policy around ocean CDR and MRV could be woven into these ecosystem-focused marine use plans and expanded to other communities using the same collaborative framework (Diggon et al., 2021, 2022). This approach would create a strong knowledge base to evaluate climate impacts and ecosystem impacts related to negative emission technologies.

2.3.2 Canadian Atlantic

Overall, the Northwest Atlantic Ocean acts as a net sink of atmospheric CO_2 (Figure 2.2). However, many coastal regions (e.g., Gulf of St. Lawrence, Scotian Shelf, and Bay of Fundy) potentially act as a source of CO_2 to the atmosphere (Figure 2.2). The Scotian shelf, for example, is a highly variable region, with CO_2 flux estimates ranging from a strong source of CO_2 to the atmosphere (Rutherford et al., 2021; Shadwick et al., 2011) to a weak sink for atmospheric CO_2 (Signorini et al., 2013). Air-sea CO_2 fluxes in the Labrador Sea are approximately 40% larger relative to that of open ocean regions in the Canadian Pacific largely due to differences in winter mixing depth between the two regions.

The Labrador Sea is a deep-water formation site where cool, dense water sinks to depth (up to 2000 m in a matter of days; Marshall *et al.*, 1998, 2001), before flowing equatorward as part of the global ocean thermohaline circulation (Wunsch, 2002). This process has the potential to move atmospheric CO_2 taken up by surface ocean waters to depth (Figure 2.4), drawing a direct connection between the atmosphere and the deep ocean, where it can remain trapped for timescales on the order of up to thousands of years (Broecker, 1979). Deep water formation renews the region's capacity to maintain high-CO_2 uptake rates by exposing deep water with little anthropogenic carbon to the atmosphere (Figure 2.2&2.4; Gruber *et al.*, 2019). Given the importance of the Labrador Sea as a region of intense anthropogenic carbon uptake (Devries, 2014; Gruber et al., 2019a; Khatiwala et al., 2013), it also represents (at present) one of the largest gaps in CO_2 observations in Canadian waters (Table A.1). Dominant processes that drive the seasonal variability of surface ocean CO_2 in the Central Labrador Sea includes deep convection in the fall and winter driven by cooling and by the cyclonic boundary currents in the basin (Figure 2.1; Rieck, Böning and Getzlaff, 2019). Deep convection brings high-CO_2 and nutrient rich water from depth to the surface, reducing oceanic uptake of atmospheric CO_2 over the winter months (Figure 2.4). In the spring, biological uptake acts to reduce CO_2 at the surface and increase air-sea CO_2 fluxes, leading to enhanced uptake of atmospheric CO_2 from spring to summer (Figure 2.4; DeGrandpre *et al.*, 2006; Körtzinger *et al.*, 2008; Atamanchuk *et al.*, 2020). Preconditioned by upwelled nutrients driven by the winter deep convection, and the increasing supply of sunlight, the North Atlantic spring phytoplankton bloom in the Labrador Sea is one of the most efficient biological carbon pumps globally (Baker et al., 2022). Following the bloom, large organic particles and aggregates sink out of the surface mixed layer due to gravity, moving CO_2 to depth (Briggs et al., 2011; Villa-Alfageme et al., 2016). Smaller particles and dissolved carbon are removed from the surface in the fall and winter by vertical mixing through deepening of the surface mixed layer (Dall'Olmo et al., 2016; Lacour et al., 2019), eddy activity (Resplandy et al., 2019), and large-scale subduction (Hansell et al., 2009). The succession of these carbon export fluxes in the Labrador Sea allows continuous carbon export to depth year round (Figure 2.4; Boyd *et al.*, 2019). Over interannual and decadal timescales, during the positive phase of the North Atlantic Oscillation, subpolar regions experience increased vertical mixing and lower sea surface temperatures, driving variability in Northwestern Atlantic Ocean CO_2 fluxes (Thomas et al., 2008; Ullman et al., 2009; Yashayaev and Loder, 2017). Under global warming, shoaling of the mixed layer depth and the addition of glacial meltwater could impact the future biological regime of the Labrador Sea by increasing stratification (von Appen et al., 2021; Balaguru et al., 2018).

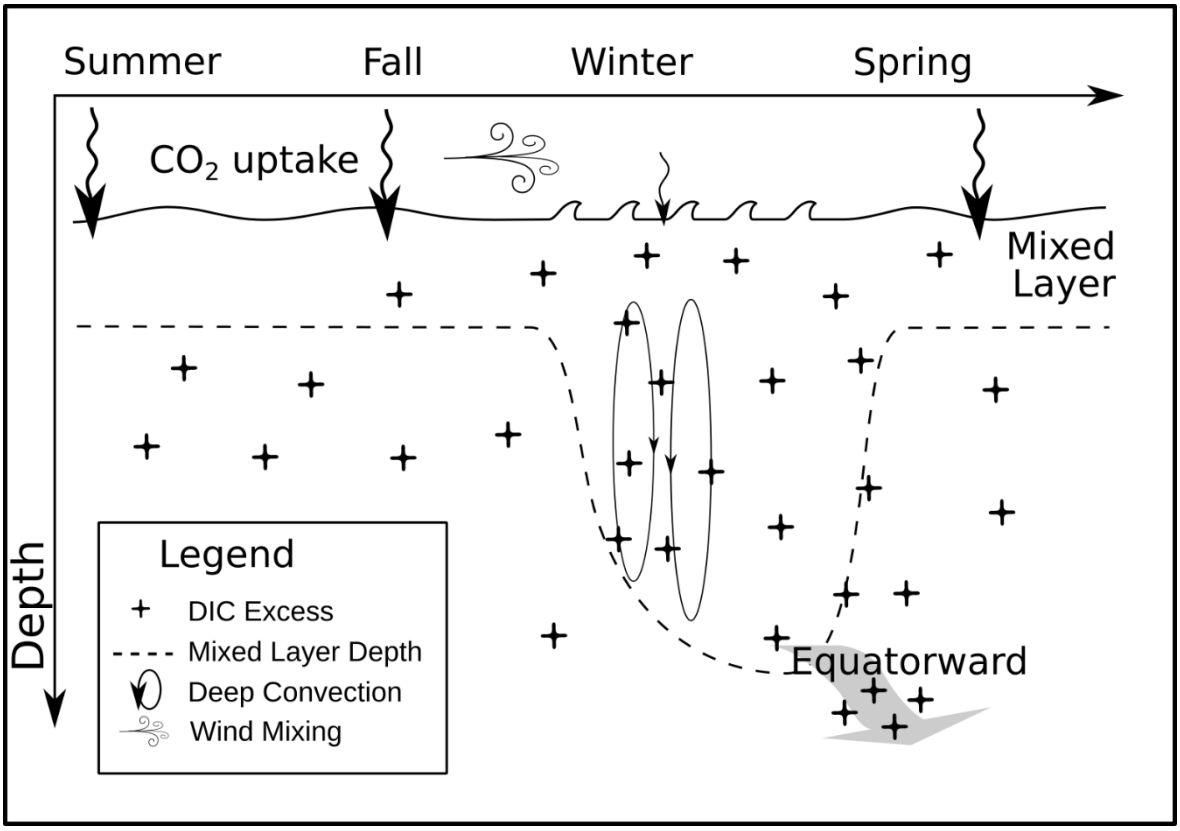

Figure 2.4 Conceptual model of subpolar Atlantic Ocean deep convection. During summer, biological production combined with strong stratification draws down surface DIC, enhancing CO_2 uptake. Increased wind and buoyancy loss in the fall encourages deeper mixing to supply higher DIC from below the summer mixed layer depth. Deep convection continues to increase DIC throughout the mixed layer in the winter, weakening CO_2 uptake. In the spring, mixed layer shoaling and increasing solar irradiance promote surface DIC removal by large-scale phytoplankton growth, subsequent export, and remineralization below the springtime mixed layer. A portion of which is exported below sequestration depth and laterally by the equatorward boundary current.

As the cold and fresh Labrador Sea current warms flowing southward along the Newfoundland-Labrador and Scotian Shelf (Figure 2.1), surface ocean CO_2 levels rise above saturation, leading to outgassing, uncharacteristic of high latitude continental shelves (Figure 2.2). This coastal environment is further complicated by upwelling of cold, high-CO_2, and nutrient rich waters along the continental slope, which increase surface ocean CO_2 levels to feed the spring phytoplankton bloom before reducing CO_2 again. This process is comparable to upwelling in the Northeast Pacific (Figure 2.3). However, unlike the West Coast of Vancouver Island, where the high-CO_2 upwelled water causes an increase in surface ocean CO_2 (Evans et al., 2012), on the Scotian Shelf, the cooling effect of the upwelled water has been shown to overwhelm the CO_2 increase, resulting in a net decrease in surface ocean CO_2 (Rutherford *et al.*, 2021). The reason for this difference is linked to global ocean circulation patterns, where subsurface waters in the Pacific tend to accumulate a greater amount of dissolved inorganic carbon due to remineralization of

organic matter (England, 1995). The competing mechanisms of upwelled water on air-sea CO_2 fluxes are highly variable spatially and temporally, making them difficult to capture in observations or numerical models. This difficulty can lead to diverging results between studies characterizing the Scotian Shelf as both a source and sink of CO_2 (e.g., Table A.1; Shadwick *et al.*, 2011; Laruelle *et al.*, 2014; Rutherford *et al.*, 2021). In the Gulf of St. Lawrence, tidal and estuarine mixing bring respired organic matter into the surface layer driving CO_2 outgassing in the shallow mouth of the estuary (Dinauer and Mucci, 2017). In the deeper oceanward part of the St. Lawrence region, enhanced biological drawdown keeps surface ocean CO_2 undersaturated driving net uptake from the atmosphere (Dinauer and Mucci, 2017). However, these fluxes may shift in the future due to increased biological production (Dinauer and Mucci, 2018).

Air-sea CO_2 fluxes at both offshore and coastal regions of the Canadian Northwest Atlantic are directly affected by the formation of Labrador Sea Water, which in turn drives variability and intensity of the Labrador current. Uncertainty in air-sea CO_2 fluxes are largely attributed to the sparsity of direct observations in the Labrador Sea and much of the subpolar North Atlantic, lack of agreement between wind speed products (Atamanchuk et al., 2020), and not enough direct estimates of the volume of Labrador Sea Water formation during any given winter (Li and Lozier, 2018). Most surface ocean CO_2 observational data in the Northwest Atlantic Ocean comes from the Ship-Of-Opportunity Program using volunteer merchant ships, with spatial coverage most densely concentrated around busy shipping tracks (Bakker et al., 2016). Regions of greatest spatial coverage include the Southern Labrador Sea, Gulf of Maine, and in the Gulf Stream region south of Nova Scotia off the east coast of the United States (Figure 2.1). Whereas the Grand Banks region, along with both the shelves of Labrador and Newfoundland, as well as the Central Labrador Sea remain very data sparse. For those data-poor regions ongoing monitoring programs like the Atlantic Zone Off-Shelf Monitoring Program and Atlantic Zone Monitoring Program (Ringuette et al., 2022; Therriault et al., 1998) are making important efforts to provide additional continuous observations, but are still limited to summer sampling programs. International monitoring programs also contribute significantly to observations in the region such as GO-SHIP (AR07W, A02, and Davis monitoring lines), Overturning in the subpolar North Atlantic Program (OSNAP), and Biogeochemical-Argo (Lacour et al., 2019). The absence of buoys measuring wind speed in the Labrador Sea also contributes to air-sea gas exchange uncertainties (Atamanchuk et al., 2020). Improving our understanding of the controls on air-sea CO_2 fluxes in the Central Labrador Sea may even lead to improved estimates for the whole North Atlantic basin (Friedrich and Oschlies, 2009). The importance of the region for global marine carbon uptake emphasises the value in maintaining the Atlantic Repeat Hydrography Line AR07W line operated by Fisheries and Oceans Canada (Hall et al., 2013) across the

Central Labrador Sea. The use of new autonomous sensing platforms for measuring CO_2 (e.g., using wave gliders as in DeYoung *et al.* 2020) may also play an important role in gap filling. The success of a few previously deployed long-term moorings in the region have greatly improved our understanding of the seasonality of CO_2 fluxes in the Labrador Sea, such as the most recent completed by the SeaCycler deployment in 2016/2017 (Atamanchuk et al., 2020), and the others deployed in the early 2000s (DeGrandpre et al., 2006; Körtzinger et al., 2008; Martz et al., 2009).

Like Pacific Canada, traditional knowledge exchange and collaboration between the scientific community, government entities, and First Nations can prove to be extremely successful. Atlantic Canada is home for many Indigenous groups offering immense opportunity for traditional knowledge exchange and for collaboration in ocean observing/monitoring efforts (Proulx et al., 2021). Alexander *et al.* (2019) mapped past research (in marine management, monitoring, and marine research) published in collaboration with Indigenous communities in Canada. In Atlantic Canada only five case studies were found in the literature, making this region the one with the least collaborations compared to Arctic and Pacific Canada. Further, in the report of Moran *et al.* (2022) there is only one community monitoring platform directly collaborating with Indigenous groups on the East Coast, located in Placentia Bay, Newfoundland. Yet, Eger *et al.* (2021) show increasing opportunities for integrated marine management with Indigenous groups in the Bay of Fundy area. While historically, Atlantic Canada is missing a myriad of opportunities within these Indigenous collaborations, there is a promising new Atlantic Regional Association of the Canadian Integrated Ocean Observing System - CIOOS (Stewart et al., 2019) pushing to create programs with Indigenous communities (Proulx et al., 2021). As early career ocean professionals, we strongly suggest that the efforts of CIOOS-Atlantic include air-sea CO_2 fluxes as a research area of focus in both coastal and offshore regions of Atlantic Canada.

2.3.3 Canadian Arctic

The Arctic Ocean is predominantly a CO_2 sink (Figure 2.2). Current estimates indicate that the pan-Arctic Ocean constitutes 5 to 14% of the global oceanic CO_2 uptake, despite covering only 3% of the global ocean area (Bates and Mathis, 2009). Uptake values reported in the Canadian Arctic are among the highest in Canadian waters (Figure 2.2), but are sparse, and highly disparate in space and time (Table A.1).

Arctic Ocean air-sea CO_2 fluxes are uniquely impacted by the presence of sea ice, which effectively prevents air-sea CO_2 exchange (Figure 2.1; Figure 2.5). Variability in ice conditions thus explains part of

the regional and temporal distribution of CO_2 uptake, with areas of longer open water seasons being stronger sinks (e.g., Chukchi Sea, Baffin Bay, Labrador Sea; Figure 2.2). Harsh Arctic weather and ice conditions induce a seasonal bias in field observations, restricting most scientific campaigns to take place over the summer months (Table A.1). This observation gap is usually waived by considering non-open water seasons as negligible to the annual contribution (e.g., Loose *et al.* 2011; Ahmed *et al.*, 2021). However, observed wintertime CO_2 fluxes in comparatively smaller scale polynyas and ice leads are one to two orders of magnitude higher than predicted by theory in open waters (Else et al., 2011). On top of the physical flux barrier, sea ice chemistry affects CO_2 fluxes through the sea ice carbon pump during both sea ice formation and melt (Rysgaard et al., 2011). During sea ice melt, dissolution of ikaite (a form of calcium carbonate in sea ice) lowers surface ocean CO_2, increasing the potential for atmospheric uptake (Figure 2.5; Rysgaard *et al.*, 2013). During sea ice formation high-CO_2 brine within the ice is rejected into the underlying seawater and sinks to depth (Figure 2.5; Rysgaard *et al.*, 2007). Both processes significantly modify air-sea CO_2 fluxes during fall and spring (DeGrandpre et al., 2019; Duke et al., 2021; Mortenson et al., 2020). Finally, sea ice also impacts biological CO_2 drawdown in a number of ways, by imparting local controls on the timing, duration and magnitude of spring and summer primary production (Arrigo et al., 2008, 2012; Rysgaard et al., 1999; Søreide et al., 2010).

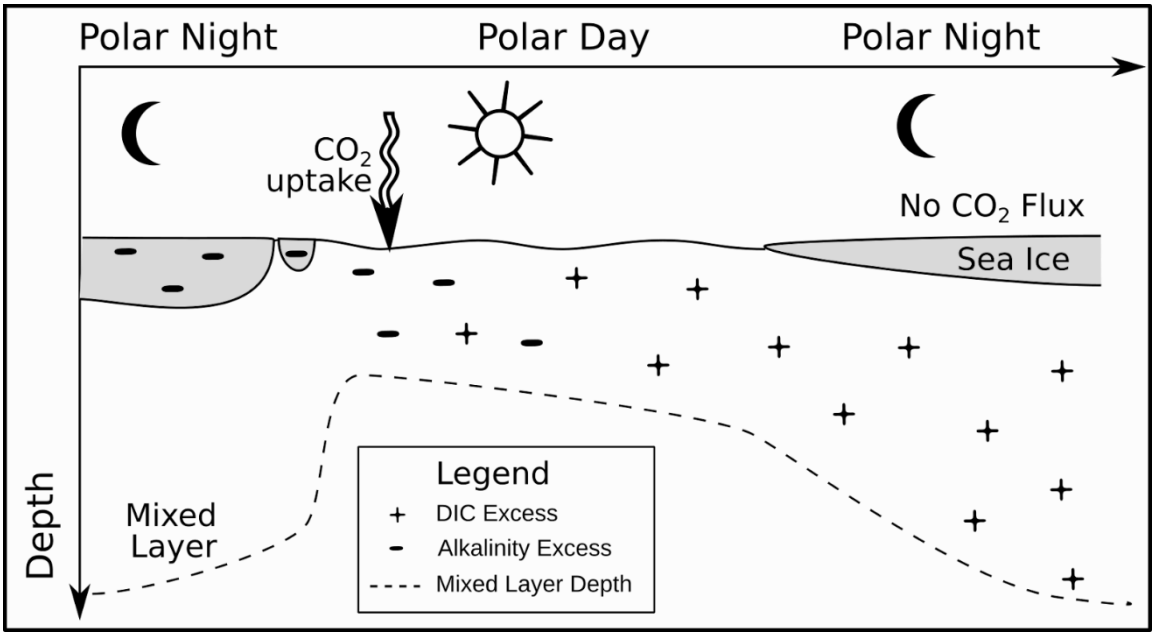

Figure 2.5 Conceptual model of Arctic Ocean sea-ice carbon pump. During summer, sea ice melt results in the dissolution of ikaite (a form of calcium carbonate in sea ice) crystals within the ice to increase surface ocean alkalinity, lowering the partial pressure of CO_2 and enhancing uptake. Additionally, primary productivity in both sea ice and the water column further reduce CO_2. Subsequent ice formation in the winter results in dissolved inorganic carbon (DIC) being rejected together with dense brine that sinks.

Regardless of the past or present state of the carbon budget in the Arctic Ocean, its future is likely to be significantly different. The Arctic is warming at two to three times the rate of global warming (IPCC, 2019). Sea ice decline is the archetype of climate change signals. The reduction of multi-year sea ice over the last decade has resulted in large portions of the Canadian Arctic becoming seasonally ice-free (Laxon et al., 2013; Wang et al., 2018; Yamamoto-Kawai et al., 2009), and a lengthening of the open water season (Maslanik et al., 2007; Perovich et al., 2007). As a result, the ocean surface is becoming increasingly exposed for atmospheric CO_2 uptake (DeGrandpre et al., 2020). In fact, Ahmed and Else (2019) estimated an increase in the CO_2 uptake in the Canadian Arctic Archipelago in the last four decades associated with increased sea ice loss and higher wind speeds. While a longer ice free season introduces greater light availability for primary production, nutrient replenishment of surface layers could either be enhanced by increased wind mixing or reduced by increased stratification due to ice melt (Lannuzel et al., 2020). Therefore the evolution and impact of primary production on the Arctic marine carbon cycle remains an open question (Arrigo et al., 2008; Lannuzel et al., 2020; Tremblay et al., 2015). Meanwhile, changes to the upper ocean's salinity and temperature structure in the Barents and Kara Seas, referred to as Arctic "Atlantification" (e.g., Årthun, Eldevik and Smedsrud 2019), may introduce potential consequences on ice formation and deep convection in the Eurasian Basins (Timmermans and Marshall, 2020). Moreover, coastal margins and the ice edge can also be important pathways for carbon export (Nishino et al., 2011), particularly as phytoplankton blooms may be stimulated by nutrients derived from coastal rivers or seeded by ice algae (Matthes et al., 2021). There is, however, some evidence that rivers may drive localized marine organic carbon respiration (Izett et al., 2022), suggesting that some Arctic regions may experience periodic net CO_2 outgassing (Manning et al., 2020). Finally, it is likely that future Arctic CO_2 fluxes will exhibit varied responses to ongoing permafrost thawing and changes in river runoff, through various effects on nutrient and organic matter inputs, and changes to local marine stratification (Prowse et al., 2015; Vonk and Gustafsson, 2013). Further, increased methane bubbling and hydrate erosion will affect the system (Westbrook et al., 2009).

In the context of this evolving Arctic Ocean with more mobile ice packs, new ice-proof, autonomous observing technologies are needed to close the fall, winter, and spring observational gaps. Those technologies already exist in the form of Ice-Tethered Profilers and Arctic Ocean Flux Buoys, capable of year-round measurements, regularly deployed in the Beaufort Gyre. Meanwhile, renewed efforts to install and maintain eddy covariance instruments in Iqaluktuttiaq (ᐃᖃᓗᖅᑐᑎᐊᖅ, Cambridge Bay; Butterworth and Else, 2018) or to expand the Barrow Strait Real Time Observatory will be instrumental in providing year-round observations. In addition to these local observations, international scientific

partnership targeting a pan-Arctic approach will be crucial to addressing the relevant questions surrounding the quantification of CO_2 fluxes in the Arctic Ocean. Examples include the Synoptic Arctic Survey (Addressing Arctic Challenges Requires a Synoptic Ocean Survey, 2023), The Pacific Arctic Group, the Distributed Biological Observatory (Moore and Grebmeier, 2018) and the Ecosystem Studies of Sub-Arctic and Arctic Seas (ESSAS). The use of numerical models, with a coupled sea ice biogeochemistry component covering the Arctic Ocean, will also be important to obtain a more comprehensive understanding of the carbon system in the northernmost Canadian Ocean. The future fate of the Arctic Ocean atmospheric CO_2 sink could "possibly increase or decrease" as detailed in Lannuzel *et al.* (2020). Such a high uncertainty is intrinsically linked to the high complexity of the Arctic carbon cycle and to the drastic environmental changes currently unfolding in that region. Enhanced efforts are required to better observe and understand this high complexity and to anticipate those drastic changes.

Scientific research conducted in the Canadian Arctic has historically been motivated, designed, and implemented from a southern, settler perspective. This results in Inuit Nunangat peoples being excluded and marginalized from the benefits of northern research. Inuit Tapiriit Kanatami (2018) provide vision and strategy implementation for empowering research in Inuit Nunangat (i.e., the Inuvialuit Settlement Region (Northwest Territories), Nunavut, Nunavik (Northern Québec), and Nunatsiavut (Northern Labrador)), at a national level. Pedersen *et al.* (2020) share 45 recommendations developed by Ikaarvik (meaning "bridge" in Inuktitut) youth and mentors for researchers aiming to meaningfully consult, engage, and incorporate Inuit communities in scientific research. This work builds from the concept of ScIQ, the combination of Inuit Qaujimajatuqangit (IQ) and science. Pedersen *et al.* (2020) describe Inuit Qaujimajatuqangit as a way of knowing, a way of life, which extends beyond traditional knowledge, including knowledge, customs, and values, encompassing relationships, attitudes, and behaviours. The recommendations describe actions researchers can take before, during, and after conducting research in the north to incorporate Inuit Qaujimajatuqangit within the entirety of the scientific process.

2.4 Research gaps

There are still prominent gaps in our understanding of air-sea CO_2 flux variability across the Pacific, Atlantic, and Arctic Ocean (Table 2.1). Scientific efforts in Canada and through international collaborations in both observations and modelling have narrowed the uncertainties associated with specific basin air-sea CO_2 fluxes (Figure 2.2; Table A.1). However, these efforts are largely focused on resolving variability in the seasonal cycle and determining mean annual flux values. We still severely lack understanding on how air-sea CO_2 flux variability is impacted on longer timescales or how fluxes may be

shifting under climate change (Table 2.1). Given the different processes that dominate spatial and temporal heterogeneity in air-sea CO_2 fluxes (Figure 2.3-2.5), we have summarized the major basin-specific, process-focused research questions needed to advance the field (Table 2.1).

Table 2.1 Overview of basin-specific research questions needed to aid resolving identified research gaps in this article.

Gap	Research question
Shared across basins	
Long term change	Where and why is the surface ocean increase in CO_2 different from the atmospheric trend, altering the ocean carbon sink?
Sub-decadal to decadal variability	How do modes of climate variability impact air-sea CO_2 fluxes (e.g., El Niño-Southern Oscillation, Pacific Decadal Oscillation, North Atlantic Oscillation)?
Ocean carbon dioxide removal verification	How can ocean carbon dioxide removal (CDR) interventions be differentiated from signals of natural variability and anthropogenic climate change?
International collaboration	Where can Canadian observation and modelling efforts collaborate with, benefit from, and contribute to international ocean understanding?
Indigenous partnerships and capacity building	How can research funding be leveraged to enhance collaboration with First Nations to increase observations, address impending ocean CDR monitoring, reporting, and verification (MRV) development, and ocean acidification action planning?
Complete marine carbon budgets	What is the complete marine carbon budget in Canada integrating carbon stocks and fluxes across other marine pools (e.g., pelagic, benthic, terrestrial to marine interface)? How can we quantify marine carbon budgets and rates of change in more variable and dynamic regions (e.g., nearshore, upwelling regions, polynya regions, etc.)? How can we combine different observation types (e.g., discrete, underway, autonomous, observation-based products) and model outputs to resolve "policymaker relevant" flux values (g C yr^{-1})?
Pacific Ocean	
Marine heatwaves	How will future longer-lasting, more frequent, and more intense marine heatwaves change regional air-sea CO_2 fluxes?

	How will these impact primary productivity in the iron-limited high-nutrient low-chlorophyll region?
Upwelling to downwelling strength	What is the balance of upwelling to downwelling strength that differentiates net annual uptake or outgassing? How is this pattern distributed spatially along the Canadian West Coast?
Atlantic Ocean	
Deep-water formation rates	How is climate change impacting Labrador Sea deep-water formation rates and depth? How is carbon storage durability being impacted?
Biological carbon pump	How will shoaling winter mixed layer depths under climate change impact phytoplankton spring blooms and dissolved inorganic carbon cycling?
Scotian Shelf processes	What is the net impact of upwelling on surface ocean CO_2? How do phytoplankton bloom initiation timing and spatial distribution change the net annual flux on the Shelf?
Arctic Ocean	
Sea ice changes	How is a younger, thinner, sea ice cover with a smaller spatial extent and longer open water season changing the sign/magnitude of air-sea CO_2 fluxes? How is this changing sea ice carbon pump dynamics?
Freshwater stratification and productivity	How will changes in surface stratification from sea ice melt, increased glacial runoff, and changes in terrestrial runoff (e.g., permafrost thaw and riverine input) impact air-sea CO_2 fluxes due to differing water mass carbon loads and equilibration time? How will this impact timing and magnitude of phytoplankton blooms?

2.5 Future directions

The next generation of oceanographers are witnessing the emergence of a new ocean state. The need to reduce present day uncertainties, enhance our understanding of tipping points, account for extreme climatic events in the ocean, and document change from the preindustrial baseline state presents exciting challenges for the oceanographic community. These challenges are particularly relevant to understanding air-sea CO_2 fluxes across all three of Canada's adjacent ocean basins. Expanded use of emerging techniques and greater cross-collaboration between observation and modelling specialists

could narrow the range of uncertainty in regional to basin-scale fluxes, improve observational coverage, inform carbon stocktake efforts, establish a baseline for proposed ocean CDR projects, and support ocean acidification mitigation and adaptation efforts (Table 2.2).

Table 2.2 Table of recommendations for addressing gaps identified and improving air-sea CO_2 flux estimates in Canada.

Category	Recommendations	Examples
Observations	1. Expand use of innovative autonomous measurement technology and support its development. 2. Submit relevant data to public repositories and invest in maintaining global data repositories/structures (national and international). 3. Integrate multiple knowledge systems.	· Instrument platforms (e.g., gliders, surface vehicles, deep-water floats, profiling moorings, ice-proof platforms). · Sensors (e.g., mobile high frequency dissolved inorganic carbon and total alkalinity, pCO_2 remote sensing capabilities). · Satellite remote sensing. · Repositories (e.g., Canadian Integrated Ocean Observing System (CIOOS), Surface Ocean CO_2 Atlas (SOCAT), Global Ocean Data Analysis Project (GLODAP)). · Mine data so earlier data are not lost. · CARE/FAIR data sharing principles. · Alternative data sources (e.g., qualitative data). · Contextualizing Western science data.
Modelling	4. Direct modeling efforts towards fit-for-purpose ocean CDR and regional process study applications.	· Observation data assimilation and evaluation. · Multi-model ensemble comparison projects. · Regional downscaling. · Use of emergent constraint techniques.
Ocean carbon dioxide removal	5. Develop transparent and robust monitoring, verification, and reporting (MRV) protocols.	· Clearly distinguishing intervention from baseline noise. · Integration of observations and models. · Establish code of conduct.

	6. Engage and consult with Indigenous communities. 7. Mobilize ocean acidification expertise.	· Adherence to community specific needs (e.g., First Nations marine governance). · Canada's Ocean Acidification Community of Practice, Ocean Acidification International Coordination Centre, Global Ocean Acidification Observing Network, DFO-NOAA Joint Ocean Acidification Framework
Indigenous co-generation of knowledge	8. Tailor community-specific approaches.	· Formulate research questions through community collaboration. · Pre-study engagement and frequent collaboration thereafter. · Collaborations built on meaningfully trusting relationships. · Participation beyond data collection.
Early career capacity building	9. Increase significance of meaningfully engaging Indigenous communities. 10. House specific projects in multidisciplinary collaborative platforms. 11. Improve equity, diversity, and inclusion.	· Required course work on Indigenous history and rights. · Contribute to established community relationship continuity. · Recognize community building activities within dissertations. · Collaborate with interdisciplinary researchers to deliver improved community-centered outcomes. · Expanded recruitment to include traditionally marginalized groups valuing non-traditional metrics of success. · Fair and equitable financial support for graduate students and postdocs.

Maturing autonomous carbon system sensor technology (Sonnichsen et al., 2023) and deployment on innovative autonomous monitoring platforms such as gliders, surface vehicles, floats, and profiling

moorings offer increased observational capacity beyond time series and sporadic underway sampling (Chai et al., 2020; Sastri et al., 2019). New and planned satellite missions offer improved observation capabilities particularly of the active gas exchange surface layer (Watson et al., 2020; Woolf et al., 2016), and of surface and vertical water transport (Ardhuin et al., 2018; Oubanas et al., 2018), enabling measurement of biogeochemical fronts associated with upwelling, marginal sea-ice zones, and across heterogeneous continental shelf boundaries and river outflows (Shutler et al., 2020). Furthermore, submission of surface ocean CO_2 observation data to global databases (e.g., Surface Ocean CO_2 Atlas; Bakker *et al.*, 2016) are extremely important to increase accessibility, quality assurance and control of data, as well as end user reusability. The principals of FAIR (Findable, Accessible, Interoperable and Re-usable; Tanhua et al., 2019) and CARE (Collective Benefit, Authority to Control, Responsibility, and Ethics; Carroll et al., 2020; when relevant using Indigenous owned data and knowledge) should be adhered to when considering a project's data lifecycle. These breakthroughs in innovative observation platforms and increasing public availability of data are coinciding with the emergence of machine learning and higher computing capacity that can be used to simulate the marine carbon system during periods or within regions devoid of sufficient observations (Landschützer et al., 2014), or to project future changes. Integrating multiple ways of knowing outside conventional western science observations can result in richer outcomes with greater breadth from a stronger framework of research questions established through early engagement (Ban et al., 2018). Indigenous peoples' communal memory, as an example, is capable of observing trends or variations in their lands that no other sensor can replicate (Alessa et al., 2016) often outside western science monitoring metrics (Table 2.2). This could include contributing alternative data sources (e.g., qualitative measures embedded in traditional laws or stories; Ban *et al.* 2018), or contextualizing, interpreting, and applying results from earth observations (e.g., Mittimatalik sea ice charts; Wilson *et al.* 2021).

Considering, specifically, the marine carbonate system, existing numerical models need to be carefully calibrated against observations, and parameterizations need to be improved. Observations are needed to evaluate the performance of existing models and carefully calibrate them through data assimilation, to narrow the spread of air-sea CO_2 flux estimates across model ensembles (Wang et al., 2016). Assimilation of observations, especially biogeochemical data, will improve understanding of historical carbon uptake conditions and drivers of variability. Data assimilation also improves near real-time seasonal to decadal predictions (forecasts) which are currently only indirectly initialized (Li et al., 2019a). Improved observational coverage, for example by autonomous biogeochemical ocean Argo floats, will improve our ocean modelling ability. Idealized model experiments like in Sarmiento *et al.* (1998), Winton

et al. (2013), and multi-model ensemble comparison projects like those in Frölicher *et al.* (2015), Cheng, Chiang, and Zhang (2013), can be used to understand the relative importance of different biogeochemical processes and their response to the changing climate. Further, these types of experiments can be important for identifying the source of model ensemble uncertainty. Model uncertainty in the ocean carbon flux is projected to be largest where surface waters are connected to deeper waters (Gooya et al., 2023). Improving ocean circulation in models, which is a primary driver of ocean carbon flux variability (McKinley et al., 2020), can reduce these uncertainties. Regional downscaling of low-resolution models to higher resolution, especially in heterogeneous regions like the Canadian Arctic Archipelago, can result in more informative model projections (Table 2.2). As an example, mesoscale eddies are quite important for mixing (and therefore also impact air-sea CO_2 fluxes; Ford *et al.*, 2022) but are often not resolved in current generations of earth system models (Frölicher et al., 2015). Further, simplified, and specialized models can analyse the efficiency and climate level feedback of various proposed ocean CDR techniques. “Sampling” from models (looking at data from where and when we have real world observations within the full model field) can be used to evaluate the performance of current observation gap-filling techniques (Gloege et al., 2021) in regions of high air-sea CO_2 fluxes and high uncertainty (e.g., high latitude oceans; Gruber, Landschutzer and Lovenduski, 2019). Moreover, new statistical tools and techniques such as emergent constraints (a way of looking at the relationship between a variable of current climate state within individual models, and future changes in a variable of interest that make up an ensemble) accelerate the development and improvement of the next generations of earth system models (e.g., Hall *et al.* 2019; Bourgeois *et al.* 2022).

Our poor understanding of air-sea CO_2 flux variability represents a major gap in current ocean CDR and carbon credit generation program standards (Table 2.1&2.2). Negative emission technologies must be additional to what would have happened by law or under a business-as-usual scenario if the project had not been carried out (Verra, 2023). Enhanced capacity and accuracy in both observations and modelling efforts mentioned above can reduce air-sea CO_2 flux uncertainty, critical to clarifying what constitutes additional removal relative to baseline noise. However, as far as developing trusted, unique, non-exchangeable carbon credits from nature-based, mechanical, or geoengineered solutions (NASEM, 2021), considerations need to be made for which carbon pool is being drawn down. Accounting must include the transboundary nature of the ocean, the timescale of carbon removal, and, most importantly, if the process actually enhances ocean atmospheric CO_2 uptake. We are much further behind in defining the marine carbon stocktake compared to the terrestrial carbon reservoir in Canada (Sothe et al., 2022). Moving forward with marine nature-based solutions that include tangible ecosystem co-benefits (e.g.,

ocean acidification mitigation) through restoration and conservation should continue to be a priority while recognizing their limitations and potential leakage (Drever et al., 2021; Roth et al., 2023; Williamson et al., 2022). Considerations also need to be given to ensuring the safety and efficacy of ocean CDR given the risk of uncertain impacts to human and environmental welfare through a comprehensive code of conduct (Loomis et al., 2022). Ocean CDR projects need to concentrate on acquiring funding at the levels highlighted in the NASEM (2021) report, and conducting feasibility and scalability testing with a focus on monitoring, reporting, and verification. The latter should be performed through a lens of governance in line with equity and justice goals (Kosar and Suarez, 2021; Loomis et al., 2022). Ocean CDR should not be used to delay carbon emission reductions (Ho, 2023b; Shutler, 2020).

Resolving air-sea CO_2 fluxes helps resolve uncertainty in ocean acidification as strong atmospheric CO_2 uptake generally leads to elevated trends and worsening ocean acidification conditions. Leveraging existing ocean acidification infrastructure, expertise, and policies offers an exceptional starting point for addressing uncertainty in air-sea CO_2 fluxes and developing ocean CDR MRV (Table 2.2). National and international ocean acidification infrastructure already exists (e.g., Canada's Ocean Acidification Community of Practice; Ocean Acidification International Coordination Centre; Hansson, Appeltans and Gattuso, 2014; Global Ocean Acidification Observing Network; Newton *et al.*, 2015; DFO-NOAA Joint Ocean Acidification Framework; Government of Canada and Fisheries and Oceans Canada, 2018) along with widespread public attention (United Nations Sustainable Development Goal 14.3; Barbière, Isensee and Schoo, 2019). Experts from these communities are well suited to address monitoring gaps in air-sea CO_2 flux observations, assess ocean CDR ecosystem impacts, and offer the public a trusted voice advancing MRV development.

Throughout this paper, we have identified Indigenous led or co-led monitoring programs and coast-specific Indigenous scientific collaborative frameworks built on recommendations from First Nations. Indigenous communities are likely to experience greater climate impacts in Canada while their contribution to the global climate crisis is negligible. Indigenous peoples are a highly sensitive population at the intersection of climate change and community health (Ford et al., 2018; Kenny et al., 2020) facing a burden of existing social disparity in health, education, food and energy security, generational trauma, and colonial legacies (Ford et al., 2010; Ford and Smit, 2004; Maldonado et al., 2013; Maru et al., 2014). With an elevated emphasis from research and government institutions on meaningfully engaging with First Nations, new collaborations could improve traditional knowledge exchange to enhance marine carbon cycle understanding. The community-specific approach would follow successes in mapping

(Bishop et al., 2022; Davies et al., 2020), coastal management (Lombard et al., 2019; Weiss et al., 2013), marine conservation (Ban et al., 2009), observational oceanography (Moran et al., 2022), and fisheries (Reid et al., 2021; Turgeon et al., 2018; Weatherdon et al., 2016). As ocean CDR and Indigenous involvement in the sector are both just emerging, any new collaborative initiative should follow recommendations made by Breckwoldt, Lopes and Selim (2021), including (1) the need for participation beyond data collection, (2) acknowledgment and mitigation of an agenda mismatch between funded and needed research, and (3) emphasizing the power of the transdisciplinary processes of learning together.

Pathways for early career researchers to meaningfully engage with Indigenous groups and collaborate on climate problems are restricted by institutional undervaluing, graduate student timelines, lack of funding, and traditional academic metrics of success (e.g., peer-reviewed journal publications). University students, and particularly international students, may lack knowledge about Canada's colonial history and systemic oppression of Indigenous peoples (Godlewska et al., 2020) and the ways that natural science research can impact Indigenous communities (Bozhkov et al., 2020; Kater, 2022). Community relationship building needs to be recognized as a priority investment and should start with mandatory course work on Indigenous history and rights taught by Indigenous instructors to enhance student understanding of the socio-political landscape around their research (Table 2.2; Wong *et al.*, 2020). Given graduate student timelines, it falls on principal investigators to identify which Indigenous government or community has jurisdiction over or interests in the proposed research. Principal investigators can create continuity in community relationship building, which is critical to establishing trust and genuinely engaging with rightsholders (Table 2.2). Early dialogue should support Indigenous peoples' self-determination, focusing on what research is being proposed and how the proposal meets the interest and priorities of Indigenous communities finding opportunities for reciprocity (Wong et al., 2020). Mainstreaming reconciliation in all aspects of the scientific endeavor, from formulation to completion as a requirement in Government of Canada tri-council funding (Wong et al., 2020), integrated as a valued component of traditional graduate student dissertations, and moving forward with both treaty-based, and resurgence-based decolonial Indigenization of academic spaces and places is severely overdue (Gaudry and Lorenz, 2018).

Training and equipping early career ocean professionals (ECOPs) with the skills needed to apply the approaches described above should be a priority moving forward in supervised academic settings as well as in government and industry work environments. Early exposure to carbon cycle concepts, interdisciplinary linkages, and skill building through undergraduate research assistantships is ideal if

accompanied with adequate compensation and professional development opportunities. Early career researchers should not be expected to become experts in all the methods outlined throughout this paper including community collaboration and engagement (Table 2.2). Rather, early career researchers should be given the opportunity to connect (as part of their research project) to a platform that enables them to collaborate with other multidisciplinary researchers bringing together social scientists, economists, and Indigenous knowledge keepers. Beyond training, at the forefront of recruiting students all the way to research chairs, the focus should be on increasing equity, diversity, and inclusion within our field to spark new ideas, solutions, and perspectives (Osiecka et al., 2022). Fair and equitable financial support for graduate student and postdoc work (Laframboise et al., 2023), mental health support, and fostering greater peer-to-peer collaborative opportunities leads to more diverse, happier, healthier, and more productive labs (Osiecka et al., 2022). The next generation of ocean scientists face significant adversity in informing policy efforts to meet global net-zero emissions targets, while grappling with past and current injustices around truth and reconciliation efforts here in Canada. Amongst this group of ECOPs, there is consensus on the need for recentering science in future policy discussions while moving forward with all available options to combat the climate crisis.

2.6 Acknowledgements

Heartfelt thanks to Roberta Hamme for her passion, enthusiasm, and support for all the early career highly qualified personnel on Canada's Marine Carbon Sink Project. We are so grateful to have so much support for our ongoing work from all the principal investigators on the project including Debby Ianson, Brent Else, Philippe Tortell, Doug Wallace, Paul Myers, Kent Moore, Katja Fennel, Brad deYoung, Dariia Atamanchuk, Frédéric Cyr, Susan Allen, Nadja Steiner, Neil Swart, Lisa Miller, Kumiko Azetsu-Scott, Jim Christian, Emmanuel Devred, Youyu Lu, Tetjana Ross, and Igor Yashayaev. We also thank fellow early career ocean carbon professionals Robert Izett, Tereza Jarníková, and Samantha Jones for their support and feedback while putting this manuscript together, as well as the two anonymous reviewers for their helpful comments. Funding for this project was provided by the Natural Sciences and Engineering Research Council of Canada (NSERC) through the Advancing Climate Change Science in Canada program (grant# ACCPJ 536173-18) to Roberta Hamme.

2.7 Author contributions

Conceptualization: PJD, BR, RA, JL, KS, PG, MMMA, MRM, CAB, KK, RP, YS, GN, ACF

Data curation: PJD, BR, RA, ACF

Formal analysis: PJD, RA, KK, ACF

Investigation: PJD, BR, RA, JL, KS, PG, MMMA, MRM, CAB, KK, RP, YS, GN

Project administration: PJD

Validation: ACF

Visualization: BR, ACF

Writing – first draft: PJD (Introduction, Canadian marine CO_2 uptake, Canadian Pacific, Research gaps, Future directions), BR (Canadian Arctic), RA (Canadian Atlantic)

Writing – original submission: PJD, BR, RA, JL, KS, PG, MMMA, MRM, CAB, KK, RP, YS, GN, ACF

Writing – review & editing: PJD, BR, RA, JL, KS, PG, MMMA, MRM, CAB, KK, RP, YS, GN, ACF

Chapter 3. Estimating Marine Carbon Uptake in the Northeast Pacific Using a Neural Network Approach

Key points:

1. High spatial resolution artificial neural network pCO_2 product shows minimal loss in performance compared to similarly trained coarser resolution estimates with internal data division being the most important tuning parameter.
2. Air-sea CO_2 flux seasonal variability:
    a. Alaskan Gyre region driven by seasonal gyre upwelling and entrainment.
    b. North Pacific Current region driven by competing temperature and dissolved inorganic carbon cycles.
3. Strength of Alaskan Gyre upwelling acts as most influential driver of sub-decadal to decadal air-sea CO_2 flux variability.
4. Impact of interannual events on air-sea CO_2 flux:
    a. 2008 ocean iron fertilization event led to a minimal increase in uptake due to strong Alaskan Gyre upwelling mode.
    b. 2013-2015 “The Blob” and 2018-2020 marine heatwave events led to a large increase in uptake due to stratification plus a weak Alaskan Gyre upwelling mode.
5. Basin-wide air-sea pCO_2 disequilibria may be increasing due to connectivity to subsurface water, implying the Northeast Pacific could be becoming a stronger sink for atmospheric CO_2.

Short summary: The ocean is both impacted by climate change and helps mitigate its effects through taking up carbon from the atmosphere. We used a machine learning approach to investigate controls on carbon uptake in the Northeast Pacific open ocean. Marine heatwaves that lasted 2–3 years increased uptake, while the upwelling strength of the Alaskan Gyre controlled uptake over 10-year time periods. The trend from 1998–2019 suggests carbon uptake in the Northeast Pacific open ocean is increasing.

This work has been published in a scientific journal as: Duke, P. J., Hamme, R. C., Ianson, D., Landschützer, P., Ahmed, M. M. M., Swart, N. C., and Covert, P. A.: Estimating marine carbon uptake in the northeast Pacific using a neural network approach, Biogeosciences, 20(18), 3919–3941, 2023, https://doi.org/10.5194/bg-20-3919-2023.

3.1 Abstract

The global ocean takes up nearly a quarter of anthropogenic CO_2 emissions annually, but the variability of this uptake at regional scales remains poorly understood. Here we use a neural network approach to

interpolate sparse observations, creating a monthly gridded seawater partial pressure of CO_2 (pCO_2) data product from January 1998 to December 2019, at 1/12°x1/12° spatial resolution, in the Northeast Pacific open ocean, a net sink region. The data product (ANN-NEP; NCEI Accession 0277836) was created from pCO_2 observations within the 2021 version of the Surface Ocean CO_2 Atlas (SOCAT), and a range of predictor variables acting as proxies for processes affecting pCO_2 to create non-linear relationships to interpolate observations at a spatial resolution four times greater than leading global products and with better overall performance. In moving to a higher resolution, we show that the internal division of training data is the most important parameter for reducing overfitting. Using our pCO_2 product, wind speed, and atmospheric CO_2, we evaluate air-sea CO_2 flux variability. On sub-decadal to decadal timescales, we find that the upwelling strength of the subpolar Alaskan Gyre, driven by large-scale atmospheric forcing, acts as the primary control on air-sea CO_2 flux variability (r^2 = 0.93, p <0.01). In the northern part of our study region, divergence with atmospheric CO_2 is enhanced by increased local wind stress curl, enhancing upwelling and entrainment of naturally CO_2-rich subsurface waters, leading to decade-long intervals of strong winter outgassing. During recent Pacific marine heatwaves from 2013 on, we find enhanced atmospheric CO_2 uptake (by as much as 45%) due to limited wintertime entrainment. Our product estimates long-term surface ocean pCO_2 increase at a rate below the atmospheric trend (1.4±0.1 μatm yr^{-1}) with the slowest increase in the center of the subpolar gyre where there is strong interaction with subsurface waters. This mismatch suggests the Northeast Pacific Ocean sink for atmospheric CO_2 may be increasing.

3.2 Introduction

As countries around the world consider updating their carbon emission reduction commitments (United Nations Environment Programme, 2022), we require a better understanding of global carbon sinks and how they may be shifting under climate change. The global ocean takes up nearly a quarter of anthropogenic carbon dioxide (CO_2) emissions annually (Friedlingstein et al., 2022b) but the temporal and spatial variability of the marine sink remains unclear on decadal or longer timescales (Fay and McKinley, 2013b; Gruber et al., 2023; McKinley et al., 2011b; Wanninkhof et al., 2013b). Potential future changes in the marine sink associated with climate change are also unclear (O'Neill et al., 2016). Extending the spatial and temporal coverage of partial pressure of CO_2 in seawater (pCO_2) observations can help address this knowledge gap (Aricò et al., 2021). Benefitting from the increasing abundance of CO_2 measurements at sea and community synthesis efforts (e.g., through the Surface Ocean CO_2 Atlas (SOCAT); Bakker et al., 2016), a variety of interpolation approaches have evolved capable of creating

continuous observation-based estimates of pCO_2 (Chen et al., 2019; Denvil-Sommer et al., 2019; Landschützer et al., 2013; Laruelle et al., 2017; Nakaoka et al., 2013; Ritter et al., 2017; Zhong et al., 2022). However, their global focus and coarse resolution limits their interpretation at regional scales (Olivier et al., 2022). Only recently, higher resolution regional pCO_2 maps have been developed for the California current system (Sharp et al., 2022) to overcome the limitations of coarse global scale pCO_2 products. These seawater pCO_2 products, combined with wind speed and atmospheric pCO_2, have informed regional to global air-sea CO_2 flux estimates of multiyear variability (Hauck et al., 2020; Landschützer et al., 2015, 2016, 2019; Wang et al., 2021).

No high-resolution observation-based air-sea CO_2 flux estimate currently exists for the North Pacific Ocean. The Northeast Pacific Ocean has been characterized as a net annual sink for atmospheric CO_2 (Wong et al., 2010; Franco et al., 2021; Sutton et al., 2017; Duke et al., 2023b). The region is divided by two dominant oceanographic features, the Alaskan Gyre system to the north, and the North Pacific Current to the south (Franco et al., 2021). With respect to surface ocean carbon measurements, the Alaskan Gyre system remains extremely sparsely sampled. The seasonal air-sea CO_2 flux of the gyre has been described as being strongly influenced by gyre upwelling with outgassing in the winter and uptake in the summer (Brady et al., 2019; Chierici et al., 2006; Palevsky et al., 2013). Along the easternmost part of the North Pacific Current, most of our understanding comes from a limited region; the Ocean Station Papa mooring at 50°N, 145°W (Sutton et al., 2017), and the Line P program (Freeland, 2007). This region has well documented seasonal cycles (Sutton et al., 2017), interannual variability (Wong et al., 2010; Wong and Chan, 1991), and long-term trends (Franco et al., 2021; Sutton et al., 2019). CO_2 uptake is mainly driven by direct ventilation of the shallow upper water column, with a small seasonal change in surface ocean pCO_2 (Sutton et al., 2017; Wong et al., 2010). The estimated long-term trend in surface ocean pCO_2 appears to be increasing at less than the atmospheric rate of increase (Franco et al., 2021).

Understanding what drives air-sea CO_2 fluxes on seasonal, interannual, and decadal timescales in the Northeast Pacific Ocean will inform how the regional sink may change in the future. This region is already experiencing persistent marine heatwaves with dramatic temperature anomalies observed during 2014 to 2016 and 2018 to 2020 events (Bond et al., 2015; Freeland and Ross, 2019), with future events predicted to become longer-lasting, more frequent, more extensive, and more intense (Frölicher et al., 2018). The impact of large-scale climate-driven decadal oscillations on the marine carbon system is just beginning to be explored in models (Hauri et al., 2021). Furthermore, this region has been targeted as a potential site of marine carbon dioxide removal, as a negative emissions technology aimed at

meeting emission reduction goals continues to grow in interest and investment (Cooley et al., 2023). Some proposed approaches look to artificially stimulate biological carbon drawdown (GESAMP, 2019; NASEM, 2021). The Northeast Pacific Ocean, as an iron-limited high-nutrient low-chlorophyll region (Aumont et al., 2003; Dugdale and Wilkerson, 1991; Freeland et al., 1984; Martin et al., 1994), has already been the location of geoengineered biological carbon drawdown experiments (Boyd et al., 2005, 2007; Ianson et al., 2012; Wong and Johnson, 2002). Thus, a firm understanding of processes driving carbon fluxes and the establishment of environmental baselines in the region is critical.

Our aim is to investigate drivers of air-sea CO_2 flux variability in the Northeast Pacific (NEP) Ocean, building a novel regional high-resolution artificial neural network (ANN) approach adopted from an existing global setup (Landschützer et al., 2013). In Section 3.3, we describe the creation of a gridded pCO_2 data product (herein referred to as ANN-NEP; NCEI Accession 0277836; Duke et al., 2023a) monthly from January 1998 to December 2019 at 1/12°x1/12° spatial resolution in the Northeast Pacific open ocean (approximately 9 km by 5km; latitude by longitude). In Section 3.4, we show that the high-resolution regional pCO_2 product is robust enough to recreate training observation data while generalizing well compared to independent withheld observation data. We also show that stepping to a higher resolution regionally with appropriate tuning of the internal training and evaluation data ratio does not hinder product performance. In Section 3.5, our results show that the upwelling strength of the subpolar Alaskan Gyre and surface ocean connectivity to subsurface waters act as the primary control on air-sea CO_2 flux variability in our study area. We conclude by calculating long-term trends in surface ocean pCO_2 and carbon uptake, examining trends relative to connectivity to subsurface waters.

3.3 Data and methods

Our study area comprises the region between latitudes 45°N and 62°N and longitudes 120°W and 155°W (Figure 3.1), with the open-oceanic/coastal boundary defined as 300 km offshore following Laruelle et al. (2017). We limit our study region to the open ocean regions with reduced variability and related drivers compared to the continental shelf regions. Creating a product on the continental shelf and in the nearshore requires different neural network considerations and is associated with high uncertainties (Laruelle et al., 2017). This work represents a four times increase in spatial resolution over previous multiyear global open ocean products, usually coarser than 1/4° (Landschützer et al., 2020b). The increased resolution derives from high-resolution predictor data used to create the product (Table 3.1). To interpolate the existing CO_2 observations in this domain, we adapt the artificial neural network (ANN) self-organizing-map-feed-forward-network (SOM-FFN) approach developed by Landschützer et al. (2013,

2014). In a first step, the method divides the region of interest into dynamic zones with similar biogeochemical features (i.e., SOM biogeochemical provinces), using a self-organizing map approach. In a second step, a feed-forward neural network is used for interpolating pCO_2 observations in each of the pre-determined provinces of step one. Specifically, non-linear functional relationships are created between pCO_2 observations (or neural network target data), where they exist in our study domain, and independent predictor variables (or neural network input data) that are known to drive the marine carbon cycle (see Section 3.3.1 below). Once the relationships are established, they can be applied where no observations exist to fill space/time gaps and create continuous sea surface pCO_2 maps from 1998-2019.

3.3.1 Predictor data

The chosen predictor variables for this study (Table 3.1) had all been used previously in observation-based pCO_2 interpolated products (Denvil-Sommer et al., 2019; Gregor et al., 2018; Landschützer et al., 2014; Telszewski et al., 2009; Zhong et al., 2022). Sea surface temperature (SST) comes from the satellite-based European Space Agency Climate Change Initiative (ESA Sea Surface Temperature Climate Change Initiative (SST_cci): Level 4 Analysis Climate Data Record, version 2.1; Merchant et al., 2019), as well as Chlorophyll-*a* concentration which served as a proxy for biological processes (ESA Ocean Colour Climate Change Initiative (Ocean_Colour_cci): Global chlorophyll-a data products gridded on a geographic projection, Version 5.0). Remaining physical process predictor data (e.g., sea surface salinity (SSS), sea surface height (SSH), and mixed layer depth (MLD)) are obtained from Copernicus Marine Environment Monitoring Service global ocean eddy-resolving reanalysis (Global Ocean Physical Reanalysis Product, E.U. Copernicus Marine Service Information GLOBAL_REANALYSIS_PHY_001_030). Jointly assimilated observations include satellite altimeter data and *in situ* vertical profiles of temperature and salinity informing the MLD reanalysis product (Table 3.1). The ocean general circulation model is based on the Nucleus for European Modelling of the Ocean (NEMO) platform, driven at the surface by the European Centre for Medium-Range Weather Forecasts ERA-Interim winds (Jean-Michel et al., 2021). Both Chlorophyll-*a* and mixed layer depth were log10-transformed to produce a distribution of values closer to normal before being used in either SOM-FFN step. Atmospheric pCO_2 in µatm was downloaded from Landschützer et al. (2020b), derived from the National Oceanic and Atmospheric Administration Earth System Research Global Monitoring Laboratory (https://gml.noaa.gov/ccgg/globalview/) atmospheric mole fraction of CO_2 (χCO_2) and SST (Reynolds et al., 2002) as well as sea level pressure (Kalnay et al., 1996) following Dickson et al. (2007). Finally, the

monthly pCO_2 climatology of Landschützer et al. (2020) was used as an additional input parameter solely for defining the SOM biogeochemical provinces.

Table 3.1 Northeast Pacific open ocean artificial neural network predictor variables and their corresponding source, original temporal and spatial resoltuions, and processing steps used for this study.

Predictor variable	Source	Original resolution		Processing
		Temporal	Spatial	
Satellite-based product				
Sea surface temperature (SST)	SST_cci Level 4 Analysis Version 2.1	Daily	1/20°x1/20°	Averaged to monthly, aggregated to 1/12°x1/12°
Chlorophyll-*a* (Chl)	Ocean_Colour_cci Version 5.0	Daily	1/24°x1/24°	Averaged to monthly, aggregated to 1/12°x1/12°, log10-transformed
Satellite and in-situ observation data assimilated reanalysis product				
Sea surface salinity (SSS)	Copernicus Marine Service Global Reanalysis PHY_001_030	Monthly	1/12°x1/12°	None
Sea surface height (SSH)				None
Mixed layer depth (MLD)				log10-transformed
Atmospheric-measurement-based interpolation product				
Atmospheric pCO_2	Landschützer et al. (2020) - NCEI Accession 0160558	Monthly	1°x1°	Interpolated to 1/12°x1/12°

3.3.2 pCO_2 observations

ANN target pCO_2 data come from the Surface Ocean CO_2 Atlas (SOCAT) v2021 (Bakker et al., 2016), as well as additional data from the Fisheries and Oceans Canada February 2019 Line P cruise (https://www.waterproperties.ca/linep/; Figure 3.1a&b). Sea surface CO_2 fugacity (fCO_2) was converted to sea surface pCO_2 (Text B.1; Körtzinger, 1999). pCO_2 observations were bin-averaged into monthly, 1/12° latitude by 1/12° longitude grid cells computing the mean and standard deviation within each grid cell. Of the 8,712,264 grid cells that represent the surface ocean gridded in three dimensions over 264 months (1998–2019) at 1/12°x1/12° resolution in the study area, just 0.39% have an associated gridded pCO_2 value (Figure 3.1a&b).

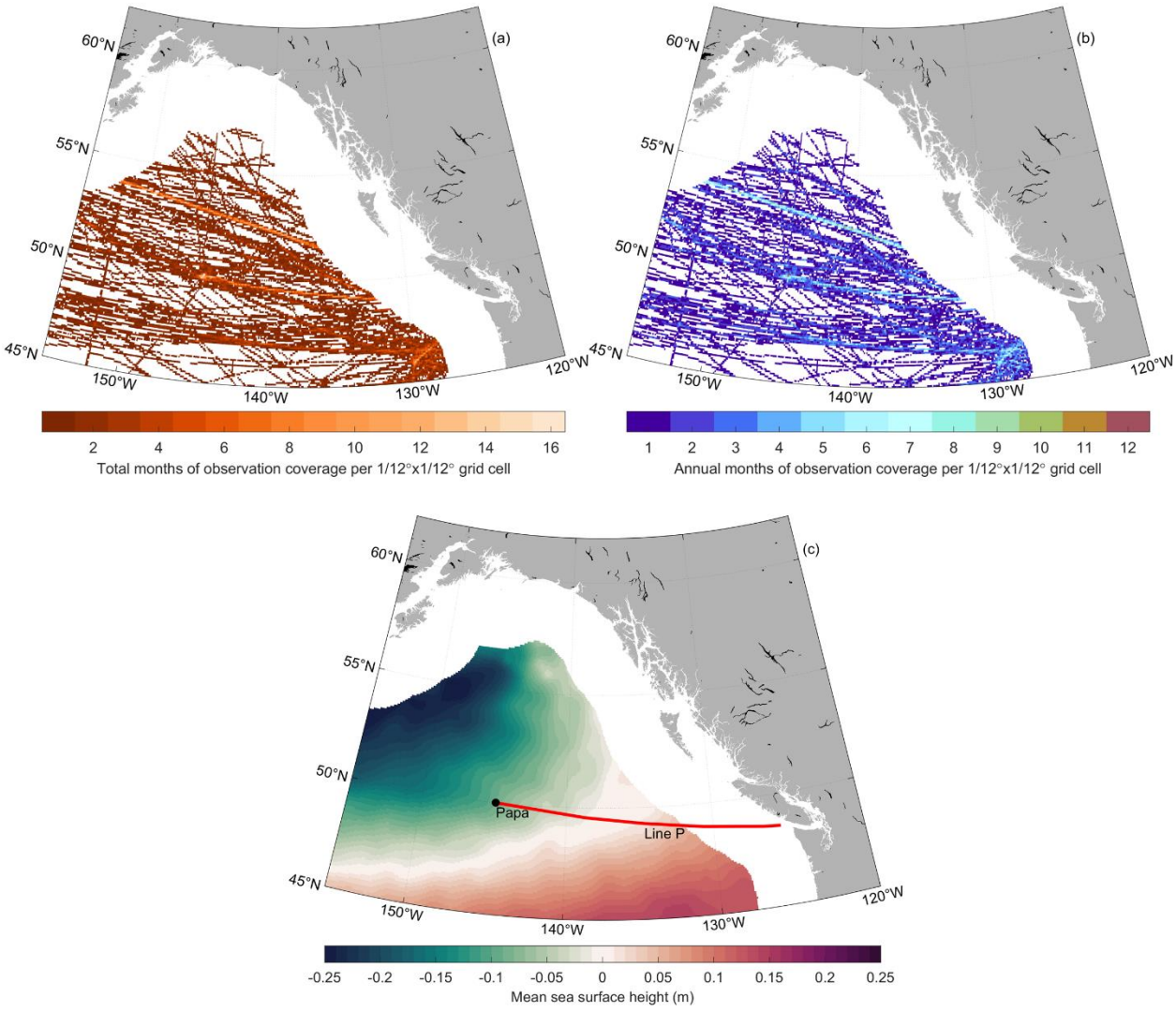

Figure 3.1 (a) Total number of months of observational coverage from Surface Ocean CO_2 Atlas (SOCAT) v2021 (Bakker et al., 2016) and additional data from Fisheries and Oceans Canada February 2019 Line P cruise (https://www.waterproperties.ca/linep/) per 1/12°x1/12° grid cell. (b) Number of unique annual months of observational coverage per 1/12°x1/12° grid cell. (c) Mean sea surface height (SSH; Table 3.1) shows relative location of the subpolar Alaskan Gyre (negative SSH values), and the North Pacific Current (SSH approximately equal to zero). Ocean Station Papa is labeled and marked with a black circle while Line P is labelled and marked with a red line.

3.3.3 Evaluation

In constructing the optimal ANN architecture, a series of SOM-FFN tuning tests were conducted comparing ANN output to training and independent withheld data. ANN performance for each tuning test was evaluated using five statistical metrics: root mean squared error (RMSE), coefficient of determination (r^2), mean absolute error (MAE), mean bias (calculated as the mean residual), and the slope of the linear regression (c_1) between the ANN and the corresponding gridded SOCAT pCO_2

observations. Independent withheld data came from randomly selected SOCAT data using associated expocodes corresponding to unique complete underway cruise tracks or mooring deployments. We tested 100 random independent withheld data splits and selected one representative of basin-wide observational coverage (summer/southern sampling bias), with winter, spring, and fall data present (Figure 3.1; Figure A.1). These independent withheld data represented approximately 5% of the total study area gridded pCO_2 data, with coverage during all seasons over a range of latitudes (Figure A.1). Ensuring selected independent withheld data is random, yet also representative of the full domain, without withholding critical end range training data is difficult. Community-based best practices are likely needed going forward to ensure continuity in reported observation-based pCO_2 product uncertainty based on independent withheld data (Section 3.4.2).

3.3.4 Neural network construction

SOM-FFN tuning tests occurred in series using the MATLAB Neural Network Toolbox, with sequential improvements impacting future tests. Optimization of the SOM-derived biogeochemical provinces involved trial-and error testing of various parameters including SOM biogeochemical province count, predictor variables choice, and static or varying province shape with each timestep (Landschützer et al., 2013). The choice of four SOM biogeochemical provinces represented the lowest number of SOM biogeochemical provinces for a typical clustering structure to emerge (Figure B.2), while keeping the ratio of gridded pCO_2 observation to the total grid cells within each province similar (0.38$\pm$0.06%). The best SOM predictor variables were SST, SSS, MLD (Table 3.1), and the Landschützer et al. (2020a) pCO_2 climatology. We did not normalize predictor data (e.g., force a mean of 0 and standard deviation of 1), implicitly weighting SOM predictors toward the pCO_2 climatology as its range is at least one order of magnitude greater than that for SST, SSS, and log(MLD) (Landschützer et al., 2013). As a result, our dynamic provinces follow the seasonal variations in the pCO_2 climatology (Landschützer et al., 2020a). Thus, non-static provinces, which changed shape from one month to the next over a climatology, proved the most useful in clustering seasonal cycle variability. This clustering does lead to clearly unphysical fronts as an artifact of the approach.

In reaching an optimal FFN architecture (i.e., number of inputs, number of hidden layers and neurons in each hidden layer), trial-and error testing of tuning parameters explored predictor variable choice, FFN training algorithm and activation functions, pre-training to determine the number of neurons in the first hidden layer, introducing a second hidden layer with a static number of neurons, and changing the internal data division ratio (optimized at 94:6; see Section 3.4.4 below).

To emphasize interannual and longer-term trends within the six predictor variables (Table 3.1), each predictor variable is used in two different forms, first in its raw form and second after deseasonalizing, bringing the total number of FFN predictors used to 12. To deseasonalize, within each grid cell, the monthly anomaly was calculated by subtracting the climatological monthly mean, removing the seasonal cycle from the data (the same approach is used when looking at anomaly values in our results; Section 3.5). Where no chlorophyll-*a* satellite data were available, the ANN was run again with the remaining predictors and output was merged to fill empty grid cells (Landschützer et al., 2014). The Levenberg–Marquardt backpropagation training algorithm and hyperbolic tangent sigmoid activation function (i.e., trainlm and tansig respectfully in MATLAB) were found to deliver the best fit. The number of neurons within the first hidden layer varied by province and the optimal number of neurons was determined in a pre-training run, where we increased the number of neurons parabolically from two up to a number where the ratio between the training sample size to the number of weights did not exceed 30 (i.e., a number that was determined by trial and error). The best output performance of the pre-training determines the best neuron setup which was then further used for the actual ANN training.

To avoid overfitting, we split all the internal training data into two subsets (i.e., one actual training dataset and one internal evaluation dataset). While most studies use a fixed ratio (usually 80:20) between these sets, we used the optimal ratio determined by a criterion suggested in Amari et al. (1997) that is dependent on the number of degrees of freedom and hence varies with the optimal number of neurons determined in the pre-training (see Section 3.4.4 below). While the training dataset is used to reconstruct the non-linear relationship between input data (Table 3.1) and pCO_2 observations, the internal evaluation data are used to stop the training before the network starts overfitting the training data. Specifically, we stopped the training when 6 consecutive iterations did not reduce the network's error compared to internal evaluation data (Hsieh, 2009). The addition of a second hidden layer with a static neuron number of five was found to slightly improve performance within the evaluation metrics.

3.3.5 Cross-evaluation and ensemble

In order to further decrease the risk of overfitting, we used a 10-fold cross-evaluation approach (Li et al., 2019b, 2020) and a bootstrapping method (Landschützer et al., 2013). Here, all SOCAT cruises (apart from the independent withheld data; Section 3.3.3) were randomly divided into ten equal subsamples using SOCAT expocodes prior to gridding. One subsample was used as 10-fold evaluation data (10% of all data), and was excluded from training, while the remaining nine subsamples were used together as training data (90% of all data). The cross-evaluation process was repeated ten times, with each of the ten

subsamples used exactly once as the 10-fold evaluation dataset. We performed ten trainings with each 10-fold training data subsample where we randomly split the ANN internal training and evaluation data based on the optimal ratio determined through testing (Section 3.4.4). The robustness and reliability of an ANN has been shown to be significantly improved by combining several ANNs into an ANN ensemble model (Fourrier et al., 2020; Linares-Rodriguez et al., 2013; Sharkey, 1999). The ten different ANN outputs trained on ten different 10-fold training data subsamples were used as an ANN ensemble, where the ten outputs were averaged to obtain the final ANN-NEP pCO_2 product (Fourrier et al., 2020).

3.3.6 Computation of air-sea fluxes

Using the ANN-NEP pCO_2 product, the air-sea CO_2 flux ($F\mathrm{CO}_2$), was calculated using Eq. 3.1:

$$F\mathrm{CO}_2 = \propto k\Delta p\mathrm{CO}_2 \,, \tag{3.1}$$

based on solubility ($\propto$) as a function of temperature and salinity using the data presented in Table 3.1 (Weiss, 1974), gas transfer velocity (k), and the gradient between pCO_2 in the surface ocean and the atmosphere (ΔpCO_2). Here, the gas transfer velocity is a function of wind-speed retrieved from monthly, 1/4° spatial resolution Cross-Calibrated Multiplatform ocean surface wind data (Mears et al., 2019) interpolated to 1/12°, the temperature dependent Schmidt number specific to CO_2, and gas transfer coefficient from Wanninkhof (2014). Negative (positive) flux values indicate CO_2 uptake (outgassing) by the ocean. Uncertainty in the air-sea CO_2 flux comes from a 20% uncertainty in k (Wanninkhof, 2014) and the overall product uncertainty in estimated pCO_2 (θ_{pCO2}; Eq. 3.2; see Section 3.4.2 below). As the uncertainty of ΔpCO_2 is dominated by the uncertainty in estimated surface ocean pCO_2, we neglect the small contribution from atmospheric CO_2 (<1 μatm; Landschützer et al. 2014).

3.4 Network performance

3.4.1 Evaluation comparing to SOCAT data

Overall, the final high-resolution regional artificial neural network Northeast Pacific pCO_2 product (ANN-NEP) obtains good fits with an overall r^2 of better than 0.8 and RMSE of around 11 μatm between the estimated pCO_2 and the gridded SOCAT pCO_2 data across both the training data (Figure 3.2a), and independent withheld data (Figure 3.2b). The mean bias is negligible (<0.8 μatm; smaller than observational uncertainty). These results also apply within individual calendar years, and within monthly groupings across all years, indicating that the temporally inhomogeneous data distribution over the time range and between seasons does not have a measurable effect on the estimates (Table B.1). There is no

clear spatial structure to the residuals, with no specific region displaying persistently positive or negative residuals (Figure B.3). When compared to local pCO_2 mooring data from Ocean Station Papa (which is included in SOCAT; Figure 3.1a&b; Sutton et al. 2017), the ANN-NEP product also performs well (r^2 = 0.86; 133 months; not shown).

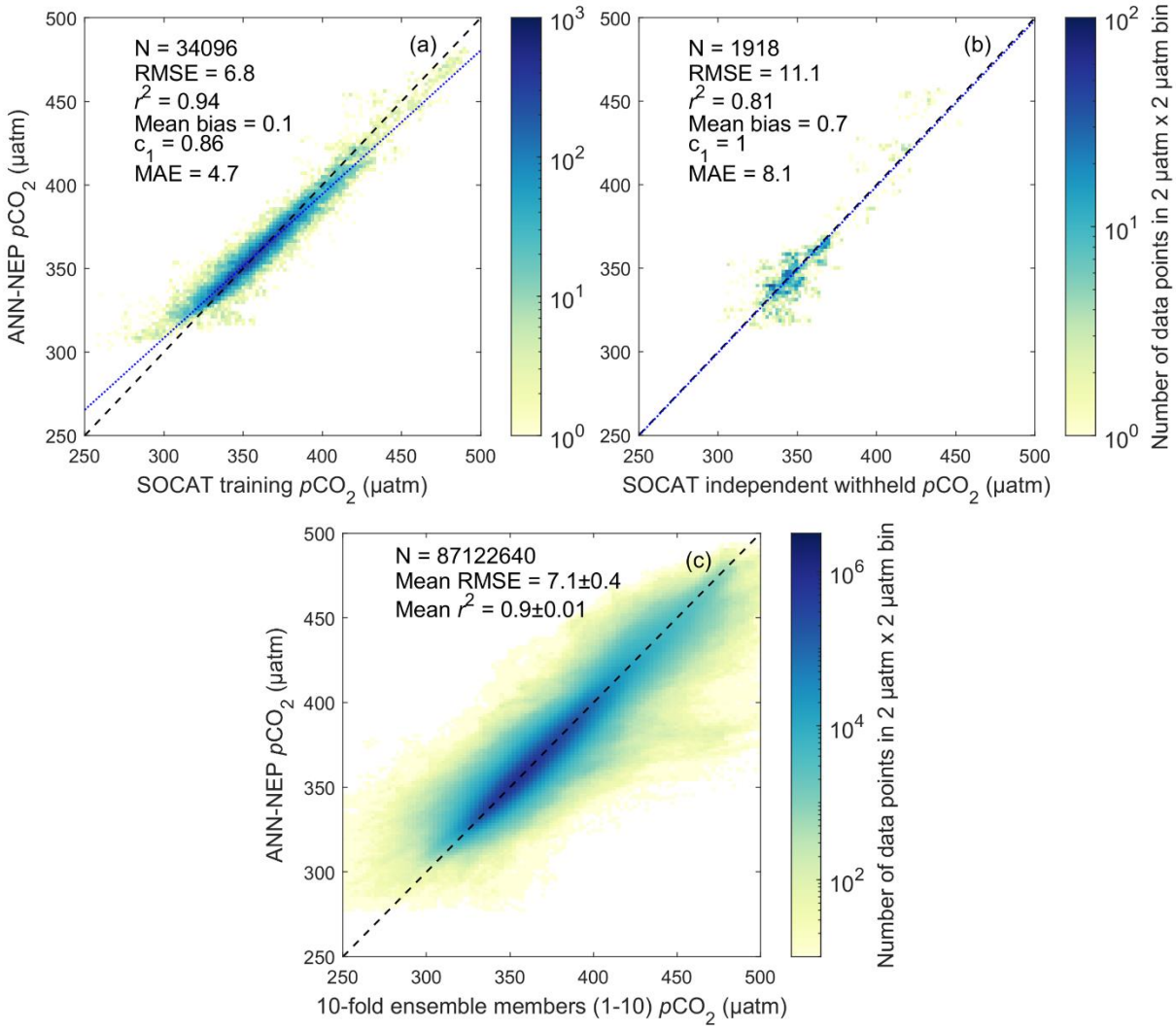

Figure 3.2 Regional high-resolution artificial neural network Northeast Pacific (ANN-NEP) ensemble mean pCO_2 against (a) training pCO_2 observation data, and (b) independent withheld pCO_2 observation data. Number of observations (N), root mean squared error (RMSE), coefficient of determination (r^2), mean absolute error (MAE), mean bias (calculated as the mean residual), and the slope of the linear regression (c_1). The observed linear relationship is represented by the dotted blue line. (c) ANN-NEP pCO_2 (ensemble mean) against individual ensemble member estimates. Total number of observations (N) across all 10-fold ensemble members (see Section 3.3.5). Across all panels data are binned into 2 µatm by 2 µatm bins. The dashed black line represents a perfect fit of slope (c_1) = 1 and intercept = 0. Colorbar shows data density on a log scale. Note the order of magnitude difference in the colorbar scale between panels.

The ANN ensemble model mean approach demonstrated improved performance metrics when compared to each individual ensemble member. The ensemble median was nearly equivalent to the ensemble mean (r^2 = 0.99; not shown). Overall, individual ensemble members showed little deviation (RMSE <8 μatm) from the ensemble mean (Figure 3.2c), with the ensemble mean still improving estimate robustness and reducing overtraining as evident in comparing the final ANN product to independently withheld data (Figure 3.2b) and the mean RMSE of individual ensemble members to independently withheld data (13±1 μatm; Figure B.4a). Each individual ensemble member also performed relatively well compared to the 10% subsample of corresponding 10-fold evaluation data (mean RMSE = 17±2 μatm; Figure B.4b). The mean standard deviation across all grid cells within the 10-fold ensemble is 2.2±1.3 μatm (mapped in Figure B.5).

3.4.2 Uncertainty calculations

Uncertainty in the ANN estimated pCO_2 product was calculated following Landschützer et al. (2018, 2014), Roobaert et al. (2019), and Keppler et al. (2020) (Eq. 3.2), where the overall pCO_2 product uncertainty (θ_{pCO2}) is calculated from the square root of the sum of the four squared errors: observational uncertainty (θ_{obs}), gridding uncertainty (θ_{grid}), ANN interpolation uncertainty (θ_{map}), and ANN run randomness uncertainty (θ_{run}).

$$\theta_{\mathrm{pCO2}} = \sqrt{\theta_{\mathrm{obs}}^2 + \theta_{\mathrm{grid}}^2 + \theta_{\mathrm{map}}^2 + \theta_{\mathrm{run}}^2}, \quad (3.2)$$

Observational uncertainty (θ_{obs} = 3.1 μatm) is the measurement uncertainty of pCO_2 in the field, evaluated as the average of the uncertainty assigned to each data point according to its SOCAT quality control (QC) flag (between 2-5 μatm). Gridding uncertainty (θ_{grid} = 1.5 μatm) is associated with gridding SOCAT observations into monthly 1/12°x1/12° bins, evaluated as the average standard deviation among pCO_2 values within each grid cell with at least 3 data points. ANN interpolation uncertainty (θ_{map} = 11.1 μatm) is uncertainty introduced by interpolating the pCO_2 observations using the SOM-FFN approach, evaluated as the RMSE from the ANN ensemble output compared to the independent withheld SOCAT data (Figure 3.2b). One limitation of our approach in assessing the uncertainty of the ANN interpolation method is that it is only applicable to grid cells where observations are available. Consequently, location-specific seasonal biases, especially in high latitudes with limited wintertime observations (Figure 3.1a&b), may not be fully captured or accounted for. The standard deviation of the ensemble (ensemble spread) gives an indication of how robust our estimate is from one run to the next using different 10-fold training data (Section 3.3.5; Keppler et al., 2020). ANN run randomness uncertainty (θ_{run} = 2.2 μatm)

comes from the mean standard deviation between 10-fold ensemble members (Section 3.3.5 & 3.4.1), which is less than the comparison of each member of the ensemble with the ensemble mean (Figure B.4; Figure B.2c).

Overall product uncertainty combining all four components according to Eq. (3.2) is 12 µatm, with the contribution of ANN interpolation uncertainty being the largest. Our product uncertainty is comparable to reported open ocean uncertainty values from global products (Landschützer et al., 2014), as well as a regional product in the California Current System (Sharp et al., 2022). Combining the reported uncertainty in the gas transfer velocity (Section 3.3.6) and the overall pCO_2 product uncertainty yields an average uncertainty of ±0.24 mol m^{-2} yr^{-1} in the air-sea gas flux, with the largest fraction of the error stemming from the uncertainty of the gas transfer velocity. The total uncertainty in the flux corresponds to roughly 20% of individual grid cell calculated flux values.

3.4.3 Improvement relative to a global product

The ANN-NEP pCO_2 product created here shows improved performance over the Landschützer et al. (2020b) global product at each timestep within the study area when compared to SOCAT data gridded at 1/12°x1/12° (Figure 3.3), illustrating the importance of regional high-resolution estimates in resolving fine scale variations. Across all evaluation metrics the global product does not perform as well in the region compared to SOCAT training data (RMSE = 14; r^2 = 0.74; mean bias = -2; c_0 = 0.68; MAE = 10; compared to Figure 3.2a). This improvement suggests a regional high-resolution product can narrow the range of variability in predictor data within the SOM clustering step and present pCO_2 observation data with greater correlation to the FFN. In the Landschützer et al. (2020b) global product, there is often only one SOM biogeochemical province covering the whole region, forcing non-linear relationships in the FFN to be built around greater variability in pCO_2 observation data from a wider range of geographic areas. The ANN-NEP regionally specific four SOM biogeochemical province grouping could alleviate this shortcoming in the FFN step. The improvement in our high-resolution product is particularly evident in the seasonal amplitude, where differences between ANN-NEP and Landschützer et al. (2020b) exceed the product uncertainty in 25% of grid cells (Figure B.6a). The largest seasonal amplitude differences occur in the north Alaskan Gyre region, and south of the North Pacific Current (Figure B.6a). The additional spatial resolution and temporal details in the regional high-resolution product provide key information to inform future observation programs including potential mooring locations. The value added in stepping to a high-resolution regional product proves particularly useful in resolving biogeochemical gradients within the subpolar Alaskan Gyre system in our study area (Section 3.5).

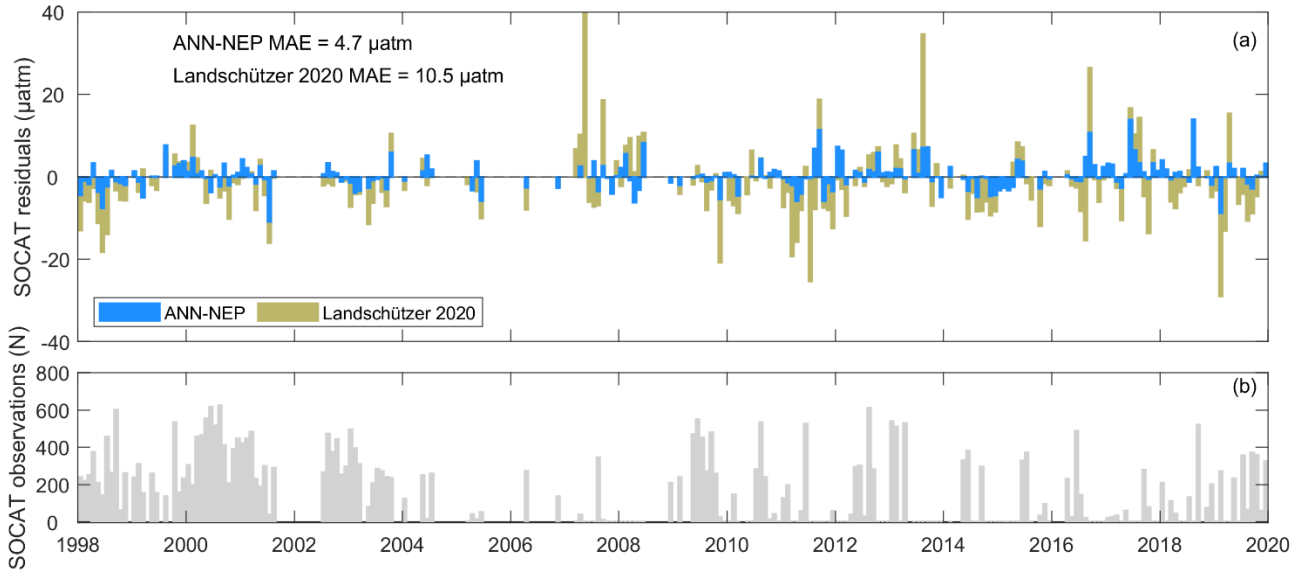

Figure 3.3 (a) Mean residuals over the full study area at each timestep of the ANN-NEP pCO_2 estimate in this study, the Landschützer et al. (2020b) product interpolated to the 1/12 °x1/12 ° grid of this study, compared to the gridded SOCAT data displaying the mean absolute error (MAE). (b) total number of gridded SOCAT observations across the study area at each timestep.

3.4.4 Performance at coarser resolutions

Stepping to a higher spatial resolution drastically decreases the ratio of gridded pCO_2 observations compared to the total number of grid cells (Figure 3.4f), nevertheless the ANN experiences minimal loss in performance across different spatial resolutions (Figure 3.4a-e). Globally, most open ocean observation-based pCO_2 products interpolate on a 1°x1° gridded resolution (Denvil-Sommer et al., 2019; Global Ocean Surface Carbon, E.U. Copernicus Marine Service Information MULTIOBS_GLO_BIO_CARBON_SURFACE_REP_015_008; Landschützer et al., 2020b; Zhong et al., 2022), with most coastal or regional products using a 1/4°x1/4° grid cell size (Hales et al., 2012; Laruelle et al., 2017; Nakaoka et al., 2013; Sharp et al., 2022), with a few regional products stepping to even higher resolutions (e.g., 1-km in Chen et al. 2016; 4-km in Parard et al. 2015, 2016; 11-km in Xu et al. 2019). To determine how the network preforms when producing a coarser resolution product, we tested the same configuration of our tuned 1/12°x1/12° ANN at various resolutions (Figure 3.4). The predictor variables and SOCAT pCO_2 observations were simply bin-averaged to coarser grid cell sizes (i.e., 1°, 1/2°, 1/4°, 1/8°).

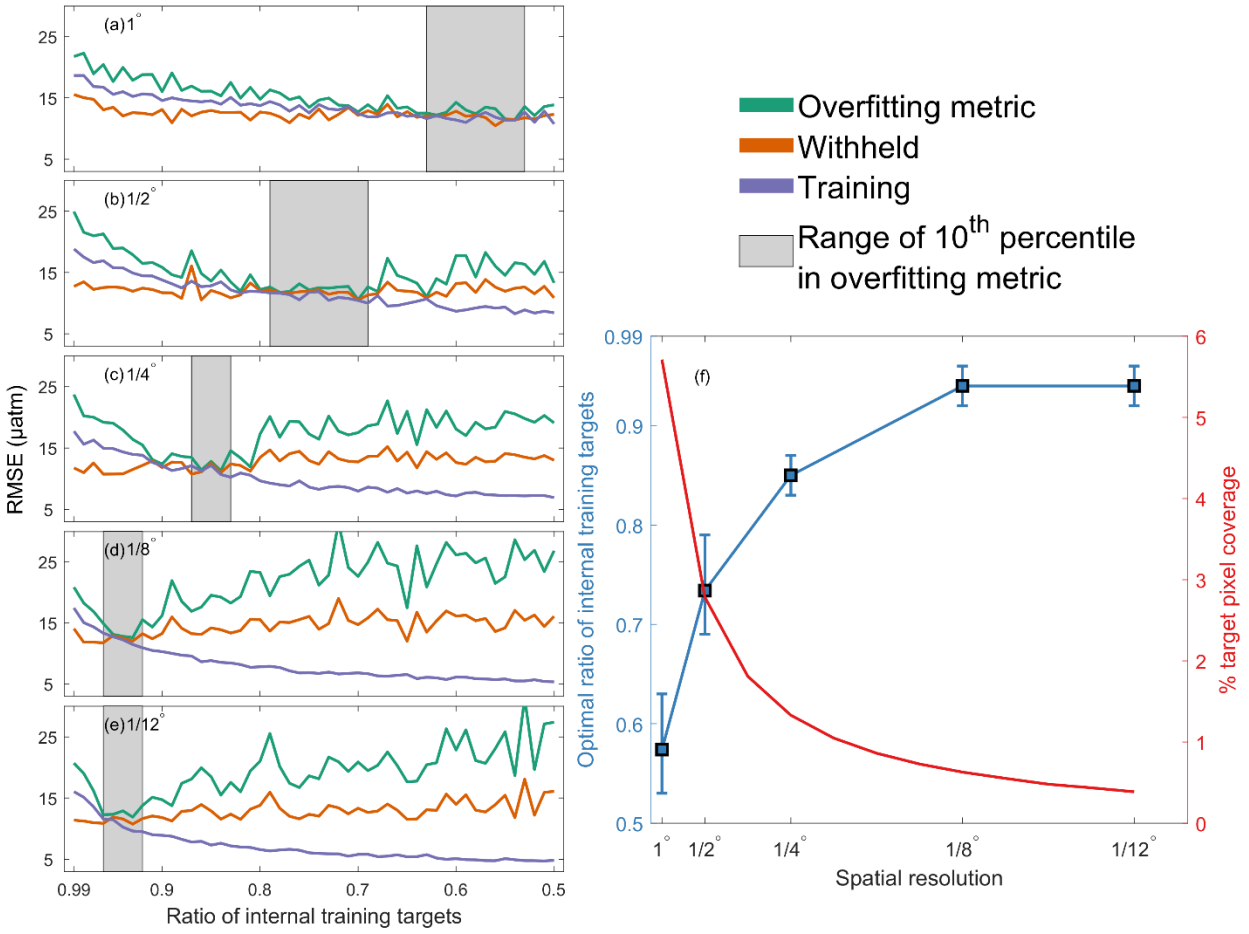

Figure 3.4 Varying spatial resolution: (a) 1°, (b) 1/2°, (c) 1/4°, (d) 1/8°, and (e) 1/12° ANN pCO_2 product performance evaluated by the mean RMSE (Section 3.3.3) of training data (blue line), independently withheld data (orange line), and an overfitting metric (green line) against internal data division ratios between the pCO_2 training data used by the ANN to train and internally evaluate. The ratios in grey show the range of the lower 10th percentile (5 of 50 runs) of overfitting metric values for each resolution. (f) At each spatial resolution, the lefthand y-axis shows the optimal internal data division ratio with error bars representing the lower 10th percentile of overfitting metric values (same as grey ranges in (a) to (e) with all resolutions converging around RMSE = 12.8±0.4 µatm). The righthand y-axis shows the percent of gridded pCO_2 observations (targets) compared to the total number of grid cells.

Using the same ANN configuration between the different resolutions (i.e., optimal SOM biogeochemical provinces, appropriate predictors, neuron number in the first hidden layer, etc., see Section 3.3.4), the most important parameter for reducing overfitting at each resolution becomes the internal data division ratio between the pCO_2 training data used by the ANN to train and internally evaluate (Figure 3.4). We tested a suite of data division ratios between 99% of data used to train / 1% used to internally evaluate to a 50/50 split at 1% intervals for each resolution (Figure 3.4). These tests were run without the 10-fold cross-evaluation ensemble approach. To quantify the optimal ratio at each resolution, we used an

overfitting metric (Eq. 3.3) equal to the larger of the training or independently withheld data RMSE, plus the absolute value of the difference between the two:

$$\text{Overfitting metric} = \max\left(\text{RMSE}_{training}, \text{RMSE}_{withheld}\right) + \left|\text{RMSE}_{training} - \text{RMSE}_{withheld}\right|, \quad (3.3)$$

Using an internal data division ratio optimized based on the overfitting metric, an ANN interpolated pCO_2 product with an uncertainty value of 12.5±0.4 μatm (see Section 3.4.2; Table B.2) is possible at each of the coarser resolutions (Figure 3.4a-e; Table B.2). For comparison, the reported uncertainty in a global product (Landschützer et al., 2014) ranges from 9 to 18 μatm. In regions with sufficient observational coverage (Figure 3.4f; Bakker et al., 2016), this finding creates a precedent for stepping to a higher resolution product with nearly no loss in performance, overcoming the overfitting concern with increased resolution (Rosenthal, 2016).

3.5 Air-sea CO_2 fluxes

With the estimated ANN pCO_2 product displaying a strong ability to accurately represent regional pCO_2 variability in the Northeast Pacific (Section 3.4), we calculate air-sea CO_2 fluxes in the region (Eq. 3.1). Long-term (1998-2019) mean pCO_2 and air-sea CO_2 fluxes display similar patterns (Figure 3.5). In the northwest of our study area, high pCO_2 and net CO_2 outgassing to the atmosphere correspond to the influence of the upwelling subpolar Alaskan Gyre system (Figure 3.5; Figure 3.1c). Lower pCO_2 values and stronger atmospheric CO_2 uptake occur in the North Pacific Current region (Figure 3.1c) to the south and along the eastern study area margin (Figure 3.5). The gradient of the gyre captured in the high-resolution estimate improves regional understanding with the largest differences between the Landschützer et al. (2020b) global product occurring in the north (basin-wide absolute difference 2-5%; Figure B.6a). ANN-NEP calculated fluxes compare well to air-sea CO_2 fluxes averaged across six unique, courser resolution, global observation-based pCO_2 products, each using five different wind speed products (r^2 = 0.81; Fay et al., 2021). However, our work suggests that the global product ensemble may underestimate the outgassing signal from the subpolar Alaskan Gyre (Figure 3.5b; Figure B.7). Higher resolution in the gyre gradient also provides regional context to carbon measurements made at the Ocean Station Papa mooring, often used to represent the Alaskan gyre (e.g., Jackson et al. 2009), which is actually situated approximately between the two regions, and along the Line P monitoring program.

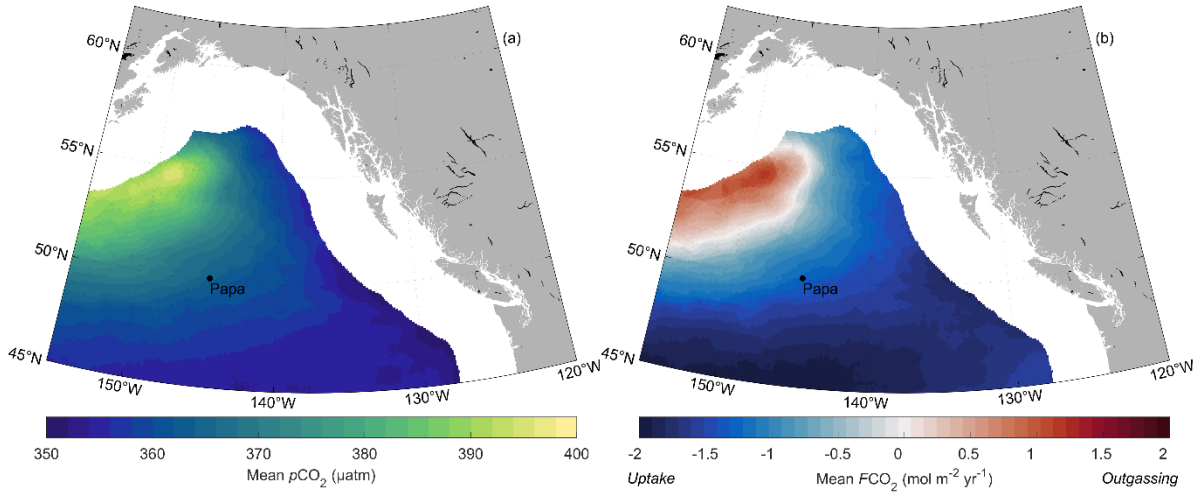

Figure 3.5 (a) Long-term (1998-2019) mean ANN-NEP pCO_2 and (b) air-sea CO_2 flux density in mol m^{-2} yr^{-1} for the open ocean Northeast Pacific. Negative (positive) flux values indicate CO_2 uptake (outgassing) by the ocean. Ocean Station Papa is shown for reference.

3.5.1 Seasonal variability

To determine seasonal cycle drivers, we decompose the climatological pCO_2 into a thermal and non-thermal component (Takahashi et al., 1993, 2002):

$$pCO_{2\,(T)} = pCO_{2\,(am)} \times \exp\left[0.0423\left(T_{(mm)} - T_{(am)}\right)\right], \tag{3.4}$$

$$pCO_{2\,(NT)} = pCO_{2\,(mm)} \times \exp\left[0.0423\left(T_{(am)} - T_{(mm)}\right)\right], \tag{3.5}$$

$$R_{(T\,NT^{-1})} = \frac{\max\left(pCO_{2\,(T)}\right) - \min\left(pCO_{2\,(T)}\right)}{\max\left(pCO_{2\,(NT)}\right) - \min\left(pCO_{2\,(NT)}\right)}, \tag{3.6}$$

Here the subscripts T and NT represent thermal and non-thermal effects, respectively, while subscripts am and mm represent annual mean and monthly mean values, respectively. Eq. 3.4 imposes the empirical temperature dependency on the annual mean pCO_2 value providing an estimate of seasonal temperature control (Sarmiento and Gruber, 2006; Takahashi et al., 2002). Eq. 3.5 removes the temperature dependency from the monthly mean pCO_2 values providing an estimate of the residual, non-thermal controls on pCO_2 including circulation, mixing, gas exchange, and biology. The ratio of the seasonal amplitudes of the two components (Eq. 3.6; $R_{(T\,NT^{-1})}$) can differentiate the dominant process, where a value greater (less) than one indicates that thermal (non-thermal) processes dominate.

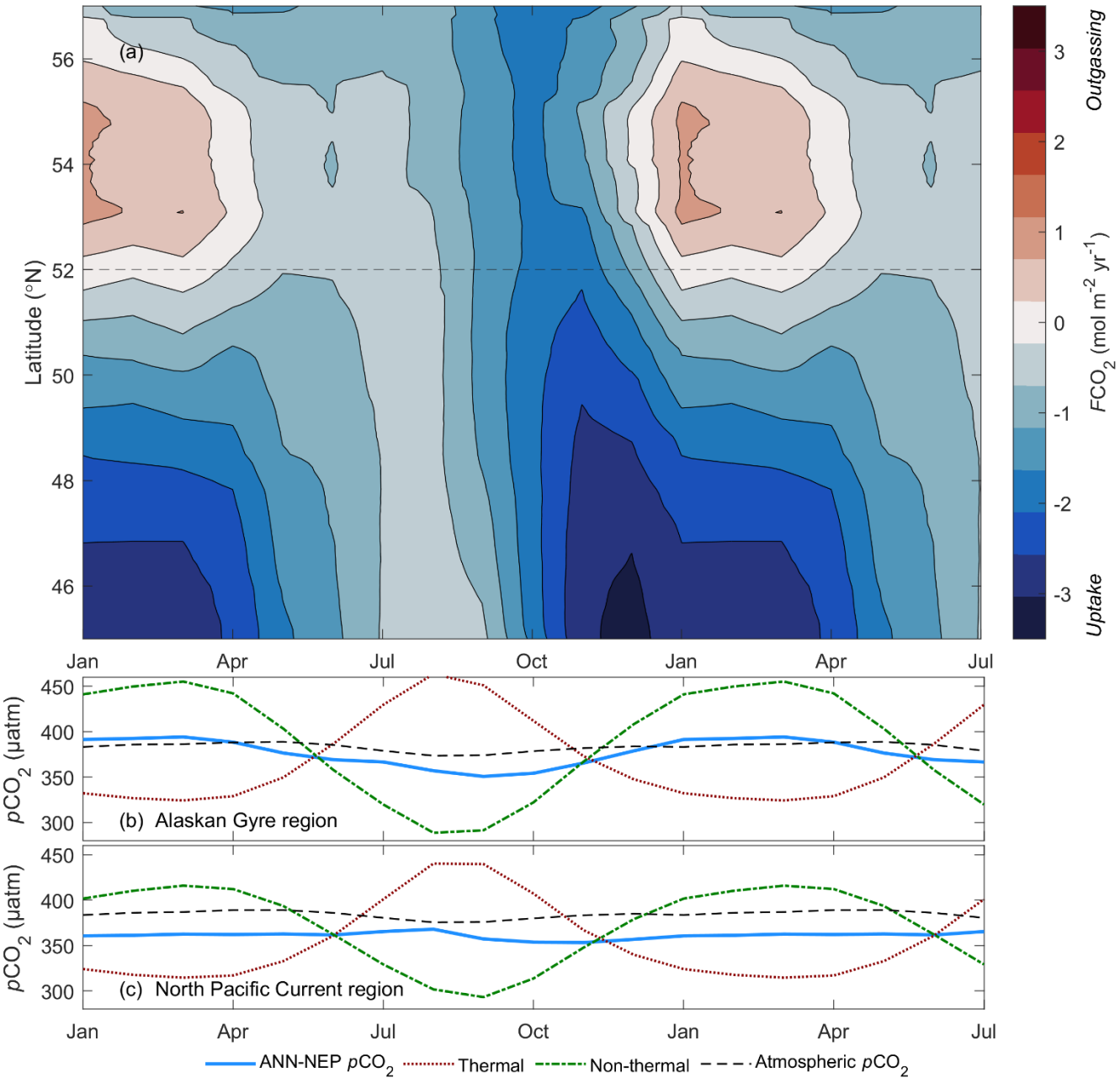

Figure 3.6 (a) Zonally averaged air-sea CO_2 flux from the ANN estimated pCO_2 product climatology along each 1/12 ° latitude band in the study area plotted against the climatological month along the x-axis (Hovmöller diagram). Negative (positive) flux values indicate CO_2 uptake (outgassing) by the ocean. The dashed grey line subdivides the Alaskan Gyre and North Pacific Current regions in the North/South with different seasonal drivers summarized in panels below. (b) Alaskan Gyre region (latitudes north of 52 °N) & (c) North Pacific Current region (latitudes south of 52 °N) area averaged monthly climatological pCO_2 (solid blue line), thermal component (i.e., changes due to temperature; Eq. 3.4; dotted red line), non-thermal component (i.e., changes due to circulation, mixing, gas exchange, and biology; Eq. 3.5; dot-dash green line), and atmospheric pCO_2 (dashed black line). The climatology is plotted over 19 months to emphasize the seasonal cycle.

Seasonally, the northern Alaskan Gyre region of our study area (latitudes north of 52°N; Figure 3.6a&b), flips from outgassing in the wintertime to uptake in the summer in the climatological air-sea CO_2 flux (Brady et al., 2019; Chierici et al., 2006; Palevsky et al., 2013). The change in the sign of the flux is driven by a 40 µatm difference between winter maxima and summer minima pCO_2 climatology values (Figure 3.6b). In the Landschützer et al. (2020a) climatology, this seasonal dipole in the Alaskan Gyre also exists displaying a 40 µatm seasonal pCO_2 range. Similar patterns exist in the Takahashi et al. (2014, 2009, 2002) climatologies as well (approximately 45-50 µatm). Increased wind stress curl drives stronger gyre circulation in the fall and winter, upwelling and entraining nutrient and CO_2-rich subsurface waters into the surface ocean, increasing the non-thermal pCO_2 component (Figure 3.6b), leading to outgassing (Figure 3.6a; Chierici et al. 2006). Through the spring and summer, biological drawdown, preconditioned by the upwelled, mixed, and entrained nutrients, decrease the surface ocean non-thermal pCO_2 component (Figure 3.6b; Harrison et al. 1999), enhancing uptake (Figure 3.6a). Although the seasonal amplitude of the temperature component is also large in the north, these non-thermal controls dominate ($R_{(T\,NT^{-1})}$ = 0.84).

In the south part of our study area, the North Pacific Current region (latitudes south of 52°N; Figure 3.6a&c) acts as a strong CO_2 sink through the winter transitioning to a weak sink through the summer. Whereas in the Alaskan Gyre region the seasonal cycle of pCO_2 is dominantly controlled by non-thermal drivers (Figure 3.6b), the North Pacific Current region experiences a near balance between opposing drivers (Figure 3.6c; $R_{(T\,NT^{-1})}$ = 1.02). In the North Pacific Current region, we see a much smaller seasonal amplitude in pCO_2 (15 µatm; Figure 3.6c), peaking in July with warming, falling to a minimum in October. The seasonal amplitude is dampened by the competing effect of temperature changes in solubility, and changes in dissolved inorganic carbon concentration through biological drawdown and changing mixed layer depth (Sutton et al., 2017; Wong et al., 2010). With minimal seasonal variation in seawater pCO_2, the seasonal change in atmospheric CO_2 uptake south of 52°N (Figure 3.6a) is dominantly driven by higher wind speed through the winter months (mean increase of 55% over summer climatological values).

3.5.2 Alaskan Gyre upwelling strength

On sub-decadal to decadal timescales, there is a strong correlation between air-sea CO_2 flux anomalies and SSH anomalies in the Alaskan Gyre region of our study area (r^2 = 0.93, p <0.01; Figure 3.7b&c; Figure B.8). In this subpolar gyre, prevailing winds cause upwelling driven by Ekman pumping (Gargett, 1991), but the strength varies. During 1998-2002 as well as 2006-2013, we observe strong winter and spring

outgassing in the Alaskan Gyre, with flux densities as high as 3.6 mol m^{-2} yr^{-1} in January 2000. In these same periods, anomalously low sea level pressure over the Alaskan Gyre led to anomalously strong wind stress curl which enhanced Ekman pumping and depressed SSH (Figure 3.7b; Mann and Lazier 2006; Hristova et al. 2019). The stronger upwelling brought CO_2-rich subsurface water to the surface (Lagerloef et al., 1998). Conversely, during the periods of anomalously high sea level pressures and positive SSH anomalies (2003-2005; 2014-2020; Figure 3.7c), there is less upwelling of CO_2-rich subsurface water to the surface, allowing primary productivity to draw down surface ocean CO_2 (McKinley et al., 2006), enhancing CO_2 uptake from the atmosphere (Figure 3.7b).

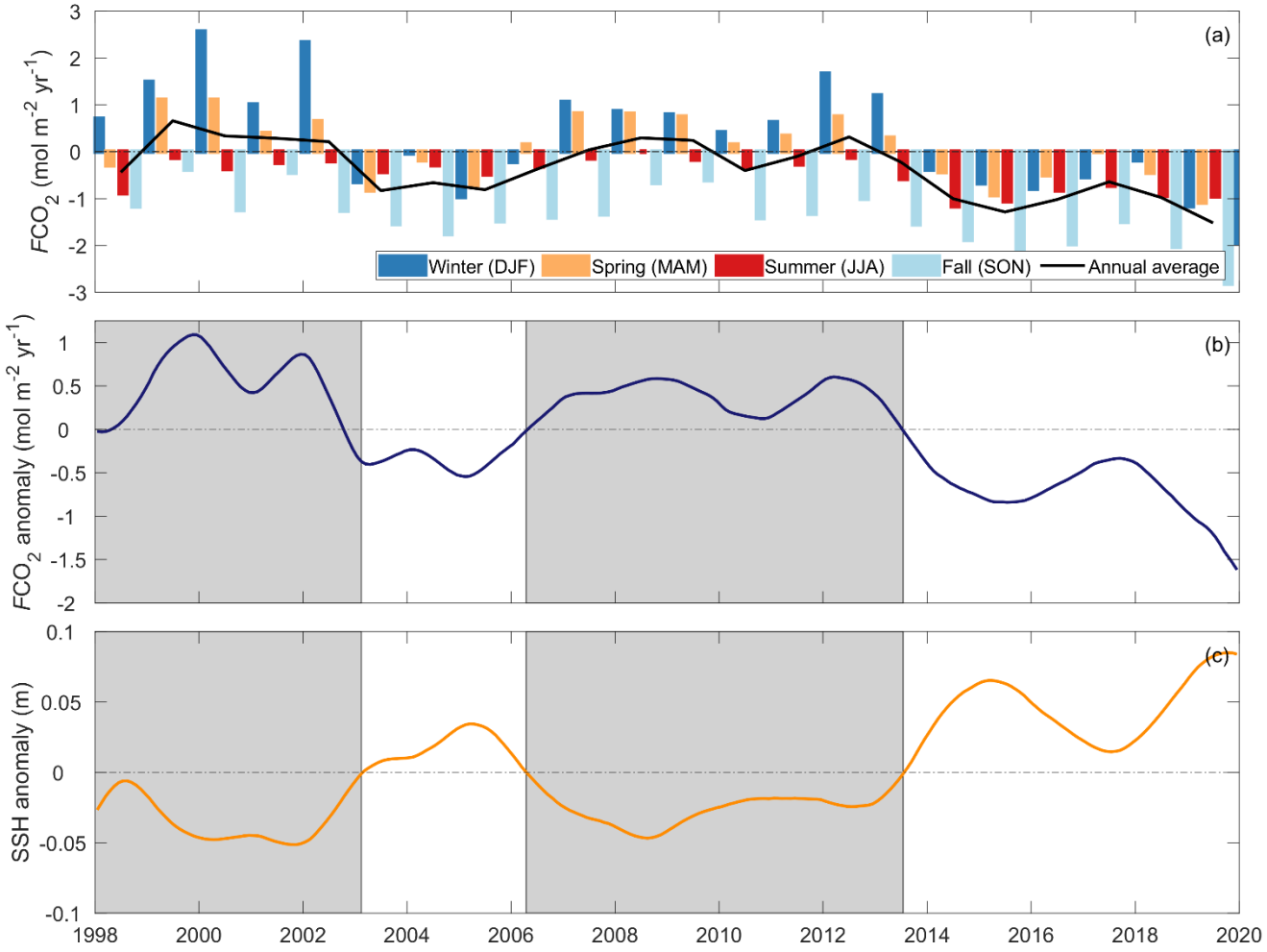

Figure 3.7 Alaskan Gyre region of our study area (latitudes north of 52 °N). (a) Air-sea CO_2 fluxes grouped by seasonal three-month bins along with the annual average (black line). (b) Air-sea CO_2 flux anomalies removing the seasonal cycle (Section 3.3.4) and applying a 12-month running mean. (c) Sea surface height (SSH) anomalies in the same region removing the seasonal cycle and applying a 12-month running mean. Grey boxes highlight periods of anomalously high Alaskan Gyre upwelling strength corresponding to negative SSH anomalies. Horizontal dashed lines mark zero in each panel. Seasonal groupings in (a) are winter (December, January, February), spring (March, April, May), summer (June, July, August), fall (September, October, November).

Our observation-based findings show strong carbon relationships with SSH in the Alaskan Gyre, with correlations between other climate indices being weaker. Over longer timescales, climate-driven regional ocean fluctuations have been shown to modulate the Alaskan Gyre surface water inorganic carbon system (Di Lorenzo et al., 2008; Hauri et al., 2021). The North Pacific Gyre Oscillation and the Pacific Decadal Oscillation indices have both been shown to strongly influence the physics, chemistry, and biology of Gulf of Alaska ecosystem (Di Lorenzo et al., 2008; Newman et al., 2016). Hauri et al. (2021) showed that the rate of ocean acidification in a hindcast model of the Gulf of Alaska was strongly related to the first empirical orthogonal function of SSH. We report the same relationship with SSH described in Hauri et al. (2021) as the dominant control of sub-decadal patterns on air-sea CO_2 fluxes from our observation-based pCO_2 product (Figure 3.7). Our estimates of the 12-month running mean air-sea CO_2 flux anomaly in the Alaskan Gyre region (Figure 3.7b) are more weakly correlated to the North Pacific Gyre Oscillation, Pacific Decadal Oscillation, and the El Niño-Southern Oscillation indices (r^2 = 0.63, 0.38, 0.22 respectively; p <0.01). This regional variation in SSH correlating with both observations and models lends strong evidence for variations in Alaskan Gyre upwelling strength explaining regional biogeochemistry on sub-decadal to decadal timescales. This relationship supports work showing that the SSH anomaly is an important climate index for the region (Cummins et al., 2005; Di Lorenzo et al., 2008). This finding also highlights the challenges of representing the regional seasonal cycle of the Northeast Pacific in a climatology within a reference period dominated by one mode of Alaskan Gyre upwelling strength (e.g., Takahashi et al., 2002, 2009, 2014).

3.5.3 Impact of interannual events

On shorter, interannual timescales, basin-wide variability in air-sea CO_2 flux is significantly influenced by the impact of extreme events, with the underlaying sub-decadal and decadal signal amplifying or dampening these impacts. During persistent marine heatwaves in the Northeast Pacific since 2013, we see strong atmospheric CO_2 uptake anomalies fueled by reduced winter mixing and increased surface density stratification (Figure 3.8; Bond et al., 2015). The strongest marine heatwave, known as “the Blob”, with sea surface temperature anomalies greater than 3°C or 4 standard deviations above normal (Freeland and Ross, 2019), persisted in the Northeast Pacific from late 2013 to the end of 2015 driven by an anomalous high-pressure atmospheric ridge (Bond et al., 2015; Di Lorenzo and Mantua, 2016). The ridge was associated with a significant decline in local wind speed, decreasing the mixing of deep, colder waters to the surface and raising sea surface temperatures (Bond et al., 2015; Scannell et al., 2020). The reduced winter mixed layer deepening and associated limiting of upwelled and entrained nutrient and

CO_2-rich subsurface waters to the surface has been linked to a relief of ocean acidification (i.e., anomalously high aragonite saturation states; Mogen et al. 2022). There has also been a reported increase in net primary production during "the Blob" in both in-situ and satellite records (Long et al., 2021; Peña et al., 2019; Yu et al., 2019). During "the Blob," we see strong negative air-sea CO_2 flux anomalies, particularly in the winter months (October to December 2014 and 2015), indicative of a 30% increase in uptake relative to climatological monthly means. The increased atmospheric CO_2 uptake is driven by reduced winter wind speeds (by approximately 7%) leading to limited winter mixed layer deepening, increased surface density stratification, while possibly being enhanced by the increase in net primary production (Figure 3.8b).

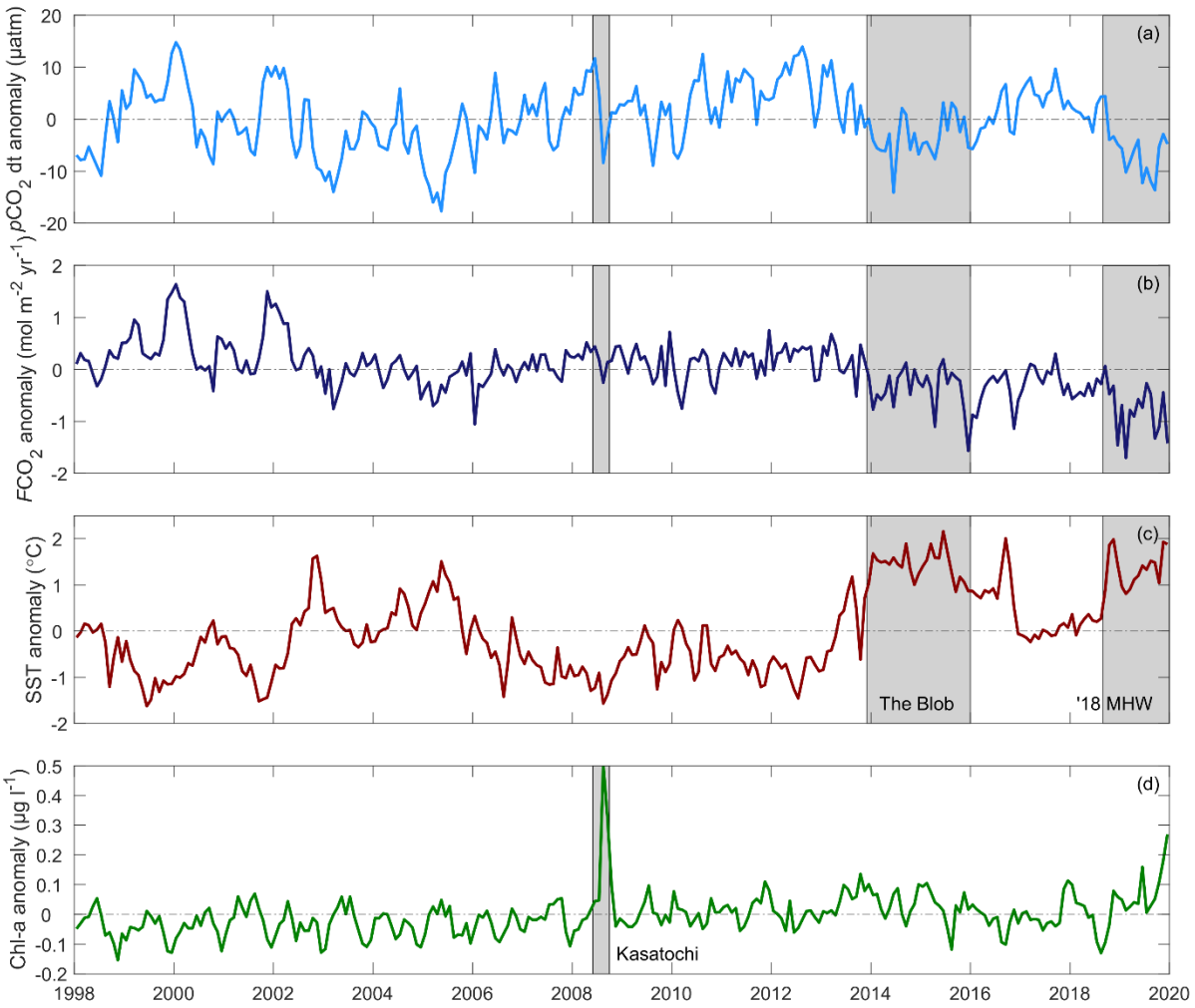

Figure 3.8 Full study area-averaged interannual variability in (a) pCO_2 anomaly removing the seasonal cycle (Section 3.3.4) and long-term trend (Section 3.5.4), (b) air-sea CO_2 flux anomaly, (c) sea surface temperature anomaly, and (d) chlorophyll-a anomaly all removing the seasonal cycle. Grey boxes highlight large interannual

events including "The Blob" marine heatwave 2014-2016, a second marine heatwave 2018-2020 ('18 MHW), and a 2008 ocean iron fertilization event following the Kasatochi volcanic eruption (Kasatochi). Horizontal dashed lines mark zero in each panel.

Through a second marine heatwave from mid-2018 to 2020 (Amaya et al., 2020; Chen et al., 2021; Scannell et al., 2020), we see a similar magnitude increase in atmospheric CO_2 uptake compared to "the Blob" event (Figure 3.8b). Through some of the largest SST anomalies (October to December 2018 and 2019) we observed large negative air-sea CO_2 flux anomalies indicating enhanced atmospheric uptake of 45% beyond corresponding climatological monthly means (Figure 3.8b), particularly in the Alaskan Gyre (Figure 3.7a&b). During this marine heatwave, a similar reduction in upper ocean mixing and limited wintertime entrainment due to reduced wind speed were observed (by approximately 9%; Amaya et al., 2020) and resultant reduced surface pCO_2 (Franco et al., 2021). Increased net primary production has also been reported (Long et al., 2021). An unusual near-surface freshwater anomaly in the Gulf of Alaska during 2019 contributed to the intensification of the marine heatwave by increasing the near-surface buoyancy and density stratification (Scannell et al., 2020).

Our result that marine heatwaves cause enhanced CO_2 uptake in the Northeast Pacific may not be applicable to a wider region. Mignot et al. (2022) described how the impact of marine heatwaves on air-sea CO_2 fluxes are the net result of two competing mechanisms: 1) increased sea surface temperatures reducing the solubility of CO_2, increasing pCO_2 and reducing CO_2 uptake, and 2) increased density stratification reducing vertical mixing and entrainment, decreasing surface dissolved inorganic carbon, and increasing CO_2 uptake. Their analysis finds that the temperature effect outweighs the advection effect during persistent marine heatwaves in the North Pacific subtropical gyre reducing CO_2 uptake by 29±11%, with the opposite true in the Tropical Pacific (Mignot et al., 2022). However, when looking at our more localized study area in the Northeast Pacific subpolar gyre, we find instead that the impact of reduced winter mixing (because of decreased winds and increased density stratification) tipped the balance toward enhanced atmospheric CO_2 uptake during these marine heatwaves, again advocating the need for high resolution local studies to better understand local climate change effects.

Through both "the Blob" and the 2019 marine heatwave, the Alaskan Gyre was in a period of weak upwelling (Figure 3.7c), leading to a decade-long negative pCO_2 anomaly (Figure 3.8a), in addition to the maximum observed ΔpCO_2 due to the diverging long-term trend with the atmosphere (Section 3.5.4). Unravelling the individual influence of these interconnected drivers (i.e., marine heatwaves, sub-decadal variability, and long-term trend) is not possible with this product but does prompt future inquiry in combination with regional models and emerging climate analysis tools (e.g., Chapman et al., 2022).

We do not observe a large change in atmospheric CO_2 uptake associated with the 2008 basin-wide ocean iron fertilization event. In August 2008, the eruption of Kasatochi volcano in the Aleutian Islands, Alaska, USA dispersed volcanic ash over an unusually large area of the subarctic Northeast Pacific fueling a massive phytoplankton bloom in the iron-limited region (Hamme et al., 2010; Langmann et al., 2010). Hamme et al. (2010) reported that enhanced biological uptake drew down pCO_2 by approximately 25 μatm at Ocean Station Papa. Basin-wide, we see a decrease of 20 μatm from July to August 2008 in the detrended, deseasonalized ANN pCO_2 following the eruption (Figure 3.8a) with a drawdown of 30 μatm at Ocean Station Papa. The neural network approach does display a tendency to slightly overestimate relatively low pCO_2 values (Figure 3.2a). Because this basin-wide enhanced primary production and surface ocean pCO_2 decrease lasted only two months, its impact on the air-sea CO_2 flux was limited (Figure 3.8b). The limited impact could be tied to weaker summer wind speeds and longer equilibration times (Jones et al., 2014). The eruption occurred during a period of enhanced Alaskan Gyre upwelling (Figure 3.7c), meaning the event was overlaid on top of an already sub-decade long positive pCO_2 anomaly (Figure 3.8a) perhaps dampening the event's impact. Unfortunately, the lack of direct pCO_2 measurements in SOCAT v2021 during this time prevents us from further investigating the underlaying causes.

3.5.4 Air-sea CO_2 flux trend

Overall, the Northeast Pacific Ocean CO_2 sink has become more negative (i.e., become a larger sink; Figure 3.9b) from 1998 to 2020 at a rate of -0.043±0.004 mol m^{-2} yr^{-2}. Looking at the start and end of the timeseries, the average flux from 1998 to 2002 appeared to be a small atmospheric CO_2 sink at -0.7 mol m^{-2} yr^{-1}, compared to the sink from 2016-2020 at -1.6 mol m^{-2} yr^{-1}. Regionally, we don't see a statistically significant trend in the satellite-based ocean surface wind speed data over this time (p >0.1; Mears et al. 2019). However, the timeseries endpoints are representative of different Alaskan Gyre upwelling modes (Figure 3.7c), with the timeseries starting in a sub-decade long positive pCO_2 anomaly and ending during a decade long negative pCO_2 anomaly. Decadal trends will be sensitive to the start and end point of the timeseries (e.g., Fay and McKinley 2013). We caution that our trend results may not be representative of longer time periods (i.e., from industrial onset).

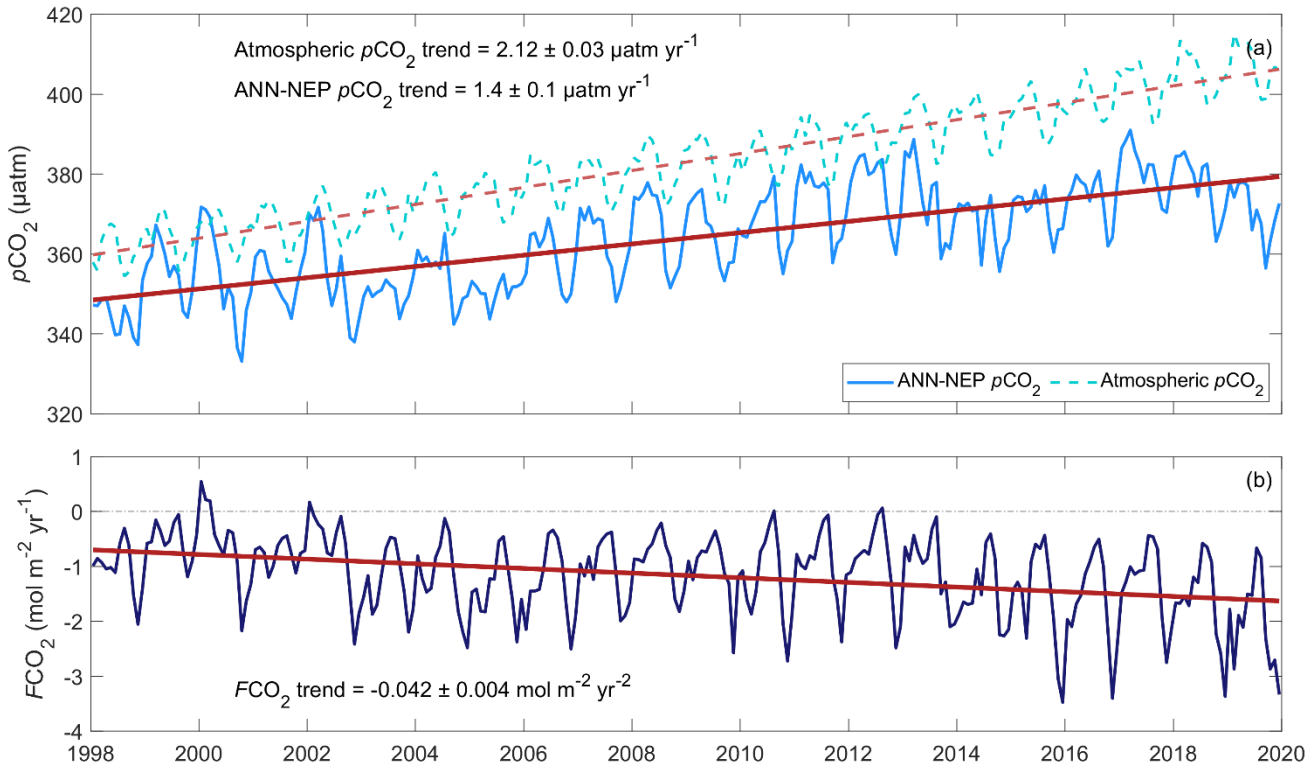

Figure 3.9 Full study area-averaged long-term trends in (a) ANN-NEP surface ocean pCO_2 (solid line) and atmospheric pCO_2 (dashed line), and (b) air-sea CO_2 flux density.

Taking the full study area deseasonalized (Section 3.3.4), area-averaged pCO_2, we calculated trends based on shorter time series within our data using different monthly timeseries start and end dates (Figure 3.10). Based on pCO_2 data timeseries ranges greater than 10 years (between 1998 and 2020), 87% of trends are less than the atmospheric trend with a mean of 1.59±0.27 µatm yr^{-1} (N = 9222 at a monthly timestep; Figure 3.10). In the remaining 13% of total timeseries start and end date combinations, there is a pronounced very steep trend exceeding the atmospheric rate of increase. Date combinations resulting in trends exceeding the atmospheric increase could be partly attributed to start and end dates coinciding with periods of weak and strong Alaskan Gyre upwelling, respectively. These upwelling modes induce negative and positive pCO_2 anomalies, which further amplify the observed trend. However, the Alaskan Gyre region makes up only about 25% of the total study area (region north of 52°N; Section 3.5.2), and trends in Figure 3.10 represent the ANN-NEP full spatial domain.

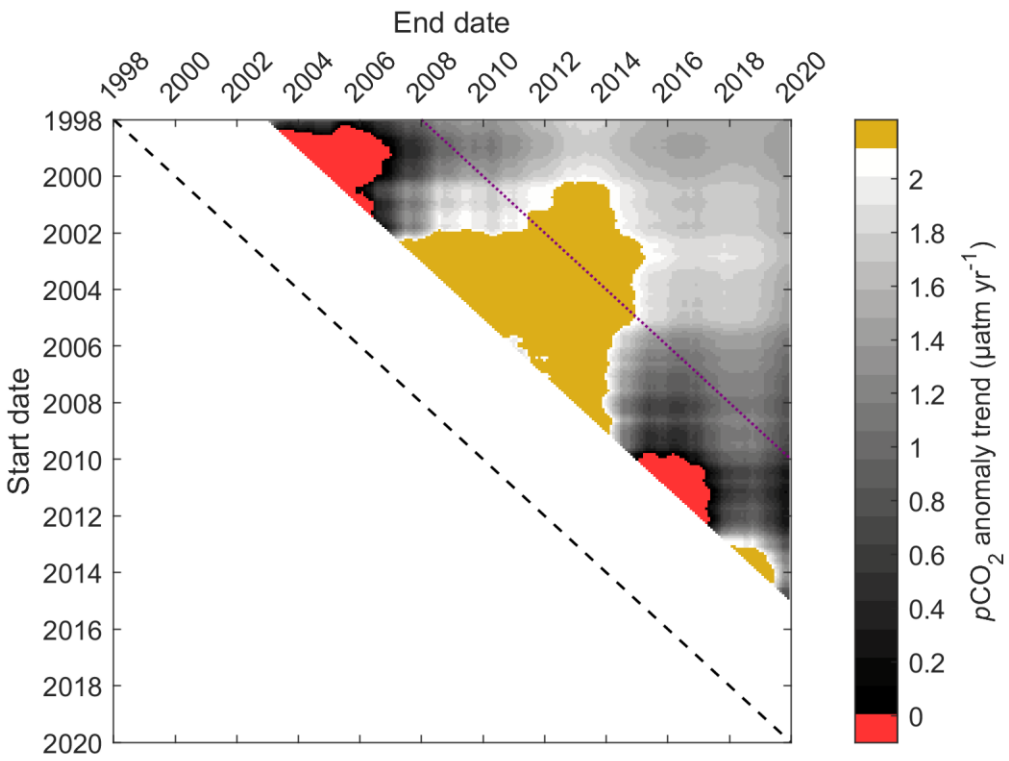

Figure 3.10 Full study area-averaged pCO_2 anomaly (removing the seasonal cycle; Section 3.3.4) linear trend calculated using different monthly timeseries start and end dates. Timeseries start from dates on the left and end on a date along the top. The dashed black line indicates equal start and end dates. Trend values are only shown for timeseries of at least a 5-year duration. Red values represent negative pCO_2 trends, gold values represent trends greater than the atmospheric rate of increase (2.12±0.01 µatm yr^{-1}). The purple dotted line indicates a 10-year timeseries duration.

The rate of change in the air-sea CO_2 flux over the study period is largely due to the increasing gradient with the atmosphere (Figure 3.9a). Over the full study area from 1998-2020, the ANN-NEP pCO_2 trend is 1.4±0.1 µatm yr^{-1}. The Landschützer et al. (2020b) global product trend in the region is similar at 1.5±0.1 µatm yr^{-1}. At Ocean Station Papa, the ANN-NEP pCO_2 trend is 1.5±0.1 µatm yr^{-1}, in agreement with the observed trend based on discrete samples collected 1–3 times per year (1.6±0.8 µatm yr^{-1} between 1990-2019; Franco et al. 2021). The ocean pCO_2 trend is not as rapid as the atmospheric increase of 2.12±0.03 µatm yr^{-1} over the same period (Figure 3.9a). Sutton et al. (2017) also reported a lag with the atmosphere at Ocean Station Papa with a ΔpCO_2 trend of -1.5±0.9 µatm yr^{-1} from the 2007-2014 mooring pCO_2 data. The ANN-NEP ΔpCO_2 trend at Ocean Station Papa is -0.67±0.05 µatm yr^{-1}.

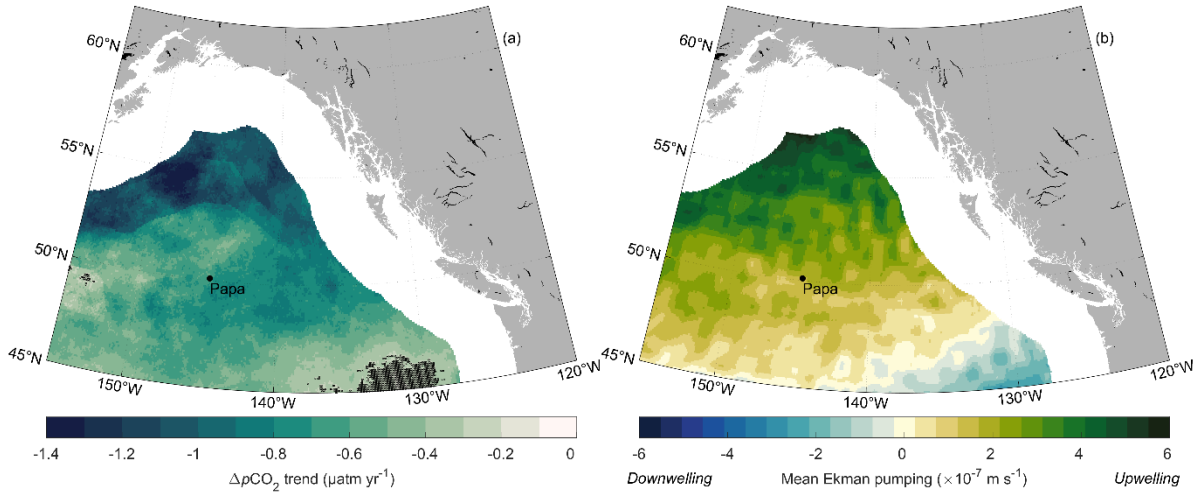

Figure 3.11 (a) Trend in ΔpCO_2 where more negative (darker) values indicate an increasing gradient with the atmosphere and a lag in the pCO_2 increase in the surface ocean. Black crosshatches show grid cells with an insignificant calculated trend (outside the 95% confidence level; $p \geq 0.05$). (b) Calculated average vertical velocity associated with Ekman pumping (calculated from zonal and meridional wind speed) where negative (blue) values indicate downwelling and positive (green) values indicate upwelling. Ocean Station Papa is shown for reference.

The observed lag in the increase in surface ocean pCO_2 with respect to atmospheric pCO_2, causing an increasing air-sea gradient (ΔpCO_2), may be attributed to interaction with subsurface water. We find a strong spatial correlation between the trend in ΔpCO_2 and the calculated average vertical velocity associated with Ekman pumping ($r^2 = 0.64$, $p < 0.01$; Figure 3.11b). Ekman pumping was calculated using the MATLAB Climate Toolbox ekman function (Greene et al., 2017, 2019; Kessler, 2002) from monthly, 1/4° spatial resolution Cross-Calibrated Multiplatform zonal and meridional ocean surface wind speeds (Mears et al., 2019) interpolated to 1/12°. Fay and McKinley (2013) describe regions impacted by upwelling from depth having shallower pCO_2 trends and greater divergence with the atmosphere based on models and observations. Dissolved inorganic carbon increases with depth, causing enhanced vertical mixing to increase surface ocean pCO_2 over the seasonal cycle (Sections 3.5.1 to 3.5.3). However, in the long-term, dissolved inorganic carbon is increasing most in surface waters, due to direct uptake of atmospheric CO_2, and least at depth. The supply to the surface of subsurface waters with low anthropogenic carbon causes a lag in the rate of increase in surface ocean pCO_2. The anthropogenic carbon signal in the intermediate to deep waters in this region are some of the smallest in the global ocean due to circulation patterns (Carter et al., 2019; Clement and Gruber, 2018; Gruber et al., 2019a; Sabine et al., 2004). Regions within our study area with greater connection between surface and deep waters, such as the center of the Alaskan Gyre in the north (Van Scoy et al., 1991), are experiencing the largest divergence with the atmosphere. With a joint increase in projected future wind speeds

(Wanninkhof and Triñanes, 2017; Young and Ribal, 2019; Zheng et al., 2016), and a growing ΔpCO_2, the region is likely to become a stronger net annual sink for atmospheric CO_2.

3.6 Conclusions

Using a high-resolution regional neural network approach, we represent pCO_2 measurement variability well in the Northeast Pacific Ocean. We interpolated sparse observations using non-linear relationships developed with a neural network approach based on predictor data from satellite and reanalysis products to create a continuous monthly pCO_2 estimate at 1/12°x1/12° spatial resolution. Using a cross-evaluation ensemble approach we were able to produce a robust pCO_2 product that represents regional variability with an uncertainty of 12 µatm. We found that stepping to a significantly higher spatial resolution, compared to typical open ocean observation-based pCO_2 products (1/4° or 1° spatial resolution), led to nearly no loss in performance despite a much lower ratio of gridded pCO_2 observations compared to the total number of grid cells. The most important parameter for reducing overfitting across regional pCO_2 products with different spatial resolutions was the internal division of training data. Higher resolution products require more direct training data and less data to internally evaluate, while still comparing to independent withheld data. This work shows that high-resolution, high-performance, observation-based neural network derived pCO_2 products can be developed when reducing the complexity of controlling processes by focusing on specific regions. However, chosen predictor variables need to be regionally specific considering "process focused" influences on the local carbon system. Our reported optimization of the internal data division ratio between network training and evaluation data indicates the importance of this choice when moving to a higher spatial resolution. Increased spatial resolution will be necessary to capture variability in regions strongly influenced by mesoscale processes, enabling resolution of oceanographic features such as eddies, upwelling regimes, and gyre system gradients.

We report pronounced variability in marine CO_2 uptake in the Northeast Pacific Ocean dominantly driven by the control of Alaskan Gyre upwelling and connectivity to subsurface waters. Overall, the open ocean Northeast Pacific acted as a net sink for atmospheric CO_2 from 1998 to 2020 with an average basin wide air-sea CO_2 flux of -1.2 mol m^{-2} yr^{-1} but with pronounced seasonality. In the northern Alaskan Gyre region, wintertime upwelling and entrainment lead to significant outgassing. In the southern North Pacific Current region, the seasonal flux cycle is largely driven by wind speed where the seasonal change in surface ocean pCO_2 remains small. Based on our product, upwelling strength of the Alaskan Gyre dominates air-sea CO_2 flux variability in that region on sub-decadal to decadal timescales. During

prolonged periods of enhanced gyre upwelling, we see strong winter outgassing driven by upwelled and entrained CO_2-rich subsurface waters. During periods of weak gyre upwelling, the northern part of our study area acts as a sink for atmospheric CO_2 year-round. During two recent marine heatwaves we see enhanced CO_2 uptake due to limited wintertime entrainment of subsurface waters resulting from weaker winds. However, we observed minimal impact on atmospheric CO_2 uptake following a 2008 volcanic eruption, with air-sea CO_2 flux anomalies linked to enhanced biological uptake via iron fertilization lasting only two months. The gradient between the Northeast Pacific surface ocean pCO_2 and atmospheric CO_2 is increasing, pushing the region towards becoming an enhanced sink for atmospheric CO_2. We see the largest increase in the gradient, and so potential for greater future uptake, at the center of the Alaskan Gyre where, through upwelling, there is a strong connection with subsurface waters low in anthropogenic CO_2.

The regional, high-resolution pCO_2 product created here could serve as a valuable baseline for regional models (e.g., Pilcher et al., 2018; Hauri et al., 2020). The pCO_2 product, and associated air-sea CO_2 flux estimates, offers continuous coverage in sparsely sampled regions informed by patterns in well sampled neighbouring waters. The product could be used to aid in model evaluation, use in data assimilation, constrain initial conditions, enhance carbon flux process understanding, and improve regional climate change projections.

Our analysis illustrates the complex interplay between factors driving air-sea CO_2 flux variability at varying temporal scales across the study domain and within broad subregions (Alaskan Gyre and North Pacific Current regions) allowing us to suggest what resources will be needed to make further advances. Improvement of estimated pCO_2 would benefit from an increase in the number of pCO_2 observations used for training. We recommend prioritizing additional measurements in the northern Alaskan Gyre region in future observational programs. Our estimated fluxes in the gyre are large (both uptake and outgassing), but observations are sparse, leading to the largest standard deviations between our cross-evaluation ensemble members (Figure B.4). The impact of sub-decadal to decadal variability on the trend in surface ocean pCO_2 and in regional atmospheric CO_2 uptake emphasises the importance of long duration timeseries sites and programs to capture the natural cycles of variability and accurately estimate change. Our findings and estimated pCO_2 product serve as environmental baselines, which could be used to inform future marine carbon dioxide removal in the Northeast Pacific at the basin and regional scale. However, use of our product at the individual grid cell level is not encouraged as errors likely remain high, whereas over broader regions these errors average away. Our study serves as an

important initial step in creating a complete carbon budget for the Northeast Pacific, with coastal, pelagic, and benthic carbon stocks and fluxes still to be resolved.

3.7 Data availability

All data used is publicly available. ANN-NEP pCO_2 and air-sea CO_2 flux fields are available through the National Center for Environmental Information (NCEI Accession 0277836; https://doi.org/10.25921/c1w8-6v02). pCO_2 data are from the Surface Ocean CO_2 Atlas (SOCAT) v2021 (available at https://www.socat.info/) as well as additional data from Fisheries and Oceans Canada February 2019 Line P cruise (available at https://www.waterproperties.ca/linep/). Sea surface temperature and chlorophyll-a are from the European Space Agency Climate Change Initiative (available at https://climate.esa.int/en/odp/#/dashboard). Sea surface salinity, sea surface height, and mixed layer depth are from Copernicus Marine Environment Monitoring Service (available at https://data.marine.copernicus.eu/product/GLOBAL_MULTIYEAR_PHY_001_030/description). Ocean surface wind data are from Cross-Calibrated Multiplatform version 2 Wind Vector Analysis Product (available at https://www.remss.com/measurements/ccmp/).

3.8 Acknowledgements

Ocean Station Papa mooring timeseries site, plus the Line P program are operated by the National Oceanic and Atmospheric Administration (NOAA) and Fisheries and Oceans Canada (DFO). Thanks to Marine Fourrier and one anonymous reviewer for their helpful comments improving the manuscript. Funding for this project was provided by the Natural Sciences and Engineering Research Council of Canada (NSERC) through the Advancing Climate Change Science in Canada program (grant# ACCPJ 536173-18) to RH. Funding from Fisheries and Oceans Canada's Aquatic Climate Change Adaptation Service Program to DI supported the analysis of recent underway pCO_2 measurements made by the Line-P program (grant# 96036). PD financial support also provided by a Natural Sciences and Engineering Research Council of Canada (NSERC) Doctoral Postgraduate Scholarship.

3.9 Author contributions

PD and PL developed the neural network code and created the product with help from RH, DI, NS, and MA. PD, RH, DI, and PL contributed to the interpretation and analysis of the results. All co-authors contributed to editing the manuscript. RH and DI supervised the project work. PC provided data and consultation. PD prepared the manuscript with contributions from all co-authors.

Chapter 4. High-resolution Neural Network Demonstrates Strong CO_2 Source-Sink Juxtaposition in the Coastal Zone

Key points

1. The coastal Northeast Pacific is a net sink for atmospheric CO_2 with increasing air-sea pCO_2 disequilibrium trends in most of the region.
2. Regional processes drive net annual air-sea CO_2 flux to be anticorrelated with air-sea CO_2 flux seasonal amplitude.
3. Estimated pCO_2 reproduces observed seasonal cycle phase and amplitude well along with broad spatial patterns of variability.

Plain language summary: The importance of the coastal ocean as a hub of exchange for carbon between terrestrial ecosystems, the open ocean, and the atmosphere is still unclear. In this study, we investigate how much carbon dioxide moves between the ocean and the atmosphere in the coastal Northeast Pacific. We use a mathematical technique (i.e., machine learning) to transform limited observational data to a high-resolution estimate of this exchange across the entire region. We found this method effectively captured the big picture patterns and seasonal changes in ocean carbon dioxide levels. We report that the coastal Northeast Pacific absorbs slightly more carbon dioxide than it releases, helping regulate atmospheric levels of this greenhouse gas. However, there are large differences regionally with some coastal zones absorbing substantial amounts of carbon dioxide and others releasing the gas, such as the nearshore. We report a trend of increasing ocean uptake over time, suggesting the region may play an increasingly important role in reducing atmospheric carbon dioxide levels. This study provides valuable baseline information for efforts to reduce carbon dioxide in the atmosphere through artificially enhancing ocean uptake in the region.

This work has been submitted to a scientific journal as: Duke, P. J., Hamme, R. C., Ianson, D., Landschützer, P., Swart, N. C., and Covert, P. A.: High-resolution Neural Network Demonstrates Strong CO_2 Source-Sink Juxtaposition in the Coastal Zone, Journal of Geophysical Research: Oceans, under review, submitted March 19, 2024, Manuscript ID: 2024JC021134.

4.1 Abstract

Coastal oceans may play an important role in regulating the concentration of carbon dioxide in the atmosphere. Quantification of carbon fluxes at this highly dynamic land-ocean interface will aid in monitoring, reporting, and verification for marine carbon dioxide removal. Here, we use a two-step neural network approach to generate basin-wide estimates from sparse observational data in the coastal

Northeast Pacific Ocean at an unprecedented spatial resolution of 1/12° with coverage in the nearshore (0 - 25 km offshore). We compiled partial pressure of carbon dioxide (pCO_2) observations as well as a range of predictor variables including satellite-based and physical oceanographic reanalysis products. With the predictor variables representing processes affecting pCO_2, we created non-linear relationships to interpolate observations from 1998-2019. Compared to *in situ* shipboard and mooring observations, our coastal pCO_2 product captures broad spatial patterns and seasonal cycle variability well. A sensitivity analysis identifies that the parameters responsible for the neural network's ability to capture regional pCO_2 variability agrees with mechanistic processes. Using wind speed and atmospheric CO_2, we calculated air-sea CO_2 fluxes. We report an anticorrelation between net annual air-sea CO_2 flux and air-sea CO_2 flux seasonal amplitude and suggest the relationship is driven by regional processes. We show the inclusion of nearshore net outgassing fluxes lowers the overall regional net flux. Overall, our results suggest that the region is a net sink (-0.7 mol m^{-2} yr^{-1}) for atmospheric CO_2 with trends indicating increasing oceanic uptake due to strong connectivity to subsurface waters.

4.2 Introduction

The global ocean takes up nearly a quarter of anthropogenic carbon dioxide (CO_2) emissions annually (Friedlingstein et al., 2023). It has been suggested coastal oceans contribute disproportionately to oceanic CO_2 uptake relative to global ocean by surface area (Bourgeois et al., 2016; Chau et al., 2022; Laruelle et al., 2014; Resplandy et al., 2024; Roobaert et al., 2019, 2024), but exhibit far greater heterogeneity in air-sea CO_2 fluxes (Liu et al., 2010) and may be changing at a different rate compared to the open ocean (Laruelle et al., 2018; Resplandy et al., 2024). Coastal oceans serve as an important hub of exchange, outgassing carbon delivered by terrestrial ecosystems to the ocean (Regnier et al., 2022), while facilitating transport between the coast and open ocean, and directly absorbing CO_2 from the atmosphere (Bauer et al., 2013; Chen and Borges, 2009; Mackenzie et al., 1998; Ward et al., 2020). However, the role of the coastal ocean in the global carbon budget is not well-constrained due to lack of observations relative to the complexity of highly localized variability (Chavez et al., 2007; Dai, 2021; Dai et al., 2022).

Gap filling approaches (i.e., methods to interpolate sparse observations) used to inform coastal ocean air-sea CO_2 flux estimates are often at coarse resolution and often operate in an opaque way. Interpolation techniques have been widely used to inform air-sea CO_2 flux estimates in the coastal ocean both regionally and globally (e.g., Chen et al., 2016; Hales et al., 2012; Laruelle et al., 2017; Parard et al., 2015, 2016; Roobaert et al., 2019, 2024; Sharp et al., 2022; Xu et al., 2019). These approaches extend

the temporal and spatial coverage of partial pressure of CO_2 in seawater (pCO_2) observations from community synthesis efforts (e.g., through the Surface Ocean CO_2 Atlas (SOCAT); Bakker et al., 2016) and can be used to calculate air-sea CO_2 fluxes using wind speed and atmospheric CO_2 (Wanninkhof, 2014). Historically, coastal ocean approaches have been adopted from their open ocean counterparts (Chau et al., 2022; Landschützer et al., 2020a), and thus most of these estimates have at best a monthly, 1/4°x1/4° latitude by longitude resolution, which is incapable of resolving smaller scale processes in coastal regions, especially nearshore, that experience high variability and short autocorrelation length scales (Jones et al., 2012). Interpolation techniques, which lack transparency, also rarely probe internal relationship dependency between variables.

Large heterogeneity in air-sea CO_2 fluxes exist in the coastal Northeast Pacific, with substantial expanses of the coast completely absent of observations (Benway et al., 2016). Large discrepancies exist between previous air-sea CO_2 flux estimates within this region, with disagreement over the net annual flux magnitude and direction (i.e., as a net sink or source for atmospheric CO_2; Duke et al., 2023b; Fennel et al., 2019). Air-sea CO_2 flux variability in the region is heavily impacted by coastal processes such as upwelling, river plumes, tidal mixing, and coastal currents (Evans et al., 2012, 2019; Evans and Mathis, 2013; Hales et al., 2005; Ianson et al., 2003; Nemcek et al., 2008). Upwelling along the Pacific eastern boundary shelf has contrasting impacts on the oceanic CO_2 sink reflected in complex interactions between biological carbon drawdown fueled by upwelled nutrient and carbon-rich waters (Hales et al., 2005; Messié and Chavez, 2015; Ribalet et al., 2010) and outgassing associated with the same subsurface waters brought to the surface (Chan et al., 2017; Christensen, 1994; Evans et al., 2011; Feely et al., 2008; Hales et al., 2005; Ianson and Allen, 2002). Closer to shore, within the Salish Sea, and along Alaska's Inside Passage, air-sea CO_2 fluxes into and out of the ocean are highly episodic and spatially heterogeneous (Evans et al., 2022; Jarníková et al., 2022b). Binning regional pCO_2 observations in three dimensions into monthly, 1/12°x1/12° grid cells over the period 1998–2019, reveals the data scarcity (Figure 4.1). Of the 6,030,816 spatial and temporal grid cells just 0.6% have an associated gridded pCO_2 value. Observations are concentrated along shipping lanes, have a summer bias, and increase in frequency during later years (Figure 4.1). No observations exist in vast areas of the coastal Gulf of Alaska and along extensive stretches of shoreline (Figure 4.1c).

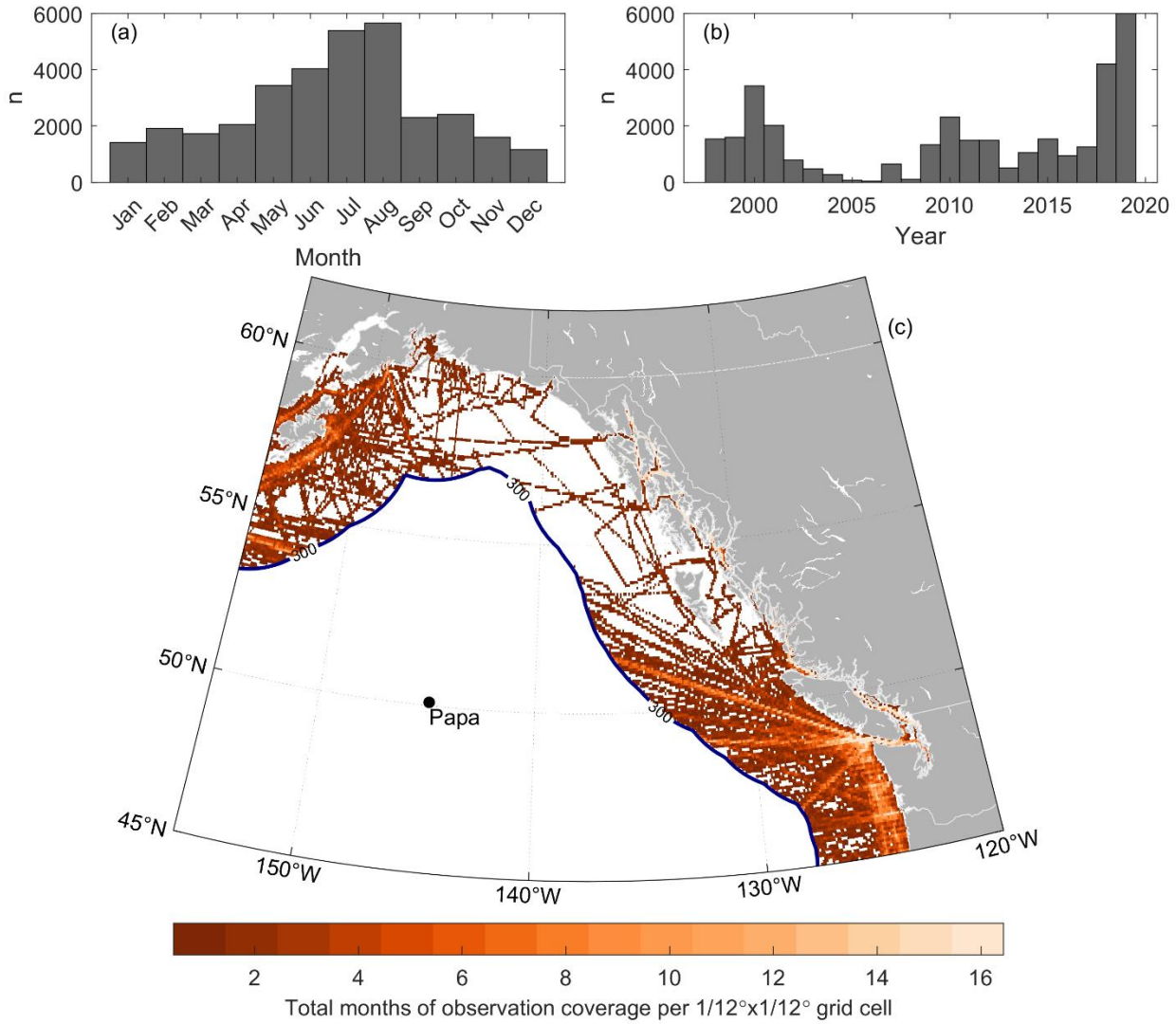

Figure 4.1 Number of grid cells (of 54782 total spatial grid cells) with coastal pCO_2 observation data (Section 4.3.1) in (a) months reveals a summer bias, and (b) years showing increased sampling closer to present. (c) Total number of months of observational coverage per grid cell displays better coverage along shipping routes. 300 km offshore line shown for coastal/open oceanic boundary used in this study (solid blue line labelled '300').

Here we investigate how well a high-resolution regional artificial neural network (ANN) approach can determine air-sea CO_2 fluxes in the coastal Northeast Pacific (NEPc). We build on an existing global setup (Landschützer et al., 2013) adopted previously in stepping to a higher spatial resolution in the open Northeast Pacific (Duke et al., 2023c). In Section 4.3, we describe the creation of a gridded pCO_2 data product for the coastal Northeast Pacific monthly from January 1998 to December 2019 at an unprecedented 1/12°x1/12° resolution to resolve coastal ocean processes. In Section 4.3, we demonstrate that our product robustly recreates gridded observation data, comparable to a less variable open ocean product. In Section 4.5, we directly compare our pCO_2 product with *in situ* shipboard and

mooring observations and detail potential capabilities and limitations in the continuous, gridded product. In Section 4.6, we examine the regional patterns of variability in the net annual air-sea CO_2 flux relative to the seasonal cycle and describe potential drivers through a spatial sensitivity analysis. We conclude by calculating surface ocean pCO_2 trends in the last decades.

4.3 Data and methods

We created a coastal pCO_2 data product spanning a geographic area between 45 - 62°N and 120 - 155°W, and within 6 to 300 km of shore building on the methods of Duke et al. (2023c). (ANN-NEPc; Duke et al., 2024). Briefly, our first step identified grid cells with similar environmental characteristics, provinces, using a self-organizing map approach (SOM) (Landschützer et al., 2013). In the second step, within each province, we used a feed-forward neural network (FFN) to create non-linear functional relationships between pCO_2 observations and independent predictor variables (Landschützer et al., 2013). Third, we applied these relationships to the predictor data to generate continuous monthly sea surface pCO_2 maps from 1998-2019 in the coastal Northeast Pacific (NEPc). ANN-NEPc fills the gap between open ocean (> 300 km offshore) pCO_2 (Duke et al., 2023c) to as close to the shoreline as reanalysis and satellite-based products reach. In stepping to 1/12° spatial resolution (approximately 9 km by 5 km, latitude by longitude), this work represents a three times increase in spatial resolution over previous 1/4° global and regional coastal ocean products with an overlapping domain (Landschützer et al., 2020a; Laruelle et al., 2017; Roobaert et al., 2024; Sharp et al., 2022), with extended coverage into the nearshore (defined here as 0 - 25 km offshore).

4.3.1 pCO_2 observations

ANN target pCO_2 data came from the Surface Ocean CO_2 Atlas (SOCAT) v2021 (Bakker et al., 2016), the Fisheries and Oceans Canada February 2019 Line P cruise (https://www.waterproperties.ca/linep/), a West Coast Ocean Acidification cruise from July and August 2010 (Evans et al., 2012), and La Perouse cruises from May 2007 and May 2010 (Tortell et al., 2012). Sea surface CO_2 fugacity (fCO_2) was converted to sea surface pCO_2 (Text C.1; Körtzinger, 1999). We did not correct *in situ* pCO_2 observations to sea surface mass boundary layer temperature, because following previous techniques introduced significant additional uncertainty in our coastal study area (Text C.2). pCO_2 observations were bin-averaged (monthly from 1998–2019, at 1/12°x1/12°), computing the mean and standard deviation within each grid cell.

4.3.2 Predictor data

Predictor data were chosen based on accessibility and ability to represent processes that mechanistically impact surface ocean pCO_2 (Table 4.1). Selected predictor variables primarily originate from satellite observations or reanalysis models (Table 4.1; Text C.3). Predictors differ slightly from a regional open ocean estimate (Duke et al., 2023c). Here, we used a high-resolution regional wind speed product and not reanalysis model derived mixed layer depth. Capturing greater variability in the coastal ocean required a high-resolution regional wind speed product over a low-resolution global product (Figure C.2). Latitude, longitude, and time were not used as predictor variables.

Table 4.1 Northeast Pacific Coastal Ocean artificial neural network predictor variables, and their corresponding source, original temporal and spatial resolutions, and processing steps used for this study.

Predictor variable	Source	Original resolution		Processing
		Temporal	Spatial	
Satellite-based product				
Sea surface temperature (SST)	SST_cci: Level 4 Analysis Climate Data Record, version 2.1	Daily	1/20°x1/20°	Averaged to monthly, aggregated to 1/12°x1/12°
Chlorophyll-*a* (Chl)	Ocean_Colour_cci: Version 5.0	Daily	1/24°x1/24°	Averaged to monthly, aggregated to 1/12°x1/12°, log10-transformed
Satellite and in-situ observation data assimilated reanalysis product				
Sea surface salinity (SSS)	Copernicus Marine Service GLOBAL_REANALYSIS_PHY_001_030	Monthly	1/12°x1/12°	None
Sea surface height (SSH)				None
Atmospheric-measurement-based interpolation product				
Atmospheric pCO_2	Landschützer et al. (2020b) - NCEI Accession 0160558	Monthly	1°x1°	Interpolated to 1/12°x1/12°
High-resolution regional forecast model				
Wind speed	Regional Deterministic Reforecast System (RDRS-v2.1)	Hourly	1/11°x1/11°	Averaged to monthly, interpolated to 1/12°x1/12°

4.3.3 Neural network construction

To reach the optimal ANN-NEPc architecture, we performed a series of tuning tests using the MATLAB Neural Network Toolbox, with sequential improvements impacting future tests (Duke et al., 2023c). The choice of three dynamic (i.e., changing shape at every timestep) self-organizing map (SOM) based clusters represented the lowest number for a typical clustering structure to emerge (Figure C.3a). All spatial grid cells within the study area belong to more than one SOM cluster at some point over 1998-2019 (Figure C.3b). SOM predictor variables (SST, SSS, SSH only; Table 4.1) were normalized to a mean of 0 and standard deviation of 1. The second FFN step used all six predictor variables in Table 4.1, in addition to each predictor variable anomaly (i.e., deseasonalized; calculated by subtracting the climatological monthly mean), bringing the total number of predictors to 12. Anomaly values were used to highlight interannual to decadal variability within our predictor data sets. The number of neurons within the first hidden layer varied by province with the optimal number of neurons determined in a pre-training run (Landschützer et al., 2013, 2014). The second hidden layer used seven static neurons, which slightly improved performance. To further decrease the risk of overfitting, we used a 10-fold cross-evaluation approach to create an ANN ensemble (Duke et al., 2023c; Li et al., 2019b, 2020) and a bootstrapping method (Landschützer et al., 2013). Observation cruises were randomly divided into 10 equal subsamples (10% each) using expocodes (i.e., unique identifiers corresponding to complete underway cruise tracks or mooring deployments) prior to gridding, leaving some data splits with more (or less) gridded pCO_2 targets (Section 4.3.1). We repeated the FFN training step 10 times, using each of the 10 subsamples once as the internally withheld evaluation dataset and the rest as the training dataset (with a separate independent data always withheld; Section 4.3.4). In each iteration, we trained the ANN for 10 rounds. The robustness and reliability of an ANN estimate has been shown to be significantly improved by combining a ANN ensemble (Duke et al., 2023c; Fourrier et al., 2020; Linares-Rodriguez et al., 2013; Sharkey, 1999). Here, we take the mean of the 10-fold estimates.

4.3.4 Evaluation

Comparisons of ANN output to training and independent withheld data were made throughout tuning tests. ANN-NEPc performance for each tuning test was evaluated using five statistical metrics: root mean squared error (RMSE), coefficient of determination (r^2), mean absolute error (MAE), mean bias (calculated as the mean residual), and the slope of the linear regression (c_1) between the ANN and the corresponding gridded pCO_2 observations. One subset of data was selected from the observation data using associated expocodes to be entirely withheld from the FFN training step. We tested 100 random

independent withheld data splits and selected the one with the best observational coverage over a wide range of seasons, years, and locations (Figure C.4). These independent withheld data represented approximately 4.5% of the total study area gridded pCO_2 data.

4.3.5 Sensitivity analysis

We used a perturbation approach to quantitatively assess the impact of each predictor variable on estimated pCO_2 (e.g., Broullón et al., 2018; Li et al., 2020; Sun et al., 2021). To diagnose how important different predictor variables were across the study area, a single set of non-linear relationships was used inside a single uniform SOM province. We then applied this single FFN to our continuous, gridded predictor dataset and to perturbed versions of that dataset. For each predictor variable separately, we introduced a perturbation increasing the value within each grid cell by 50% of the standard deviation within that grid cell ($X' = X + 0.5(std(X))$; N = 264 months per grid cell; de Oña & Garrido, 2014) and calculated the resulting predicted pCO_2. We then took the difference between the perturbed run and a baseline run using unperturbed predictor variables.

4.3.6 Computation of air-sea fluxes

Using our pCO_2 product, we calculated the air-sea CO_2 flux (FCO_2; mol m^{-2} yr^{-1}):

$$FCO_2 = K_0 k \Delta pCO_2 , \quad (4.1)$$

from the Henry's Law solubility constant (K_0; mmol m^{-3} μatm^{-1}) as a function of temperature and salinity (Table 4.1; Weiss, 1974), gas transfer velocity (k; m day^{-1}), and the gradient between pCO_2 in the surface ocean and the atmosphere (ΔpCO_2; μatm). Here, the gas transfer velocity is derived from Wanninkhof (2014), a function of wind-speed at 10 meter elevation (Table 4.1) and the temperature dependent Schmidt number specific to CO_2 (Wanninkhof, 2014). Negative flux values indicate CO_2 uptake by the ocean. We assume that the uncertainty in our air-sea CO_2 flux estimate results from a 20% uncertainty in k (Wanninkhof, 2014) and the overall product uncertainty in estimated pCO_2 (θpCO_2; Section 4.4.3 below). As the uncertainty of ΔpCO_2 is dominated by the uncertainty in estimated surface ocean pCO_2, we neglect the small contribution from atmospheric CO_2 (< 1 μatm; Landschützer et al., 2014). Wind speed product uncertainty which would contribute to a larger overall flux uncertainty is not included. This uncertainty is difficult to evaluate in the nearshore where the standard deviation of global wind speed products (Atamanchuk et al., 2020; Roobaert et al., 2018) is likely not an appropriate measure of the uncertainty of our specifically chosen coastal wind product (Figure C.2).

4.4 Network performance

4.4.1 Evaluation with respect to observational data

Comparing our estimated pCO_2 product with the gridded observations across both the training data (Figure 4.2a) and independent withheld data (Figure 4.2b) demonstrates fits with an MAE less than 30 μatm and RMSE of around 40 μatm. The mean bias is negligible over the full range (< 0.2 μatm, smaller than observational uncertainty; Section 4.4.3). 70% of the calculated residuals fall within the -20 to 20 μatm range, while 47% of the grid cells have absolute residuals < 10 μatm especially further offshore (Figure C.5). Despite seasonal and annual biases in observations (Figure 4.1; Section 4.3.1), our product performs similarly across different months and years (Table C.1). The ANN ensemble model mean demonstrated improved performance compared to each individual ensemble member (Figure C.6; Text C.4).

Larger bias exists at the upper and lower limits of the gridded pCO_2 observational range. Our product underestimates pCO_2 observations greater than the 90th percentile (> 412 μatm; mean bias = -28 μatm), and overestimates values less than the 10th percentile (< 306 μatm; mean bias = 13 μatm). The spatial structure of the residuals reflects this bias distribution (Figure C.5), with negative residuals in the strong mixing regions of the Salish Sea commonly characterized by high pCO_2 (Evans et al., 2012, 2019; Jarníková et al., 2022b), and positive residuals along the upwelling zone off the west coast of Oregon and Washington States characterized by low pCO_2 (Evans et al., 2011). Observation-based pCO_2 products commonly overestimate pCO_2 in highly biologically productive coastal upwelling regions (Chau et al., 2022; Hales et al., 2012; Roobaert et al., 2024; Sharp et al., 2022). Chlorophyll (Table 4.1) as a proxy for biological productivity in training may not fully represent biological control on pCO_2. Ford et al. (2022) showed that in regions with high biological activity and nutrients supplied from depth (i.e., South Atlantic upwelling mesoscale eddies) regional, algorithm-derived net community production estimates (Ford et al., 2021) improved ANN pCO_2 estimates. Creation of coastal, regionally specific net community production algorithms, and inclusion as a predictor variable, may help reduce bias of low pCO_2 values in our study area.

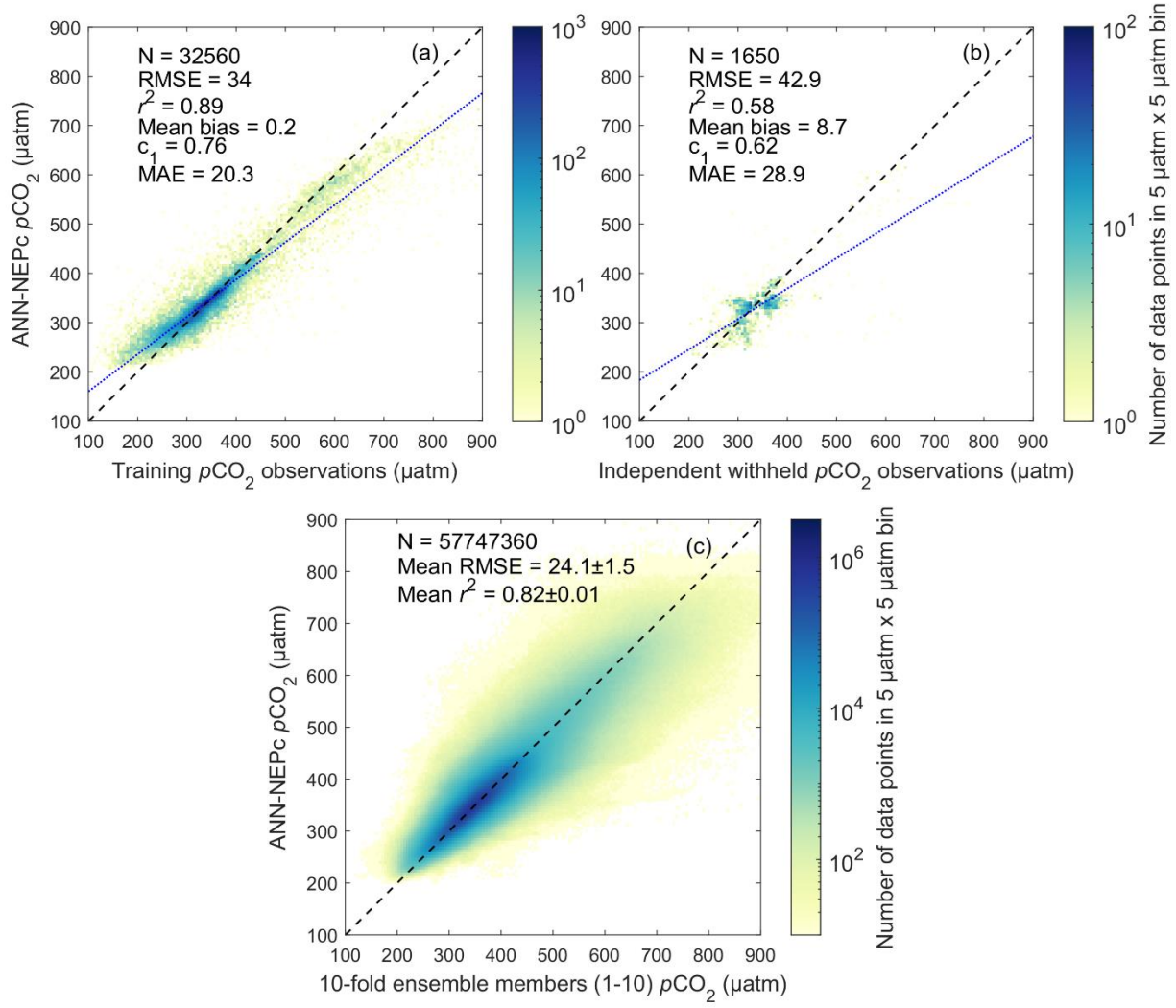

Figure 4.2 Our ensemble mean pCO_2 estimate (ANN-NEPc) against (a) observed pCO_2 training data, (b) observed pCO_2 independently withheld data, and (c) individual ensemble member estimates. Data are binned into 5 µatm by 5 µatm bins with data density shown in the colorbar on a log scale (note order of magnitude difference between panels). Dashed black line is the 1:1. Dotted blue line is the least squares best fit. Also shown are number of observations (N), root mean squared error (RMSE), coefficient of determination (r^2), mean absolute error (MAE), mean bias (calculated as the mean residual), and the slope of the linear regression (c_1).

In relative terms, our pCO_2 product performs nearly as well as an open ocean product, even nearshore (Table 4.2). Nearshore pCO_2 exhibits a much larger range of variability compared to the continental shelf and the offshore marine environment. Table 4.2 displays relative percent error (RPE) binned by distance offshore (d) calculated as:

$$\mathrm{RPE}_d = \mathrm{RMSE}_d / [\mathrm{prctile}_{95}(pCO_{2\,d}^{obs}) - \mathrm{prctile}_5(pCO_{2\,d}^{obs})] \times 100, \quad (4.2)$$

where RMSE_d is the RMSE from gridded observational data averaged over the distance bin, $\mathrm{prctile}_{95}(pCO_{2\,d}^{obs})$ is the 95th percentile observed pCO_2 in that distance bin and $\mathrm{prctile}_5(pCO_{2\,d}^{obs})$ is the

5th percentile. Compared to a high-performance, regional open ocean product (Table 4.2; Duke et al., 2023a), RMSE increases moving toward shore but so does the range in pCO_2 such that the RPE is constant within a factor of two.

Table 4.2 Error statistics for our ensemble mean pCO_2 estimate against all gridded observation data binned by distance offshore: number of observations (N) per bin, observed range of variability (range; difference between the 95th and 5th percentile), root mean squared error (RMSE), and relative percent error (RPE; Eq. 4.2).

Distance offshore (km)	N	Range (μatm)	RMSE (μatm)	RPE (%)
0-25 (nearshore)	8669	481	54	11
25-50	4763	215	33	16
50-100	5770	153	24	15
100-150	3324	114	16	14
150-200	3317	90	12	13
200-300	6501	106	10	10
High-resolution Northeast Pacific open ocean product (Duke et al., 2023a)				
> 300	34096	83	7	8

4.4.2 Comparison to other products

Our pCO_2 estimate agrees well with one other Northeast Pacific coastal ocean estimate but diverges from coarser resolution global products (Figure C.7). The regional Sharp et al. (2022) product within the northern extension of the California current system (45 °N to 59 °N, east of 140 °W) is nearly equivalent to our pCO_2 product within reported uncertainties (r^2 = 0.57; Figure C.7a). However, our product produces estimates closer to shore (Section 4.6.2 below). Compared to our product and *in situ* observations, a global coastal climatology (Landschützer et al., 2020a; Laruelle et al., 2017) and multiyear product (Roobaert et al., 2024) do not capture the same pCO_2 range (Figure C.7c&e; Figure C.8). For example, both global products underestimate winter pCO_2 values closer to shore in the coastal Gulf of Alaska region (> 52 °N & < 50 km offshore; area-averaged climatological winter pCO_2 of 300 μatm and 290 μatm respectively compared to 330 μatm in this study; Figure C.7d&f), highlighting the importance of finer resolution in coastal systems. This region also has the scarcest pCO_2 observations within our study area (0.37% coverage; Figure 4.1). Global SOM clusters commonly group the California current system with the Northwest European shelf and Sea of Japan (Laruelle et al., 2017; Roobaert et al., 2024). FFN non-linear relationships inside such clusters may not be suitable for regionally specific processes dominated by downwelling (Stabeno et al., 2004), glacial runoff (Pilcher et al., 2018; Siedlecki

et al., 2017), significant seasonal biological productivity (Coyle et al., 2012; Fiechter and Moore, 2009; Hermann et al., 2009), and the influence of the upwelling subpolar Alaskan Gyre (Duke et al., 2023c; Hauri et al., 2021). This finding supports the Sharp et al. (2022) recommendation of increasing the number of SOM clusters for observation-based coastal ocean pCO_2 estimates to capture more regionally specific non-linear relationships, cognizant of SOCAT observation data density.

4.4.3 Uncertainty estimate

Uncertainty in the ANN-NEPc estimated pCO_2 product was determined following Duke et al. (2023c). The overall pCO_2 product uncertainty (θpCO_2 = 50 µatm in our coastal product) is calculated from the square root of the sum of the four squared errors: observational uncertainty based on reported SOCAT QA/QC flags (θ_{obs} = 3.7 µatm), gridding uncertainty based on the average standard deviation from gridding observations into monthly 1/12°x1/12° bins (θ_{grid} = 22.4 µatm; with an increasing gradient shoreward), ANN interpolation uncertainty based on the RMSE comparing the ANN-NEPc estimated pCO_2 to independent withheld data (θ_{map} = 42.9 µatm; Section 4.4.1), and ANN run randomness uncertainty based on the mean standard deviation between 10-fold ensemble members (θ_{run} = 6.8 µatm; Figure C.9). ANN interpolation uncertainty is the largest contribution overall. Combining the reported uncertainty in the gas transfer velocity (Section 4.3.6) and the overall pCO_2 product uncertainty yields an average uncertainty of $\pm$0.2 mol-C m^{-2} yr^{-1} in the air-sea gas flux, neglecting the uncertainty in wind speed products (Section 4.3.6), across all grid cells, with the largest fraction of the error stemming from the uncertainty in the gas transfer velocity.

Our reported total uncertainty may appear high relative to other coastal pCO_2 products, but we include higher variability regions and more stringent error estimates. Other observation-based interpolated pCO_2 products in the coastal ocean report lower uncertainty values (RMSE values generally between 10 and 35 µatm in regional estimates detailed in S. Chen et al., (2016); 29 µatm globally in Roobaert et al. (2024); approximately 30 µatm in the California current system in Sharp et al. (2022); 55 µatm in the coastal subpolar Pacific in Chau et al. (2022)). However, most other estimates did not use independent withheld data to report total product uncertainty. Roobaert et al. (2024) point out their largest RMSE values are calculated along the Cascadia Shelf in our study area (62 µatm). Our pCO_2 product is also the only estimate that includes the nearshore, introducing higher variability (Table 4.2). Excluding the nearshore across all components of the uncertainty calculation yields an overall uncertainty of 40 µatm, more comparable to other coastal ocean estimates.

4.5 Comparison to high-resolution observations

Comparison to *in situ* observations shows that our ANN-NEPc estimated pCO_2 product resolves seasonal variability and broad spatial patterns well. Despite high spatial resolution, our design of a monthly timestep product means the ANN cannot reproduce short temporal (e.g., days) events. Predictor variable inaccuracy also contributes to pCO_2 estimate uncertainty, particularly in the nearshore where data assimilation into reanalysis models is limited (e.g., SSS and coastal limitations of Argo float array) and retrieval issues affect satellite estimates (e.g., SST and cloud masking, impact of aerosols, diurnal variability, uncertainty estimation, and validation). *In situ* measurements show that biogeochemical and hydrographic variability in our region occurs on spatial scales of less than 20 km (Nemcek et al., 2008), with spatial autocorrelation lengths increasing offshore (Murphy et al., 2001), and timescales of days to weeks (Evans et al., 2011, 2012, 2019; Fassbender et al., 2018b). Our product is constrained by initial binning of observations to 1/12°x1/12° (approximately 9 km by 5 km) and a monthly time step, as well as scarcity of observations used to train (Figure 4.1). Comparing it directly with *in situ* mooring and shipboard underway pCO_2 system measurements in the coastal zone provides insight into when and where the ANN is both capable and incapable of resolving variability.

Our pCO_2 estimate captures the observed seasonal cycle (phase and amplitude) at regional mooring time series sites well (Figure 4.3; full time series at all five regional mooring sites in Figure C.8). At NOAA's Gulf of Alaska Ocean Acidification (GAKOA) site south of Alaska's Kenai Peninsula, our product tends to overestimate seasonal summer minima and winter maxima values. However, it captures seasonal cycle timing well with a similar average seasonal amplitude even when not all mooring data are included in SOCATv2021 (this study = 144 µatm; GAKOA = 169 µatm; Figure 4.3b). At another NOAA Gulf of Alaska mooring site south of Kodiak Island, our estimate also captures the phase of the seasonal cycle well (r^2 = 0.89; N = 31 months; Figure C.8a).

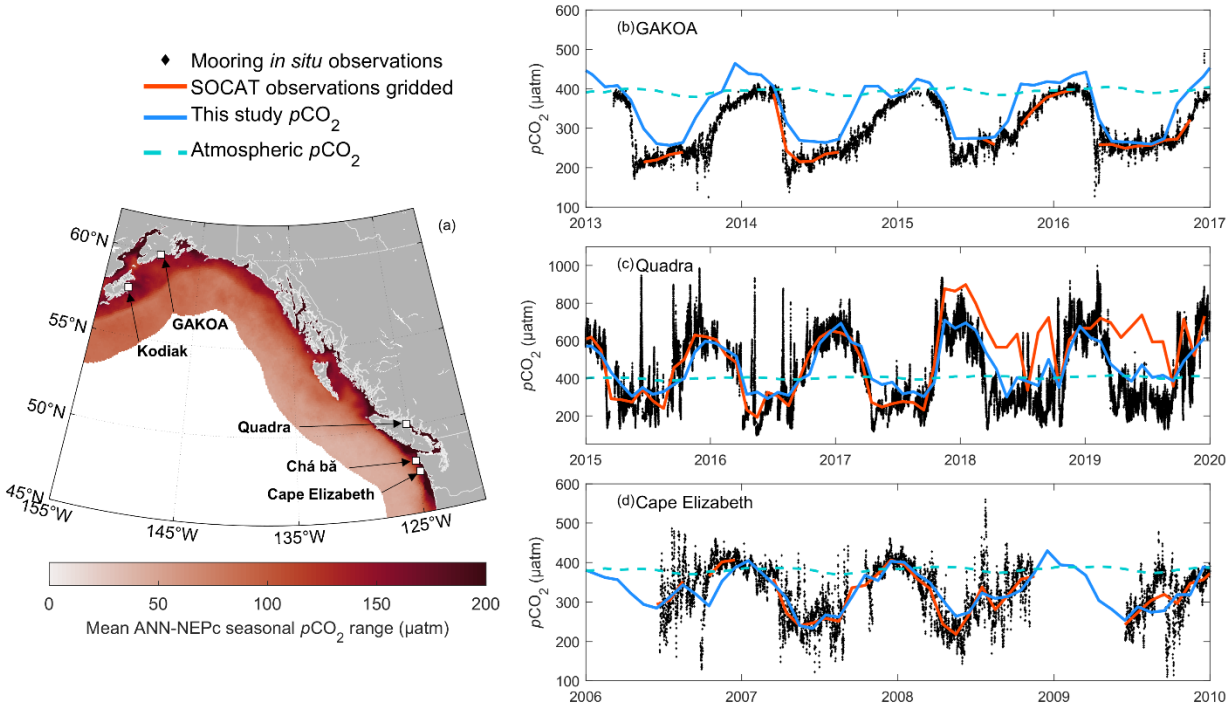

Figure 4.3 (a) Map of mean estimated surface ocean pCO_2 seasonal amplitude (1998-2019; range; annual maximum minus minimum) in µatm. Nearshore mooring time series at (b) Gulf of Alaska Ocean Acidification mooring (GAKOA), (c) Quadra, and (d) Cape Elizabeth mooring in situ pCO_2 data (black diamonds; not all included in SOCATv2021) plotted with co-located gridded SOCATv2021 (orange solid line), this study pCO_2 (blue solid line), and atmospheric pCO_2 (light blue dashed line). Kodiak and Chá bă and Roobaert et al. (2024) comparison time series in Figure C.8.

The ANN recreates the seasonal cycle well at Hakai Institute's Quadra Island Station, but its monthly timestep does not capture higher frequency variability (Figure 4.3c). In some instances, measured pCO_2 at the Quadra mooring increases over 500 µatm within three days (e.g., June 9-12, 2015), leading to a strong outgassing signal. The ANN monthly estimate does not capture such short events. Monthly binning impacts net annual air-sea CO_2 fluxes within a single grid cell (2015 mean annual flux from daily mooring pCO_2 and wind speed: 0.08 mol m^{-2} yr^{-1}; compared to this study: 0.26 mol m^{-2} yr^{-1}) but likely has a smaller impact when quantifying the larger regional flux. Near the end of the time series (late 2017 to 2020), the gridded SOCAT data deviates from the *in situ* mooring data due to inclusion of nearby shipboard data, yet our estimated pCO_2 continues to better represent the mooring seasonal cycle. When evaluating ANN performance (Section 4.4.3), this difference from the gridded observation data contributes to a higher measure of uncertainty, yet in situ representation is still preserved compared to the mooring data.

The ANN does capture part of the signal from somewhat longer (i.e., weeks) summer high pCO_2 events at NOAA's Cape Elizabeth mooring off the west coast of Washington State (Figure 4.3d). Horizontal advection of freshwater (July 2007) or upwelling events (> 500 µatm; July 2008; Evans et al., 2015) can cause high summer pCO_2 values. These extreme events impact bin-averaged training data, allowing the ANN to recover some of the short duration signal, albeit at a lower value. Our product reproduces both persistent, weeks long events < 35 km offshore, in line with the monthly averaged observations.

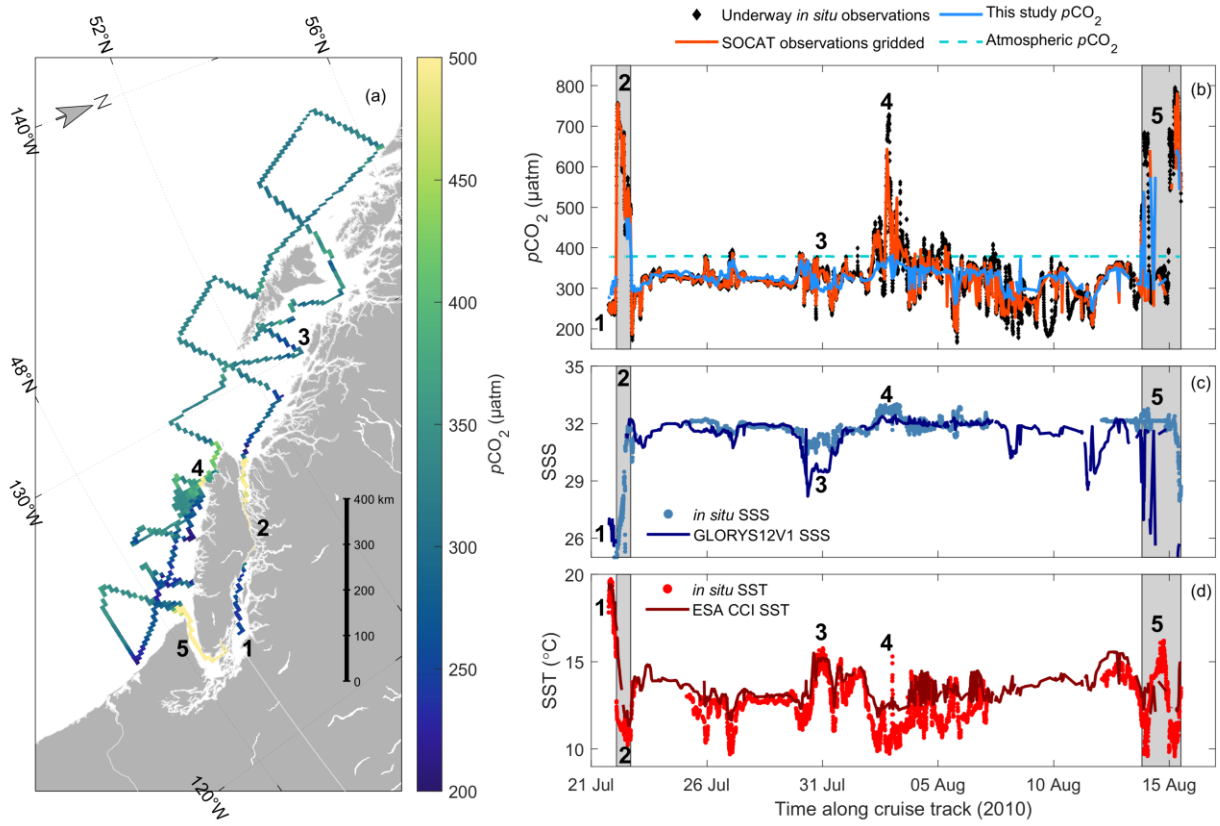

Figure 4.4 (a) pCO_2 along 2010 West Coast Ocean Acidification cruise track from 21 Jul 2010 to 15 Aug 2010 (Evans et al., 2012). Data is gridded into 1/12 ° by 1/12 ° bins. Events indicate (1) cruise start, (2) Johnstone Strait, (3) Hecate Strait, (4) intense upwelling plume near Brooks Peninsula, and (5) Juan de Fuca Strait respectively. Subplots against time along cruise track for (b) pCO_2 where underway in situ pCO_2 data (black diamonds) are plotted with co-located monthly gridded data (orange solid line), this study pCO_2 (blue solid line), and atmospheric pCO_2 (light blue dashed line). (c) Sea surface salinity (SSS) with underway in situ SSS (light blue dots) and co-located reanalysis SSS (dark blue solid line; used as a predictor variable). SSS values near cruise start as low as 15 in situ and 24 from reanalysis (not shown). (d) Sea surface temperature (SST) with underway in situ SST (red dots) and co-located satellite-based SST (dark red solid line; used as a predictor variable). Gray boxes highlight tidal mixing zones (e.g., Johnstone Strait, Juan de Fuca and Haro Straits and connecting waters).

Direct comparison to a cruise from July/August 2010 provides another example of our pCO_2 product's ability to capture broadscale patterns. The ANN estimate resolves undersaturated pCO_2 conditions in the Salish Sea at the start of the cruise well (point 1; Figure 4.4). Through Johnstone Strait (50.5 °N, 126.5

°W), a strong tidal mixing zone (Evans et al., 2022), lack of predictor data coverage prevents estimation of pCO_2 in those grid cells at all (point 2; Figure 4.4). The ANN captures the lower variability continental shelf and slope environment in Queen Charlotte Sound and around Haida Gwaii well (between points 2 and 4; Figure 4.4). Differences between estimated and observed pCO_2 exist in Hecate Strait (point 3; Figure 4.4) likely due to strong underestimation of SSS as a predictor in the reanalysis product (point 3; Figure 4.4c). Along the west coast of Vancouver Island, shipboard observations captured an upwelling event off Brooks Peninsula (50.14 °N, 127.78 °W; Asher et al., 2017), visible in decreased temperatures, elevated salinity, and very high *in situ* pCO_2 (point 4; Figure 4.4). The ANN does not replicate this short upwelling event (i.e., days; Asher et al., 2017). High pCO_2 driven by tidal mixing in the Juan de Fuca and Haro Straits are captured by the ANN (point 5; Figure 4.4; Jarníková, Olson, et al., 2022). An abundance of consistently high pCO_2 observations results in a strong reconstruction by the ANN in this region (Evans et al., 2012).

4.6 Air-sea CO_2 flux and pCO_2 drivers

Long-term (1998–2019) mean air-sea CO_2 fluxes display a pronounced juxtaposition between strong uptake and outgassing regions in the coastal Northeast Pacific Ocean (Figure 4.5c). Overall, air-sea CO_2 flux estimates from our product show this coastal zone acts as a net sink for atmospheric CO_2, drawing down 0.96±0.25 Tg C yr^{-1} with a mean flux of -0.7 mol m^{-2} yr^{-1} but high variability with a standard deviation of 1.4 mol m^{-2} yr^{-1}. Mean pCO_2 and air-sea CO_2 fluxes display similar patterns, with high pCO_2 nearshore leading to outgassing and low pCO_2 along the transition zone and continental shelf environments taking up atmospheric CO_2 (Figure 4.5a&c). Canada's West Coast exclusive economic zone has a CO_2 uptake of 0.61±0.11 Tg C yr^{-1}. Compared to the open ocean region of the Northeast Pacific (Duke et al., 2023c), the adjacent coastal ocean is a weaker sink for atmospheric CO_2 by area (40% weaker compared to -1.2 mol m^{-2} yr^{-1} in the open ocean), taking up 64% less CO_2 total within 40% less area (open ocean uptake = 2.63±0.53 Tg C yr^{-1}; open ocean surface area = 1.8×10^6 km^2; coastal ocean surface area = 1.1×10^6 km^2). Elevated pCO_2 and outgassing is also reported in the subpolar Alaskan Gyre system (Figure 4.5a&c), consistent with Duke et al. (2023c).

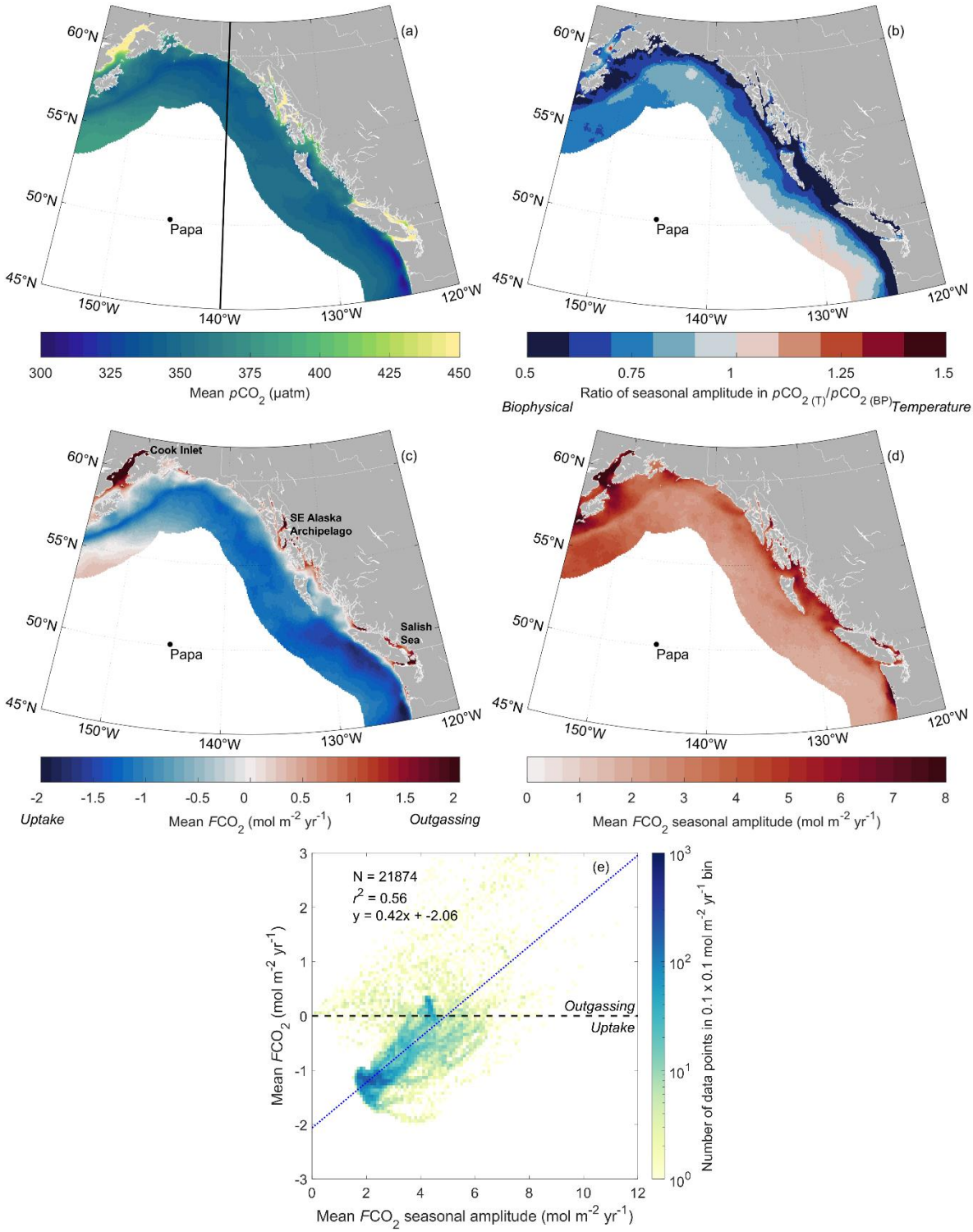

Figure 4.5 (a) Mean pCO_2 (1998-2019) in µatm. 140 °W meridian divide used in Section 4.6.2 analysis shown for reference. (b) Ratio of pCO_2 seasonal amplitude in thermal component (i.e., changes due to temperature; $pCO_{2\,(T)}$) and biophysical component (i.e., changes due to circulation, mixing, gas exchange, and biology; $pCO_{2\,(BP)}$). (c) Mean air–sea CO_2 flux (1998-2019) in mol m^{-2} yr^{-1}. Negative flux values indicate CO_2 uptake by the ocean. (d) Mean air-sea CO_2 flux seasonal amplitude (range; annual maximum minus minimum) in mol m^{-2} yr^{-1}. (e) Mean air-sea CO_2

flux vs. mean air-sea CO_2 flux seasonal amplitude (grid cell by grid cell). Dotted blue line is the least squares best fit. Dashed black line separates values of outgassing (positive) from uptake (negative).

4.6.1 Regional patterns

Spatially, the study area can be divided into four distinct regions based on air-sea CO_2 flux patterns in our product. The net annual air-sea CO_2 flux is anti-correlated with the mean air-sea CO_2 flux seasonal amplitude ($r^2 = 0.56$; $p < 0.01$; Figure 4.5e). We identify four regions that drive this pattern from most offshore to inshore: the transitional zone connecting the open ocean and the coast is a net sink with a small seasonal cycle, the Cascadia Shelf where the net sink is even stronger but the seasonal cycle remains low, nearshore regions with large seasonal cycles, and semi-enclosed estuaries with strong outgassing. To further disentangle driving processes between these four regions we decompose the estimated pCO_2 into a thermal ($pCO_{2\,(T)}$) and biophysical ($pCO_{2\,(BP)}$) component (Text C.5; Takahashi et al., 1993, 2002). We then take the ratio ($R_{T\,BP}^{-1}$) of the seasonal amplitude (climatological maximum minus minimum) of the two components ($pCO_{2\,(T)}/pCO_{2\,(BP)}$; Figure 4.5b), where biophysical processes dominate if $R_{T\,BP}^{-1}$ is less than one and vice versa.

Much of the offshore transitional zone (medium blue colours in Figure 4.5c) acts as a sink for atmospheric CO_2 year-round where thermal and biophysical pCO_2 components are nearly balanced. Low air-sea CO_2 flux seasonal amplitudes in the transitional zone (> 50 km offshore; excluding the subpolar Alaska Gyre) correspond to net annual atmospheric CO_2 uptake. In the southeast of the study area (Figure 4.5b), the North Pacific Current region experiences a relative balance of opposing thermal and biophysical pCO_2 components seasonally ($R_{T\,NT}^{-1}$ approximately = 1; Duke et al., 2023c; Sutton et al., 2017; Takahashi et al., 2006; Wong et al., 2010). Along most of the transitional zone where $R_{T\,NT}^{-1}$ is closer to one (Figure 4.5b), we also report low pCO_2 seasonal amplitudes (Figure 3a) allowing for continuous pCO_2 undersaturation with respect to the atmosphere and continuous annual uptake with low air-sea CO_2 flux seasonal amplitudes (Figure C.12; Figure 4.5d). Advection of low pCO_2 (Duke et al., 2023c; Takahashi et al., 2006) water by the North Pacific Current from the open ocean toward the coast causes overall pCO_2 undersaturation in this region (Reed and Schumacher, 1986; Thomson, 1981; Weingartner et al., 2002). The low pCO_2 amplitudes are maintained by the effect of temperature on pCO_2 (increasing during warming and decreasing during cooling) dampening changes due to spring phytoplankton blooms (drawing down pCO_2) and winter surface mixed layer deepening (increasing pCO_2).

The most prominent CO_2 sink region is found along the Cascadia Shelf, inshore of the transitional zone, with a mean flux of -1.5 mol m^{-2} yr^{-1} (darkest blue colours in Figure 4.5c). Along the continental shelf and within much of the nearshore, biophysical processes (e.g., coastal upwelling, seasonal biological drawdown, mixing) dominate the seasonal cycle of pCO_2 with $R_{T\,NT}^{-1}$ values < 1. Summer upwelling fuels primary productivity causing surface pCO_2 drawdown as waters are advected offshore (Hales et al., 2005; Teeter et al., 2018; Ware and Thomson, 2005). Winter downwelling drives onshore transport of low pCO_2 offshore waters and limits subsurface waters, with elevated respiratory CO_2, from mixing to the surface (i.e., coastal nutrient trap; Ianson et al., 2009; F. A. Whitney et al., 2005; Wilkerson & Dugdale, 1987). This general circulation of shelf waters maintains low seasonal flux amplitudes and strong CO_2 uptake on the Cascadia Shelf.

Much of the nearshore tends to experience seasonally strong, juxtaposing air-sea CO_2 fluxes, leading to near zero net annual CO_2 fluxes (nearshore white colours in Figure 4.5c). For example, closer to shore north of 50 °N and south of the Southeast Alaska Archipelago, winter mixed layer deepening brings water rich in nutrients and CO_2 from respired organic matter to the surface, increasing pCO_2, leading to strong CO_2 outgassing to the atmosphere when light is limiting (Figure C.12a; Marchese et al., 2022). In the spring, substantial primary productivity draws down pCO_2 (Marchese et al., 2022), reverting the region to a prominent sink for atmospheric CO_2 (Figure C.12b). This large seasonal amplitude results in a net neutral flux.

Semi-enclosed, nearshore estuarine environments display strong CO_2 outgassing in our product, which is not always observed in regional high-resolution models. High pCO_2 values and outgassing fluxes (mean CO_2 flux of 0.7 mol m^{-2} yr^{-1}) occur in Cook Inlet, the Salish Sea, and the Southeastern Alaska Archipelago (Figure 4.5c). Globally, the source strength of these integrated estuarine environments is comparable to (or smaller than) other nearshore source regions that decrease averaged coastal ocean CO_2 uptake (Section 4.6.2 below; Duke et al., 2023b; Fennel et al., 2019; Laruelle et al., 2018). In high-resolution regional models, the Salish Sea has been reported as a weak net annual source (this study: 1.0 mol m^{-2} yr^{-1}; comparable to Jarníková et al., 2022b): 0.69 mol m^{-2} yr^{-1}), and Cook Inlet as a net sink (Hauri et al., 2020; Pilcher et al., 2018). Limited observations used to constrain both our observation-based estimate and regional models may create discrepancies between them. Our estimate is based on all available surface ocean pCO_2 observations along with a suite of predictor variables (Figure 4.1; Table 4.1), whereas regional process-based models using data for boundary conditions simplify and parameterise mechanisms (Hauri et al., 2020; Jarníková et al., 2022b; Pilcher et al., 2018). Global observation-based

estimates and models also disagree, where model fluxes are often more negative (stronger sink) at northern latitudes, attributed to a smaller seasonal pCO_2 amplitude (Resplandy et al., 2024).

4.6.2 Nearshore fluxes

The nearshore coastal environment (0 - 25 km offshore) exhibits large air-sea CO_2 fluxes, over a relatively small surface area, impacting regional marine carbon budgeting. As our estimate wraps around the coast from primarily E-W to primarily N-S, we split the region along the 140 °W meridian (Figure 4.5a). Averaging grid cells approximately parallel to the regional coastline along longitudinal bands (155 °W to 140 °W west of 140 °W; Figure 4.6a&b) and along latitudinal bands (56 °N to 45 °N east of 140 °W; Figure 4.6c&d), the inclusion or exclusion of the nearshore environment creates large differences in estimated net annual air-sea CO_2 fluxes, for example, between 154 °W to 149 °W encompassing Cook Inlet (absolute flux difference of 250%, switching from a net sink to a source; Figure 4.6b). North to south from 56 °N to the northern extension of the California current system at 45°N (Figure 4.6d), including the nearshore leads to a slightly weaker net annual sink for atmospheric CO_2. The difference is largest within latitudinal bands inclusive of the Salish Sea (49-51 °N; 20% weaker). Differences in zonally averaged pCO_2 and air-sea CO_2 fluxes also exist between products with varying nearshore coverage (Section 4.4.2; Roobaert et al., 2024; Sharp et al., 2022). Basin-wide, inclusion of the nearshore changes the annual exchange with the atmosphere within the study area by 0.06 Tg C yr^{-1} (6%). These results highlight the importance of including the nearshore in regional marine carbon budgets.

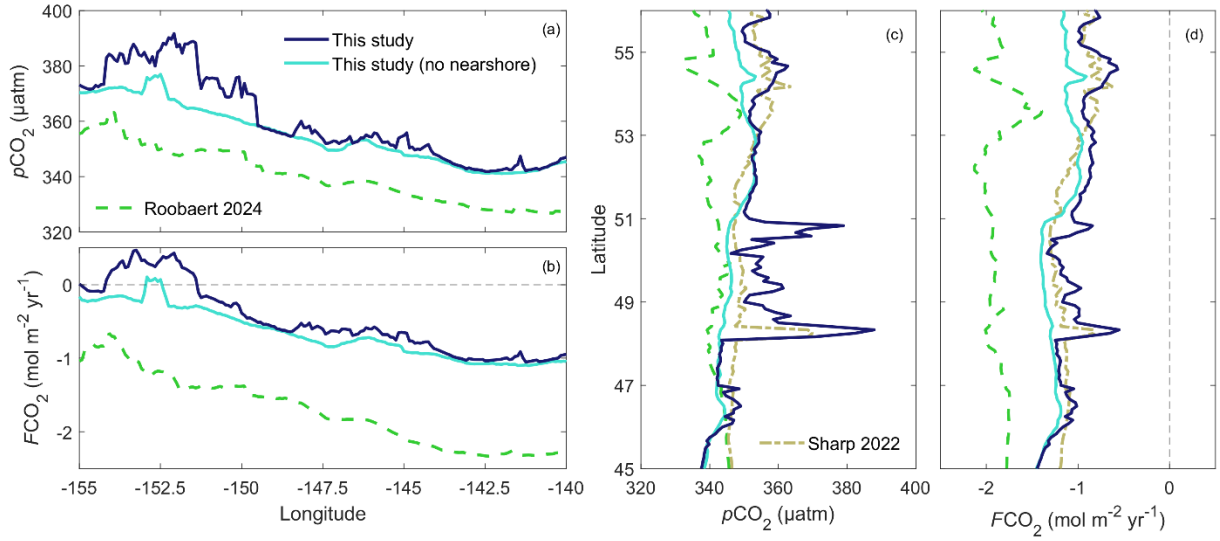

Figure 4.6 Longitudinally averaged estimates west of 140 °W of mean (a) pCO2 and (b) air-sea CO2 flux of: this study (dark blue), this study removing the nearshore (cyan). (c) and (d) are latitudinally averaged estimates east of 140 °W respectively. Additional observation-based estimates with overlapping domains including Sharp et al.

(2022) (dot-dash beige), and Roobaert et al. (2024) (dashed lime green). Sharp et al. (2022) air-sea CO2 fluxes calculated following Section 4.3.6.

4.6.3 Dominant controls on variability

Four distinct tiers of predictor variable importance rankings emerged from a perturbation-based spatial sensitivity analysis in estimated pCO_2 (Figure 4.7a). The ANN is purely a set of empirical, not mechanistic, relationships between pCO_2 observations and predictor variables, though variables were selected with mechanism in mind (Table 4.1). We used a perturbation-based spatial sensitivity analysis (Section 4.3.5) to probe the dependency of the ANN relationships on each variable, as they cannot be viewed directly (unlike a multiple linear regression). Atmospheric pCO_2 and atmospheric pCO_2 anomaly (removing the seasonal cycle; Section 4.3.3) are the most important predictors, followed by SST, and then process-driven controls whose importance varies spatially. Atmospheric pCO_2 and atmospheric pCO_2 anomaly are the only two predictor variables that capture a trend in time from 1998 to 2019 (i.e., increase of 2.12 $\mu atm\ yr^{-1}$ due to anthropogenic emissions). Due to the trend, these variables also experienced the largest absolute value perturbation (mean basin-wide increase of 7 μatm), at least one order of magnitude greater than other variables. The third most important predictor for estimating pCO_2 is SST. Basin-wide, the sensitivity test introduced a mean SST increase of 1.5 °C, resulting in a mixed pCO_2 response where generally there was a decrease, outside of the Gulf of Alaska central glacial drainage basin where pCO_2 increased (Figure C.13a). This result does not follow the mechanistic reduced solubility of CO_2 in warmer water. However, it emphasizes the importance of the SST seasonal cycle as a predictor (strong correlation, typically negative, between pCO_2 and SST; Figure C.13b).

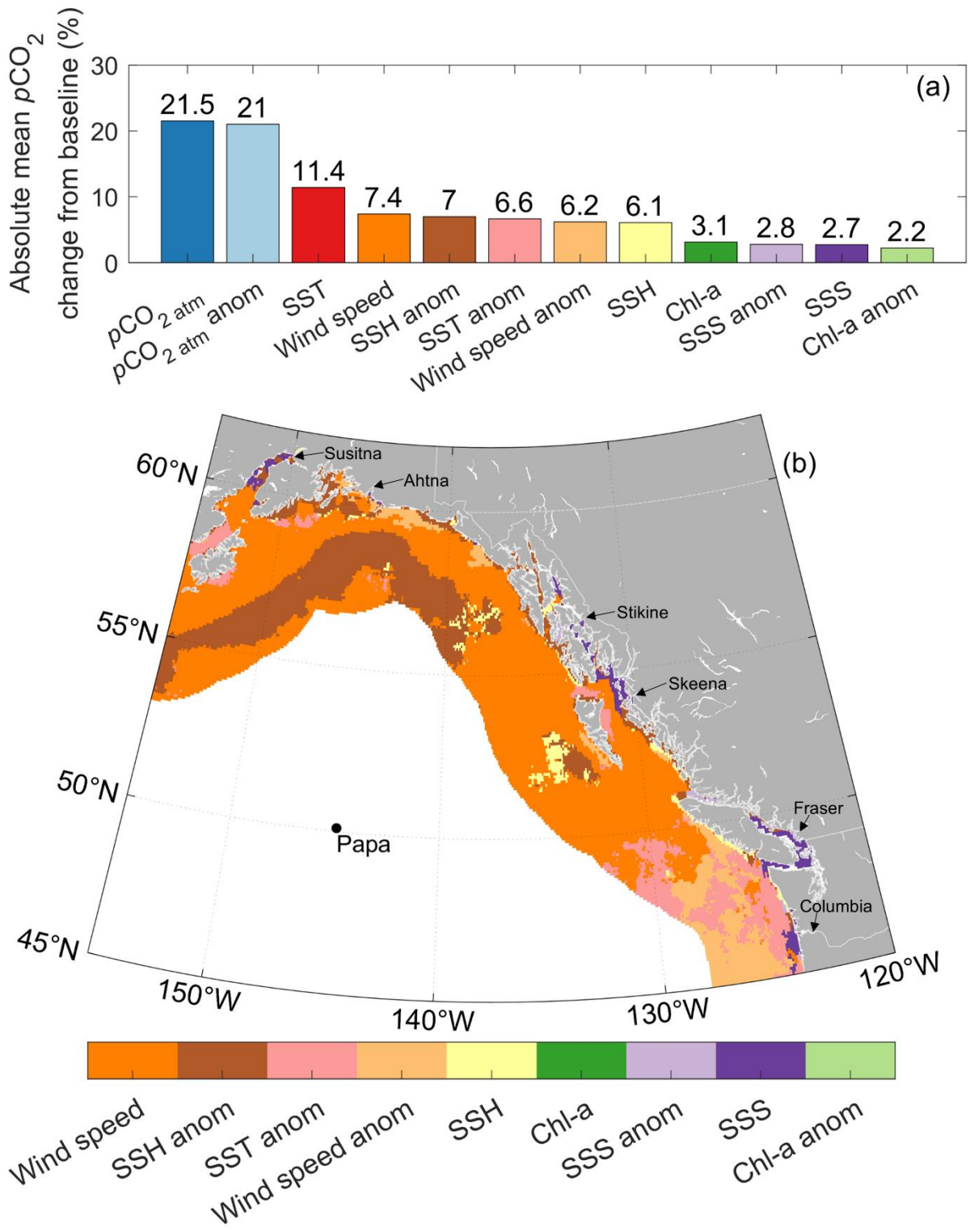

Figure 4.7 (a) Predictor variables ordered by absolute mean pCO_2 change from baseline run during perturbation-based spatial sensitivity analysis (Section 4.3.5). (b) Most dominant process-based predictor variable mapped by largest absolute mean pCO_2 change from baseline run during perturbation-based spatial sensitivity analysis (excluding top three variables from (a)). No grid cells displayed Chl or Chl anomaly as the largest absolute mean

pCO_2 change from baseline over the full study time range (1998-2019). Major river outflows are labelled for reference.

Excluding the three most dominate controls (atmospheric pCO_2, atmospheric pCO_2 anomaly, and SST), the spatial distribution of predictor variable importance rankings can be explained by mechanistic drivers even though the ANN is purely empirical. SSH anomaly is important along the Alaskan Gyre boundary, where the upwelling gyre exerts control over local biogeochemistry (Figure 4.7b; Duke et al., 2023c; Hauri et al., 2021). Wind speed (as a proxy for mixed layer depth) is important throughout most regions along the continental shelf and the outer coast as winter mixed layer deepening brings CO_2-rich subsurface waters to the surface (mean basin-wide perturbation increase of 0.4 m s^{-1} resulting in a pCO_2 increase of 1.7%; Figure 4.7b). SSH and SSH anomaly are additionally important offshore of Sitka, Alaska (57 °N, 143 °W) and Haida Gwaii (52 °N, 133 °W) where mesoscale anticyclonic eddies with enhanced primary productivity and high SSH propagate away from the continental margin (Figure 4.7b; Batten and Crawford, 2005; Crawford et al., 2007; Crawford and Whitney, 1999; Whitney et al., 2005; Whitney and Robert, 2002). In the North Pacific Current influenced region southeast of the study area, SST anomaly and wind speed anomaly are the most important predictors linked to the relative balance of opposing mechanisms (i.e., thermal and biophysical pCO_2 components; Figure 4.5b).

Nearshore regions experience a range of predictors with prominent features mostly controlled by salinity (SSS and SSS anomaly) in coastal estuarine areas (Figure 4.7b), and tidally mixed areas (e.g., Juan de Fuca Strait, Johnstone Strait; Figure 4a). In additional regions where freshwater discharge is important (e.g., Table C.2), SSH and SSH anomaly emerge as important predictors potentially linked to discharge associated changes to nearshore sea level (Figure 4.7b; Durand et al., 2019). Neither perturbation to Chl nor Chl anomaly resulted in the largest absolute mean pCO_2 change from baseline over 264 months in a single grid cell (Figure 4.7b). However, seasonally Chl emerges as a prominent predictor in scattered grid cells along nearshore West Coast Vancouver Island and in the Southeast Alaska Archipelago during the spring (i.e., March, April, and May; not shown).

4.6.4 Air-sea pCO_2 trends

Trends in the last decades (1998-2019) in ΔpCO_2 (sea – air) display spatial heterogeneity in the coastal Northeast Pacific, with a gradient of smaller trends moving offshore. A linear fit was applied to the full ΔpCO_2 anomaly (i.e., deseasonalized; Section 4.3.3) time series within each grid cell to calculate the trend and standard error. Regions that experience an increase in surface ocean pCO_2 close to the increase in atmospheric (i.e., resulting in a small ΔpCO_2 trend) are spatially distinct from those that have

an insignificant trend in pCO_2 leading to a large divergence with the atmosphere (i.e., large ΔpCO_2 trend). Grid cells with a small ΔpCO_2 trend are dominantly located in the outer coast (> 50 km offshore) and in the southeast of the study area (Figure 4.8a). Trends are closer to the atmospheric trend in this region (2.12 μatm yr^{-1}), meaning any change in the carbon sink due to anthropogenic climate change will require long observation time series to detect, as the signal is small relative to internal variability (Gooya et al., 2023; McKinley et al., 2016; Resplandy et al., 2015; Sutton et al., 2019). We report trends in pCO_2 that are similar to those observed at time series sites along Fisheries and Ocean Canada Line P stations (this study: P4 = 1.3±0.1 μatm yr^{-1}; P12 = 1.6±0.1 μatm yr^{-1}; comparable to Franco et al. (2021): P4 = 1.0±1.4 μatm yr^{-1}; P12 = 1.5±0.6 μatm yr^{-1}).

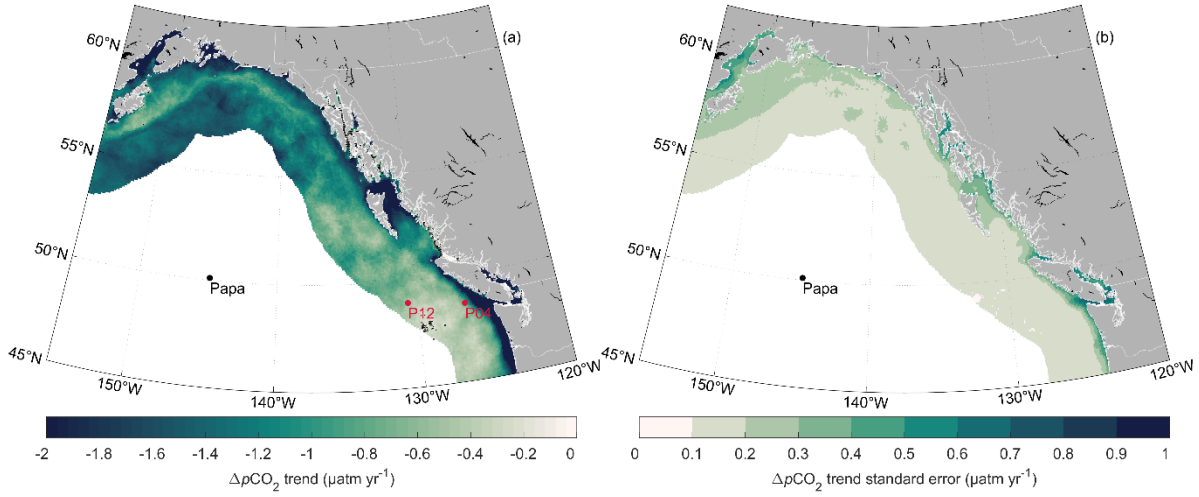

Figure 4.8 1998-2019 trend in (a) ΔpCO_2 anomaly (i.e., deseasonalized) where more negative (darker) values indicate an increase in air-sea pCO_2 disequilibria with time. Black crosshatches show grid cells with an insignificant calculated trend (outside the 95% confidence level; p ≥ 0.05; 0.4% of total grid cells). (b) Standard error of the estimated slope in the ΔpCO_2 trend fit.

Large ΔpCO_2 trends (and low or insignificant pCO_2 trends) occur in regions experiencing strong connectivity to the older subsurface waters of the Northeast Pacific (e.g., subpolar Alaskan Gyre, west coast upwelling zone; Figure 4.8a). This older water has a lower anthropogenic carbon load (Carter et al., 2019; Clement and Gruber, 2018; Gruber et al., 2019a; Sabine et al., 2004), which may be responsible for the lag in the increase in surface ocean pCO_2 (e.g., Duke et al., 2023c). The ΔpCO_2 trend in the Alaska Gyre is dominated by the winter trend, whereas the west coast upwelling zone is dominated by the summer trend (Figure C.14). These seasonal trends coincide with the timing of greatest connectivity to depth in each region. Strongest Alaskan gyre upwelling occurs in winter (Gargett, 1991; Talley, 1985), whereas the coastal upwelling season is spring and summer (Dorman and Winant, 1995; Hsieh et al.,

1995) with downwelling occurring in the winter (Section 4.6.1; Thomson & Ware, 1996). In the nearshore (e.g., Southeast Alaska Archipelago, Salish Sea), subsurface waters exchange through estuarine flow and tidal mixing. In these regions, we report low or insignificant winter ΔpCO_2 trends and large negative summer trends in agreement with regional model results (e.g., Jarníková et al., 2022b). Increasing summer air-sea pCO_2 disequilibria enhances ocean CO_2 uptake, whereas winter air-sea disequilibria has remained relatively constant, maintaining ocean outgassing. In winter, light limits biological productivity, resulting in higher total CO_2 in the surface (Evans et al., 2019; Ianson et al., 2016; Simpson et al., 2022). This increase in total CO_2 reduces the buffer capacity of the carbonate system (Revelle and Suess, 1957), so that the pCO_2 increase due to anthropogenic carbon uptake is larger than it is in summer in many temperate zones (e.g., Jarníková et al., 2022b; Landschützer et al., 2018). Our findings are consistent with global ΔpCO_2 trend estimates where most coastal regions appear to exhibit negative ΔpCO_2 trends likely becoming stronger atmospheric CO_2 sinks or weaker sources (Fennel et al., 2019; Laruelle et al., 2018; Resplandy et al., 2024; Roobaert et al., 2024; Wang et al., 2017). However, the rate of change in the air-sea CO_2 flux can be amplified or dampened in some regions by changes in wind speed patterns (Griffin et al., 2010; Resplandy et al., 2024; Roobaert et al., 2024).

4.7 Conclusions

Our high-resolution, neural network created pCO_2 product reproduces observed coastal Northeast Pacific Ocean variability well, from the outer transitional zone to the nearshore (0 – 25 km offshore). We interpolated sparse observations using non-linear relationships developed with a neural network based on predictor data from satellite and reanalysis products to create a continuous, gridded monthly pCO_2 estimate at a 1/12° spatial resolution, inclusive of the nearshore. This pCO_2 product provides a baseline environmental context for pCO_2 and air-sea CO_2 flux variability in the study area with an uncertainty of 50 µatm and 0.2 mol-C m^{-2} yr^{-1}, respectively. The product resolves seasonal variability (phase and amplitude) and broad spatial patterns well compared to high-resolution *in situ* observations. The product is not designed to capture daily – weekly variability.

A unique ANN sensitivity analysis shows that variations in pCO_2 results agree with mechanistic drivers even though the ANN itself is purely empirical. ANNs are not based on predefined equations but their ability to capture information inherent to the training data, preventing any explicit explanation of how predictor variables and their output are related. We suggest a new systematic sensitivity analysis introducing perturbations to predictor variables, with a consideration for natural spatial variability, to

produce mapped variable importance rankings. This approach offers insight providing greater transparency to complex ANN techniques.

We describe the coastal Northeast Pacific as a net sink for atmospheric CO_2 with large spatial heterogeneity between outgassing in the nearshore and uptake on the outer coast. Net annual air-sea CO_2 flux is largely anticorrelated with seasonal air-sea CO_2 flux amplitude. Patterns inherent to specific regions drive this anticorrelation, including circulation and opposing seasonal upwelling or relaxation vs. downwelling, and may make the relationship regionally specific rather than applicable to the wider global coastal ocean. Our results also emphasize the importance of including nearshore fluxes (often omitted by other coastal products), which are likely to be a source reducing the net coastal sink, when constructing marine carbon budgets (e.g., Legge et al., 2020). These findings could be potentially important considerations for reporting marine carbon dioxide removal approaches in the study area, as interventions impacting source areas are treated differently from those enhancing natural sinks (Verra, 2023).

Trends over the last decades show outer coast pCO_2 may be experiencing the largest increase in air-sea pCO_2 disequilibrium, due to strong connectivity with subsurface waters low in anthropogenic CO_2, while pCO_2 in the North Pacific Current region tracks increasing atmospheric pCO_2 more closely. Trends reported here across the coastal Northeast Pacific indicate most regions are likely to become stronger atmospheric CO_2 sinks or weaker sources.

Improving regional observational coverage and continuity and advancing the ANN approach will improve future air-sea CO_2 flux estimates. Some regions in the coastal Gulf of Alaska display large net annual air-sea CO_2 fluxes (e.g., Cook Inlet) yet are extremely sparsely monitored. A higher temporal resolution, such as daily, could enable the ANN to capture highly episodic air-sea CO_2 flux events common to the nearshore. However, this approach would dramatically reduce the percent coverage of observation training targets. A solution may be creating ANN non-linear relationships to interpolate pCO_2 directly from *in situ* observations. Using high frequency, collocated sensors and non-uniform “highest available resolution” satellite and reanalysis datasets for predictor variables not collected *in situ*, a higher temporal and/or spatial resolution coastal product could be developed without substantial loss in ANN training targets.

4.8 Data availability

All data used is publicly available. ANN-NEPc pCO_2 and air-sea CO_2 flux fields created for this publication are available through the National Center for Environmental Information (NCEI Accession 0290365; https://doi.org/10.25921/4jvk-y051). pCO_2 data are from the Surface Ocean CO_2 Atlas (SOCAT) v2021 (available at https://www.socat.info/) as well as additional data from the Fisheries and Oceans Canada February 2019 Line P cruise, a West Coast Ocean Acidification cruise from July and August 2010 (Evans et al., 2012), and La Perouse cruises from May 2007 and May 2010 (available at https://www.waterproperties.ca/linep/). Sea surface temperature and chlorophyll-a are from the European Space Agency Climate Change Initiative (available at https://climate.esa.int/en/odp/#/dashboard). Sea surface salinity and sea surface height are from Copernicus Marine Environment Monitoring Service (available at https://data.marine.copernicus.eu/product/GLOBAL_MULTIYEAR_PHY_001_030/description). Ocean surface wind data at 10 m height are from Regional Deterministic Reforecast System (available at https://caspar-data.ca/; detailed here https://github.com/julemai/CaSPAr). Mooring data used in analysis are also available through the National Center for Environmental Information (NOAA moorings: NCEI Accession 0173932; and Hakai Institute Quadra Island Field Station: NCEI Accession 0208638).

4.9 Acknowledgments

Funding for this project was provided by the Natural Sciences and Engineering Research Council of Canada (NSERC) through the Advancing Climate Change Science in Canada program (grant# ACCPJ 536173-18) to RH. Funding from Fisheries and Oceans Canada's Aquatic Climate Change Adaptation Service Program to DI supported the analysis of recent underway pCO_2 measurements made by the Line-P program (grant# 96036). PD financial support also provided by a Natural Sciences and Engineering Research Council of Canada (NSERC) Doctoral Postgraduate Scholarship and the joint Fisheries and Oceans Canada (DFO) and National Oceanic and Atmospheric Administration (NOAA) Ocean Acidification Collaborative Funding Initiative.

Fisheries and Oceans Canada (DFO) runs the Line P monitoring program. National Oceanic and Atmospheric Administration (NOAA) operates the Kodiak, Gulf of Alaska Ocean Acidification, Chá bă, and Cape Elizabeth moorings. Hakai Institute operates Quadra Island Station. We extend our thanks to Jamie Shutler and Dan Ford for their valuable brainstorming efforts regarding the pCO_2 temperature correction section. We are grateful to Wiley Evans for sharing previously published pCO_2 data from the 2010 West

Coast Ocean Acidification cruise. We also want to thank Philippe Tortell and Robert Izett for providing previously published pCO_2 data from the May 2007 and May 2010 La Perouse cruises.

4.10 Author contributions

PD and PL developed the neural network code and created the product with help from RH, DI. PD, RH, and DI contributed to the interpretation and analysis of the results. All co-authors contributed to editing the manuscript. RH and DI supervised the project work. PC provided data and consultation. PD prepared the manuscript with contributions from all co-authors.

Chapter 5. Comparing Regional pCO_2 Product Boundaries

5.1 Introduction

Observation-based pCO_2 data products commonly delineate between the coastal ocean and the open ocean (Duke et al., 2023c; Hales et al., 2012; Landschützer et al., 2014; Laruelle et al., 2017; Roobaert et al., 2024; Sharp et al., 2022). Spatial domains of past data products vary with how nearshore or offshore they extend (e.g., 200 nautical mile limit of national Exclusive Economic Zones, Hales et al. (2012); offshore to 140 °W, Sharp et al. (2022); 300 km offshore, Duke et al. (2023c) & Laruelle et al. (2017); outer limit of the shelf break, Roobaert et al. (2024); exclusion of estuarine systems, Roobaert et al. (2024) & Laruelle et al. (2017)). These differing boundary definitions create discontinuity between regional and global ocean air-sea CO_2 flux estimates (Landschützer et al., 2020a). The choice of boundary definition has important implications on the observations and environmental characteristics included in informing the gap-filling approaches used, causing differences between products within overlapping domains (Landschützer et al., 2020a).

In this Chapter, I conduct additional analysis comparing overlapping boundaries between two regional Northeast Pacific observation-based pCO_2 data products spanning the coastal and open ocean. Previous Chapters investigated high-resolution, observation-based pCO_2 data products (with associated air-sea CO_2 fluxes) in the open ocean (Duke et al., 2023c) and coastal regions (Chapter 4). Both studies defined the coastal–open-oceanic boundary as 300 km offshore following Laruelle et al. (2017), adding a 10 km buffer, leading to a uniform 20 km overlapping domain along the 300 km offshore contour between the two products. Here I investigate how well the coastal–open-ocean continuum is reconstructed across the overlapping domain given independent gap-filling approaches.

5.2 Product background

I compare Northeast Pacific open ocean (Duke et al., 2023a) and coastal ocean pCO_2 products (Duke et al., 2024) described in Duke et al. (2023b) and Chapter 4 respectively. Both products offer continuous monthly sea surface pCO_2 maps from 1998-2019 in the Northeast Pacific spanning 45 - 62°N and 120 - 155°W, at 1/12° spatial resolution (approximately 9 km by 5 km, latitude by longitude), with the coastal product extending to typically < 6 km of shore (Figure 4.5). Overall pCO_2 product uncertainty was reported as 12 µatm in the open ocean and 49 µatm in the coastal ocean. Products used a gap-filling approach to make basin-wide estimates from sparce pCO_2 observations by adapting a two-step artificial neural network (SOM-FFN) interpolation method developed by Landschützer et al. (2013, 2014). The

approach first groups provinces of grid cells with similar environmental characteristics using a self-organizing map approach (SOM); then, within each province, a feed-forward neural network (FFN) was used to create non-linear functional relationships between pCO_2 observations and independent predictor variables that are known to influence surface ocean CO_2. These relationships were then applied to the gridded predictor data to generate continuous estimated pCO_2 maps.

The largest differences between approaches used to create the two pCO_2 products included differing SOM approaches, slightly differing predictor variables used in each FFN, and different wind speed products used to estimate the air-sea CO_2 flux. The open ocean product used four unique SOM biogeochemical provinces changing shape over a monthly climatology with the clustering defined using an open ocean pCO_2 climatology (Landschützer et al., 2020a) as a predictor in addition to sea surface temperature, salinity, and mixed layer depth. In contrast, the coastal product used three unique provinces changing shape at each timestep with the clustering defined by only sea surface temperature, salinity, and height. The coastal FFN incorporated high-resolution regional wind data (1/11° spatial resolution Regional Deterministic Reforecast System; RDRS; Gasset et al., 2021) instead of reanalysis model derived mixed layer depth (Copernicus Marine Environment Monitoring Service global ocean eddy-resolving reanalysis; Jean-Michel et al., 2021) used in the open ocean FFN. The change was prompted by data assimilation limitations of the Argo float array used in the reanalysis mixed layer depth (i.e., generally deployed in waters with depths > 2 km; Bittig et al., 2019), and the common use of wind speed as a proxy for mixed layer depth in observation-based coastal ocean estimates (e.g., Roobaert et al., 2024; Laruelle et al., 2017). In calculating the air-sea CO_2 flux, the same regional high-resolution wind speed product was used for the coastal estimate while the open ocean estimate used a global wind speed product (1/4° spatial resolution Cross-Calibrated Multiplatform (CCMP) ocean surface wind data; Mears et al., 2019). Capturing greater variability in the coastal ocean required a high-resolution regional wind speed product over a low-resolution global product, reducing needed downscaling by nearly a third to match the desired output spatial resolution. On average, RDRS wind speeds are 1.19 m s^{-1} lower than CCMP wind speeds within the full coastal ocean product domain (Figure C.2).

5.3 Combined pCO_2 product evaluation

How well the two products reconstruct estimated pCO_2 along the boundary provides insight into how robust the FFN non-linear relationships that I created were. Relationships informing boundary grid cell estimates were created inside associated SOM provinces unique to each product, meaning they are based on different environmental conditions. Even with similar input data, each FFN could be capturing

these non-linear relationships in distinctive ways. Across the unified Northeast Pacific Ocean data product, the boundary appears more gradual for pCO_2 compared to air-sea CO_2 flux (Figure 5.1).

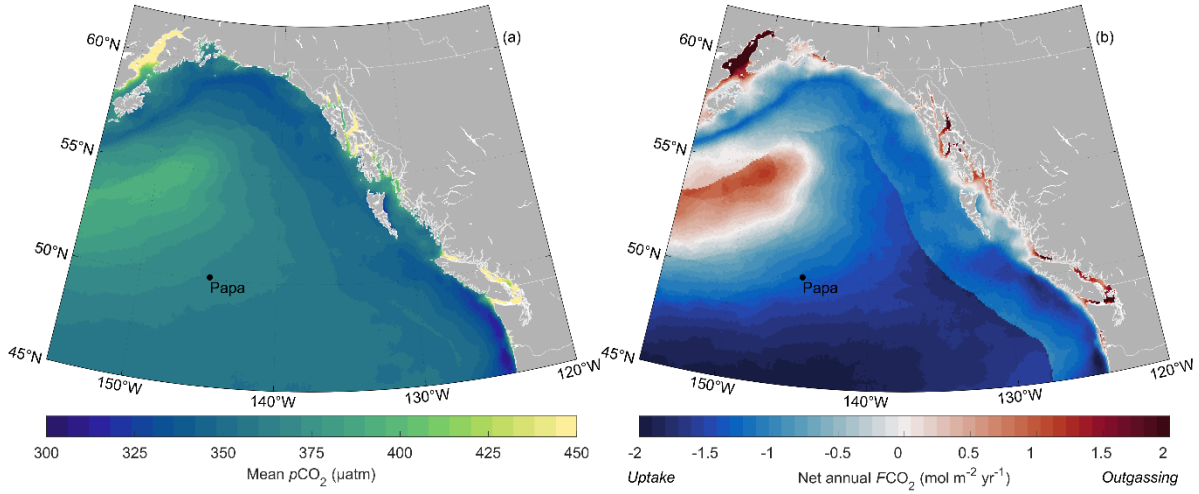

Figure 5.1 (a) Long-term (1998-2019) mean pCO_2 in µatm and (b) air-sea CO_2 flux in mol m^{-2} yr^{-1} across both Northeast Pacific data products (ANN-NEP & ANN-NEPc). Negative flux values indicate CO_2 uptake by the ocean. Ocean Station Papa is shown for reference.

The individual coastal ocean and open ocean data products replicate pCO_2 patterns well within the overlapping domain. Mean absolute error between the two products is approximately equal to the reported open ocean pCO_2 uncertainty (13 µatm; Figure 5.2a). There is a larger difference between products within the Alaskan Gyre influenced part of the overlapping domain, with the open ocean product estimating higher pCO_2 values relative to the coastal product (Figure 5.2b). The gyre region suffers from a scarcity of observations (Duke et al., 2023c). This lack of data coincides with increased biogeochemical complexity due to gyre forcing (Duke et al., 2023c). It cannot be determined which product is biased high or low, only that there is a difference. There is no statistically significant difference between products when compared to gridded observations within the overlapping domain (RMSE $\leq$ 10 µatm; Figure D.1). Differences between products appear larger during summer months and in later years (Figure D.2). The difference between products tends to be closer to zero in months and years with high observation counts (Figure D.2).

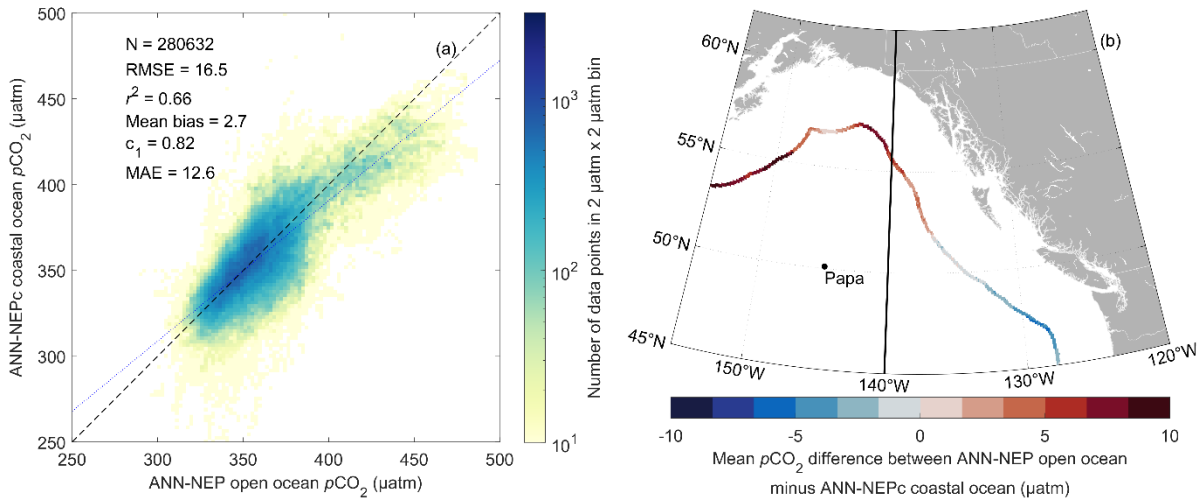

Figure 5.2 (a) Coastal pCO_2 estimate (ANN-NEPc) against open ocean pCO_2 estimate (ANN-NEP) within overlapping domain (grid cell by grid cell). Data are binned into 2 µatm by 2 µatm bins with data density shown in the colorbar on a log scale. Dashed black line is the 1:1. Dotted blue line is the least squares best fit. Also shown are number of overlapping grid cells in space and time (N), root mean squared error (RMSE), coefficient of determination (r^2), mean bias (calculated as the mean residual), the slope of the linear regression (c_1), and the mean absolute error (MAE). (b) Mapped mean difference between the open ocean pCO_2 estimate (ANN-NEP) and the coastal pCO_2 estimate (ANN-NEPc). 140 °W meridian divide used in Figure 5.3 & 5.4 analysis shown for reference.

Differences in air-sea CO_2 fluxes between the two products are influenced by ΔpCO_2 (sea - air) and the choice of wind speed product. Figure 5.3 averages grid cells within the overlapping domain approximately parallel to the 300 km offshore contour along longitudinal bands (northwest gyre region, 155 °W to 140 °W west of 140 °W: Figure 5.3a&b) and along latitudinal bands (eastern Cascadia Shelf border, 56 °N to 45 °N east of 140 °W; Figure 5.3c&d). Mean zonal differences in pCO_2 are relatively small with the largest difference being in the Alaskan Gyre influenced region compared to along the eastern Cascadia Shelf border (9 µatm and 5 µatm respectively; Figure 5.3a&c). Mean wind speed difference (1.15 m s^{-1}) within the overlapping domain between CCMP and RDRS results in a large difference in the gas transfer velocity parameterization (Wanninkhof, 2014) dependent on quadratic wind speed (gridded wind speed squared mean of CCMP: 72.6 m^2 s^{-2}; compared to RDRS: 53.5 m^2 s^{-2}) impacting flux estimates (Roobaert et al., 2018). Recalculating air-sea CO_2 fluxes using CCMP wind speed rather than RDRS wind speed within the coastal ocean pCO_2 product reduces differences with the open ocean estimate (Figure 5.3b&d), especially along the eastern Cascadia Shelf border (Figure 5.3d). West of 150 °W, differences in ΔpCO_2 maintain large flux differences regardless of wind speed product used. The open ocean product captures twice as many grid cells with a ΔpCO_2 greater than 50 µatm compared to the coastal product (14% and 7% respectively), resulting in stronger outgassing.

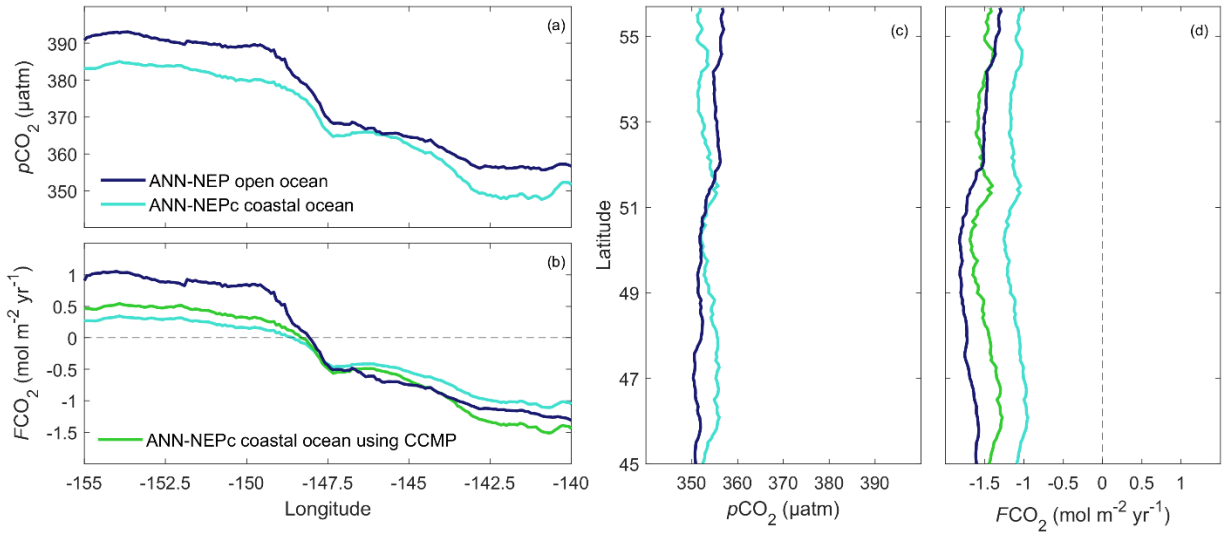

Figure 5.3 Longitudinally averaged estimates for the Alaskan Gyre region (west of 140 °W) of mean (a) pCO_2 and (b) air-sea CO_2 flux of: open ocean estimate (ANN-NEP) (dark blue), coastal estimate (ANN-NEPc) (turquoise), and the coastal flux estimate recalculated using CCMP wind speed (lime green). (c) and (d) are latitudinally averaged estimates for the eastern Cascadia Shelf border (east of 140 °W) respectively.

Varying wind speed estimates are a prominent source of air-sea CO_2 flux uncertainty (Atamanchuk et al., 2020; Otero et al., 2013; Roobaert et al., 2018). Wind speed products along the West Coast of North America can show large discrepancies compared to winds observed at buoy sites (Bylhouwer et al., 2013; Tinis et al., 2006; Wallcraft et al., 2009). Inclusion of wind speed uncertainty (calculated following Roobaert et al. (2018) as the standard deviation of calculated fluxes from four unique wind speed products scaled to monthly, 1/12° resolution: RDRS, Gasset et al. (2021); CCMP, Mears et al. (2019), NCEP2, Kanamitsu et al. (2002); ERA5, Hersbach et al. (2020)) added in quadrature with uncertainties in the gas transfer velocity (Wanninkhof, 2014) and overall pCO_2 product uncertainty (Section 3.4.2 & 4.4.3) yields a larger mean flux uncertainty in the overlapping domain for both products (±0.5 mol m^{-2} yr^{-1} compared to ±0.2 mol m^{-2} yr^{-1}; Section 3.4.2 & 4.4.3). Mean calculated fluxes from the different wind speed products are shown in Figure 5.4 (averaged approximately parallel to the 300 km offshore contour same as Figure 5.3). Calculated fluxes using CCMP and ERA5 wind speed products are nearly identical, while RDRS appears to exhibit similar spatial patterns. In contrast, NCEP2 calculated fluxes are much closer to zero in both the Alaskan Gyre and eastern Cascadia Shelf border regions (Figure 5.4). Roobaert et al. (2018) and Wallcraft et al. (2009) also highlighted a marked difference between NCEP2 and the other wind speed products with NCEP2 shown to be inconsistent in magnitude and wind pattern over the ocean. Roobaert et al. (2018) attribute their calculated 40% global air-sea CO_2 flux uncertainty mainly to the use of NCEP2 (only 12-20% excluding NCEP2 using various gas transfer velocity parameterizations).

Excluding NCEP2 in this analysis, the overall air-sea CO_2 flux uncertainty within the overlapping domain is ±0.4 mol m^{-2} yr^{-1}, with flux differences between products within this revised uncertainty estimate.

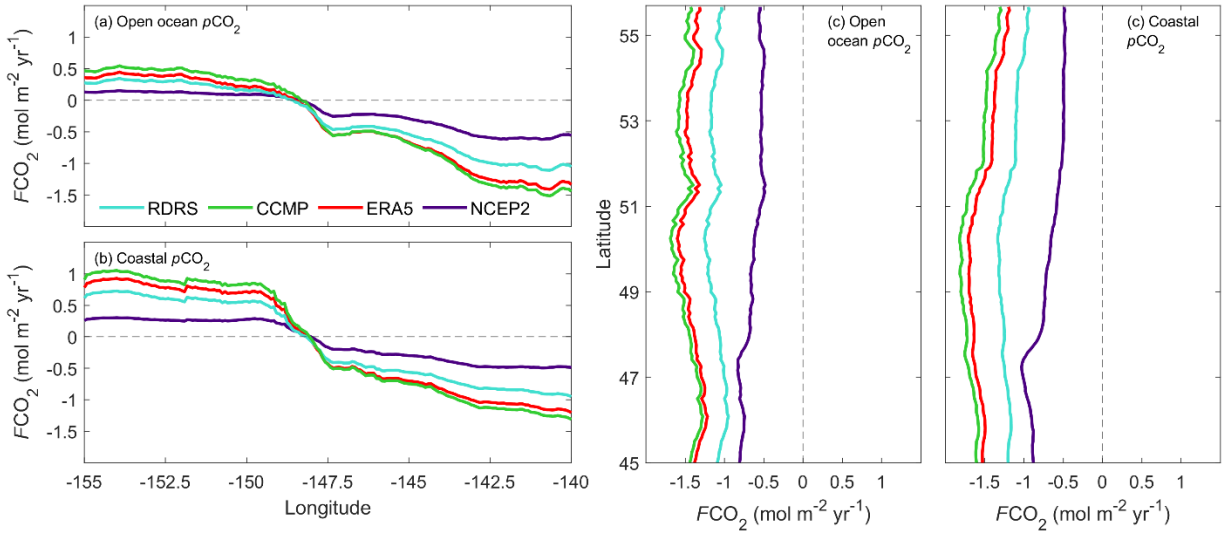

Figure 5.4 Longitudinally averaged estimates for the northwest gyre region (west of 140 °W) of mean (a) open ocean air-sea CO_2 flux (ANN-NEP pCO_2) and (b) coastal ocean air-sea CO_2 flux (ANN-NEPc pCO_2) calculated using various wind speed products: RDRS (turquoise; Gasset et al., 2021), CCMP (lime green; Mears et al., 2019), NCEP2 (indigo; Kanamitsu et al., 2002); ERA5 (red; Hersbach et al., 2020). (c) and (d) are latitudinally averaged estimates for the eastern Cascadia Shelf border (east of 140 °W) respectively.

The combination of overlapping SOM biogeochemical provinces informing FFN non-linear relationships within each, impact the difference in pCO_2 between products. The largest pCO_2 differences occur within the overlapping domains of province 1 and 5, and province 4 and 5 (Figure 5.4a). Provinces 1 and 5 have a winter and spring overlap, whereas provinces 4 and 5 overlap in summer and fall (Figure D.3). These provinces roughly correspond to the center of the Alaskan Gyre (1) and a southern and summer dominant province in the open ocean product (4) with the gyre influenced region in the coastal product (5; Figure 5.4b). High winter pCO_2 extremes estimated in province 1 lead to large air-sea CO_2 flux differences between products west of 150 °W (Figure 5.3b). Provinces 1 and 5 are the most observation scarce (total count and percent coverage; Figure 5.4c), likely impacting the robustness of FFN non-linear relationships created. The combination of provinces 4 and 5 likely diverge due to the differing physical and biogeochemical regimes encompassed by each province across products. Province 4 includes substantial training data from the North Pacific Current influenced region where there is almost no connectivity to depth (Duke et al., 2023c). Province 5 is relatively seasonally stable with training data influenced dominantly by gyre forcing and transition zone Gulf of Alaska waters (Chapter 4). Training data inside each province domain impact the relationships created to estimate pCO_2 along the boundary. The most frequently occurring province overlap (between 4 and 7; Figure 5.4) along the eastern Cascadia

Shelf border also leads to the smallest pCO_2 difference between products (Figure 5.3c; Figure 5.4a) as both approximately follow sea surface temperature variability (i.e., increasing and decreasing in size seasonally along a latitudinal gradient; Figure D.3).

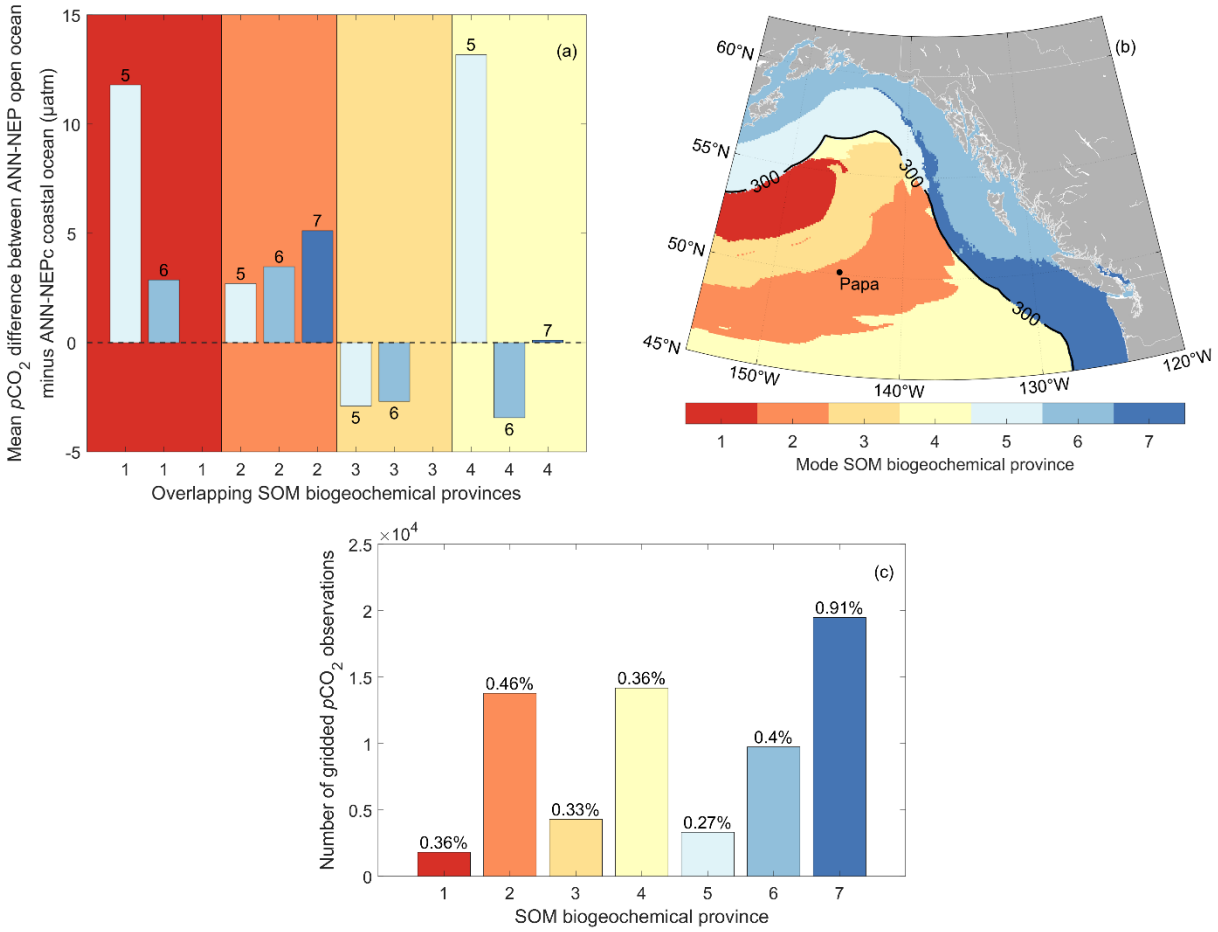

Figure 5.5 (a) Mean difference between the open ocean pCO_2 estimate (ANN-NEP) and the coastal pCO_2 estimate (ANN-NEPc) grouped by overlapping SOM biogeochemical province combination. Open ocean provinces are shown along the x axis and coastal ocean provinces are shown on each bar. Missing bars are where provinces do not overlap. (b) Mapped mode of SOM biogeochemical province (i.e., most frequent occurrence) from January 1998 to December 2019 across both regional pCO_2 data products. 300 km offshore line shown for coastal–open-oceanic boundary used in this study (solid black line labelled '300'). Color scheme matches provinces in (a) and (b). (c) Numbers of gridded Surface Ocean CO_2 Atlas (SOCAT) v2021 (Bakker et al., 2016) pCO_2 observations within each SOM biogeochemical province. Provinces 1-4 relate to the open ocean pCO_2 estimate (ANN-NEP) whereas 5-7 relate to the coastal pCO2 estimate (ANN-NEPc). Numbers above each bar represent the percent coverage of gridded pCO_2 observations to the total grid cells within each province.

5.4 Conclusions

Two independent observation-based pCO_2 data products agree reasonably well within the overlapping domain in the Northeast Pacific Ocean. Neither product displayed a large pCO_2 bias compared to gridded observations. The spatial distribution of the differences between products are much larger in the Alaskan

Gyre region, and smaller in the North Pacific Current region. Both ΔpCO_2 extremes and the choice of wind speed significantly impacted air-sea CO_2 flux estimates in the Alaskan Gyre region, leading to large differences between products (mean flux difference of 340%). However, flux differences between products are within the envelope of estimated total flux uncertainty with the inclusion of wind speed product uncertainty. The environmental characteristics captured by each unique SOM biogeochemical province and the number of observations available inside each province to train FFN non-linear relationships potentially act as overarching controls on observed differences. Differences are largest with provinces containing few observations and between provinces that capture vastly different physical and biogeochemical regimes. This additional analysis lends confidence to both products' ability to reconstruct pCO_2 from non-linear relationships established between observations and predictor variables in more observation dense regions.

Future observation-based interpolation approaches to estimating surface ocean pCO_2, and associated air-sea CO_2 fluxes, may not need to be divided along an arbitrary coastal–open-oceanic boundary definition. Dynamic provinces in the first unsupervised SOM clustering step could delineate any boundary more objectively based on environmental predictor data. Additionally, province-specific predictor variables based on a stepwise FFN regression algorithm could be used to account for differences between the drivers across the coastal–open-oceanic continuum (Zhong et al., 2022). Alternatively, interpolation approaches that do not rely on a clustering-based method could offer continuous estimates absent of aphysical fronts (e.g., random forest regression, Sharp et al. (2022); gradient-boost algorithm, Sun et al. (2021)). This advance would remove the need to merge products with boundary discontinuities and allow greater continuity at regional to global scales.

5.5 Data availability

Data used in this chapter but not already documented in other chapters comes from NCEP/DOE AMIP-II Reanalysis (Reanalysis-2) monthly mean of forecast wind speed at 10 m from 6-hourly values (available at https://psl.noaa.gov/data/gridded/data.ncep.reanalysis2.html). ERA5 monthly mean 10 m wind speed comes from the ECMWF Integrated Forecasting System (available at https://cds.climate.copernicus.eu/cdsapp#!/dataset/reanalysis-era5-single-levels-monthly-means?tab=overview).

Chapter 6. Conclusions

6.1 Connecting chapters

This dissertation enhances our understanding of air-sea CO_2 exchange in the Northeast Pacific Ocean with attention to coastal and nearshore zones. Chapter 2 reviewed current understanding of air-sea CO_2 fluxes in Canadian waters demonstrating agreement between net annual Northeast Pacific Open Ocean sink estimates, while highlighting a lack of understanding of variability over a range of timescales. Widely varying previous flux estimates in the coastal Northeast Pacific Ocean especially revealed a gap in our understanding of spatial variability. In Chapter 3 and 4, development of a novel, artificial neural network approach demonstrated the capability of estimating pCO_2at an unprecedented spatial resolution. A unique sensitivity analysis offered insight into providing greater transparency for non-linear interpolation approaches. The creation of observation-based pCO_2 data products for the Northeast Pacific open ocean and coastal ocean facilitated the investigation of air-sea CO_2 flux variability which allowed regional drivers to be explored. In Chapter 5, merging the two products demonstrated the robustness of each independent estimate with small pCO_2 differences across the coastal–open-oceanic boundary. Consolidating dissertation chapters, answers can be offered to the primary research questions posed in Chapter 1:

(1) What is the present-day net annual air-sea CO_2 flux of Northeast Pacific Ocean? The region is a net sink of 3.54$\pm$0.77 Pg yr^{-1} with a mean flux of -0.99 mol m^{-2} yr^{-1} and standard deviation of 1.45 mol m^{-2} yr^{-1}.

(2) What drives variability over seasonal, interannual, decadal timescales? In the open ocean, the upwelling strength of the subpolar Alaskan Gyre appears to be a primary control on air-sea CO_2 flux variability. In the coastal ocean, an anticorrelation between net annual air-sea CO_2 flux and air-sea CO_2 flux seasonal amplitude is likely driven by processes inherent to specific regions including circulation, opposing seasonal upwelling or relaxation vs. downwelling, and the effects of winter mixing and primary productivity.

(3) How has the air-sea CO_2 flux changed over the past decades? Over 1998-2019 surface ocean pCO_2 is estimated to have increased at a rate of 1.3$\pm$0.5 μatm yr^{-1}, below the rate of atmospheric increase due to subsurface connectivity, with the region likely becoming a stronger net annual sink for atmospheric CO_2.

6.2 Method development

In developing the pCO_2 and associated air-sea CO_2 flux products addressing the primary research questions above, significant contributions were made to machine learning method development in estimating marine carbon uptake. Adapting the ANN SOM-FFN approach developed by Landschützer et al. (2013, 2014) for the global open ocean (also used by Laruelle et al. (2017) and Roobaert et al. (2024) in the global coastal ocean) included a number of advances. In Chapter 3, I demonstrated that stepping to a significantly higher spatial resolution (1/12°), compared to typical open ocean observation-based pCO_2 products (1/4° or 1°), led to nearly no loss in performance despite a much lower ratio of gridded pCO_2 observations compared to the total number of grid cells. I identified the internal division of training data as the most important parameter for reducing overfitting with higher resolution products requiring more direct training data and less data to internally evaluate, while still comparing to independent withheld data. The use of an ANN ensemble approach provided an additional tool to prevent overfitting and could also be used as a measure of ANN run randomness uncertainty. In Chapter 4, I suggest a new systematic sensitivity analysis introducing perturbations to predictor variables, with a consideration for natural spatial variability, to produce mapped variable importance rankings. This approach provides greater insight into ANN non-linear relationships through comparing variations between perturbation test pCO_2 estimates with mechanistic driver understanding. Improved product performance here (Duke et al., 2023a, 2024) compared to global products (i.e., Landschützer et al., 2020b; Roobaert et al., 2024) represents the enhanced ability of FFN relationships within regionally specific SOM biogeochemical provinces (including innovative provinces changing shape at each time step; Chapter 4) to better capture local-scale variability compared to global data relationships.

6.3 Future recommendations

This dissertation serves as an important step in creating a complete marine carbon budget for the Northeast Pacific. However, discrepancies still exist between estimates made in this dissertation and regional process-based models that need to be investigated (e.g., Hauri et al., 2020; Pilcher et al., 2018; Jarníková et al., 2022). Models could utilize the data products created here to aid in model evaluation and improve carbon flux process understanding. Such an action could be an important step in reconciling large, reported differences between air-sea CO_2 flux estimates in the region (i.e., between observations, interpolation-based products, and process-based models; Duke et al., 2023b) and integrating approaches towards a “policymaker relevant” flux value (Section 2.3). This dissertation only delved into one component of a complete marine carbon budget (i.e., exchange with the atmosphere; Legge et al.,

2020). Carbon stocks and fluxes of the terrestrial-oceanic interface, pelagic, and benthic environments still need to be resolved and integrated (Legge et al., 2020).

Improved observational coverage and continuity will help improve future air-sea CO_2 flux estimates. The subpolar Alaskan Gyre is a region severely undersampled while exerting strong controls impacting regional marine biogeochemical variability (Duke et al., 2023c). Some regions in the coastal Gulf of Alaska display large net annual air-sea CO_2 fluxes (e.g., Cook Inlet; Chapter 4) or are projected to experience large changes in flux magnitude due to climate change impacts (e.g., Gulf of Alaska central coast glacial drainage basin; Pilcher et al., 2018) yet are extremely sparsely monitored (< 350 and < 700 gridded observations respectively; Chapter 4). Improved monitoring is needed as these region are expected to experience greater future changes to their marine carbon budgets due to depleting sea ice (Poole and Hufford, 1982), shifting freshwater runoff sources (Pilcher et al., 2018), and changing circulation in the coastal Gulf of Alaska (Royer, 1979; Royer and Grosch, 2006).

Expanded observations are valuable beyond observation-based product training and model assimilation. There are limitations to the data products created in Chapter 3 and 4. Elaborating beyond reported uncertainty values, the estimates fill temporal and spatial observing gaps and are not designed to supersede *in situ* observations which provide something entirely unique (Fassbender et al., 2018b). Moorings offer sustained, high-frequency observations resolving temporal variability, integrating over (often) unknown spatial scales (Fassbender et al., 2018b). Shipboard underway data provide a snapshot in time unveiling the connectivity of spatial domains, but are limited by spatial heterogeneity (e.g., Nemcek et al., 2008) and the range of temporal scales over which variability can occur in the coastal zone (e.g., Evans et al., 2019, 2012, 2011; Fassbender et al., 2018b). *In situ* observations are costly and time intensive to collect and are susceptible to biases that may result from inhomogeneous conditions (e.g., proximity to freshwater input, upwelling zone, or mesoscale eddies), interannual variability, or anomalous events (e.g., marine heatwaves, strong upwelling events). The products created here do not fully capture that inhomogeneity, but rather offer a robust overview of conditions regionally with some compromise over the temporal and spatial scales they can describe. A similar compromise exists in capturing *in situ* conditions for the pCO_2 measurements used to inform the estimate. The products are not designed to capture daily – weekly variability over small spatial scales (< 20 km). Compromise at this scale might be an important consideration for pCO_2 data product use combined with another marine carbonate system parameter (e.g., alkalinity; Carter et al., 2018) in local ecosystem assessments addressing ocean acidification concerns (event intensity, duration, and severity; Bednaršek et al., 2020).

Observations are more than synthesised target data in observation-based products and serve to further understanding of marine carbon variability alongside a variety of tools (e.g., observation-based products, satellites, models, etc.).

Marine carbon estimates need to be operationalized to function as a tool assessing mCDR monitoring, reporting, and verification (Sutton-Grier et al., 2014). This work established static regional baselines for air-sea CO_2 fluxes from 1998-2019. Observation-based products created here can inform mCDR interventions through these baselines and the deeper understanding of regional fluxes mined in this dissertation. Described regional drivers operating on different spatial and temporal scales offer important considerations when attempting to maximize mCDR intervention efficacy (GESAMP, 2019; Oschlies et al., 2023). Both products offer regional air-sea CO_2 flux context when planning pilot studies with pCO_2 maps offering initial estimates for what is required to enhance the sink or weaken the source of a particular area within the region (i.e., macroalgae cultivation in the Salish Sea, ocean alkalinity enhancement in the Alaskan Gyre, etc.). Future product updates (if requested), incorporating the latest version of SOCAT (Bakker et al., 2016) and up to date predictor data (Section 3.3.1 & 4.3.2), could offer regional baseline estimates absent of intervention signals. These estimates could be used post-intervention to independently evaluate mechanistic model validation baseline runs (Ho et al., 2023). The inability of ocean observation-based products to represent mCDR interventions (at realized scale; Gt per year removal) from past observations combined with satellite and reanalysis data presents an emerging issue for global carbon budget considerations (Friedlingstein et al., 2023). Comparison to individual grid cell estimates is not possible as errors likely remain high, whereas over broader regions these errors average away. For use in verification, near-real time estimates to short term forecasts of air-sea CO_2 fluxes are required. Addressing this need would incorporate machine learning methods with high-resolution process-based regional biogeochemical models (Fennel et al., 2023) along a “surface ocean carbon value chain” covering measuring, storing, synthesising, and mapping surface ocean carbon information (International Ocean Carbon Coordination Project, 2023). The development trajectory needed for large-scale data collection, assimilation, and output along a “surface ocean carbon value chain” could follow a path analogous to the historical development of weather forecasting (Namias, 1968; Teague and Gallicchio, 2017). The benefits of this system would extend beyond mCDR into ocean acidification ecosystem monitoring, and track the ocean carbon sink climate change response, informing policymakers of potential tipping points as well as necessary adjustment of emission reduction pledges.

Bibliography

Ahmed, M. and Else, B. G. T.: The Ocean CO 2 Sink in the Canadian Arctic Archipelago: A Present-Day Budget and Past Trends Due to Climate Change, Geophys. Res. Lett., 46, https://doi.org/10.1029/2019gl083547, 2019.

Ahmed, M. M. M., Else, B. G. T., Butterworth, B., and Capelle, D. W.: Widespread surface water pCO 2 undersaturation during ice-melt season in an Arctic continental shelf sea (Hudson Bay, Canada), Elem Sci Anth, 9, 1–22, https://doi.org/10.1525/elementa.2020.00130, 2021.

Alessa, L., Kliskey, A., Gamble, J., Fidel, M., Beaujean, G., and Gosz, J.: The role of Indigenous science and local knowledge in integrated observing systems: moving toward adaptive capacity indices and early warning systems, Sustain. Sci., 11, 91–102, https://doi.org/10.1007/s11625-015-0295-7, 2016.

Alexander, S. M., Provencher, J. F., Henri, D. A., Taylor, J. J., Lloren, J. I., Nanayakkara, L., Johnson, J. T., and Cooke, S. J.: Bridging Indigenous and science-based knowledge in coastal and marine research, monitoring, and management in Canada, Environ. Evid., 8, 1–24, https://doi.org/10.1186/s13750-019-0181-3, 2019.

Amari, S., Murata, N., Müller, K.-R., Finke, M., and Yang, H. H.: Asymptotic Statistical Theory of Overtraining and Cross-Validation, IEEE T Neural Netw., 8, 985–996, 1997.

Amaya, D. J., Miller, A. J., Xie, S. P., and Kosaka, Y.: Physical drivers of the summer 2019 North Pacific marine heatwave, Nat. Commun., 11, 1–9, https://doi.org/10.1038/s41467-020-15820-w, 2020.

Anderson, L. G. and Kaltin, S.: Carbon fluxes in the Arctic Ocean—potential impact by climate change, Polar Res., 20, 225–232, https://doi.org/10.3402/polar.v20i2.6521, 2001.

Anderson, L. G., Drange, H., Chierici, M., Fransson, A., Johannessen, T., Skjelvam, I., and Rey, F.: Annual carbon fluxes in the upper Greenland Sea based on measurements and a box-model approach, Tellus Ser. B Chem. Phys. Meteorol., 52, 1013–1024, https://doi.org/10.1034/j.1600-0889.2000.d01-9.x, 2000.

von Appen, W. J., Waite, A. M., Bergmann, M., Bienhold, C., Boebel, O., Bracher, A., Cisewski, B., Hagemann, J., Hoppema, M., Iversen, M. H., Konrad, C., Krumpen, T., Lochthofen, N., Metfies, K., Niehoff, B., Nöthig, E. M., Purser, A., Salter, I., Schaber, M., Scholz, D., Soltwedel, T., Torres-Valdes, S., Wekerle, C., Wenzhöfer, F., Wietz, M., and Boetius, A.: Sea-ice derived meltwater stratification slows the biological carbon pump: results from continuous observations, Nat. Commun., 12, 1–16, https://doi.org/10.1038/s41467-021-26943-z, 2021.

Ardhuin, F., Aksenov, Y., Benetazzo, A., Bertino, L., Brandt, P., Caubet, E., Chapron, B., Collard, F., Cravatte, S., Delouis, J. M., Dias, F., Dibarboure, G., Gaultier, L., Johannessen, J., Korosov, A., Manucharyan, G., Menemenlis, D., Menendez, M., Monnier, G., Mouche, A., Nouguier, F., Nurser, G., Rampal, P., Reniers, A., Rodriguez, E., Stopa, J., Tison, C., Ubelmann, C., Van Sebille, E., and Xie, J.: Measuring currents, ice drift, and waves from space: The Sea surface KInematics Multiscale monitoring (SKIM) concept, Ocean Sci., 14, 337–354, https://doi.org/10.5194/os-14-337-2018, 2018.

Aricò, S., Arrieta, J. M., Bakker, D. C. E., Boyd, P. W., Cotrim da Cunha, L., Chai, F., Dai, M., Gruber, N., Isensee, K., Ishii, M., Jiao, N., Lauvset, S. K., McKinley, G. A., Monteiro, P., Robinson, C., Sabine, C., Sanders, R., Schoo, K. L., Schuster, U., Shutler, J. D., Thomas, H., Wanninkhof, R., Watson, A. J., Bopp, L., Boss, E., Bracco, A., Cai, W., Fay, A., Feely, R. A., Gregor, L., Hauck, J., Heinze, C., Henson, S., Hwang, J., Post, J., Suntharalingam, P., Telszewski, M., Tilbrook, B., Valsala, V., and ojas Aldana, A.: Integrated Ocean Carbon Research: A Summary of Ocean Carbon Research, and Vision of Coordinated Ocean Carbon Research and Observations for the Next Decade, 46, https://doi.org/10.25607/h0gj-pq41, 2021.

Armstrong, J. L., Boldt, J. L., Cross, A. D., Moss, J. H., Davis, N. D., Myers, K. W., Walker, R. V., Beauchamp, D. A., and Haldorson, L. J.: Distribution, size, and interannual, seasonal and diel food habits of northern Gulf of Alaska juvenile pink salmon, Oncorhynchus gorbuscha, Deep-Sea Res. Part II Top. Stud. Oceanogr., 52, 247–265, https://doi.org/10.1016/j.dsr2.2004.09.019, 2005.

Arrigo, K. R., van Dijken, G., and Pabi, S.: Impact of a shrinking Arctic ice cover on marine primary production, Geophys. Res. Lett., 35, 1–6, https://doi.org/10.1029/2008GL035028, 2008.

Arrigo, K. R., Pabi, S., Van Dijken, G. L., and Maslowski, W.: Air-sea flux of CO2 in the Arctic Ocean, 1998-2003, J. Geophys. Res. Biogeosciences, 115, 1998–2003, https://doi.org/10.1029/2009JG001224, 2010.

Arrigo, K. R., Perovich, D. K., Pickart, R. S., Brown, Z. W., Van Dijken, G. L., Lowry, K. E., Mills, M. M., Palmer, M. A., Balch, W. M., Bahr, F., Bates, N. R., Benitez-nelson, C., Bowler, B., Brownlee, E., Ehn, J. K., Frey, K. E., Garley, R., Laney, S. R., Lubelczyk, L., Mathis, J., Matsuoka, A., Mitchell, B. G., Moore, G. W. K., Ortega-retuerta, E., Pal, S., Polashenski, C. M., Reynolds, R. A., Schieber, B., Sosik, H. M., Stephens, M., and Swift, J. H.: Massive Phytoplankton Blooms Under Arctic Sea Ice, Science, 336, 1408, https://doi.org/10.1126/science.1215065, 2012.

Årthun, M., Eldevik, T., and Smedsrud, L. H.: The role of Atlantic heat transport in future Arctic winter sea ice loss, J. Clim., 32, 3327–3341, https://doi.org/10.1175/JCLI-D-18-0750.1, 2019.

Asher, E., Dacey, J. W., Ianson, D., Peña, A., and Tortell, P. D.: Concentrations and cycling of DMS, DMSP, and DMSO in coastal and offshore waters of the Subarctic Pacific during summer, 2010-2011, J. Geophys. Res. Oceans, 122, 2647–2651, https://doi.org/10.1002/2016JC012465.Received, 2017.

Atamanchuk, D., Koelling, J., Send, U., and Wallace, D. W. R.: Rapid transfer of oxygen to the deep ocean mediated by bubbles, Nat. Geosci., 13, 232–237, https://doi.org/10.1038/s41561-020-0532-2, 2020.

Atlas, W., Housty, W., and Moore, J.: Indigenous Community Partnerships towards Foundational Understanding of Wild Salmon Survival, Tech. Rep., 69–70, https://doi.org/10.23849/npafctr15/69.70., 2019.

Aumont, O., Maier-Reimer, E., Blain, S., and Monfray, P.: An ecosystem model of the global ocean including Fe, Si, P colimitations, Glob. Biogeochem. Cycles, 17, https://doi.org/10.1029/2001gb001745, 2003.

Azetsu-Scott, K., Clarke, A., Falkner, K., Hamilton, J., Jones, E. P., Lee, C., Petrie, B., Prinsenberg, S., Starr, M., and Yeats, P.: Calcium carbonate saturation states in the waters of the Canadian Arctic Archipelago and the Labrador Sea, J. Geophys. Res. Oceans, 115, 1–18, https://doi.org/10.1029/2009JC005917, 2010.

Bach, L. T., Gill, S. J., Rickaby, R. E. M., Gore, S., and Renforth, P.: CO2 Removal With Enhanced Weathering and Ocean Alkalinity Enhancement: Potential Risks and Co-benefits for Marine Pelagic Ecosystems, Front. Clim., 1, https://doi.org/10.3389/fclim.2019.00007, 2019.

Baker, C. A., Martin, A. P., Yool, A., and Popova, E.: Biological Carbon Pump Sequestration Efficiency in the North Atlantic: A Leaky or a Long-Term Sink?, Glob. Biogeochem. Cycles, 36, https://doi.org/10.1029/2021gb007286, 2022.

Bakker, D. C. E., Pfeil, B., Landa, C. S., Metzl, N., O'Brien, K. M., Olsen, A., Smith, K., Cosca, C., Harasawa, S., Jones, S. D., Nakaoka, S. I., Nojiri, Y., Schuster, U., Steinhoff, T., Sweeney, C., Takahashi, T., Tilbrook, B., Wada, C., Wanninkhof, R., Alin, S. R., Balestrini, C. F., Barbero, L., Bates, N. R., Bianchi, A. A., Bonou, F., Boutin, J., Bozec, Y., Burger, E. F., Cai, W. J., Castle, R. D., Chen, L., Chierici, M., Currie, K., Evans, W., Featherstone, C., Feely, R. A., Fransson, A., Goyet, C., Greenwood, N., Gregor, L., Hankin, S., Hardman-Mountford, N. J., Harlay, J., Hauck, J., Hoppema, M., Humphreys, M. P., Hunt, C. W., Huss, B., Ibánhez, J. S. P., Johannessen, T., Keeling, R., Kitidis, V., Körtzinger, A., Kozyr, A., Krasakopoulou, E., Kuwata, A., Landschützer, P., Lauvset, S. K., Lefèvre, N., Lo Monaco, C., Manke, A., Mathis, J. T., Merlivat, L., Millero, F. J., Monteiro, P. M. S., Munro, D. R., Murata, A., Newberger, T., Omar, A. M., Ono, T., Paterson, K., Pearce, D., Pierrot, D., Robbins, L. L., Saito, S., Salisbury, J., Schlitzer, R., Schneider, B., Schweitzer, R., Sieger, R., Skjelvan, I., Sullivan, K. F., Sutherland, S. C., Sutton, A. J., Tadokoro, K., Telszewski, M., Tuma, M., Van Heuven, S. M. A. C., Vandemark, D., Ward, B., Watson, A. J., and Xu, S.: A multi-decade record of high-quality fCO2 data in version 3 of the Surface Ocean CO2 Atlas (SOCAT), Earth Syst. Sci. Data, 8, 383–413, https://doi.org/10.5194/essd-8-383-2016, 2016.

Balaguru, K., Doney, S. C., Bianucci, L., Rasch, P. J., Leung, L. R., Yoon, J. H., and Lima, I. D.: Linking deep convection and phytoplankton blooms in the northern Labrador Sea in a changing climate, PLoS ONE, 13, 1–17, https://doi.org/10.1371/journal.pone.0191509, 2018.

Ballinger, T. J., Bhatt, U. S., Bieniek, P. A., Brettschneider, B., Lader, R. T., Littell, J. S., Thoman, R. L., Waigl, C. F., Walsh, J. E., and Webster, M. A.: Alaska Terrestrial and Marine Climate Trends, 1957–2021, J. Clim., 36, 4375–4391, https://doi.org/10.1175/JCLI-D-22-0434.1, 2023.

Ban, N. C., Picard, C. R., and Vincent, A. C. J.: Comparing and integrating community-based and science-based approaches to prioritizing marine areas for protection, Conserv. Biol., 23, 899–910, https://doi.org/10.1111/j.1523-1739.2009.01185.x, 2009.

Ban, N. C., Frid, A., Reid, M., Edgar, B., Shaw, D., and Siwallace, P.: Incorporate Indigenous perspectives for impactful research and effective management, Nat. Ecol. Evol., 2, 1680–1683, https://doi.org/10.1038/s41559-018-0706-0, 2018.

Barbière, J., Isensee, K., and Schoo, K.: SDG 14.3.1 indicator methodology, 2019.

Barton, A., Hales, B., Waldbusser, G. G., Langdon, C., and Feelyd, R. A.: The Pacific oyster, Crassostrea gigas, shows negative correlation to naturally elevated carbon dioxide levels: Implications for near-term ocean acidification effects, Limnol. Oceanogr., 57, 698–710, https://doi.org/10.4319/lo.2012.57.3.0698, 2012.

Bates, N. R. and Mathis, J. T.: The Arctic Ocean marine carbon cycle: evaluation of air-sea CO2 exchanges, ocean acidification impacts and potential feedbacks, Biogeosciences, 6, 2433–2459, https://doi.org/10.5194/bg-6-2433-2009, 2009.

Bates, N. R., Moran, S. B., Hansell, D. A., and Mathis, J. T.: An increasing CO2 sink in the Arctic Ocean due to sea-ice loss, Geophys. Res. Lett., 33, L23609, https://doi.org/10.1029/2006GL027028, 2006.

Batten, S. D. and Crawford, W. R.: The influence of coastal origin eddies on oceanic plankton distributions in the eastern Gulf of Alaska, Deep-Sea Res. Part II Top. Stud. Oceanogr., 52, 991–1009, https://doi.org/10.1016/j.dsr2.2005.02.009, 2005.

Bauer, J. E., Cai, W.-J., Raymond, P. A., Bianchi, T. S., Hopkinson, C. S., and Regnier, P. A. G.: The changing carbon cycle of the coastal ocean, Nature, 504, 61–70, https://doi.org/10.1038/nature12857, 2013.

Bednaršek, N., Pelletier, G., Ahmed, A., Feely, R. A., and Krumhardt, K. M.: Chemical Exposure Due to Anthropogenic Ocean Acidification Increases Risks for Estuarine Calcifiers in the Salish Sea : Biogeochemical Model Scenarios, Front. Mar. Sci., 7, 1–19, https://doi.org/10.3389/fmars.2020.00580, 2020.

Bélair, S., Roch, M., Leduc, A.-M., Vaillancourt, P. A., Laroche, S., and Mailhot, J.: Medium-Range Quantitative Precipitation Forecasts from Canada's New 33-km Deterministic Global Operational System, Weather Forecast., 24, 690–708, https://doi.org/10.1175/2008WAF2222175.1, 2009.

Benway, H., Alin, S., Boyer, E., Cai, W. J., Coble, P., Cross, J., Friedrichs, M., Goñi, M., Griffith, P., Herrmann, M., Lohrenz, S., Mathis, J., McKinley, G., Najjar, R., Pilskaln, C., Siedlecki, S., and Smith, R.: A Science Plan for Carbon Cycle Research in North American Coastal Waters. Report of the Coastal CARbon Synthesis (CCARS) community workshop, August 19-21, 2014, , 84, https://doi.org/10.1575/1912/7777, 2016.

Bianucci, L., Denman, K. L., and Ianson, D.: Low oxygen and high inorganic carbon on the Vancouver Island Shelf, J. Geophys. Res. Oceans, 116, 1–20, https://doi.org/10.1029/2010JC006720, 2011.

Bishop, B., Oliver, E. C. J., and Aporta, C.: Co-producing maps as boundary objects: Bridging Labrador Inuit knowledge and oceanographic research, J. Cult. Geogr., 39, 55–89, https://doi.org/10.1080/08873631.2021.1998992, 2022.

Bittig, H. C., Steinhoff, T., Claustre, H., Fiedler, B., Williams, N. L., Sauzède, R., Körtzinger, A., and Gattuso, J. P.: An alternative to static climatologies: Robust estimation of open ocean CO2 variables and nutrient concentrations from T, S, and O2 data using Bayesian neural networks, Front. Mar. Sci., 5, 1–29, https://doi.org/10.3389/fmars.2018.00328, 2018.

Bittig, H. C., Maurer, T. L., Plant, J. N., Schmechtig, C., Wong, A. P. S., Claustre, H., Trull, T. W., Udaya Bhaskar, T. V. S., Boss, E., Dall'Olmo, G., Organelli, E., Poteau, A., Johnson, K. S., Hanstein, C., Leymarie, E., Le Reste, S., Riser, S. C., Rupan, A. R., Taillandier, V., Thierry, V., and Xing, X.: A BGC-Argo Guide: Planning, Deployment, Data Handling and Usage, Front. Mar. Sci., 6, https://doi.org/10.3389/fmars.2019.00502, 2019.

Boldt, J. L. and Haldorson, L. J.: Seasonal and Geographic Variation in Juvenile Pink Salmon Diets in the Northern Gulf of Alaska and Prince William Sound, Trans. Am. Fish. Soc., 132, 1035–1052, https://doi.org/10.1577/t02-091, 2003.

Bond, N. A., Cronin, M. F., Freeland, H., and Mantua, N.: Causes and impacts of the 2014 warm anomaly in the NE Pacific, Geophys. Res. Lett., 42, 3414–3420, https://doi.org/10.1002/2015GL063306, 2015.

Borges, A. V., Delille, B., and Frankignoulle, M.: Budgeting sinks and sources of CO2 in the coastal ocean: Diversity of ecosystem counts, Geophys. Res. Lett., 32, L14601, https://doi.org/10.1029/2005GL023053, 2005.

Bourgeois, T., Orr, J. C., Resplandy, L., Terhaar, J., Ethé, C., Gehlen, M., Bopp, L., Ipsl, L., and Paris-saclay, U.: Coastal-ocean uptake of anthropogenic carbon, Biogeosciences, 13, 4167–4185, https://doi.org/10.5194/bg-13-4167-2016, 2016.

Bourgeois, T., Goris, N., Schwinger, J., and Tjiputra, J. F.: Stratification constrains future heat and carbon uptake in the Southern Ocean between 30°S and 55°S, Nat. Commun., 13, 1–8, https://doi.org/10.1038/s41467-022-27979-5, 2022.

Boyce, J. K.: Carbon Pricing: Effectiveness and Equity, Ecol. Econ., 150, 52–61, https://doi.org/10.1016/j.ecolecon.2018.03.030, 2018.

Boyd, P. W., Strzepek, R., Jackson, G., Wong, C. S., Mckay, R. M., Law, C., Sherry, N., Johnson, K., and Gower, J.: The evolution and termination of an iron-induced mesoscale bloom in the northeast subarctic Pacific, Limnol. Oceanogr., 50, 1872–1886, https://doi.org/10.4319/lo.2005.50.6.1872, 2005.

Boyd, P. W., Jickells, T., Law, C. S., Blain, S., Boyle, E. A., Buesseler, K. O., Coale, K. H., Cullen, J. J., Baar, H. J. W. D., Follows, M., Harvey, M., Lancelot, C., and Levasseur, M.: Mesoscale Iron Enrichment Experiments 1993 – 2005: Synthesis and Future Directions, Science, 315, 612–618, https://doi.org/10.1126/science.1131669, 2007.

Boyd, P. W., Claustre, H., Levy, M., Siegel, D. A., and Weber, T.: Multi-faceted particle pumps drive carbon sequestration in the ocean, Nature, 568, 327–335, https://doi.org/10.1038/s41586-019-1098-2, 2019.

Bozhkov, E., Walker, C., McCourt, V., and Castleden, H.: Are the natural sciences ready for truth, healing, and reconciliation with Indigenous peoples in Canada? Exploring 'settler readiness' at a world-class freshwater research station, J. Environ. Stud. Sci., 10, 226–241, https://doi.org/10.1007/s13412-020-00601-0, 2020.

Brady, R. X., Lovenduski, N. S., Alexander, M. A., Jacox, M., and Gruber, N.: On the role of climate modes in modulating the air-sea CO 2 fluxes in eastern boundary upwelling systems, Biogeosciences, 16, 329–346, https://doi.org/10.5194/bg-16-329-2019, 2019.

Breckwoldt, A., Lopes, P. F. M., and Selim, S. A.: Look Who's Asking—Reflections on Participatory and Transdisciplinary Marine Research Approaches, Front. Mar. Sci., 8, https://doi.org/10.3389/fmars.2021.627502, 2021.

Briggs, N., Perry, M. J., Cetinić, I., Lee, C., D'Asaro, E., Gray, A. M., and Rehm, E.: High-resolution observations of aggregate flux during a sub-polar North Atlantic spring bloom, Deep-Sea Res. Part Oceanogr. Res. Pap., 58, 1031–1039, https://doi.org/10.1016/j.dsr.2011.07.007, 2011.

British Columbia Ocean Acidification and Hypoxia Action Plan Advisory Committee: British Columbia Ocean Acidification and Hypoxia Action Plan, Ministry of Agriculture and Food, Province of British Columbia, 2023.

Broecker, W. S.: A revised estimate for the radiocarbon age of North Atlantic deep water, J. Geophys. Res., 84, 3218, https://doi.org/10.1029/jc084ic06p03218, 1979.

Broullón, D., Pérez, F. F., Velo, A., Hoppema, M., Olsen, A., Takahashi, T., Key, R. M., González-Dávila, M., Tanhua, T., Jeansson, E., Kozyr, A., and van Heuven, S. M. A. C.: A global monthly climatology of total alkalinity: a neural network approach, Earth Syst. Sci. Data Discuss., 2013, 1–31, https://doi.org/10.5194/essd-2018-111, 2018.

Bushinsky, S. M., Landschützer, P., Rödenbeck, C., Gray, A. R., Baker, D., Mazloff, M. R., Resplandy, L., Johnson, K. S., and Sarmiento, J. L.: Reassessing Southern Ocean Air-Sea CO2 Flux Estimates With the Addition of Biogeochemical Float Observations, Glob. Biogeochem. Cycles, 33, 1370–1388, https://doi.org/10.1029/2019GB006176, 2019.

Butterworth, B. J. and Else, B. G. T.: Dried, closed-path eddy covariance method for measuring carbon dioxide flux over sea ice, Atmos Meas Tech, 11, 6075–6090, https://doi.org/10.5194/amt-11-6075-2018, 2018.

Bylhouwer, B., Ianson, D., and Kohfeld, K.: Changes in the onset and intensity of wind-driven upwelling and downwelling along the North American Pacific coast, J. Geophys. Res. Oceans, 118, 2565–2580, https://doi.org/10.1002/jgrc.20194, 2013.

Cai, W.-J., Dai, M., and Wang, Y.: Air-sea exchange of carbon dioxide in ocean margins: A province-based synthesis, Geophys. Res. Lett., 33, https://doi.org/10.1029/2006GL026219, 2006.

Capotondi, A., Alexander, M. A., Bond, N. A., Curchitser, E. N., and Scott, J. D.: Enhanced upper ocean stratification with climate change in the CMIP3 models, J. Geophys. Res., 117, C04031, https://doi.org/10.1029/2011JC007409, 2012.

Carley, S. and Konisky, D. M.: The justice and equity implications of the clean energy transition, Nat. Energy, 5, 569–577, https://doi.org/10.1038/s41560-020-0641-6, 2020.

Carroll, S. R., Garba, I., Figueroa-Rodríguez, O. L., Holbrook, J., Lovett, R., Materechera, S., Parsons, M., Raseroka, K., Rodriguez-Lonebear, D., Rowe, R., Sara, R., Walker, J. D., Anderson, J., and Hudson, M.: The CARE Principles for Indigenous Data Governance, Data Sci. J., 19, 43, https://doi.org/10.5334/dsj-2020-043, 2020.

Carter, B. R., Toggweiler, J. R., Key, R. M., and Sarmiento, J. L.: Processes determining the marine alkalinity and calcium carbonate saturation state distributions, Biogeosciences, 11, 7349–7362, https://doi.org/10.5194/bg-11-7349-2014, 2014.

Carter, B. R., Williams, N. L., Gray, A. R., and Feely, R. A.: Locally interpolated alkalinity regression for global alkalinity estimation, Limnol. Oceanogr. Methods, 14, 268–277, https://doi.org/10.1002/lom3.10087, 2016.

Carter, B. R., Feely, R. A., Williams, N. L., Dickson, A. G., Fong, M. B., and Takeshita, Y.: Updated methods for global locally interpolated estimation of alkalinity, pH, and nitrate, Limnol. Oceanogr. Methods, 16, 119–131, https://doi.org/10.1002/lom3.10232, 2018.

Carter, B. R., Feely, R. A., Wanninkhof, R., Kouketsu, S., Sonnerup, R. E., Pardo, P. C., Sabine, C. L., Johnson, G. C., Sloyan, B. M., Murata, A., Mecking, S., Tilbrook, B., Speer, K., Talley, L. D., Millero, F. J., Wijffels, S. E., Macdonald, A. M., Gruber, N., and Bullister, J. L.: Pacific Anthropogenic Carbon Between 1991 and 2017, Glob. Biogeochem. Cycles, 33, 597–617, https://doi.org/10.1029/2018GB006154, 2019.

Chai, F., Johnson, K. S., Claustre, H., Xing, X., Wang, Y., Boss, E., Riser, S., Fennel, K., Schofield, O., and Sutton, A.: Monitoring ocean biogeochemistry with autonomous platforms, Nat. Rev. Earth Environ., 1, 315–326, https://doi.org/10.1038/s43017-020-0053-y, 2020.

Chan, F., Barth, J. A., Blanchette, C. A., Byrne, R. H., Chavez, F., Cheriton, O., Feely, R. A., Friederich, G., Gaylord, B., Gouhier, T., Hacker, S., Hill, T., Hofmann, G., McManus, M. A., Menge, B. A., Nielsen, K. J., Russell, A., Sanford, E., Sevadjian, J., and Washburn, L.: Persistent spatial structuring of coastal ocean acidification in the California Current System, Sci. Rep., 7, 1–7, https://doi.org/10.1038/s41598-017-02777-y, 2017.

Chapman, C. C., Monselesan, D. P., Risbey, J. S., Feng, M., and Sloyan, B. M.: A large-scale view of marine heatwaves revealed by archetype analysis, Nat. Commun., 13, 7843, https://doi.org/10.1038/s41467-022-35493-x, 2022.

Chau, T. T. T., Gehlen, M., and Chevallier, F.: A seamless ensemble-based reconstruction of surface ocean pCO2 and air-sea CO2 fluxes over the global coastal and open oceans, Biogeosciences, 19, 1087–1109, https://doi.org/10.5194/bg-19-1087-2022, 2022.

Chavez, F. P., Takahashi, T., Cai, W. J., Friederich, G., Hales, B., Wanninkhof, R., and Feely, R. A.: Coastal oceans, in: The First State of the Carbon Cycle Report (SOCCR): The North American Carbon Budget and Implications for the Global Carbon Cycle, US Climate Change Science Program, Washington, DC, 157–166, 2007.

Chen, C.-T. A. and Borges, A. V.: Reconciling opposing views on carbon cycling in the coastal ocean: Continental shelves as sinks and near-shore ecosystems as sources of atmospheric CO2, Deep-Sea Res. Part II Top. Stud. Oceanogr., 56, 578–590, https://doi.org/10.1016/j.dsr2.2008.12.009, 2009.

Chen, S., Hu, C., Byrne, R. H., Robbins, L. L., and Yang, B.: Remote estimation of surface pCO2 on the West Florida Shelf, Cont. Shelf Res., 128, 10–25, https://doi.org/10.1016/j.csr.2016.09.004, 2016.

Chen, S., Hu, C., Barnes, B. B., Wanninkhof, R., Cai, W. J., Barbero, L., and Pierrot, D.: A machine learning approach to estimate surface ocean pCO2 from satellite measurements, Remote Sens. Environ., 228, 203–226, https://doi.org/10.1016/j.rse.2019.04.019, 2019.

Chen, Z., Shi, J., Liu, Q., Chen, H., and Li, C.: A Persistent and Intense Marine Heatwave in the Northeast Pacific During 2019–2020, Geophys. Res. Lett., 48, 1–9, https://doi.org/10.1029/2021GL093239, 2021.

Cheng, W., Chiang, J. C. H., and Zhang, D.: Atlantic meridional overturning circulation (AMOC) in CMIP5 Models: RCP and historical simulations, J. Clim., 26, 7187–7197, https://doi.org/10.1175/JCLI-D-12-00496.1, 2013.

Chierici, M., Fransson, A., and Nojiri, Y.: Biogeochemical processes as drivers of surface fCO2 in contrasting provinces in the subarctic North Pacific Ocean, Glob. Biogeochem. Cycles, 20, 1–16, https://doi.org/10.1029/2004GB002356, 2006.

Christensen, J. P.: Carbon export from continental shelves, denitrification and atmospheric carbon dioxide, Cont. Shelf Res., 14, 547–576, https://doi.org/10.1016/0278-4343(94)90103-1, 1994.

Clement, D. and Gruber, N.: The eMLR (C *) Method to Determine Decadal Changes in the Global Ocean Storage of Anthropogenic CO 2, 654–679, https://doi.org/10.1002/2017GB005819, 2018.

Cooley, S. R., Klinsky, S., Morrow, D. R., and Satterfield, T.: Sociotechnical Considerations About Ocean Carbon Dioxide Removal, Annu. Rev. Mar. Sci., 15, 41–66, https://doi.org/10.1146/annurev-marine-032122-113850, 2023.

Côté, J., Gravel, S., Méthot, A., Patoine, A., Roch, M., and Staniforth, A.: The Operational CMC–MRB Global Environmental Multiscale (GEM) Model. Part I: Design Considerations and Formulation, Mon. Weather Rev., 126, 1373–1395, https://doi.org/10.1175/1520-0493(1998)126<1373:TOCMGE>2.0.CO;2, 1998.

Coyle, K. O., Cheng, W., Hinckley, S. L., Lessard, E. J., Whitledge, T., Hermann, A. J., and Hedstrom, K.: Model and field observations of effects of circulation on the timing and magnitude of nitrate utilization and production on the northern Gulf of Alaska shelf, Prog. Oceanogr., 103, 16–41, https://doi.org/10.1016/j.pocean.2012.03.002, 2012.

Crawford, W. R. and Whitney, F. A.: Mesoscale eddy aswirl with data in Gulf of Alaska, Eos, 80, 365–370, https://doi.org/10.1029/EO080i033p00365-01, 1999.

Crawford, W. R., Brickley, P. J., and Thomas, A. C.: Mesoscale eddies dominate surface phytoplankton in northern Gulf of Alaska, Prog. Oceanogr., 75, 287–303, https://doi.org/10.1016/j.pocean.2007.08.016, 2007.

Cross, J. N., Gledhill, D. K., Sweeney, C., Butler, J., Jewett, E. B., Feely, R. A., Theuerkauf, S., Stein, T., Kitch, G., Alin, S., Barbero, L., Briggs, R., Chu, S., Dunne, J. P., John, J. G., Harris, J., Krepp, A., Longmire, K., Litzow, M., Mcelhany, P., Sutton, A., Tedesco, K., Vaughan, L., and Alexander, S.: NOAA Carbon Dioxide Removal Research: A White Paper documenting a Potential NOAA CDR Science Strategy as an element of NOAA's Climate Mitigation Portfolio, National Oceanic and Atmospheric Administration, 2022.

Cross, J. N., Sweeney, C., Jewett, E. B., Feely, R. A., McElhany, P., Carter, B., Stein, T., Kitch, G. D., and Gledhill, D. K.: Strategy for NOAA Carbon Dioxide Removal (CDR) Research: A White Paper documenting a potential NOAA CDR Science Strategy as an element of NOAA's Climate Interventions Portfolio, https://doi.org/10.25923/gzke-8730, 2023.

Crossland, C. J., Kremer, H. H., Lindeboom, H. J., Marshall Crossland, J. I., and LeTissier, M. D. A.: Coastal Fluxes in the Anthropocene: The Land-Ocean Interactions in the Coastal Zone, Springer-Verlag, Berlin, Heidelberg, Germany, 2005.

Cummins, P. F. and Ross, T.: Secular trends in water properties at Station P in the northeast Pacific : An updated analysis, Prog. Oceanogr., 186, 102329, https://doi.org/10.1016/j.pocean.2020.102329, 2020.

Cummins, P. F., Lagerloef, G. S. E., and Mitchum, G.: A regional index of northeast Pacific variability based on satellite altimeter data, Geophys. Res. Lett., 32, https://doi.org/10.1029/2005GL023642, 2005.

Dai, M.: What are the exchanges of carbon between the land-ocean-ice continuum?, in: Integrated ocean carbon research: a summary of ocean carbon research, and vision of coordinated ocean carbon research and observations for the next decade, Intergovernmental Oceanographic Commission, Paris, France, 20, 2021.

Dai, M., Su, J., Zhao, Y., Hofmann, E. E., Cao, Z., Cai, W., Gan, J., Lacroix, F., Laruelle, G. G., Meng, F., Müller, J. D., Regnier, P. A. G., Wang, G., and Wang, Z.: Carbon Fluxes in the Coastal Ocean: Synthesis, Boundary Processes, and Future Trends, Annu. Rev. Earth Planet. Sci., 50, 593–626, https://doi.org/10.1146/annurev-earth-032320-090746, 2022.

Dall'Olmo, G., Dingle, J., Polimene, L., Brewin, R. J. W., and Claustre, H.: Substantial energy input to the mesopelagic ecosystem from the seasonal mixed-layer pump, Nat. Geosci., 9, 820–823, https://doi.org/10.1038/ngeo2818, 2016.

Davies, H. N., Gould, J., Hovey, R. K., Radford, B., and Kendrick, G. A.: Mapping the Marine Environment Through a Cross-Cultural Collaboration, Front. Mar. Sci., 7, 1–15, https://doi.org/10.3389/fmars.2020.00716, 2020.

DeGrandpre, M., Evans, W., Timmermans, M.-L., Krishfield, R., Williams, B., and Steele, M.: Changes in the Arctic Ocean Carbon Cycle With Diminishing Ice Cover, Geophys. Res. Lett., 47, e2020GL088051, https://doi.org/10.1029/2020GL088051, 2020.

DeGrandpre, M. D., Körtzinger, A., Send, U., Wallace, D. W. R., and Bellerby, R. G. J.: Uptake and sequestration of atmospheric CO2 in the Labrador Sea deep convection region, Geophys. Res. Lett., 33, 1–5, https://doi.org/10.1029/2006GL026881, 2006.

DeGrandpre, M. D., Lai, C. Z., Timmermans, M. L., Krishfield, R. A., Proshutinsky, A., and Torres, D.: Inorganic Carbon and pCO2 Variability During Ice Formation in the Beaufort Gyre of the Canada Basin, J. Geophys. Res. Oceans, 124, 4017–4028, https://doi.org/10.1029/2019JC015109, 2019.

Denvil-Sommer, A., Gehlen, M., Vrac, M., and Mejia, C.: LSCE-FFNN-v1: A two-step neural network model for the reconstruction of surface ocean pCO2 over the global ocean, Geosci. Model Dev., 12, 2091–2105, https://doi.org/10.5194/gmd-12-2091-2019, 2019.

Deprez, A., Leadley, P., Dooley, K., Williamson, P., Cramer, W., Gattuso, J.-P., Rankovic, A., Carlson, E. L., and Creutzig, F.: Sustainability limits needed for CO2 removal, Science, 383, 484–486, https://doi.org/10.1126/science.adj6171, 2024.

Devries, T.: The oceanic anthropogenic CO2 sink: Storage, air-sea fluxes, and transports over the industrial era, Glob. Biogeochem. Cycles, 28, 631–647, https://doi.org/10.1002/2013GB004739, 2014.

DeVries, T., Le Quéré, C., Andrews, O., Berthet, S., Hauck, J., Ilyina, T., Landschützer, P., Lenton, A., Lima, I. D., Nowicki, M., Schwinger, J., and Séférian, R.: Decadal trends in the ocean carbon sink, Proc. Natl. Acad. Sci. U. S. A., 116, 11646–11651, https://doi.org/10.1073/pnas.1900371116, 2019.

deYoung, B., Frajka-Williams, E., Oppeln-Bronikowski, N. von, and Woodward, S.: Technicalities: exploring the Labrador sea with autonomous vehicles, J. Ocean Technol., 15, 134–139, 2020.

Di Lorenzo, E. and Mantua, N.: Multi-year persistence of the 2014/15 North Pacific marine heatwave, Nat. Clim. Change, 6, 1042–1047, https://doi.org/10.1038/nclimate3082, 2016.

Di Lorenzo, E., Schneider, N., Cobb, K. M., Franks, P. J. S., Chhak, K., Miller, A. J., McWilliams, J. C., Bograd, S. J., Arango, H., Curchitser, E., Powell, T. M., and Rivière, P.: North Pacific Gyre Oscillation links ocean climate and ecosystem change, Geophys. Res. Lett., 35, 2–7, https://doi.org/10.1029/2007GL032838, 2008.

Dickson, A. G., Sabine, C. L., and Christian, J. R.: Guide to Best Practices for Ocean CO2 Measurements, 191 pp., 2007.

Diggon, S., Butler, C., Heidt, A., Bones, J., Jones, R., and Outhet, C.: The Marine Plan Partnership: Indigenous community-based marine spatial planning, Mar. Policy, 132, 103510, https://doi.org/10.1016/j.marpol.2019.04.014, 2021.

Diggon, S., Bones, J., Short, C. J., Smith, J. L., Dickinson, M., Wozniak, K., Topelko, K., and Pawluk, K. A.: The Marine Plan Partnership for the North Pacific Coast – MaPP: A collaborative and co-led marine planning process in British Columbia, Mar. Policy, 142, 104065, https://doi.org/10.1016/j.marpol.2020.104065, 2022.

Dinauer, A. and Mucci, A.: Spatial variability in surface-water pCO2 and gas exchange in the world's largest semi-enclosed estuarine system: St. Lawrence Estuary (Canada), Biogeosciences, 14, 3221–3237, https://doi.org/10.5194/bg-14-3221-2017, 2017.

Dinauer, A. and Mucci, A.: Distinguishing between physical and biological controls on the spatial variability of pCO2: A novel approach using OMP water mass analysis (St. Lawrence, Canada), Mar. Chem., 204, 107–120, https://doi.org/10.1016/j.marchem.2018.03.007, 2018.

Dion, J., Kanduth, A., Moorhouse, J., and Beugin, D.: Canada's net zero future: Finding our way in the global transition, , 131, 2021.

Doney, S. C., Ruckelshaus, M., Emmett Duffy, J., Barry, J. P., Chan, F., English, C. A., Galindo, H. M., Grebmeier, J. M., Hollowed, A. B., Knowlton, N., Polovina, J., Rabalais, N. N., Sydeman, W. J., and Talley, L. D.: Climate change impacts on marine ecosystems, Annu. Rev. Mar. Sci., 4, 11–37, https://doi.org/10.1146/annurev-marine-041911-111611, 2012.

Doney, S. C., Busch, D. S., Cooley, S. R., and Kroeker, K. J.: The Impacts of Ocean Acidification on Marine Ecosystems and Reliant Human Communities, Annu. Rev. Environ. Resour., 45, 83–112, https://doi.org/10.1146/annurev-environ-012320- 083019, 2020.

Dong, Y., Bakker, D. C. E., Bell, T. G., Huang, B., Landschützer, P., Liss, P. S., and Yang, M.: Update on the Temperature Corrections of Global Air-Sea CO2 Flux Estimates, Glob. Biogeochem. Cycles, 36, https://doi.org/10.1029/2022GB007360, 2022.

Dorman, C. E. and Winant, C. D.: Buoy observations of the atmosphere along the west coast of the United States, 1981-1990, J. Geophys. Res., 100, 16029–16044, 1995.

Drever, C. R., Cook-Patton, S. C., Akhter, F., Badiou, P. H., Chmura, G. L., Davidson, S. J., Desjardins, R. L., Dyk, A., Fargione, J. E., Fellows, M., Filewod, B., Hessing-Lewis, M., Jayasundara, S., Keeton, W. S., Kroeger, T., Lark, T. J., Le, E., Leavitt, S. M., LeClerc, M. E., Lemprière, T. C., Metsaranta, J., McConkey, B., Neilson, E., St-Laurent, G. P., Puric-Mladenovic, D., Rodrigue, S., Soolanayakanahally, R. Y., Spawn, S. A., Strack, M., Smyth, C., Thevathasan, N., Voicu, M., Williams, C. A., Woodbury, P. B., Worth, D. E., Xu, Z., Yeo, S., and Kurz, W. A.: Natural climate solutions for Canada, Sci. Adv., 7, 1–14, https://doi.org/10.1126/sciadv.abd6034, 2021.

Dugdale, R. C. and Wilkerson, F. P.: Low Specific Nitrate Uptake Rate: A Common Feature of High-Nutrient, Low-Chlorophyll Marine Ecosystems, Limnol. Oceanogr., 36, 1678–1688, https://doi.org/10.4319/lo.1991.36.8.1678, 1991.

Duke, P. J., Else, B., Miller, L. A., Sastri, A. R., Gonski, S. F., Jones, S., Marriott, S., Dewey, R. K., and Thomas, H.: Seasonal Marine Carbon System Processes in an Arctic Coastal Landfast Sea Ice Environment Using an Innovative Underwater Sensor Platform, Elem Sci Anth, 9, 1–21, https://doi.org/10.1525/elementa.2021.00103, 2021.

Duke, P. J., Hamme, R. C., Ianson, D., Landschützer, P., Ahmed, M. M. M., Swart, N. C., and Covert, P. A.: ANN-NEP: A monthly surface pCO2 product for the Northeast Pacific open ocean from 1998-01-01 to 2019-12-31 (NCEI Accession 0277836), https://doi.org/10.25921/c1w8-6v02, 2023a.

Duke, P. J., Richaud, B., Arruda, R., Länger, J., Schuler, K., Gooya, P., Ahmed, M. M. M., Miller, M. R., Braybrook, C. A., Kam, K., Piunno, R., Sezginer, Y., Nickoloff, G., and Franco, A. C.: Canada's marine carbon sink: an early career perspective on the state of research and existing knowledge gaps, Facets, 8, 1–21, https://doi.org/10.1139/facets-2022-0214, 2023b.

Duke, P. J., Hamme, R. C., Ianson, D., Landschützer, P., Ahmed, M. M. M., Swart, N. C., and Covert, P. A.: Estimating marine carbon uptake in the northeast Pacific using a neural network approach, Biogeosciences, 20, 3919–3941, https://doi.org/10.5194/bg-20-3919-2023, 2023c.

Duke, P. J., Hamme, R. C., Ianson, D., Landschützer, P., Swart, N. C., and Covert, P. A.: ANN-NEPc: A monthly surface pCO2 product for the Northeast Pacific coastal ocean from 1998-01-01 to 2019-12-31 (NCEI Accession 0290365), 2024.

Durack, P. J., Wijffels, S. E., and Matear, R. J.: Ocean Salinities Reveal Strong Global Water Cycle Intensification During 1950 to 2000, Science, 336, 455–459, https://doi.org/10.1126/science.1212222, 2012.

Durand, F., Piecuch, C. G., Becker, M., Papa, F., Raju, S. V., Khan, J. U., and Ponte, R. M.: Impact of Continental Freshwater Runoff on Coastal Sea Level, Surv. Geophys., 40, 1437–1466, https://doi.org/10.1007/s10712-019-09536-w, 2019.

Eger, S. L., Stephenson, R. L., Armitage, D., Flannery, W., and Courtenay, S. C.: Revisiting Integrated Coastal and Marine Management in Canada: Opportunities in the Bay of Fundy, Front. Mar. Sci., 8, 1–20, https://doi.org/10.3389/fmars.2021.652778, 2021.

Ekstrom, J. A., Suatoni, L., Cooley, S. R., Pendleton, L. H., Waldbusser, G. G., Cinner, J. E., Ritter, J., Langdon, C., Van Hooidonk, R., Gledhill, D., Wellman, K., Beck, M. W., Brander, L. M., Rittschof, D., Doherty, C., Edwards, P. E. T., and Portela, R.: Vulnerability and adaptation of US shellfisheries to ocean acidification, Nat. Clim. Change, 5, 207–214, https://doi.org/10.1038/nclimate2508, 2015.

Else, B. G. T., Papakyriakou, T. N., Granskog, M. A., and Yackel, J. J.: Observations of sea surface fCO2 distributions and estimated air-sea CO2 fluxes in the Hudson Bay region (Canada) during the open water season, J. Geophys. Res. Oceans, 113, 1–12, https://doi.org/10.1029/2007JC004389, 2008a.

Else, B. G. T., Yackel, J. J., and Papakyriakou, T. N.: Remote Sensing of Environment Application of satellite remote sensing techniques for estimating air – sea CO 2 fl uxes in Hudson Bay , Canada during the ice-free season, 112, 3550–3562, https://doi.org/10.1016/j.rse.2008.04.013, 2008b.

Else, B. G. T., Papakyriakou, T. N., Galley, R. J., Drennan, W. M., Miller, L. A., and Thomas, H.: Wintertime CO2 fluxes in an Arctic polynya using eddy covariance: Evidence for enhanced air-sea gas transfer during ice formation, J. Geophys. Res., 116, 1–15, https://doi.org/10.1029/2010JC006760, 2011.

Else, B. G. T., Papakyriakou, T. N., Asplin, M. G., Barber, D. G., Galley, R. J., Miller, L. A., and Mucci, A.: Annual cycle of air-sea CO2 exchange in an Arctic Polynya Region, Glob. Biogeochem. Cycles, 27, 388–398, https://doi.org/10.1002/gbc.20016, 2013.

England, M. H.: The Age of Water and Ventilation Timescales in a Global Ocean Model, J. Phys. Oceanogr., 25, 2756–2777, https://doi.org/10.1175/1520-0485(1995)025<2756:TAOWAV>2.0.CO;2, 1995.

Environment and Climate Change Canada: 2019 Canadian Carbon Cycle Research Workshop: report on key gaps and next steps, 1–20 pp., 2020.

Espinosa, A. L.: Determination of the acidification state of Canadian Pacific coastal waters using empirical relationships with hydrographic data, University of Victoria, 2012.

Geoengineering Map: https://map.geoengineeringmonitor.org/, last access: 6 October 2023.

Evans, W. and Mathis, J. T.: The Gulf of Alaska coastal ocean as an atmospheric CO2 sink, Cont. Shelf Res., 65, 52–63, https://doi.org/10.1016/j.csr.2013.06.013, 2013.

Evans, W., Hales, B., and Strutton, P. G.: Seasonal cycle of surface ocean p CO $_2$ on the Oregon shelf, J. Geophys. Res., 116, C05012, https://doi.org/10.1029/2010JC006625, 2011.

Evans, W., Hales, B., Strutton, P. G., and Ianson, D.: Sea-air CO 2 fluxes in the western Canadian coastal ocean, Prog. Oceanogr., 101, 78–91, https://doi.org/10.1016/j.pocean.2012.01.003, 2012.

Evans, W., Mathis, J. T., Winsor, P., Statscewich, H., and Whitledge, T. E.: A regression modeling approach for studying carbonate system variability in the northern Gulf of Alaska, J. Geophys. Res. Oceans, 118, 476–489, https://doi.org/10.1029/2012JC008246, 2013a.

Evans, W., Hales, B., and Strutton, P. G.: pCO2 distributions and air–water CO2 fluxes in the Columbia River estuary, Estuar. Coast. Shelf Sci., 117, 260–272, https://doi.org/10.1016/j.ecss.2012.12.003, 2013b.

Evans, W., Mathis, J. T., and Cross, J. N.: Calcium carbonate corrosivity in an Alaskan inland sea, Biogeosciences, 11, 365–379, https://doi.org/10.5194/bg-11-365-2014, 2014.

Evans, W., Hales, B., Strutton, P. G., Shearman, R. K., and Barth, J. A.: Failure to bloom: Intense upwelling results in negligible phytoplankton response and prolonged CO2 outgassing over the Oregon shelf, J. Geophys. Res. Oceans, 120, 1446–1461, https://doi.org/10.1002/2014JC010580, 2015a.

Evans, W., Mathis, J. T., Cross, J. N., Bates, N. R., Frey, K. E., Else, B. G. T., Papkyriakou, T. N., DeGrandpre, M. D., Islam, F., Cai, Wei.-Jun., Chen, B., Yamamoto-Kawai, M., Carmack, E., Williams, William. J., and Takahashi, T.: Sea-air CO2 exchange in the western Arctic coastal ocean, Glob. Biogeochem. Cycles, n/a-n/a, https://doi.org/10.1002/2015GB005153, 2015b.

Evans, W., Pocock, K., Hare, A., Weekes, C., Hales, B., Jackson, J., Gurney-Smith, H., Mathis, J. T., Alin, S. R., and Feely, R. A.: Marine CO2 patterns in the Northern Salish Sea, Front. Mar. Sci., 5, 1–18, https://doi.org/10.3389/fmars.2018.00536, 2019.

Evans, W., Lebon, G. T., Harrington, C. D., Takeshita, Y., Bidlack, A., and Bay, H.: Marine CO2 system variability along the northeast Pacific Inside Passage determined from an Alaskan ferry, Biogeosciences, 19, 1277–1301, https://doi.org/10.5194/bg-19-1277-2022, 2022.

Fabry, V. J., Seibel, B. A., Feely, R. A., and Orr, J. C.: Impacts of ocean acidification on marine biodiversity, ICES J. Mar. Sci., 65, 414–432, https://doi.org/10.1093/icesjms/fsn048, 2008.

Fabry, V. J., McClintock, J. B., Mathis, J. T., and Grebmeier, J. M.: Ocean acidification at high latitudes: The Bellwether, Oceanography, 22, 160–171, https://doi.org/10.5670/oceanog.2009.105, 2009.

Fassbender, A. J., Rodgers, K. B., Palevsky, H. I., and Sabine, C. L.: Seasonal Asymmetry in the Evolution of Surface Ocean pCO2 and pH Thermodynamic Drivers and the Influence on Sea-Air CO2 Flux, Glob. Biogeochem. Cycles, 32, 1476–1497, https://doi.org/10.1029/2017GB005855, 2018a.

Fassbender, A. J., Alin, S. R., Feely, R. A., Sutton, A. J., Newton, J. A., Krembs, C., Bos, J., Keyzers, M., Devol, A., Ruef, W., and Pelletier, G.: Seasonal carbonate chemistry variability in marine surface waters of the US Pacific Northwest, Earth Syst. Sci. Data, 10, 1367–1401, https://doi.org/10.5194/essd-10-1367-2018, 2018b.

Fay, A. R. and McKinley, G. A.: Global trends in surface ocean pCO2 from in situ data, Glob. Biogeochem. Cycles, 27, 541–557, https://doi.org/10.1002/gbc.20051, 2013a.

Fay, A. R. and McKinley, G. A.: Global trends in surface ocean pCO2 from in situ data, Glob. Biogeochem. Cycles, 27, 541–557, https://doi.org/10.1002/gbc.20051, 2013b.

Fay, A. R., Gregor, L., Landschützer, P., McKinley, G. A., Gruber, N., Gehlen, M., Iida, Y., Laruelle, G. G., Rödenbeck, C., Roobaert, A., and Zeng, J.: SeaFlux: Harmonization of air-sea CO2 fluxes from surface pCO2 data products using a standardized approach, Earth Syst. Sci. Data, 13, 4693–4710, https://doi.org/10.5194/essd-13-4693-2021, 2021.

Feely, R. A., Sabine, C. L., Lee, K., Berelson, W., Kleypas, J., Fabry, V. J., and Millero, F. J.: Impact of anthropogenic CO2 on the CaCO3 system in the oceans, Science, 305, 362–366, https://doi.org/10.1126/science.1097329, 2004.

Feely, R. A., Sabine, C. L., Hernandez-Ayon, J. M., Ianson, D., and Hales, B.: Evidence for upwelling of corrosive “acidified” water onto the continental shelf, Science, 320, 1490–1492, https://doi.org/10.1126/science.1155676, 2008.

Feely, R. A., Sabine, C. L., Byrne, R. H., Millero, F. J., Dickson, A. G., Wanninkhof, R., Murata, A., Miller, L. A., and Greeley, D.: Decadal changes in the aragonite and calcite saturation state of the Pacific Ocean, Glob. Biogeochem. Cycles, 26, 1–15, https://doi.org/10.1029/2011GB004157, 2012.

Fennel, K., Alin, S., Barbero, L., Evans, W., Bourgeois, T., Cooley, S., Dunne, J., Feely, R. A., Hernandez-Ayon, J. M., Hu, X., Lohrenz, S., Muller-Karger, F., Najjar, R., Robbins, L., Shadwick, E., Siedlecki, S., Steiner, N., Sutton, A., Turk, D., Vlahos, P., and Wang, Z. A.: Carbon Cycling in the North American Coastal Ocean: A Synthesis, Biogeosciences, 16, 1281–1304, https://doi.org/10.5194/bg-16-1281-2019, 2019.

Fennel, K., Long, M. C., Algar, C., Carter, B., Keller, D., Laurent, A., Mattern, J. P., Musgrave, R., Oschlies, A., Ostiguy, J., Palter, J. B., and Whitt, D. B.: Modelling considerations for research on ocean alkalinity enhancement (OAE), State Planet, 2-oae2023, 1–29, https://doi.org/10.5194/sp-2-oae2023-9-2023, 2023.

Fiechter, J. and Moore, A. M.: Interannual spring bloom variability and Ekman pumping in the coastal Gulf of Alaska, J. Geophys. Res. Oceans, 114, https://doi.org/10.1029/2008JC005140, 2009.

Aquaculture Value Added: https://www.dfo-mpo.gc.ca/stats/aqua/va19pub-eng.htm, last access: 21 March 2022.

Seafisheries Value Added: https://www.dfo-mpo.gc.ca/stats/cfs-spc/tab/cfs-spc-tab1-eng.htm, last access: 21 March 2022.

Fong, C. and MacDougall, S.: Engineered Carbon Dioxide Removal in a Net-Zero Canada: Opportunities and challenges for non-biological CDR deployment, The Pembina Institute, Calgary, Alberta, Canada, 2023.

Ford, D. J., Tilstone, G. H., Shutler, J. D., Kitidis, V., Lobanova, P., Schwarz, J., Poulton, A. J., Serret, P., Lamont, T., Chuqui, M., Barlow, R., Lozano, J., Kampel, M., and Brandini, F.: Wind speed and mesoscale features drive net autotrophy in the South Atlantic Ocean, Remote Sens. Environ., 260, 112435, https://doi.org/10.1016/j.rse.2021.112435, 2021.

Ford, D. J., Tilstone, G. H., Shutler, J. D., and Kitidis, V.: Derivation of seawater p CO 2 from net community production identifies the South Atlantic Ocean as a CO 2 source, Biogeosciences, 19, 93–115, https://doi.org/10.5194/bg-19-93-2022, 2022a.

Ford, D. J., Tilstone, G. H., Shutler, J. D., and Kitidis, V.: Identifying the biological control of the annual and multi-year variations in South Atlantic air-sea CO2flux, Biogeosciences, 19, 4287–4304, https://doi.org/10.5194/bg-19-4287-2022, 2022b.

Ford, J. D. and Smit, B.: A Framework for the Vulnerability of Communities Arctic Assessing to Risks Associated with Climate Change, Arcticic, 57, 389–400, 2004.

Ford, J. D., Berrang-Ford, L., King, M., and Furgal, C.: Vulnerability of Aboriginal health systems in Canada to climate change, Glob. Environ. Change, 20, 668–680, https://doi.org/10.1016/j.gloenvcha.2010.05.003, 2010.

Ford, J. D., Sherman, M., Berrang-Ford, L., Llanos, A., Carcamo, C., Harper, S., Lwasa, S., Namanya, D., Marcello, T., Maillet, M., and Edge, V.: Preparing for the health impacts of climate change in Indigenous communities: The role of community-based adaptation, Glob. Environ. Change, 49, 129–139, https://doi.org/10.1016/j.gloenvcha.2018.02.006, 2018.

Fourrier, M., Coppola, L., Claustre, H., D'Ortenzio, F., Sauzède, R., and Gattuso, J. P.: A Regional Neural Network Approach to Estimate Water-Column Nutrient Concentrations and Carbonate System Variables in the Mediterranean Sea: CANYON-MED, Front. Mar. Sci., 7, 1–20, https://doi.org/10.3389/fmars.2020.00620, 2020.

Franco, A. C., Ianson, D., Ross, T., Hamme, R. C., Monahan, A. H., Christian, J. R., Davelaar, M., Johnson, W. K., Miller, L. A., Robert, M., and Tortell, P. D.: Anthropogenic and climatic contributions to observed carbon system trends in the Northeast Pacific, Glob. Biogeochem. Cycles, 1–21, https://doi.org/10.1029/2020gb006829, 2021.

Fransson, A., Chierici, M., Anderson, L. G., Bussman, I., Kattner, G., Jones, E. P., and Swift, J. H.: The importance of shelf processes for the modification of chemical constituents in the waters of the eastern Arctic Ocean. Cont. Shelf Res., 21 , 225-242, 2001, Cont. Shelf Res., 21, 225–242, 2001.

Freeland, H.: A short history of Ocean Station Papa and Line P, Prog. Oceanogr., 75, 120–125, https://doi.org/10.1016/j.pocean.2007.08.005, 2007.

Freeland, H. and Ross, T.: 'The Blob' - or, how unusual were ocean temperatures in the Northeast Pacific during 2014-2018?, Deep-Sea Res. Part Oceanogr. Res. Pap., 150, 103061, https://doi.org/10.1016/j.dsr.2019.06.007, 2019.

Freeland, H. J.: Evidence of Change in the Winter Mixed Layer in the Northeast Pacific Ocean : A Problem Revisited, Atmosphere-Ocean, 51, 126–133, https://doi.org/10.1080/07055900.2012.754330, 2013.

Freeland, H. J., Crawford, W. R., and Thomson, R. E.: Currents along the pacific coast of canada, Atmosphere - Ocean, 22, 151–172, https://doi.org/10.1080/07055900.1984.9649191, 1984.

Friedlingstein, P., Sullivan, M. O., Jones, M. W., Andrew, R. M., Gregor, L., Hauck, J., Quéré, C. L., Luijkx, I. T., Olsen, A., Peters, G. P., and Peters, W.: Global Carbon Budget 2022, Earth Syst. Sci. Data, 14, 4811–4900, https://doi.org/10.5194/essd-14-4811-2022, 2022a.

Friedlingstein, P., Sullivan, M. O., Jones, M. W., Andrew, R. M., Gregor, L., Hauck, J., Quéré, C. L., Luijkx, I. T., Olsen, A., Peters, G. P., and Peters, W.: Global Carbon Budget 2022, Earth Syst. Sci. Data, 14, 4811–4900, https://doi.org/10.5194/essd-14-4811-2022, 2022b.

Friedlingstein, P., O'Sullivan, M., Jones, M. W., Andrew, R. M., Bakker, D. C. E., Hauck, J., Landschützer, P., Le Quéré, C., Luijkx, I. T., Peters, G. P., Peters, W., Pongratz, J., Schwingshackl, C., Sitch, S., Canadell, J. G., Ciais, P., Jackson, R. B., Alin, S. R., Anthoni, P., Barbero, L., Bates, N. R., Becker, M., Bellouin, N., Decharme, B., Bopp, L., Brasika, I. B. M., Cadule, P., Chamberlain, M. A., Chandra, N., Chau, T.-T.-T., Chevallier, F., Chini, L. P., Cronin, M., Dou, X., Enyo, K., Evans, W., Falk, S., Feely, R. A., Feng, L., Ford, D. J., Gasser, T., Ghattas, J., Gkritzalis, T., Grassi, G., Gregor, L., Gruber, N., Gürses, Ö., Harris, I., Hefner, M., Heinke, J., Houghton, R. A., Hurtt, G. C., Iida, Y., Ilyina, T., Jacobson, A. R., Jain, A., Jarníková, T., Jersild, A., Jiang, F., Jin, Z., Joos, F., Kato, E., Keeling, R. F., Kennedy, D., Klein Goldewijk, K., Knauer, J., Korsbakken, J. I., Körtzinger, A., Lan, X., Lefèvre, N., Li, H., Liu, J., Liu, Z., Ma, L., Marland, G., Mayot, N., McGuire, P. C., McKinley, G. A., Meyer, G., Morgan, E. J., Munro, D. R., Nakaoka, S.-I., Niwa, Y., O'Brien, K. M., Olsen, A., Omar, A. M., Ono, T., Paulsen, M., Pierrot, D., Pocock, K., Poulter, B., Powis, C. M., Rehder, G., Resplandy, L., Robertson, E., Rödenbeck, C., Rosan, T. M., Schwinger, J., Séférian, R., et al.: Global Carbon Budget 2023, Earth Syst. Sci. Data, 15, 5301–5369, https://doi.org/10.5194/essd-15-5301-2023, 2023.

Friedrich, T. and Oschlies, A.: Neural network-based estimates of North Atlantic surface pCO2 from satellite data: A methodological study, J. Geophys. Res. Oceans, 114, 1–12, https://doi.org/10.1029/2007JC004646, 2009.

Frölicher, T. L., Sarmiento, J. L., Paynter, D. J., Dunne, J. P., Krasting, J. P., and Winton, M.: Dominance of the Southern Ocean in anthropogenic carbon and heat uptake in CMIP5 models, J. Clim., 28, https://doi.org/10.1175/JCLI-D-14-00117.1, 2015.

Frölicher, T. L., Fischer, E. M., and Gruber, N.: Marine heatwaves under global warming, Nature, 560, 360–364, https://doi.org/10.1038/s41586-018-0383-9, 2018.

Gannon, K. E. and Hulme, M.: Geoengineering at the "Edge of the World": Exploring perceptions of ocean fertilisation through the Haida Salmon Restoration Corporation, Geo Geogr. Environ., 5, e00054, https://doi.org/10.1002/geo2.54, 2018.

Gargett, A. E.: Physical processes and the maintenance of nutrient-rich euphotic zones, Limnol. Oceanogr., 36, 1527–1545, https://doi.org/10.4319/lo.1991.36.8.1527, 1991.

Gasset, N., Fortin, V., Dimitrijevic, M., Carrera, M., Bilodeau, B., Muncaster, R., Gaborit, É., Roy, G., Pentcheva, N., Bulat, M., Wang, X., Pavlovic, R., Lespinas, F., Khedhaouiria, D., and Mai, J.: A 10 km North American precipitation and land-surface reanalysis based on the GEM atmospheric model, Hydrol. Earth Syst. Sci., 25, 4917–4945, https://doi.org/10.5194/hess-25-4917-2021, 2021.

Gaudry, A. and Lorenz, D.: Indigenization as inclusion, reconciliation, and decolonization: navigating the different visions for indigenizing the Canadian Academy, AlterNative, 14, 218–227, https://doi.org/10.1177/1177180118785382, 2018.

GESAMP: High level review of a wide range of proposed marine geoengineering techniques, GESAMP Reports and Studies, Joint Group of Experts on the Scientific Aspects of Marine Environmental Protections, 2019.

Global Ocean Surface Carbon, E.U. Copernicus Marine Service Information MULTIOBS_GLO_BIO_CARBON_SURFACE_REP_015_008:

Global Ocean Physical Reanalysis Product, E.U. Copernicus Marine Service Information GLOBAL_REANALYSIS_PHY_001_030:

Gloege, L., McKinley, G. A., Landschützer, P., and Fay, A. R.: Quantifying Errors in Observationally Based Estimates of Ocean Carbon Sink Variability Global Biogeochemical Cycles, Glob. Biogeochem. Cycles, 35, https://doi.org/10.1029/2020GB006788, 2021.

Goddijn-Murphy, L. M., Woolf, D. K., Land, P. E., Shutler, J. D., and Donlon, C.: The OceanFlux Greenhouse Gases methodology for deriving a sea surface climatology of CO2 fugacity in support of air-sea gas flux studies, Ocean Sci., 11, 519–541, https://doi.org/10.5194/os-11-519-2015, 2015.

Godlewska, A. M. C., Schaefli, L. M., Forcione, M., Lamb, C., Nelson, E., and Talan, B.: Canadian colonialism, ignorance and education. A study of graduating students at Queen's University, J. Pedagogy, 11, 147–176, https://doi.org/10.2478/jped-2020-0008, 2020.

ESA Sea Surface Temperature Climate Change Initiative (SST_cci): Level 4 Analysis Climate Data Record, version 2.1:

Gooya, P., Swart, N. C., and Hamme, R. C.: Time-varying changes and uncertainties in the CMIP6 ocean carbon sink from global to local scale, Earth Syst. Dyn., 14, 383–398, https://doi.org/10.5194/esd-14-383-2023, 2023.

Government of British Columbia: Roadmap to 2030, Government of British Columbia, Victoria, BC Canada, 2021.

Government of British Columbia: A Coastal Marine Strategy for British Columbia: Policy Intentions Paper, Government of British Columbia, 2022.

Government of Canada: Pan-Canadian Framework on Clean Growth and Climate Change : Canada's plan to address climate change and grow the economy., 86 pp., 2016.

A collaborative framework for joint DFO/NOAA ocean acidification research and monitoring: https://www.dfo-mpo.gc.ca/science/publications/accasp-psaccma/noaa-collaborative/index-eng.html, last access: 2 April 2023.

Greene, C. A., Blankenship, D. D., Gwyther, D. E., Silvano, A., and van Wijk, E.: Wind causes Totten Ice Shelf melt and acceleration, Sci. Adv., 3, e1701681, https://doi.org/10.1126/sciadv.1701681, 2017.

Greene, C. A., Thirumalai, K., Kearney, K. A., Delgado, J. M., Schwanghart, W., Wolfenbarger, N. S., Thyng, K. M., Gwyther, D. E., Gardner, A. S., and Blankenship, D. D.: The Climate Data Toolbox for MATLAB, Geochem. Geophys. Geosystems, 20, 3774–3781, https://doi.org/10.1029/2019GC008392, 2019.

Greenfield, P.: Revealed: more than 90% of rainforest carbon offsets by biggest certifier are worthless, analysis shows, The Guardian, 18th January, 2023.

Gregor, L., Kok, S., and Monteiro, P. M. S.: Interannual drivers of the seasonal cycle of CO2 in the Southern Ocean, Biogeosciences, 15, 2361–2378, https://doi.org/10.5194/bg-15-2361-2018, 2018.

Griffin, B. J., Kohfeld, K. E., Cooper, A. B., and Boenisch, G.: Importance of location for describing typical and extreme wind speed behavior, Geophys. Res. Lett., 37, https://doi.org/10.1029/2010GL045052, 2010.

Gruber, N., Clement, D., Carter, B. R., Feely, R. A., van Heuven, S., Hoppema, M., Ishii, M., Key, R. M., Kozyr, A., Lauvset, S. K., Monaco, C. L., Mathis, J. T., Murata, A., Olsen, A., Perez, F. F., Sabine, C. L., Tanhua, T., and Wanninkhof, R.: The oceanic sink for anthropogenic CO2 from 1994 to 2007, Science, 363, 1193–1199, https://doi.org/10.1126/science.aau5153, 2019a.

Gruber, N., Landschutzer, P., and Lovenduski, N. S.: The variable southern ocean carbon sink, Annu. Rev. Mar. Sci., 11, https://doi.org/10.1146/annurev-marine-121916- 063407, 2019b.

Gruber, N., Bakker, D. C. E., Devries, T., Gregor, L., Hauck, J., Landschützer, P., Mckinley, G. A., and Müller, J. D.: Trends and variability in the ocean carbon sink, Nat. Rev. Earth Environ., 1–16, https://doi.org/10.1038/s43017-022-00381-x, 2023.

Haggan, N., Jackson, G. D., and Lacroix, P.: Salmon and Eulachon in Ecosystem Space and Time: A Plea for Wider Collaboration and Data Integration, Chall. Diadromous Fishes Dyn. Glob. Environ., 69, 619–636, 2009.

Haigh, R., Ianson, D., Holt, C. A., Neate, H. E., and Edwards, A. M.: Effects of ocean acidification on temperate coastal marine ecosystems and fisheries in the northeast pacific, PLoS ONE, 10, 1–46, https://doi.org/10.1371/journal.pone.0117533, 2015.

Hales, B., Takahashi, T., and Bandstra, L.: Atmospheric CO2 uptake by a coastal upwelling system, Glob. Biogeochem. Cycles, 19, https://doi.org/10.1029/2004GB002295, 2005.

Hales, B., Strutton, P. G., Saraceno, M., Letelier, R., Takahashi, T., Feely, R., Sabine, C., and Chavez, F.: Satellite-based prediction of pCO 2 in coastal waters of the eastern North Pacific, Prog. Oceanogr., 103, 1–15, https://doi.org/10.1016/j.pocean.2012.03.001, 2012.

Hall, A., Cox, P., Huntingford, C., and Klein, S.: Progressing emergent constraints on future climate change, Nat. Clim. Change, 9, 269–278, https://doi.org/10.1038/s41558-019-0436-6, 2019.

Hall, M. M., Torres, D. J., and Yashayaev, I.: Absolute velocity along the AR7W section in the Labrador Sea, Deep-Sea Res. Part Oceanogr. Res. Pap., 72, 72–87, https://doi.org/10.1016/j.dsr.2012.11.005, 2013.

Hamme, R. C., Webley, P. W., Crawford, W. R., Whitney, F. A., Degrandpre, M. D., Emerson, S. R., Eriksen, C. C., Giesbrecht, K. E., Gower, J. F. R., Kavanaugh, M. T., Pea, M. A., Sabine, C. L., Batten, S. D., Coogan, L. A., Grundle, D. S., and Lockwood, D.: Volcanic ash fuels anomalous plankton bloom in subarctic northeast Pacific, Geophys. Res. Lett., 37, 1–5, https://doi.org/10.1029/2010GL044629, 2010.

Hansell, D. A., Carlson, C. A., Repeta, D. J., and Schlitzerography, R.: Dissolved organic matter in the ocean: A controversy stimulates new insights, Oceanography, 22, 202–211, 2009.

Hansson, L., Appeltans, W., and Gattuso, J.-P.: Promoting International Collaboration on Ocean Acidification Data Management, Eos Trans. Am. Geophys. Union, 95, 421–422, https://doi.org/10.1002/2014EO460006, 2014.

Harrison, P. J., Boyd, P. W., Varela, D. E., Takeda, S., Shiomoto, A., and Odate, T.: Comparison of factors controlling phytoplankton productivity in the NE and NW subarctic Pacific gyres, Prog. Oceanogr., 43, 205–234, https://doi.org/10.1016/S0079-6611(99)00015-4, 1999.

Hauck, J., Zeising, M., Le Quéré, C., Gruber, N., Bakker, D. C. E., Bopp, L., Chau, T. T. T., Gürses, Ö., Ilyina, T., Landschützer, P., Lenton, A., Resplandy, L., Rödenbeck, C., Schwinger, J., and Séférian, R.: Consistency and Challenges in the Ocean Carbon Sink Estimate for the Global Carbon Budget, Front. Mar. Sci., 7, 1–22, https://doi.org/10.3389/fmars.2020.571720, 2020.

Hauri, C., Schultz, C., Hedstrom, K., Danielson, S., Irving, B., C. Doney, S., Dussin, R., N. Curchitser, E., F. Hill, D., and A. Stock, C.: A regional hindcast model simulating ecosystem dynamics, inorganic carbon chemistry, and ocean acidification in the Gulf of Alaska, Biogeosciences, 17, 3837–3857, https://doi.org/10.5194/bg-17-3837-2020, 2020.

Hauri, C., Pagès, R., McDonnell, A. M. P., Stuecker, M. F., Danielson, S. L., Hedstrom, K., Irving, B., Schultz, C., and Doney, S. C.: Modulation of ocean acidification by decadal climate variability in the Gulf of Alaska, Commun. Earth Environ., 2, 1–7, https://doi.org/10.1038/s43247-021-00254-z, 2021.

Hermann, A. J., Hinckley, S., Dobbins, E. L., Haidvogel, D. B., Bond, N. A., Mordy, C., Kachel, N., and Stabeno, P. J.: Quantifying cross-shelf and vertical nutrient flux in the Coastal Gulf of Alaska with a spatially nested, coupled biophysical model, Deep Sea Res. Part II Top. Stud. Oceanogr., 56, 2474–2486, https://doi.org/10.1016/j.dsr2.2009.02.008, 2009.

Hersbach, H., Bell, B., Berrisford, P., Hirahara, S., Horányi, A., Muñoz-Sabater, J., Nicolas, J., Peubey, C., Radu, R., Schepers, D., Simmons, A., Soci, C., Abdalla, S., Abellan, X., Balsamo, G., Bechtold, P., Biavati, G., Bidlot, J., Bonavita, M., De Chiara, G., Dahlgren, P., Dee, D., Diamantakis, M., Dragani, R., Flemming, J., Forbes, R., Fuentes, M., Geer, A., Haimberger, L., Healy, S., Hogan, R. J., Hólm, E., Janisková, M., Keeley, S., Laloyaux, P., Lopez, P., Lupu, C., Radnoti, G., de Rosnay, P., Rozum, I., Vamborg, F., Villaume, S., and Thépaut, J.-N.: The ERA5 global reanalysis, Q. J. R. Meteorol. Soc., 146, 1999–2049, https://doi.org/10.1002/qj.3803, 2020.

Ho, D. T.: Carbon dioxide removal is not a current climate solution — we need to change the narrative, Nature, 616, 9–9, https://doi.org/10.1038/d41586-023-00953-x, 2023a.

Ho, D. T.: Carbon dioxide removal is not a current climate solution — we need to change the narrative, Nature, 616, 9–9, https://doi.org/10.1038/d41586-023-00953-x, 2023b.

Ho, D. T., Bopp, L., Palter, J. B., Long, M. C., Boyd, P. W., Neukermans, G., and Bach, L. T.: Monitoring, reporting, and verification for ocean alkalinity enhancement, State Planet, 2-oae2023, 1–12, https://doi.org/10.5194/sp-2-oae2023-12-2023, 2023.

Horwitz, R. M., Hay, A. E., Burt, W. J., Cheel, R. A., Salisbury, J., and Thomas, H.: High-frequency variability of CO2 in Grand Passage, Bay of Fundy, Nova Scotia, Biogeosciences, 16, 605–616, https://doi.org/10.5194/bg-16-605-2019, 2019.

Hristova, H. G., Ladd, C., and Stabeno, P. J.: Variability and Trends of the Alaska Gyre From Argo and Satellite Altimetry, J. Geophys. Res. Oceans, 124, 5870–5887, https://doi.org/10.1029/2019JC015231, 2019.

Hsieh, W. W.: Machine Learning Methods in the Environmental Sciences: Neural Networks and Kernels, Cambridge University Press, Vancouver, BC, Canada, 364 pp., 2009.

Hsieh, W. W., Ware, D. A., and Thornson, R. E.: Wind-induced upwelling along the west coast of North America, 1899-1988, Can. J. Fish. Aquat. Sci., 52, 325–334, 1995.

Hunter, K. L., Ross, A. R. S., Ianson, D., Miller, L. A., Pearce, C. M., Christian, J. R., and Pena, M. A.: Pacific Ocean Acidification Working Group – 2014 / 2015 Report. Canadian Manuscript Report of Fisheries and Aquatic Sciences 3070, 2015.

Hurd, C. L., Law, C. S., Bach, L. T., Britton, D., Hovenden, M., Paine, E., Raven, J. A., Tamsitt, V., and Boyd, P. W.: Forensic carbon accounting: Assessing the role of seaweeds for carbon sequestration, J. Phycol., 58, 347–363, https://doi.org/10.1111/jpy.13249, 2022.

Ianson, D. and Allen, S. E.: A two-dimensional nitrogen and carbon flux model in a coastal upwelling region, Glob. Biogeochem. Cycles, 16, 2002.

Ianson, D., Allen, S. E., Harris, S. L., Orians, K. J., Varela, D. E., and Wong, C. S.: The inorganic carbon system in the coastal upwelling region west of Vancouver Island, Canada, Deep-Sea Res. Part Oceanogr. Res. Pap., 50, 1023–1042, https://doi.org/10.1016/S0967-0637(03)00114-6, 2003.

Ianson, D., Feely, R. A., Sabine, C. L., and Juranek, L. W.: Features of coastal upwelling regions that determine net air-sea CO 2 flux, J. Oceanogr., 65, 677–687, https://doi.org/10.1007/s10872-009-0059-z, 2009.

Ianson, D., Völker, C., Denman, K. L., Kunze, E., and Steiner, N.: The effect of vertical and horizontal dilution on fertilized patch experiments, Glob. Biogeochem. Cycles, 26, 1–14, https://doi.org/10.1029/2010GB004008, 2012.

Ianson, D., Allen, S. E., Moore-Maley, B. L., Johannessen, S. C., and Macdonald, R. W.: Vulnerability of a semienclosed estuarine sea to ocean acidification in contrast with hypoxia, Geophys. Res. Lett., 43, 5793–5801, https://doi.org/10.1002/2016GL068996, 2016.

International Ocean Carbon Coordination Project: Declaration on Operationalising the Surface Ocean Carbon Value Chain, International Ocean Carbon Coordination Project, Oostende, Belgium, 2023.

Inuit Tapiriit Kanatami: National Inuit Strategy on Research: Implementation Plan, 22 pp., 2018.

IPCC: IPCC, 2013: Climate Change 2013: The Physical Science Basis. Contribution of Working Group I to the Fifth Assessment Report of the Intergovernmental Panel on Climate Change, Intergovernmental Panel of Climate Change, https://doi.org/10.1017/CBO9781107415324, 2013.

IPCC: Chapter 5: Changing ocean, marine ecosystems, and dependent communities, Intergov. Panel Clim. Change Spec. Rep. Ocean Cryosphere Chang. Clim., 1–198, 2019.

IPCC: AR6 Synthesis Report: Climate Change 2023 — IPCC, Cambridge University Press, Cambridge University Press, Cambridge, UK and New York, NY, USA, 2023a.

IPCC: Climate Change 2022 – Impacts, Adaptation and Vulnerability: Working Group II Contribution to the Sixth Assessment Report of the Intergovernmental Panel on Climate Change, 1st ed., Cambridge University Press, https://doi.org/10.1017/9781009325844, 2023b.

Islam, F., DeGrandpre, M., Beatty, C., Krishfield, R., and Toole, J.: Gas exchange of CO_2 and O_2 in partially ice-covered regions of the Arctic Ocean investigated using *in situ* sensors, IOP Conf. Ser. Earth Environ. Sci., 35, 012018, https://doi.org/10.1088/1755-1315/35/1/012018, 2016.

Izett, R. W., Castro de la Guardia, L., Chanona, M., Myers, P. G., Waterman, S., and Tortell, P. D.: Impact of Vertical Mixing on Summertime Net Community Production in Canadian Arctic and Subarctic Waters: Insights From In Situ Measurements and Numerical Simulations, J. Geophys. Res. Oceans, 127, 1–26, https://doi.org/10.1029/2021JC018215, 2022.

Jackson, J. M., Myers, P. G., and Ianson, D.: An examination of mixed layer sensitivity in the northeast Pacific Ocean from July 2001–July 2005 using the general ocean turbulence model and Argo data, Atmosphere-Ocean, 47, 139–153, https://doi.org/10.3137/OC308.2009, 2009.

Jarníková, T., Olson, E. M., Allen, S. E., Ianson, D., and Suchy, K. D.: A clustering approach to determine biophysical provinces and physical drivers of productivity dynamics in a complex coastal sea, Ocean Sci., 18, 1451–1475, https://doi.org/10.5194/os-18-1451-2022, 2022a.

Jarníková, T., Ianson, D., Allen, S. E., Shao, A., and Olson, E. M.: Anthropogenic carbon increase has caused critical shifts in aragonite saturation across a sensitive coastal system, Glob. Biogeochem. Cycles, https://doi.org/10.1029/2021GB007024, 2022b.

Jean-Michel, L., Eric, G., Romain, B.-B., Gilles, G., Angélique, M., Marie, D., Clément, B., Mathieu, H., and Lea, D. J.: The Copernicus Global 1 / 12 ° Oceanic and Sea Ice GLORYS12 Reanalysis, Front. Earth Sci., 9, 1–27, https://doi.org/10.3389/feart.2021.698876, 2021.

Jiang, L. Q., Feely, R. A., Wanninkhof, R., Greeley, D., Barbero, L., Alin, S., Carter, B. R., Pierrot, D., Featherstone, C., Hooper, J., Melrose, C., Monacci, N., Sharp, J. D., Shellito, S., Xu, Y. Y., Kozyr, A., Byrne, R. H., Cai, W. J., Cross, J., Johnson, G. C., Hales, B., Langdon, C., Mathis, J., Salisbury, J., and Townsend, D. W.: Coastal Ocean Data Analysis Product in North America (CODAP-NA)-an internally consistent data product for discrete inorganic carbon, oxygen, and nutrients on the North American ocean margins, Earth Syst. Sci. Data, 13, 2777–2799, https://doi.org/10.5194/essd-13-2777-2021, 2021.

Jones, D. C., Ito, T., Takano, Y., and Hsu, W.: Spatial and seasonal variability of the air-sea equilibration timescale of carbon dioxide, Glob. Biogeochem. Cycles, 28, 1163–1178, https://doi.org/10.1002/2014GB004813, 2014.

Jones, S. D., Le Quéré, C., and Rdenbeck, C.: Autocorrelation characteristics of surface ocean pCO2 and air-sea CO2 fluxes, Glob. Biogeochem. Cycles, 26, 1–12, https://doi.org/10.1029/2010GB004017, 2012.

Juranek, L. W., Feely, R. A., Gilbert, D., Freeland, H., and Miller, L. A.: Real-time estimation of pH and aragonite saturation state from Argo profiling floats: Prospects for an autonomous carbon observing strategy, Geophys. Res. Lett., 38, 1–7, https://doi.org/10.1029/2011GL048580, 2011.

Kalnay, E., Kanamitsu, M., Kistler, R., Collins, W., Deaven, D., Gandin, L., Iredell, M., Saha, S., White, G., Woollen, J., Zhu, Y., Chelliah, M., Ebisuzaki, W., Higgins, W., Janowiak, J., Mo, K. C., Ropelewski, C., Wang, J., Leetmaa, A., Reynolds, R., Jenne, R., and Joseph, D.: The NCEP/NCAR 40-Year Reanalysis Project, Bull. Am. Meteorol. Soc., 77, 437–472, https://doi.org/10.1175/1520-0477(1996)077<0437:TNYRP>2.0.CO;2, 1996.

Kaltin, S., Anderson, L. G., Olsson, K., Fransson, A., and Chierici, M.: Uptake of atmospheric carbon dioxide in the Barents Sea, J. Mar. Syst., 38, 31–45, https://doi.org/10.1016/S0924-7963(02)00168-9, 2002.

Kanamitsu, M., Ebisuzaki, W., Woollen, J., Yang, S.-K., Hnilo, J. J., Fiorino, M., and Potter, G. L.: NCEP–DOE AMIP-II Reanalysis (R-2), Bull. Am. Meteorol. Soc., 83, 1631–1644, https://doi.org/10.1175/BAMS-83-11-1631, 2002.

Kater, I.: Natural and Indigenous sciences: reflections on an attempt to collaborate, Reg. Environ. Change, 22, 109, https://doi.org/10.1007/s10113-022-01967-3, 2022.

Kenny, T. A., Archambault, P., Ayotte, P., Batal, M., Chan, H. M., Cheung, W., Eddy, T. D., Little, M., Ota, Y., Pétrin-Desrosiers, C., Plante, S., Poitras, J., Polanco, F., Singh, G., and Lemire, M.: Oceans and human health—navigating changes on Canada's coasts, Facets, 5, 1037–1070, https://doi.org/10.1139/FACETS-2020-0035, 2020.

Keppler, L., Landschützer, P., Gruber, N., Lauvset, S. K., and Stemmler, I.: Seasonal Carbon Dynamics in the Near-Global Ocean, Glob. Biogeochem. Cycles, 34, e2020GB006571, https://doi.org/10.1029/2020GB006571, 2020.

Kessler, W. S.: Mean Three-Dimensional Circulation in the Northeast Tropical Pacific, J. Phys. Oceanogr., 32, 2457–2471, https://doi.org/10.1175/1520-0485(2002)032<2457:MTDCIT>2.0.CO;2, 2002.

Khatiwala, S., Tanhua, T., Mikaloff Fletcher, S., Gerber, M., Doney, S. C., Graven, H. D., Gruber, N., McKinley, G. A., Murata, A., Ríos, A. F., and Sabine, C. L.: Global ocean storage of anthropogenic carbon, Biogeosciences, 10, 2169–2191, https://doi.org/10.5194/bg-10-2169-2013, 2013.

Körtzinger, A.: Determination of carbon dioxide partial pressure (pCO2), in: Methods of Seawater Analysis, Verlag Chemie, 149–158, 1999.

Körtzinger, A., Send, U., Wallace, D. W. R., Karstensen, J., and de Grandpre, M.: Seasonal cycle of O2 and pCO2 in the central Labrador Sea: Atmospheric, biological, and physical implications, Glob. Biogeochem. Cycles, 22, 1–16, https://doi.org/10.1029/2007GB003029, 2008.

Kosar, U. and Suarez, V.: Removing Forward: Centering Equity and Justice in a Carbon-Removing Future, Carbon180, Carbon180, https://doi.org/10.1016/j.cdev.2021.203654, 2021.

Kovach, M.: Indigenous Methodologies: Characteristics, Conversations, and Contexts, Second Edition, University of Toronto Press, 326 pp., 2021.

Lacour, L., Briggs, N., Claustre, H., Ardyna, M., and Dall'Olmo, G.: The Intraseasonal Dynamics of the Mixed Layer Pump in the Subpolar North Atlantic Ocean: A Biogeochemical-Argo Float Approach, Glob. Biogeochem. Cycles, 33, 266–281, https://doi.org/10.1029/2018GB005997, 2019.

Laframboise, S. J., Bailey, T., Dang, A.-T., Rose, M., Zhou, Z., Berg, M. D., Holland, S., Abdul, S. A., O'Connor, K., El-Sahli, S., Boucher, D. M., Fairman, G., Deng, J., Shaw, K., Noblett, N., D'Addario, A., Empey, M., and Sinclair, K.: Analysis of financial challenges faced by graduate students in Canada, Biochem. Cell Biol., https://doi.org/10.1139/bcb-2023-0021, 2023.

Lagerloef, G. S. E., Lukas, R., Weller, R. A., and Anderson, S. P.: Pacific warm pool temperature regulation during TOGA COARE: Upper ocean feedback, J. Clim., 11, 2297–2309, https://doi.org/10.1175/1520-0442(1998)011<2297:PWPTRD>2.0.CO;2, 1998.

Land, P. E., Shutler, J. D., Cowling, R. D., Woolf, D. K., Walker, P., Findlay, H. S., Upstill-Goddard, R. C., and Donlon, C. J.: Climate change impacts on sea-air fluxes of CO2 in three Arctic seas: A sensitivity study using Earth observation, Biogeosciences, 10, 8109–8128, https://doi.org/10.5194/bg-10-8109-2013, 2013.

Landschützer, P., Gruber, N., Bakker, D. C. E., Schuster, U., Nakaoka, S., Payne, M. R., Sasse, T. P., and Zeng, J.: A neural network-based estimate of the seasonal to inter-annual variability of the Atlantic Ocean carbon sink, Biogeosciences, 10, 7793–7815, https://doi.org/10.5194/bg-10-7793-2013, 2013.

Landschützer, P., Gruber, N., D.C.E.Bakker, and Schuster, U.: Recent variability of the global ocean carbon sink, Glob. Biogeochem. Cycles, 28, 927–949, https://doi.org/10.1002/2014GB004853, 2014.

Landschützer, P., Gruber, N., Haumann, F. A., Rödenbeck, C., Bakker, D. C. E., Heuven, S. V., Hoppema, M., Metzl, N., Sweeney, C., and Takahashi, T.: The reinvigoration of the Southern Ocean carbon sink, Science, 349, 1221–1224, https://doi.org/10.1126/science.aab2620, 2015.

Landschützer, P., Gruber, N., and Bakker, D. C. E.: Decadal variations and trends of the global ocean carbon sink, Glob. Biogeochem. Cycles, 30, 1396–1417, https://doi.org/10.1002/2015GB005359, 2016.

Landschützer, P., Gruber, N., Bakker, D. C. E., Stemmler, I., and Six, K. D.: Strengthening seasonal marine CO2 variations due to increasing atmospheric CO2, Nat. Clim. Change, 8, 146–150, https://doi.org/10.1038/s41558-017-0057-x, 2018.

Landschützer, P., Ilyina, T., and Lovenduski, N. S.: Detecting Regional Modes of Variability in Observation-Based Surface Ocean pCO2, Geophys. Res. Lett., 46, 2670–2679, https://doi.org/10.1029/2018GL081756, 2019.

Landschützer, P., Laruelle, G. G., Roobaert, A., and Regnier, P.: A uniform pCO2 climatology combining open and coastal oceans, Earth Syst. Sci. Data, 12, 2537–2553, https://doi.org/10.5194/essd-12-2537-2020, 2020a.

Landschützer, P., Gruber, N., and Bakker, D. C. E.: An observation-based global monthly gridded sea surface pCO2 and air-sea CO2 flux product from 1982 onward and its monthly climatology, NCEI Access., 160558, https://doi.org/10.7289/v5z899n6, 2020b.

Langmann, B., Zakšek, K., Hort, M., and Duggen, S.: Volcanic ash as fertiliser for the surface ocean, Atmospheric Chem. Phys., 10, 3891–3899, https://doi.org/10.5194/acp-10-3891-2010, 2010.

Lannuzel, D., Tedesco, L., van Leeuwe, M., Campbell, K., Flores, H., Delille, B., Miller, L., Stefels, J., Assmy, P., Bowman, J., Brown, K., Castellani, G., Chierici, M., Crabeck, O., Damm, E., Else, B., Fransson, A., Fripiat, F., Geilfus, N. X., Jacques, C., Jones, E., Kaartokallio, H., Kotovitch, M., Meiners, K., Moreau, S., Nomura, D., Peeken, I., Rintala, J. M., Steiner, N., Tison, J. L., Vancoppenolle, M., Van der Linden, F., Vichi, M., and Wongpan, P.: The future of Arctic sea-ice biogeochemistry and ice-associated ecosystems, Nat. Clim. Change, 10, 983–992, https://doi.org/10.1038/s41558-020-00940-4, 2020.

Laruelle, G. G., Lauerwald, R., Pfeil, B., and Regnier, P.: Regionalized global budget of the CO2 exchange at the air-water interface in continental shelf seas, Glob. Biogeochem. Cycles, 28, 1199–1214, https://doi.org/10.1002/2014GB004832.Received, 2014.

Laruelle, G. G., Landschützer, P., Gruber, N., Tison, J.-L., Delille, B., and Regnier, P.: Global high-resolution monthly pCO2 climatology for the coastal ocean derived from neural network interpolation, Biogeosciences Discuss., 1–40, https://doi.org/10.5194/bg-2017-64, 2017.

Laruelle, G. G., Cai, W.-J., Hu, X., Gruber, N., Mackenzie, F. T., and Regnier, P.: Continental shelves as a variable but increasing global sink for atmospheric carbon dioxide, Nat. Commun., 9, 1–11, https://doi.org/10.1038/s41467-017-02738-z, 2018.

Lauvset, S. K., Chierici, M., Counillon, F., Omar, A., Nondal, G., Johannessen, T., and Olsen, A.: Annual and seasonal fCO2 and air-sea CO2 fluxes in the Barents Sea, J. Mar. Syst., 113–114, 62–74, https://doi.org/10.1016/j.jmarsys.2012.12.011, 2013.

Lauvset, S. K., Lange, N., Tanhua, T., Bittig, H. C., Olsen, A., Kozyr, A., Alin, S., Álvarez, M., Azetsu-Scott, K., Barbero, L., Becker, S., Brown, P. J., Carter, B. R., da Cunha, L. C., Feely, R. A., Hoppema, M., Humphreys, M. P., Ishii, M., Jeansson, E., Jiang, L.-Q., Jones, S. D., Lo Monaco, C., Murata, A., Müller, J. D., Pérez, F. F., Pfeil, B., Schirnick, C., Steinfeldt, R., Suzuki, T., Tilbrook, B., Ulfsbo, A., Velo, A., Woosley, R. J., and Key, R. M.: GLODAPv2.2022: the latest version of the global interior ocean biogeochemical data product, Earth Syst. Sci. Data, 14, 5543–5572, https://doi.org/10.5194/essd-14-5543-2022, 2022.

Laxon, S. W., Giles, K. A., Ridout, A. L., Wingham, D. J., Willatt, R., Cullen, R., Kwok, R., Schweiger, A., Zhang, J., Haas, C., Hendricks, S., Krishfield, R., Kurtz, N., Farrell, S., and Davidson, M.: CryoSat-2 estimates of Arctic sea ice thickness and volume, Geophys. Res. Lett., 40, 732–737, https://doi.org/10.1002/grl.50193, 2013.

Le Quéré, C., Rödenbeck, C., Buitenhuis, E. T., Conway, T. J., Langenfelds, R., Gomez, A., Labuschagne, C., Ramonet, M., Nakazawa, T., Metzl, N., Gillett, N., and Heimann, M.: Saturation of the Southern Ocean CO2 Sink Due to Recent Climate Change, Science, 316, 1735–1738, https://doi.org/10.1126/science.1136188, 2007.

Lee, K., Tong, L. T., Millero, F. J., Sabine, C. L., Dickson, A. G., Goyet, C., Park, G. H., Wanninkhof, R., Feely, R. A., and Key, R. M.: Global relationships of total alkalinity with salinity and temperature in surface waters of the world's oceans, Geophys. Res. Lett., 33, 1–5, https://doi.org/10.1029/2006GL027207, 2006.

Legge, O., Johnson, M., Hicks, N., Jickells, T., Diesing, M., Aldridge, J., Andrews, J., Artioli, Y., Bakker, D. C. E., Burrows, M. T., Carr, N., Cripps, G., Felgate, S. L., Fernand, L., Greenwood, N., Hartman, S., Kröger, S., Lessin, G., Mahaffey, C., Mayor, D. J., Parker, R., Queirós, A. M., Shutler, J. D., Silva, T., Stahl, H., Tinker, J., Underwood, G. J. C., Van Der Molen, J., Wakelin, S., Weston, K., and Williamson, P.: Carbon on the Northwest European Shelf: Contemporary Budget and Future Influences, Front. Mar. Sci., 7, https://doi.org/10.3389/fmars.2020.00143, 2020.

Lezaun, J.: Hugging the Shore: Tackling Marine Carbon Dioxide Removal as a Local Governance Problem, Front. Clim., 3, 1–6, https://doi.org/10.3389/fclim.2021.684063, 2021.

Li, F. and Lozier, M. S.: On the linkage between Labrador Sea Water volume and overturning circulation in the Labrador Sea: A case study on proxies, J. Clim., 31, 5225–5241, https://doi.org/10.1175/JCLI-D-17-0692.1, 2018.

Li, H., Ilyina, T., Müller, W. A., and Landschützer, P.: Predicting the variable ocean carbon sink, Sci. Adv., 5, 1–9, https://doi.org/10.1126/sciadv.aav6471, 2019a.

Li, X., Bellerby, R., Ge, J., Wallhead, P., Liu, J., and Yang, A.: Retrieving monthly and interannual total-scale pH on the East China Sea shelf using an artificial neural network: ANN-pH-v1, Geosci. Model Dev. Discuss., 1–15, https://doi.org/10.5194/gmd-2019-236, 2019b.

Li, X., Bellerby, R. G. J., Wallhead, P., Ge, J., Liu, J., Liu, J., and Yang, A.: A Neural Network-Based Analysis of the Seasonal Variability of Surface Total Alkalinity on the East China Sea Shelf, Front. Mar. Sci., 7, https://doi.org/10.3389/fmars.2020.00219, 2020.

Linares-Rodriguez, A., Ruiz-Arias, J. A., Pozo-Vazquez, D., and Tovar-Pescador, J.: An artificial neural network ensemble model for estimating global solar radiation from Meteosat satellite images, Energy, 61, 636–645, https://doi.org/10.1016/j.energy.2013.09.008, 2013.

Lindoso, V.: Choices Made Now Are Critical for the Future of Our Ocean and Cryosphere, 2019.

Liu, K.-K., Atkinson, L., Quinones, R., and Talaue-McManus, L.: Carbon and Nutrient Fluxes in Continental Margins, Glob. Change – IGBP Ser., 2010.

Lockwood, D., Quay, P. D., Kavanaugh, M. T., Juranek, L. W., and Feely, R. A.: High-resolution estimates of net community production and air-sea CO 2 flux in the northeast Pacific, Glob. Biogeochem. Cycles, 26, 1–16, https://doi.org/10.1029/2012GB004380, 2012.

Lombard, A. T., Ban, N. C., Smith, J. L., Lester, S. E., Sink, K. J., Wood, S. A., Jacob, A. L., Kyriazi, Z., Tingey, R., and Sims, H. E.: Practical approaches and advances in spatial tools to achieve multi-objective marine spatial planning, Front. Mar. Sci., 6, 1–9, https://doi.org/10.3389/fmars.2019.00166, 2019.

Long, J. S., Fassbender, A. J., and Estapa, M. L.: Depth-Resolved Net Primary Production in the Northeast Pacific Ocean: A Comparison of Satellite and Profiling Float Estimates in the Context of Two Marine Heatwaves, Geophys. Res. Lett., 48, 1–11, https://doi.org/10.1029/2021GL093462, 2021.

Loomis, R., Cooley, S. R., Collins, J. R., Engler, S., and Suatoni, L.: A Code of Conduct Is Imperative for Ocean Carbon Dioxide Removal Research, Front. Mar. Sci., 9, 2022.

Loose, B., Miller, L. A., Elliott, S., and Papakyriakou., T.: Sea ice biogeochemistry and material transport across the frozen interface, Oceanography, 24, 202–218, https://doi.org/10.5670/oceanog.2011.65, 2011.

Mackenzie, F. T., Lerman, A., and Ver, L. M. B.: Role of the continental margin in the global carbon balance during the past three centuries, Geology, 26, 423–426, https://doi.org/10.1130/0091-7613(1998)026<0423:ROTCMI>2.3.CO;2, 1998.

Maldonado, J. K., Shearer, C., Bronen, R., Peterson, K., and Lazrus, H.: The impact of climate change on tribal communities in the US: Displacement, relocation, and human rights, Clim. Change, 120, 601–614, https://doi.org/10.1007/s10584-013-0746-z, 2013.

Manizza, M., Follows, M. J., Dutkiewicz, S., Menemenlis, D., Hill, C. N., and Key, R. M.: Changes in the Arctic Ocean CO2 sink (1996-2007): A regional model analysis, Glob. Biogeochem. Cycles, 27, 1108–1118, https://doi.org/10.1002/2012GB004491, 2013.

Mann, K. H. and Lazier, J. R.: Dynamics of Marine Ecosystems: Biological-Physical Interactions in the Oceans, Blackwell Publishing, 2006.

Manning, C. C., Preston, V. L., Jones, S. F., Michel, A. P. M., Nicholson, D. P., Duke, P. J., Ahmed, M. M. M., Manganini, K., Else, B. G. T., and Tortell, P. D.: River inflow dominates methane emissions in an Arctic coastal system, Geophys. Res. Lett., 47, e2020GL087669, https://doi.org/10.1029/2020gl087669, 2020.

Marchese, C., Hunt, B. P. V., Giannini, F., Ehrler, M., and Costa, M.: Bioregionalization of the coastal and open oceans of British Columbia and Southeast Alaska based on Sentinel-3A satellite-derived phytoplankton seasonality, Front. Mar. Sci., 9, 1–22, https://doi.org/10.3389/fmars.2022.968470, 2022.

Marine Planning Partnership Initiative: Central Coast Marine Plan, 2015a.

Marine Planning Partnership Initiative: Haida Gwaii Marine Plan, 2015b.

Marine Planning Partnership Initiative: North Coast Marine Plan, 2015c.

Marine Planning Partnership Initiative: North Vancouver Island Marine Plan, 2015d.

Marshall, J., Dobson, F., Moore, K., Rhines, P., Visbeck, M., D'Asaro, E., Bumke, K., Chang, S., Davis, R., Fischer, K., Garwood, R., Guest, P., Harcourt, R., Herbaut, C., Holt, T., Lazier, J., Legg, S., McWilliams, J., Pickart, R., Prater, M., Renfrew, I., Schott, F., Send, U., and Smethie, W.: The Labrador Sea Deep Convection Experiment, Bull. Am. Meteorol. Soc., 79, 2033–2058, https://doi.org/10.1175/1520-0477(1998)079<2033:tlsdce>2.0.co;2, 1998.

Marshall, J., Kushnir, Y., Battisti, D., Chang, P., Czaja, A., Dickson, R., Hurrell, J., McCartney, M., Saravanan, R., and Visbeck, M.: North Atlantic climate variability: Phenomena, impacts and mechanisms, Int. J. Climatol., 21, 1863–1898, https://doi.org/10.1002/joc.693, 2001.

Martin, J., KH, C., KS, J., SE, F., RM, G., SJ, T., CN, H., VA, E., JL, N., and TL, C.: Testing the iron hypothesis in ecosystems of the equatorial Pacific Ocean, Nature, 371, 123–129, https://doi.org/10.1038/371123a0, 1994.

Martz, T. R., DeGrandpre, M. D., Strutton, P. G., McGillis, W. R., and Drennan, W. M.: Sea surface pC02 and carbon export during the Labrador Sea spring-summer bloom: An in situ mass balance approach, J. Geophys. Res. Oceans, 114, 1–12, https://doi.org/10.1029/2008JC005060, 2009.

Maru, Y. T., Stafford Smith, M., Sparrow, A., Pinho, P. F., and Dube, O. P.: A linked vulnerability and resilience framework for adaptation pathways in remote disadvantaged communities, Glob. Environ. Change, 28, 337–350, https://doi.org/10.1016/j.gloenvcha.2013.12.007, 2014.

Maslanik, J. A., Fowler, C., Stroeve, J., Drobot, S., Zwally, J., Yi, D., and Emery, W.: A younger, thinner Arctic ice cover: Increased potential for rapid, extensive sea-ice loss, Geophys. Res. Lett., 34, https://doi.org/10.1029/2007GL032043, 2007.

Mathis, J. T., Cooley, S. R., Lucey, N., Colt, S., Ekstrom, J., Hurst, T., Hauri, C., Evans, W., Cross, J. N., and Feely, R. A.: Ocean acidification risk assessment for Alaska's fishery sector, Prog. Oceanogr., 136, 71–91, https://doi.org/10.1016/j.pocean.2014.07.001, 2015.

Matthes, L. C., Ehn, J. K., Dalman, L. A., Babb, D. G., Peeken, I., Harasyn, M., Kirillov, S., Lee, J., Bélanger, S., Tremblay, J.-É., Barber, D. G., and Mundy, C. J.: Environmental drivers of spring primary production in Hudson Bay, Elem. Sci. Anthr., 9, 00160, https://doi.org/10.1525/elementa.2020.00160, 2021.

McGregor, D.: From "decolonized" to reconciliation research in Canada: Drawing from indigenous research paradigms, Acme, 17, 810–831, 2018.

McKinley, G. A., Takahashi, T., Buitenhuis, E., Chai, F., Christian, J. R., Doney, S. C., Jiang, M. S., Lindsay, K., Moore, J. K., Le Quéré, C., Lima, I., Murtugudde, R., Shi, L., and Wetzel, P.: North Pacific carbon cycle response to climate variability on seasonal to decadal timescales, J. Geophys. Res. Oceans, 111, https://doi.org/10.1029/2005JC003173, 2006.

McKinley, G. A., Fay, A. R., Takahashi, T., and Metzl, N.: Convergence of atmospheric and North Atlantic carbon dioxide trends on multidecadal timescales, Nat. Geosci., 4, https://doi.org/10.1038/ngeo1193, 2011a.

McKinley, G. A., Fay, A. R., Takahashi, T., and Metzl, N.: Convergence of atmospheric and North Atlantic carbon dioxide trends on multidecadal timescales, Nat. Geosci., 4, https://doi.org/10.1038/ngeo1193, 2011b.

McKinley, G. A., Pilcher, D. J., Fay, A. R., Lindsay, K., Long, M. C., and Lovenduski, N. S.: Timescales for detection of trends in the ocean carbon sink, Nature, 530, 469–472, https://doi.org/10.1038/nature16958, 2016.

McKinley, G. A., Fay, A. R., Eddebbar, Y. A., Gloege, L., and Lovenduski, N. S.: External Forcing Explains Recent Decadal Variability of the Ocean Carbon Sink, AGU Adv., 1, 1–10, https://doi.org/10.1029/2019av000149, 2020.

McLean, E. L., Katenka, N. V., and Seibel, B. A.: Decreased growth and increased shell disease in early benthic phase Homarus americanus in response to elevated CO2, Mar. Ecol. Prog. Ser., 596, 113–126, https://doi.org/10.3354/meps12586, 2018.

Mears, C. A., Scott, J., Wentz, F. J., Ricciardulli, L., Leidner, S. M., Hoffman, R., and Atlas, R.: A Near-Real-Time Version of the Cross-Calibrated Multiplatform (CCMP) Ocean Surface Wind Velocity Data Set, J. Geophys. Res. Oceans, 124, 6997–7010, https://doi.org/10.1029/2019JC015367, 2019.

Merchant, C. J., Embury, O., Bulgin, C. E., Block, T., Corlett, G. K., Fiedler, E., Good, S. A., Mittaz, J., Rayner, N. A., Berry, D., Eastwood, S., Taylor, M., Tsushima, Y., Waterfall, A., Wilson, R., and Donlon, C.: Satellite-based time-series of sea-surface temperature since 1981 for climate applications, Sci. Data, 6, 1–18, https://doi.org/10.1038/s41597-019-0236-x, 2019.

Messié, M. and Chavez, F. P.: Seasonal regulation of primary production in eastern boundary upwelling systems, Prog. Oceanogr., 134, 1–18, https://doi.org/10.1016/j.pocean.2014.10.011, 2015.

Mignot, A., Schuckmann, K. V., Landschützer, P., Gasparin, F., Gennip, S. V., Perruche, C., Lamouroux, J., and Amm, T.: Decrease in air-sea CO 2 fluxes caused by persistent marine heatwaves, Nat. Commun., 13, 1–9, https://doi.org/10.1038/s41467-022-31983-0, 2022.

Miller, L. A., Yager, P. L., Erickson, K. A., Amiel, D., Bâcle, J., Kirk Cochran, J., Garneau, M. È., Gosselin, M., Hirschberg, D. J., Klein, B., LeBlanc, B., and Miller, W. L.: Carbon distributions and fluxes in the North Water, 1998 and 1999, Deep-Sea Res. Part II Top. Stud. Oceanogr., 49, 5151–5170, https://doi.org/10.1016/S0967-0645(02)00183-2, 2002.

Mogen, S., Lovenduski, N. S., Dallman, A. R., Gregor, L., Sutton, A. J., Bograd, S. J., Cordero Quiros, N., Di Lorenzo, E., Hazen, E. L., Jacox, M. G., and et al.: Ocean biogeochemical signatures of the North Pacific Blob, Earth Space Sci. Open Arch., 49, e2021GL096938, https://doi.org/10.1029/2021GL096938, 2022.

Moore, S. E. and Grebmeier, J. M.: The Distributed Biological Observatory: Linking Physics to Biology in the Pacific Arctic Region, Arctic, 71, 1–7, https://doi.org/10.14430/arctic4606, 2018.

Moran, K., Boutin, B., Juniper, S. K., Pirenne, B., and Round, A.: A multi-use and multi-stakeholder ocean observing platform system, OCEANS 2019 MTS/IEEE Seattle, https://doi.org/10.23919/OCEANS40490.2019.8962711, 2022.

Morrison, J., Foreman, M. G. G., and Masson, D.: A Method for Estimating Monthly Freshwater Discharge Affecting British Columbia Coastal Waters, Atmosphere-Ocean ISSN, 5900, https://doi.org/10.1080/07055900.2011.637667, 2012.

Mortenson, E., Steiner, N., Monahan, A. H., Hayashida, H., Sou, T., and Shao, A.: Modeled Impacts of Sea Ice Exchange Processes on Arctic Ocean Carbon Uptake and Acidification (1980–2015), J. Geophys. Res. Oceans, 125, 1–20, https://doi.org/10.1029/2019JC015782, 2020.

Murata, A. and Takizawa, T.: Summertime CO2 sinks in shelf and slope waters of the western Arctic Ocean, Cont. Shelf Res., 23, 753–776, https://doi.org/10.1016/S0278-4343(03)00046-3, 2003.

Murata, A., Inoue, J., Nishino, S., and Yasunaka, S.: Early Wintertime CO 2 Uptake in the Western Arctic Ocean, J. Geophys. Res. Oceans, 127, e2021JC018037, https://doi.org/10.1029/2021JC018037, 2018.

Murphy, P. P., Nojiri, Y., Harrison, D. E., and Larkin, N. K.: Scales of spatial variability for surface ocean pCO2 in the Gulf of Alaska and Bering Sea: Toward a sampling strategy, Geophys. Res. Lett., 28, 1047–1050, https://doi.org/10.1029/2000GL012375, 2001.

Nakaoka, S., Telszewski, M., Nojiri, Y., Yasunaka, S., Miyazaki, C., Mukai, H., and Usui, N.: Estimating temporal and spatial variation of ocean surface pCO2 in the North Pacific using a self-organizing map neural network technique, Biogeosciences, 10, 6093–6106, https://doi.org/10.5194/bg-10-6093-2013, 2013.

Nakaoka, S. I., Aoki, S., Nakazawa, T., Hashida, G., Morimoto, S., Yamanouchi, T., and Yoshikawa-Inoue, H.: Temporal and spatial variations of oceanic pCO2 and air-sea CO2 flux in the Greenland Sea and the Barents Sea, Tellus Ser. B Chem. Phys. Meteorol., 58, 148–161, https://doi.org/10.1111/j.1600-0889.2006.00178.x, 2006.

Namias, J.: long range weather forecasting—history, current status and outlook, Bull. Am. Meteorol. Soc., 49, 438–470, https://doi.org/10.1175/1520-0477-49.5.438, 1968.

NASEM: A Research Strategy for Ocean-based Carbon Dioxide Removal and Sequestration, A Research Strategy for Ocean-based Carbon Dioxide Removal and Sequestration, National Academies of Sciences, Engineering, and Medicine, Washington, DC, https://doi.org/10.17226/26278, 2021.

NASEM: A Research Strategy for Ocean-based Carbon Dioxide Removal and Sequestration, National Academies Press, Washington, D.C., https://doi.org/10.17226/26278, 2022.

Nemcek, N., Ianson, D., and Tortell, P. D.: A high-resolution survey of DMS, CO2, and O2/Ar distributions in productive coastal waters, Glob. Biogeochem. Cycles, 22, 1–13, https://doi.org/10.1029/2006GB002879, 2008.

Newman, M., Alexander, M. A., Ault, T. R., Cobb, K. M., Deser, C., Di Lorenzo, E., Mantua, N. J., Miller, A. J., Minobe, S., Nakamura, H., Schneider, N., Vimont, D. J., Phillips, A. S., Scott, J. D., and Smith, C. A.: The Pacific decadal oscillation, revisited, J. Clim., 29, 4399–4427, https://doi.org/10.1175/JCLI-D-15-0508.1, 2016.

Newton, J. A., Feely, R. A., Jewett, E. B., Williamson, P., and Mathis, J.: Global Ocean Acidification Observing Network: Requirements and Governance Plan, 57 pp., 2015.

Nishino, S., Itoh, M., Kawaguchi, Y., Kikuchi, T., and Aoyama, M.: Impact of an unusually large warm-core eddy on distributions of nutrients and phytoplankton in the southwestern Canada Basin during late summer/early fall 2010, Geophys. Res. Lett., 38, 1–6, https://doi.org/10.1029/2011GL047885, 2011.

Nitishinsky, M., Anderson, L. G., and Hölemann, J. A.: Inorganic carbon and nutrient fluxes on the Arctic Shelf, Cont. Shelf Res., 27, 1584–1599, https://doi.org/10.1016/j.csr.2007.01.019, 2007.

Novick, K., Williams, C., Runkle, B., Anderegg, W. R. L., Hollinger, D., Litvak, M., Normile, C., Shrestha, G., Almaraz, M., Anderson, C., Barnes, M., Baldocchi, D., Colburn, L., Cullenward, D., Evans, M., Guan, K., Keenan, T., Lamb, R., Larson, E., Oldfield, E., Poulter, B., Reyes, J., Sanderman, J., Selmants, P., Sepulveda Carlo, E., Torn, M. S., Trugman, A., and Woodall, C.: The science needed for robust, scalable, and credible nature-based climate solutions in the United States, https://doi.org/10.5967/n7r9-7j83, 2022.

O'Carroll, A. G., Armstrong, E. M., Beggs, H. M., Bouali, M., Casey, K. S., Corlett, G. K., Dash, P., Donlon, C. J., Gentemann, C. L., Høyer, J. L., Ignatov, A., Kabobah, K., Kachi, M., Kurihara, Y., Karagali, I., Maturi, E., Merchant, C. J., Marullo, S., Minnett, P. J., Pennybacker, M., Ramakrishnan, B., Ramsankaran, R., Santoleri, R., Sunder, S.,

Saux Picart, S., Vázquez-Cuervo, J., and Wimmer, W.: Observational Needs of Sea Surface Temperature, Front. Mar. Sci., 6, 2019.

Olivier, L., Boutin, J., Reverdin, G., Lefèvre, N., Landschützer, P., Speich, S., Karstensen, J., Labaste, M., Noisel, C., Ritschel, M., and Steinhoff, T.: Wintertime process study of the North Brazil Current rings reveals the region as a larger sink for CO 2 than expected, Biogeosciences, 19, 2969–2988, https://doi.org/10.5194/bg-19-2969-2022, 2022.

Omar, A. M., Johannessen, T., Olsen, A., Kaltin, S., and Rey, F.: Seasonal and interannual variability of the air-sea CO2 flux in the Atlantic sector of the Barents Sea, Mar. Chem., 104, 203–213, https://doi.org/10.1016/j.marchem.2006.11.002, 2007.

de Oña, J. and Garrido, C.: Extracting the contribution of independent variables in neural network models: A new approach to handle instability, Neural Comput. Appl., 25, 859–869, https://doi.org/10.1007/s00521-014-1573-5, 2014.

O'Neill, B. C., Tebaldi, C., Vuuren, D. P. V., Eyring, V., Friedlingstein, P., Hurtt, G., Knutti, R., Kriegler, E., Lamarque, J., Lowe, J., Meehl, G. A., and Moss, R.: The Scenario Model Intercomparison Project (ScenarioMIP) for CMIP6, 3461–3482, https://doi.org/10.5194/gmd-9-3461-2016, 2016.

Orr, J. C., Fabry, V. J., Aumont, O., Bopp, L., Doney, S. C., Feely, R. A., Gnanadesikan, A., Gruber, N., Ishida, A., Joos, F., Key, R. M., Lindsay, K., Maier-Reimer, E., Matear, R., Monfray, P., Mouchet, A., Najjar, R. G., Plattner, G. K., Rodgers, K. B., Sabine, C. L., Sarmiento, J. L., Schlitzer, R., Slater, R. D., Totterdell, I. J., Weirig, M. F., Yamanaka, Y., and Yool, A.: Anthropogenic ocean acidification over the twenty-first century and its impact on calcifying organisms, Nature, 437, 681–686, https://doi.org/10.1038/nature04095, 2005.

Orr, J. C., Epitalon, J. M., Dickson, A. G., and Gattuso, J. P.: Routine uncertainty propagation for the marine carbon dioxide system, Mar. Chem., 207, 84–107, https://doi.org/10.1016/j.marchem.2018.10.006, 2018.

Oschlies, A., Stevenson, A., Bach, L. T., Fennel, K., Rickaby, R. E. M., Satterfield, T., Webb, R., and Gattuso, J. P.: Guide to Best Practices in Ocean Alkalinity Enhancement Research (OAE Guide 23), State Planet SP, 2-oae2023, 1–242, https://doi.org/10.5194/sp-2-oae2023, 2023.

Osiecka, A. N., Wrobel, A., Hendricks, I.-W., and Osiecka-Brzeska, K.: Being ERC in marine science: Results of a survey among early-career marine scientists and conservationists, Front. Mar. Sci., 9, 835692, https://doi.org/10.3389/fmars.2022.835692, 2022.

Otero, P., Padin, X. A., Ruiz-Villarreal, M., García-García, L. M., Ríos, A. F., and Pérez, F. F.: Net sea–air CO_2 flux uncertainties in the Bay of Biscay based on the choice of wind speed products and gas transfer parameterizations, Biogeosciences, 10, 2993–3005, https://doi.org/10.5194/bg-10-2993-2013, 2013.

Oubanas, H., Gejadze, I., Malaterre, P. O., Durand, M., Wei, R., Frasson, R. P. M., and Domeneghetti, A.: Discharge Estimation in Ungauged Basins Through Variational Data Assimilation: The Potential of the SWOT Mission, Water Resour. Res., 54, 2405–2423, https://doi.org/10.1002/2017WR021735, 2018.

Addressing Arctic Challenges Requires a Synoptic Ocean Survey: http://eos.org/opinions/addressing-arctic-challenges-requires-a-synoptic-ocean-survey, last access: 6 April 2023.

Palevsky, H. I., Ribalet, F., Swalwell, J. E., Cosca, C. E., Cokelet, E. D., Feely, R. A., Armbrust, E. V., and Quay, P. D.: The influence of net community production and phytoplankton community structure on CO2 uptake in the Gulf of Alaska, 664–676 pp., https://doi.org/10.1002/gbc.20058, 2013.

Parard, G., Charantonis, A. A., and Rutgerson, A.: Remote sensing the sea surface CO2 of the Baltic Sea using the SOMLO methodology, Biogeosciences, 12, 3369–3384, https://doi.org/10.5194/bg-12-3369-2015, 2015.

Parard, G., Charantonis, A. A., and Rutgersson, A.: Using satellite data to estimate partial pressure of CO2 in the Baltic Sea, J. Geophys. Res. G Biogeosciences, 121, 1002–1015, https://doi.org/10.1002/2015JG003064, 2016.

Pedersen, C., Otokiak, M., Koonoo, I., Milton, J., Maktar, E., Anaviapik, A., Milton, M., Porter, G., Scott, A., Newman, C., Porter, C., Aaluk, T., Tiriraniaq, B., Pedersen, A., Riffi, M., Solomon, E., and Elverum, S.: ScIQ: An invitation and recommendations to combine science and Inuit Qaujimajatuqangit for meaningful engagement of inuit communities in research, Arct. Sci., 6, 326–339, https://doi.org/10.1139/as-2020-0015, 2020.

Peña, M. A., Nemcek, N., and Robert, M.: Phytoplankton responses to the 2014–2016 warming anomaly in the northeast subarctic Pacific Ocean, Limnol. Oceanogr., 64, 515–525, https://doi.org/10.1002/lno.11056, 2019.

Peng, W.: Trade-offs for equitable climate policy assessed, Nature, 588, 225–226, https://doi.org/10.1038/d41586-020-03392-0, 2020.

Perovich, D. K., Light, B., Eicken, H., Jones, K. F., Runciman, K., and Nghiem, S. V.: Increasing solar heating of the Arctic Ocean and adjacent seas, 1979-2005: Attribution and role in the ice-albedo feedback, Geophys. Res. Lett., 34, https://doi.org/10.1029/2007GL031480, 2007.

Peters, G. P., Le Quéré, C., Andrew, R. M., Canadell, J. G., Friedlingstein, P., Ilyina, T., Jackson, R. B., Joos, F., Korsbakken, J. I., McKinley, G. A., Sitch, S., and Tans, P.: Towards real-time verification of CO2 emissions, Nat. Clim. Change, 7, 848–850, https://doi.org/10.1038/s41558-017-0013-9, 2017.

Pilcher, D. J., Siedlecki, S. A., Hermann, A. J., Coyle, K. O., Mathis, J. T., and Evans, W.: Simulated Impact of Glacial Runoff on CO2 Uptake in the Gulf of Alaska, Geophys. Res. Lett., 45, 880–890, https://doi.org/10.1002/2017GL075910, 2018.

Pipko, I. I., Semiletov, I. P., and Pugach, S. P.: Interannual variability of air-sea CO 2 fluxes and carbon system in the East Siberian Sea, Biogeosciences, 8, 1987–2007, https://doi.org/10.5194/bg-8-1987-2011, 2011.

Pipko, I. I., Pugach, S. P., Semiletov, I. P., Anderson, L. G., and Shakhova, N. E.: The spatial and interannual dynamics of the surface water carbonate system and air – sea CO 2 fluxes in the outer shelf and slope of the Eurasian Arctic Ocean, Ocean Sci., 13, 997–1016, https://doi.org/10.5194/os-13-997-2017, 2017.

Poole, F. W. and Hufford, G. L.: Meteorological and oceanographic factors affecting sea ice in Cook Inlet., J. Geophys. Res., 87, 2061–2070, https://doi.org/10.1029/JC087iC03p02061, 1982.

Pörtner, H. O., Roberts, D. C., Masson-Delmotte, V., Zhai, P., Tignor, M., Poloczanska, E., Mintenbeck, K., Nicolai, M., Okem, A., Petzold, J., and Rama, B.: IPCC special report on the ocean and cryosphere in a changing climate, IPCC Intergovernmental Panel on Climate Change: Geneva, Switzerland, 2019.

Proulx, M. J., Ross, L., Macdonald, C., Fitzsimmons, S., and Smit, M.: Indigenous Traditional Ecological Knowledge and Ocean Observing: A Review of Successful Partnerships, Front. Mar. Sci., 8, 1–18, https://doi.org/10.3389/fmars.2021.703938, 2021.

Prowse, T., Bring, A., Mård, J., Carmack, E., Holland, M., Instanes, A., Vihma, T., and Wrona, F. J.: Arctic Freshwater Synthesis: Summary of key emerging issues, J. Geophys. Res. Biogeosciences, 120, 1887–1893, https://doi.org/10.1002/2015JG003128, 2015.

Reed, R. K. and Schumacher, J. D.: Current Measurements along the Shelf Break in the Gulf of Alaska, J. Phys. Oceanogr., 16, 1985–1990, https://doi.org/10.1175/1520-0485(1986)016<1985:CMATSB>2.0.CO;2, 1986.

Regnier, P., Resplandy, L., Najjar, R. G., and Ciais, P.: The land-to-ocean loops of the global carbon cycle, Nature, 603, 401–410, https://doi.org/10.1038/s41586-021-04339-9, 2022.

Reid, A. J., Eckert, L. E., Lane, J. F., Young, N., Hinch, S. G., Darimont, C. T., Cooke, S. J., Ban, N. C., and Marshall, A.: “Two-Eyed Seeing”: An Indigenous framework to transform fisheries research and management, Fish Fish., 22, 243–261, https://doi.org/10.1111/faf.12516, 2021.

Resplandy, L., Séférian, R., and Bopp, L.: Natural variability of CO2 and O2 fluxes: What can we learn from centuries-long climate models simulations?, J. Geophys. Res. Oceans, 120, 384–404, https://doi.org/10.1002/2014JC010463, 2015.

Resplandy, L., Lévy, M., and McGillicuddy, D. J.: Effects of Eddy-Driven Subduction on Ocean Biological Carbon Pump, Glob. Biogeochem. Cycles, 33, 1071–1084, https://doi.org/10.1029/2018GB006125, 2019.

Resplandy, L., Hogikyan, A., Müller, J. D., Najjar, R. G., Bange, H. W., Bianchi, D., Weber, T., Cai, W.-J., Doney, S. C., Fennel, K., Gehlen, M., Hauck, J., Lacroix, F., Landschützer, P., Le Quéré, C., Roobaert, A., Schwinger, J., Berthet, S., Bopp, L., Chau, T. T. T., Dai, M., Gruber, N., Ilyina, T., Kock, A., Manizza, M., Lachkar, Z., Laruelle, G. G., Liao, E., Lima, I. D., Nissen, C., Rödenbeck, C., Séférian, R., Toyama, K., Tsujino, H., and Regnier, P.: A Synthesis of Global Coastal Ocean Greenhouse Gas Fluxes, Glob. Biogeochem. Cycles, 38, e2023GB007803, https://doi.org/10.1029/2023GB007803, 2024.

Revelle, R. and Suess, H. E.: Carbon Dioxide Exchange Between Atmosphere and Ocean and the Question of an Increase of Atmospheric CO2 during the Past Decades, Tellus, 9, 18–27, https://doi.org/10.3402/tellusa.v9i1.9075, 1957.

Reynolds, R. W., Rayner, N. A., Smith, T. M., Stokes, D. C., and Wang, W.: An Improved In Situ and Satellite SST Analysis for Climate, J. Clim., 15, 1609–1625, https://doi.org/10.1175/1520-0442(2002)015<1609:AIISAS>2.0.CO;2, 2002.

Ribalet, F., Marchetti, A., Hubbard, K. A., Brown, K., Durkin, C. A., Morales, R., Robert, M., Swalwell, J. E., Tortell, P. D., and Armbrust, E. V.: Unveiling a phytoplankton hotspot at a narrow boundary between coastal and offshore waters, Proc. Natl. Acad. Sci. U. S. A., 107, 16571–16576, https://doi.org/10.1073/pnas.1005638107, 2010.

Rieck, J. K., Böning, C. W., and Getzlaff, K.: The nature of eddy kinetic energy in the labrador sea: Different types of mesoscale eddies, their temporal variability, and impact on deep convection, J. Phys. Oceanogr., 49, 2075–2094, https://doi.org/10.1175/JPO-D-18-0243.1, 2019.

Ringuette, M., Devred, E., Azetsu-Scott, K., Head, E., Punshon, S., Casault, B., and Clay, S.: Optical, Chemical, and Biological Oceanographic Conditions in the Labrador Sea between 2014 and 2018, v + 38 p pp., 2022.

Ritter, R., Landschützer, P., Gruber, N., Fay, A. R., Iida, Y., Jones, S., Nakaoka, S., Park, G. H., Peylin, P., Rödenbeck, C., Rodgers, K. B., Shutler, J. D., and Zeng, J.: Observation-Based Trends of the Southern Ocean Carbon Sink, Geophys. Res. Lett., 44, 12,339-12,348, https://doi.org/10.1002/2017GL074837, 2017.

Rivers, N., Strand, M., Fernandes, M., Metuge, M., Lemahieu, A., CL, C. L., Benkenstein, A., and Snow, B.: Pathways to integrate Indigenous and local knowledge in ocean governance processes: Lessons from the Algoa Bay Project, Front. Mar. Sci., 9, https://doi.org/10.3389/fmars.2022.1084674, 2023.

Rödenbeck, C., Keeling, R. F., Bakker, D. C. E., Metzl, N., Olsen, A., Sabine, C., and Heimann, M.: Global surface-ocean pCO2 and sea-Air CO2 flux variability from an observation-driven ocean mixed-layer scheme, Ocean Sci., 9, 193–216, https://doi.org/10.5194/os-9-193-2013, 2013.

Rogelj, J., Popp, A., Calvin, K. V., Luderer, G., Emmerling, J., Gernaat, D., Fujimori, S., Strefler, J., Hasegawa, T., Marangoni, G., Krey, V., Kriegler, E., Riahi, K., Van Vuuren, D. P., Doelman, J., Drouet, L., Edmonds, J., Fricko, O., Harmsen, M., Havlík, P., Humpenöder, F., Stehfest, E., and Tavoni, M.: Scenarios towards limiting global mean temperature increase below 1.5 °C, Nat. Clim. Change, 8, 325–332, https://doi.org/10.1038/s41558-018-0091-3, 2018.

Roobaert, A., Laruelle, G. G., Landschützer, P., and Regnier, P.: Uncertainty in the global oceanic CO2 uptake induced by wind forcing: Quantification and spatial analysis, Biogeosciences, 15, 1701–1720, https://doi.org/10.5194/bg-15-1701-2018, 2018.

Roobaert, A., Laruelle, G. G., Landschützer, P., Gruber, N., Chou, L., and Regnier, P.: The Spatiotemporal Dynamics of the Sources and Sinks of CO2 in the Global Coastal Ocean, Glob. Biogeochem. Cycles, 33, 1693–1714, https://doi.org/10.1029/2019GB006239, 2019.

Roobaert, A., Regnier, P., Landschützer, P., and Laruelle, G. G.: A novel sea surface pCO_2-product for the global coastal ocean resolving trends over 1982–2020, Earth Syst. Sci. Data, 16, 421–441, https://doi.org/10.5194/essd-16-421-2024, 2024.

Rosenthal, P. B.: Testing the validity of single-particle maps at low and high resolution, Methods Enzymol., 579, 227–253, https://doi.org/10.1016/bs.mie.2016.06.004, 2016.

Ross, T., Fisher, J., Bond, N., Galbraith, M., and Whitney, F.: The Northeast Pacific: Current status and recent trends, PICES Press, 27, 36–39, 2019.

Roth, F., Broman, E., Sun, X., Bonaglia, S., Nascimento, F., Prytherch, J., Brüchert, V., Lundevall Zara, M., Brunberg, M., Geibel, M. C., Humborg, C., and Norkko, A.: Methane emissions offset atmospheric carbon dioxide uptake in coastal macroalgae, mixed vegetation and sediment ecosystems, Nat. Commun., 14, 42, https://doi.org/10.1038/s41467-022-35673-9, 2023.

Royer, T. C.: On the Effect of Precipitation and Runoff on Coastal Circulation in the Gulf of Alaska, J. Phys. Oceanogr., 9, 555–563, https://doi.org/10.1175/1520-0485(1979)009<0555:OTEOPA>2.0.CO;2, 1979.

Royer, T. C. and Grosch, C. E.: Ocean warming and freshening in the northern Gulf of Alaska, Geophys. Res. Lett., 33, https://doi.org/10.1029/2006GL026767, 2006.

Rutherford, K., Fennel, K., Atamanchuk, D., Wallace, D., and Thomas, H.: A modelling study of temporal and spatial pCO2 variability on the biologically active and temperature-dominated Scotian Shelf, Biogeosciences, 18, 6271–6286, https://doi.org/10.5194/bg-18-6271-2021, 2021.

Rysgaard, S., Nielsen, T. G., and Hansen, B. W.: Seasonal variation in nutrients, pelagic primary production and grazing in a high-Arctic coastal marine ecosystem, Young Sound, Northeast Greenland, Mar. Ecol. Prog. Ser., 179, 13–25, https://doi.org/10.3354/meps179013, 1999.

Rysgaard, S., Glud, R. N., Sejr, M. K., Bendtsen, J., and Christensen, P. B.: Inorganic carbon transport during sea ice growth and decay: A carbon pump in polar seas, J. Geophys. Res., 112, 1–8, https://doi.org/10.1029/2006JC003572, 2007.

Rysgaard, S., Bendtsen, J., Delille, B., Dieckmann, G. S., Glud, R. N., Kennedy, H., Mortensen, J., Papadimitriou, S., Thomas, D. N., and Tison, J. L.: Sea ice contribution to the air-sea CO2 exchange in the Arctic and Southern Oceans, Tellus Ser. B Chem. Phys. Meteorol., 63, 823–830, https://doi.org/10.1111/j.1600-0889.2011.00571.x, 2011.

Rysgaard, S., Søgaard, D. H., Cooper, M., Pućko, M., Lennert, K., Papakyriakou, T. N., Wang, F., Geilfus, N. X., Glud, R. N., Ehn, J., McGinnis, D. F., Attard, K., Sievers, J., Deming, J. W., and Barber, D.: Ikaite crystal distribution in winter sea ice and implications for CO 2 system dynamics, The Cryosphere, 7, 707–718, https://doi.org/10.5194/tc-7-707-2013, 2013.

Sabine, C. L., Feely, R. A., Gruber, N., Key, R. M., Lee, K., Bullister, J. L., Wanninkhof, R., Wong, C. S., Wallace, D. W. R., Tilbrook, B., Millero, F. J., Peng, T., and Kozyr, A.: The Oceanic Sink for Anthropogenic CO 2, Science, 305, 367–372, https://doi.org/10.1126/science.1097403, 2004.

Sarmiento, J. L. and Gruber, N.: Ocean Biogeochemical Dynamics, Princeton University Press, Princeton, 1–503 pp., 2006.

Sarmiento, J. L., Hughes, T., Stouffer, R. J., and Manabe, S.: Simulated response of the ocean carbon cycle to anthropogenic climate warming, Nature, 393, 245–249, https://doi.org/10.1038/30455, 1998.

Sastri, A. R., Christian, J. R., Achterberg, E. P., Atamanchuk, D., Buck, J. J. H., Bresnahan, P., Duke, P. J., Evans, W., Gonski, S. F., Johnson, B., Juniper, S. K., Mihaly, S., Miller, L. A., Morley, M., Murphy, D., Nakaoka, S., Ono, T., and Christian, J. R.: Perspectives on in situ Sensors for Ocean Acidification Research, Front. Mar. Sci., 6:653, https://doi.org/10.3389/fmars.2019.00653, 2019.

ESA Ocean Colour Climate Change Initiative (Ocean_Colour_cci): Global chlorophyll-a data products gridded on a geographic projection, Version 5.0: https://catalogue.ceda.ac.uk/uuid/e9f82908fd9c48138b31e5cfaa6d692b.

Scannell, H. A., Johnson, G. C., Thompson, L., Lyman, J. M., and Riser, S. C.: Subsurface Evolution and Persistence of Marine Heatwaves in the Northeast Pacific, Geophys. Res. Lett., 47, 1–10, https://doi.org/10.1029/2020GL090548, 2020.

Semiletov, I. P., Pipko, I. I., Repina, I., and Shakhova, N. E.: Carbonate chemistry dynamics and carbon dioxide fluxes across the atmosphere-ice-water interfaces in the Arctic Ocean: Pacific sector of the Arctic, J. Mar. Syst., 66, 204–226, https://doi.org/10.1016/j.jmarsys.2006.05.012, 2007.

Shadwick, E. H., Thomas, H., Azetsu-Scott, K., Greenan, B. J. W., Head, E., and Horne, E.: Seasonal variability of dissolved inorganic carbon and surface water pCO2 in the Scotian Shelf region of the Northwestern Atlantic, Mar. Chem., 124, 23–37, https://doi.org/10.1016/j.marchem.2010.11.004, 2011.

Sharkey, A. J. C.: Combining Artificial Neural Nets: Ensemble and Modular Multi-Net Systems, Springer, Berlin, 1999.

Sharp, J. D., Fassbender, A. J., Carter, B. R., Lavin, P. D., and Sutton, A. J.: A monthly surface pCO2product for the California Current Large Marine Ecosystem, Earth Syst. Sci. Data, 14, 2081–2108, https://doi.org/10.5194/essd-14-2081-2022, 2022.

Shutler, J. D.: Offsetting is a dangerous smokescreen for inaction, Front. Ecol. Environ., 18, 486, https://doi.org/10.1002/fee.2262, 2020.

Shutler, J. D., Land, P. E., Piolle, J. F., Woolf, D. K., Goddijn-Murphy, L., Paul, F., Girard-Ardhuin, F., Chapron, B., and Donlon, C. J.: FluxEngine: A flexible processing system for calculating atmosphere-ocean carbon dioxide gas fluxes and climatologies, J. Atmospheric Ocean. Technol., 33, 741–756, https://doi.org/10.1175/JTECH-D-14-00204.1, 2016.

Shutler, J. D., Wanninkhof, R., Nightingale, P. D., Woolf, D. K., Bakker, D. C. E., Watson, A., Ashton, I., Holding, T., Chapron, B., Quilfen, Y., Fairall, C., Schuster, U., Nakajima, M., and Donlon, C. J.: Satellites will address critical science priorities for quantifying ocean carbon, Front. Ecol. Environ., 18, 27–35, https://doi.org/10.1002/fee.2129, 2020.

Shutler, J. D., Gruber, N., Findlay, H. S., Land, P. E., Gregor, L., Holding, T., Sims, R. P., Green, H., Piolle, J.-F., Chapron, B., Sathyendranath, S., Rousseaux, C. S., Donlon, C. J., Cooley, S., Turner, J., Valauri-Orton, A., Lowder, K., Widdicombe, S., Newton, J., Sabia, R., Rio, M.-H., and Gaultier, L.: The increasing importance of satellite observations to assess the ocean carbon sink and ocean acidification, Earth-Sci. Rev., 250, 104682, https://doi.org/10.1016/j.earscirev.2024.104682, 2024.

Siedlecki, S. A., Pilcher, D. J., Hermann, A. J., Coyle, K., and Mathis, J.: The Importance of Freshwater to Spatial Variability of Aragonite Saturation State in the Gulf of Alaska, J. Geophys. Res. Oceans, 122, 8482–8502, https://doi.org/10.1002/2017JC012791, 2017.

Siegenthaler, U. and Sarmiento, J. L.: Atmospheric carbon dioxide and the ocean, Nature, 365, 119–125, https://doi.org/10.1038/365119a0, 1993.

Signorini, S. R., Mannino, A., Najjar, R. G., Friedrichs, M. A. M., Cai, W. J., Salisbury, J., Wang, Z. A., Thomas, H., and Shadwick, E.: Surface ocean pCO2 seasonality and sea-air CO2 flux estimates for the North American east coast, J. Geophys. Res. Oceans, 118, 5439–5460, https://doi.org/10.1002/jgrc.20369, 2013.

Simpson, E., Ianson, D., and Kohfeld, K. E.: Using End-Member Models to Estimate Seasonal Carbonate Chemistry and Acidification Sensitivity in Temperate Estuaries, Geophys. Res. Lett., 49, e2021GL095579, https://doi.org/10.1029/2021GL095579, 2022.

Smith, S., Geden, O., Nemet, G., Gidden, M., Lamb, W., Powis, C., Bellamy, R., Callaghan, M., Cowie, A., Cox, E., Fuss, S., Gasser, T., Grassi, G., Greene, J., Lueck, S., Mohan, A., Müller-Hansen, F., Peters, G., Pratama, Y., Repke, T., Riahi, K., Schenuit, F., Steinhauser, J., Strefler, J., Valenzuela, J., and Minx, J.: State of Carbon Dioxide Removal - 1st Edition, https://doi.org/10.17605/OSF.IO/W3B4Z, 2023.

Sonnichsen, C., Atamanchuk, D., Hendricks, A., Morgan, S., Smith, J., Grundke, I., Luy, E., and Sieben, V. J.: An Automated Microfluidic Analyzer for In Situ Monitoring of Total Alkalinity, ACS Sens., 8, 344–352, https://doi.org/10.1021/acssensors.2c02343, 2023.

Søreide, J. E., Leu, E. V. A., Berge, Jør., Graeve, M., and Falk-Petersen, S.: Timing of blooms, algal food quality and Calanus glacialis reproduction and growth in a changing Arctic, Glob. Change Biol., 16, 3154–3163, https://doi.org/10.1111/j.1365-2486.2010.02175.x, 2010.

Sothe, C., Gonsamo, A., Arabian, J., Kurz, W. A., Finkelstein, S. A., and Snider, J.: Large Soil Carbon Storage in Terrestrial Ecosystems of Canada, Glob. Biogeochem. Cycles, 36, 1–18, https://doi.org/10.1029/2021gb007213, 2022.

Stabeno, P. J., Reed, R. K., and Schumacher, J. D.: The Alaska Coastal Current: Continuity of transport and forcing, J. Geophys. Res. Oceans, 100, 2477–2485, 1995.

Stabeno, P. J., Bond, N. A., Hermann, A. J., Kachel, N. B., Mordy, C. W., and Overland, J. E.: Meteorology and oceanography of the Northern Gulf of Alaska, 859–897 pp., https://doi.org/10.1016/j.csr.2004.02.007, 2004.

Stewart, A., deYoung, B., Smit, M., Donaldson, K., Reedman, A., Bastien, A., Brunsting, R., Carter, B., Covey, B., Kelly, R., Peterson, E., Pirenne, B., Plourde, A., Ste-Marie, A.-S., Tollefsen, C., Wallace, D., and Whoriskey, F.: The Development of a Canadian Integrated Ocean Observing System (CIOOS), Front. Mar. Sci., 6, 2019.

Sun, H., He, J., Chen, Y., and Zhao, B.: Space-Time Sea Surface pCO2 Estimation in the North Atlantic Based on CatBoost, Remote Sens., 13, 2805, https://doi.org/10.3390/rs13142805, 2021.

Sutton, A. J., Wanninkhof, R., Sabine, C. L., Feely, R. A., Cronin, M. F., and Weller, R. A.: Variability and trends in surface seawater pCO 2 and CO 2 flux in the Pacific Ocean, Geophys. Res. Lett., 44, 5627–5636, https://doi.org/10.1002/2017GL073814, 2017.

Sutton, A. J., Feely, R. A., Maenner-Jones, S., Musielwicz, S., Osborne, J., Dietrich, C., Monacci, N., Cross, J., Bott, R., Kozyr, A., Andersson, A. J., Bates, N. R., Cai, W. J., Cronin, M. F., De Carlo, E. H., Hales, B., Howden, S. D., Lee, C. M., Manzello, D. P., McPhaden, M. J., Meléndez, M., Mickett, J. B., Newton, J. A., Noakes, S. E., Noh, J. H., Olafsdottir, S. R., Salisbury, J. E., Send, U., Trull, T. W., Vandemark, D. C., and Weller, R. A.: Autonomous seawater pCO 2 and pH time series from 40 surface buoys and the emergence of anthropogenic trends, Earth Syst. Sci. Data, 11, 421–439, https://doi.org/10.5194/essd-11-421-2019, 2019.

Sutton-Grier, A. E., Moore, A. K., Wiley, P. C., and Edwards, P. E. T.: Incorporating ecosystem services into the implementation of existing U.S. natural resource management regulations: Operationalizing carbon sequestration and storage, Mar. Policy, 43, 246–253, https://doi.org/10.1016/j.marpol.2013.06.003, 2014.

Tabata, S.: The general circulation of the Pacific Ocean and a brief account of the oceanographic structure of the North Pacific Ocean Part I - circulation and volume transports, Atmosphere, 13, 133–168, https://doi.org/10.1080/00046973.1975.9648394, 1975.

Takahashi, T., Olafsson, J., Goddard, J. G., Chipman, D. W., and Sutherland, S. C.: Seasonal variation of CO2 and nutrients in the high-latitude surface oceans: A comparative study, Glob. Biogeochem. Cycles, 7, 843–878, https://doi.org/10.1029/93GB02263, 1993.

Takahashi, T., Takahashi, T. T., Sutherland, S. C., Williams, R. G., Eglinton, G., Elderfield, H., Whitfield, M., and Williams, P. J. Le. B.: An assessment of the role of the North Atlantic as a CO2 sink, Philos. Trans. R. Soc. Lond. B. Biol. Sci., 348, 143–152, https://doi.org/10.1098/rstb.1995.0056, 1995.

Takahashi, T., Feely, R. A., Weiss, R. F., Wanninkhof, R. H., Chipman, D. W., Sutherland, S. C., and Takahashi, T. T.: Global air-sea flux of CO2: An estimate based on measurements of sea–air pCO2 difference, Proc. Natl. Acad. Sci., 94, 8292–8299, https://doi.org/10.1073/pnas.94.16.8292, 1997.

Takahashi, T., Sutherland, S. C., Sweeney, C., Poisson, A., Metzl, N., Tilbrook, B., Bates, N., Wanninkhof, R., Feely, R. A., Sabine, C., Olafsson, J., and Nojiri, Y.: Global sea-air CO2 flux based on climatological surface ocean pCO2, and seasonal biological and temperature effects, Deep-Sea Res. Part II Top. Stud. Oceanogr., 49, 1601–1622, https://doi.org/10.1016/S0967-0645(02)00003-6, 2002.

Takahashi, T., Sutherland, S. C., Feely, R. A., and Wanninkhof, R.: Decadal change of the surface water pCO_2 in the North Pacific: A synthesis of 35 years of observations, J. Geophys. Res., 111, C07S05, https://doi.org/10.1029/2005JC003074, 2006.

Takahashi, T., Sutherland, S. C., Wanninkhof, R., Sweeney, C., Feely, R. A., Chipman, D. W., Hales, B., Friederich, G., Chavez, F., Sabine, C., Watson, A., Bakker, D. C. E., Schuster, U., Metzl, N., Yoshikawa-Inoue, H., Ishii, M., Midorikawa, T., Nojiri, Y., Körtzinger, A., Steinhoff, T., Hoppema, M., Olafsson, J., Arnarson, T. S., Tilbrook, B., Johannessen, T., Olsen, A., Bellerby, R., Wong, C. S., Delille, B., Bates, N. R., and de Baar, H. J. W.: Climatological mean and decadal change in surface ocean pCO2, and net sea-air CO2 flux over the global oceans, Deep-Sea Res. Part II Top. Stud. Oceanogr., 56, 554–577, https://doi.org/10.1016/j.dsr2.2008.12.009, 2009.

Takahashi, T., Sutherland, S. C., Chipman, D. W., Goddard, J. G., and Ho, C.: Climatological distributions of pH, pCO2, total CO2, alkalinity, and CaCO3 saturation in the global surface ocean, and temporal changes at selected locations, Mar. Chem., 164, 95–125, https://doi.org/10.1016/j.marchem.2014.06.004, 2014.

Takatani, Y., Kazutaka, E., and Iida, Y.: Relationships between total alkalinity in surface water and sea surface dynamic height in the Pacific Ocean, J. Geophys. Res. Oceans, 119, 6121–6139, https://doi.org/10.1002/2013JC009739.Received, 2014.

Talley, L. D.: Ventilation of the Subtropical North Pacific: The Shallow Salinity Minimum, J. Phys. Oceanogr., 15, 633–649, https://doi.org/10.1175/1520-0485(1985)015<0633:VOTSNP>2.0.CO;2, 1985.

Tanhua, T., Pouliquen, S., Hausman, J., O'Brien, K., Bricher, P., de Bruin, T., Buck, J. J. H., Burger, E. F., Carval, T., Casey, K. S., Diggs, S., Giorgetti, A., Glaves, H., Harscoat, V., Kinkade, D., Muelbert, J. H., Novellino, A., Pfeil, B., Pulsifer, P. L., Van de Putte, A., Robinson, E., Schaap, D., Smirnov, A., Smith, N., Snowden, D., Spears, T., Stall, S., Tacoma, M., Thijsse, P., Tronstad, S., Vandenberghe, T., Wengren, M., Wyborn, L., and Zhao, Z.: Ocean FAIR Data Services, Front. Mar. Sci., 6, 2019.

Teague, K. A. and Gallicchio, N.: The Evolution of Meteorology: A Look into the Past, Present, and Future of Weather Forecasting, John Wiley & Sons, 285 pp., 2017.

Teeter, L., Hamme, R. C., Ianson, D., and Bianucci, L.: Accurate Estimation of Net Community Production From O2/Ar Measurements, Glob. Biogeochem. Cycles, 32, 1163–1181, https://doi.org/10.1029/2017GB005874, 2018.

Telszewski, M., Chazottes, A., Schuster, U., Watson, A. J., Moulin, C., Bakker, D. C. E., González-Dávila, M., Johannessen, T., Körtzinger, A., Lüger, H., Olsen, A., Omar, A., Padin, X. A., Ríos, A. F., Steinhoff, T., Santana-Casiano, M., Wallace, D. W. R., and Wanninkhof, R.: Estimating the monthly pCO2 distribution in the north Atlantic using a self-organizing neural network, Biogeosciences, 6, 1405–1421, https://doi.org/10.5194/bg-6-1405-2009, 2009.

Therriault, J.-C., Petrie, B., Pepin, P., Gagnon, J., Gregory, D., Helbig, J., Herman, A., Lefaivre, D., Mitchell, M., Pelchat, B., Runge, J., and Sameoto, D.: Proposal for a northwest Atlantic zonal monitoring program, Can Tech Rep Hydrogr Ocean Sci, 194, vii+57p, 1998.

Thomas, H., Prowe, A. E. F., Lima, I. D., Doney, S. C., Wanninkhof, R., Greatbatch, R. J., Schuster, U., and Corbière, A.: Changes in the North Atlantic Oscillation influence CO2 uptake in the North Atlantic over the past 2 decades, Glob. Biogeochem. Cycles, 22, 1–13, https://doi.org/10.1029/2007GB003167, 2008.

Thomson, R. E.: Oceanography of the British Columbia Coast, 291pp. pp., 1981.

Thomson, R. E. and Ware, D. M.: A current velocity index of ocean variability, J. Geophys. Res. Oceans, 101, 14297–14310, https://doi.org/10.1029/96JC01055, 1996.

Timmermans, M. L. and Marshall, J.: Understanding Arctic Ocean Circulation: A Review of Ocean Dynamics in a Changing Climate, J. Geophys. Res. Oceans, 125, 1–35, https://doi.org/10.1029/2018JC014378, 2020.

Tinis, S. W., Thomson, R. E., Mass, C. F., and Hickey, B. M.: Comparison of MM5 and meteorological buoy winds from British Columbia to northern California, Atmosphere - Ocean, 44, 65–81, https://doi.org/10.3137/ao.440105, 2006.

Tortell, P. D., Merzouk, A., Ianson, D., Pawlowicz, R., and Yelland, D. R.: Influence of regional climate forcing on surface water pCO 2,ΔO 2/Ar and dimethylsulfide (DMS) along the southern British Columbia coast, Cont. Shelf Res., 47, 119–132, https://doi.org/10.1016/j.csr.2012.07.007, 2012.

Tremblay, J.-éric, Anderson, L. G., Matrai, P., Coupel, P., Bélanger, S., Michel, C., and Reigstad, M.: Global and regional drivers of nutrient supply, primary production and CO2 drawdown in the changing Arctic Ocean, Prog. Oceanogr., 139, 171–196, https://doi.org/10.1016/j.pocean.2015.08.009, 2015.

Truth and Reconciliation Commission of Canada: Truth and Reconciliation Commission of Canada: Calls to Action, Calls to Action, Winnipeg, Manitoba, Canada, 2015.

Turgeon, K., Hawkshaw, S. C. F., Dinning, K. M., Quinn, B. K., Edwards, D. N., Wor, C., Parlee, C. E., Debertin, A., Hawkshaw, M., Nelson, B. W., Zhang, F., Benestan, L., Angel, E., Morse, B. L., and Mombourquette, D.: Enhancing fisheries education and research through the Canadian Fisheries Research Network: A student perspective on interdisciplinarity, collaboration and inclusivity, Facets, 3, 963–980, https://doi.org/10.1139/facets-2017-0038, 2018.

Ullman, D. J., McKinley, G. A., Bennington, V., and Dutkiewicz, S.: Trends in the North Atlantic carbon sink: 1992-2006, Glob. Biogeochem. Cycles, 23, 1992–2006, https://doi.org/10.1029/2008GB003383, 2009.

UNFCCC: Adoption of the Paris Agreement. Proposal by the President., , 21932, 32, 2015.

United Nations Environment Programme: Emissions Gap Report 2022: The Closing Window — Climate crisis calls for rapid transformation of societies, Nairobi, 1 pp., 2022.

Van Scoy, K. A., Olson, D. B., and Fine, R. A.: Ventilation of North Pacific intermediate waters: The role of the Alaskan Gyre, J. Geophys. Res. Oceans, 96, 16801–16810, https://doi.org/10.1029/91JC01783, 1991.

Vandemark, D., Salisbury, J. E., Hunt, C. W., Shellito, S. M., Irish, J. D., McGillis, W. R., Sabine, C. L., and Maenner, S. M.: Temporal and spatial dynamics of CO2 air-sea flux in the Gulf of Maine, J. Geophys. Res. Oceans, 116, 1–14, https://doi.org/10.1029/2010JC006408, 2011.

Verra: Verified Carbon Standard Program Guide v4.5, Verra, 2023.

Villa-Alfageme, M., Soto, F. C. de, Ceballos, E., Giering, S. L. C., Moigne, F. A. C. L., Henson, S., Mas, J. L., and Sanders, R. J.: Geographical, seasonal, and depth variation in sinking particle speeds in the North Atlantic, Geophys. Res. Lett., 43, 8609–8616, https://doi.org/10.1002/2016GL069233, 2016.

Vonk, J. E. and Gustafsson, Ö.: Permafrost-carbon complexities, Nat. Geosci., 6, 675–676, https://doi.org/10.1038/ngeo1937, 2013.

Wallcraft, A. J., Kara, A. B., Barron, C. N., Metzger, E. J., Pauley, R. L., and Bourassa, M. A.: Comparisons of monthly mean 10 m wind speeds from satellites and NWP products over the global ocean, J. Geophys. Res. Atmospheres, 114, https://doi.org/10.1029/2008JD011696, 2009.

Wang, H., Hu, X., and Sterba-Boatwright, B.: A new statistical approach for interpreting oceanic fCO2 data, Mar. Chem., 183, 41–49, https://doi.org/10.1016/j.marchem.2016.05.007, 2016.

Wang, H., Hu, X., Cai, W.-J., and Sterba-Boatwright, B.: Decadal fCO2 trends in global ocean margins and adjacent boundary current-influenced areas, Geophys. Res. Lett., 44, 8962–8970, https://doi.org/10.1002/2017GL074724, 2017.

Wang, J., Jin, M., and Musgrave, D. L.: A hydrological digital elevation model for freshwater discharge into the Gulf of Alaska, 109, 1–15, https://doi.org/10.1029/2002JC001430, 2004.

Wang, Q., Wekerle, C., Danilov, S., Koldunov, N., Sidorenko, D., Sein, D., Rabe, B., and Jung, T.: Arctic Sea Ice Decline Significantly Contributed to the Unprecedented Liquid Freshwater Accumulation in the Beaufort Gyre of the Arctic Ocean, Geophys. Res. Lett., 45, 4956–4964, https://doi.org/10.1029/2018GL077901, 2018.

Wang, Y., Li, X., Song, J., Li, X., Zhong, G., and Zhang, B.: Carbon sinks and variations of pCO2 in the Southern Ocean from 1998 to 2018 based on a deep learning approach, IEEE J. Sel. Top. Appl. Earth Obs. Remote Sens., 14, 3495–3503, https://doi.org/10.1109/JSTARS.2021.3066552, 2021.

Wanninkhof, R.: Relationship between wind speed and gas exchange over the ocean revisited, Limnol. Oceanogr. Methods, 12, 351–362, https://doi.org/10.4319/lom.2014.12.351, 2014.

Wanninkhof, R. and Triñanes, J.: The impact of changing wind speeds on gas transfer and its effect on global air-sea CO2 fluxes, Glob. Biogeochem. Cycles, 31, 961–974, https://doi.org/10.1002/2016GB005592, 2017.

Wanninkhof, R., Asher, W. E., Ho, D. T., Sweeney, C., and McGillis, W. R.: Advances in quantifying air-sea gas exchange and environmental forcing, Annu. Rev. Mar. Sci., 1, 213–244, https://doi.org/10.1146/annurev.marine.010908.163742, 2009.

Wanninkhof, R., Park, G.-H., Takahashi, T., Sweeney, C., Feely, R., Nojiri, Y., Gruber, N., Doney, S. C., McKinley, G. A., Lenton, A., Qu´er´e, C. L., Heinze, C., Schwinger, J., Graven, H., and Khatiwala, S.: Global ocean carbon uptake : magnitude , variability and trends, Biogeosciences, 10, 1983–2000, https://doi.org/10.5194/bg-10-1983-2013, 2013a.

Wanninkhof, R., Park, G.-H., Takahashi, T., Sweeney, C., Feely, R., Nojiri, Y., Gruber, N., Doney, S. C., McKinley, G. A., Lenton, A., Qu´er´e, C. L., Heinze, C., Schwinger, J., Graven, H., and Khatiwala, S.: Global ocean carbon uptake : magnitude , variability and trends, Biogeosciences, 10, 1983–2000, https://doi.org/10.5194/bg-10-1983-2013, 2013b.

Ward, N. D., Megonigal, J. P., Bond-Lamberty, B., Bailey, V. L., Butman, D., Canuel, E. A., Diefenderfer, H., Ganju, N. K., Goñi, M. A., Graham, E. B., Hopkinson, C. S., Khangaonkar, T., Langley, J. A., McDowell, N. G., Myers-Pigg, A. N., Neumann, R. B., Osburn, C. L., Price, R. M., Rowland, J., Sengupta, A., Simard, M., Thornton, P. E., Tzortziou, M., Vargas, R., Weisenhorn, P. B., and Windham-Myers, L.: Representing the function and sensitivity of

coastal interfaces in Earth system models, Nat. Commun., 11, 2458, https://doi.org/10.1038/s41467-020-16236-2, 2020.

Ware, D. M. and Thomson, R. E.: Bottom-Up Ecosystem Trophic Dynamics Determine Fish Production in the Northeast Pacific, Science, 308, 1280–1284, https://doi.org/10.1126/science.1109049, 2005.

Watson, A. J., Schuster, U., Shutler, J. D., Holding, T., Ashton, I. G. C., Landschützer, P., Woolf, D. K., and Goddijn-Murphy, L.: Revised estimates of ocean-atmosphere CO2 flux are consistent with ocean carbon inventory, Nat. Commun., 11, 1–6, https://doi.org/10.1038/s41467-020-18203-3, 2020.

Weatherdon, L. V., Ota, Y., Jones, M. C., Close, D. A., and Cheung, W. W. L.: Projected scenarios for coastal first nations' fisheries catch potential under climate change: Management challenges and opportunities, PLoS ONE, 11, 1–28, https://doi.org/10.1371/journal.pone.0145285, 2016.

Weingartner, T. J., Coyle, K., Finney, B., Hopcroft, R., Whitledge, T., Brodeur, R., Dagg, M., Farley, E., Haidvogel, D., Haldorson, L., Hermann, A. I., Hinckley, S., Napp, J., Stabeno, P., Kline, T., Lee, C., Lessard, E., Royer, T., and Strom, S.: The Northeast Pacific GLOBEC Program: Coastal Gulf of Alaska, Oceanography, 15, 48–63, https://doi.org/10.5670/oceanog.2002.21, 2002.

Weiss, K., Hamann, M., and Marsh, H.: Bridging Knowledges: Understanding and Applying Indigenous and Western Scientific Knowledge for Marine Wildlife Management, Soc. Nat. Resour., 26, 285–302, https://doi.org/10.1080/08941920.2012.690065, 2013.

Weiss, R. F.: Carbon dioxide in water and seawater: the solubility of a non-ideal gas, Mar. Chem., 2, 203–215, https://doi.org/10.1016/0304-4203(74)90015-2, 1974.

Westbrook, G. K., Thatcher, K. E., Rohling, E. J., Piotrowski, A. M., Pälike, H., Osborne, A. H., Nisbet, E. G., Minshull, T. A., Lanoisellé, M., James, R. H., Hühnerbach, V., Green, D., Fisher, R. E., Crocker, A. J., Chabert, A., Bolton, C., Beszczynska-Möller, A., Berndt, C., and Aquilina, A.: Escape of methane gas from the seabed along the West Spitsbergen continental margin, Geophys. Res. Lett., 36, 1–5, https://doi.org/10.1029/2009GL039191, 2009.

Whitney, F. and Robert, M.: Structure of Haida Eddies and their transport of nutrient from coastal margins into the NE pacific ocean, J. Oceanogr., 58, 715–723, https://doi.org/10.1023/A:1022850508403, 2002.

Whitney, F. A. and Freeland, H. J.: Variability in upper-ocean water properties in the NE Pacific Ocean, Deep-Sea Res. Part II Top. Stud. Oceanogr., 46, 2351–2370, https://doi.org/10.1016/S0967-0645(99)00067-3, 1999.

Whitney, F. A., Crawford, W. R., and Harrison, P. J.: Physical processes that enhance nutrient transport and primary productivity in the coastal and open ocean of the subarctic NE Pacific, Deep-Sea Res. Part II Top. Stud. Oceanogr., 52, 681–706, https://doi.org/10.1016/j.dsr2.2004.12.023, 2005.

Wilkerson, F. P. and Dugdale, R. C.: The use of large shipboard barrels and drifters to study the effects of coastal upwelling on phytoplankton dynamics1, 2, Limnol. Oceanogr., 32, 368–382, https://doi.org/10.4319/lo.1987.32.2.0368, 1987.

Williamson, P., Gattuso, J., and Pearce, C. R.: Carbon Removal Using Coastal Blue Carbon Ecosystems Is Uncertain and Unreliable , With Questionable Climatic Cost-Effectiveness, Front. Clim., 4, 1–14, https://doi.org/10.3389/fclim.2022.853666, 2022.

Wilson, K., Arreak, A., Sikumiut Committee, Bell, T., and Ljubicic, G.: The Mittimatalik Siku Asijjipallianinga (Sea Ice Climate Atlas): How Inuit Knowledge, Earth Observations, and Sea Ice Charts Can Fill IPCC Climate Knowledge Gaps, Front. Clim., 3, 2021.

Winton, M., Griffies, S. M., Samuels, B. L., Sarmiento, J. L., and Licher, T. L. F.: Connecting changing ocean circulation with changing climate, J. Clim., 26, 2268–2278, https://doi.org/10.1175/JCLI-D-12-00296.1, 2013.

Wong, C., Ballegooyen, K., Ignace, L., Johnson, M. J., and Swanson, H.: Towards reconciliation: 10 Calls to Action to natural scientists working in Canada, Facets, 5, 769–783, https://doi.org/10.1139/FACETS-2020-0005, 2020.

Wong, C. S. and Chan, Y.-H.: Temporal variations in the partial pressure and flux of CO2 at ocean station P in the subarctic northeast Pacific Ocean, Tellus, 43B, 206–223, https://doi.org/10.1034/j.1600-0889.1991.00014.x, 1991.

Wong, C. S. and Johnson, W. K.: Subarctic Ecosystem Response to Iron Enrichment Study (SERIES): Eastern Subarctic Pacific, July 2002, Institute of Ocean Sciences, Sidney, B.C, 2002.

Wong, C. S., Christian, J. R., Emmy Wong, S. K., Page, J., Xie, L., and Johannessen, S.: Carbon dioxide in surface seawater of the eastern North Pacific Ocean (Line P), 1973-2005, Deep-Sea Res. Part Oceanogr. Res. Pap., 57, 687–695, https://doi.org/10.1016/j.dsr.2010.02.003, 2010.

Woolf, D. K., Land, P. E., Shutler, J. D., Goddijn-Murphy, L. M., and Donlon, C. J.: On the calculation of air-sea fluxes of CO2 in the presence of temperature and salinity gradients, J. Geophys. Res. Oceans, 121, 3010–3028, https://doi.org/10.1002/2015JC011516, 2016.

Wunsch, C.: What Is the Predictive Ecology, Science, 298, 1179–1180, 2002.

Xu, S., Park, K., Wang, Y., Chen, L., Qi, D., and Li, B.: Variations in the summer oceanic pCO 2 and carbon sink in Prydz Bay using the self-organizing map analysis approach, Biogeosciences, 16, 797–810, https://doi.org/10.5194/bg-16-797-2019, 2019.

Yamamoto-Kawai, M., McLaughlin, F. A., Carmack, E. C., Nishino, S., Shimada, K., and Kurita, N.: Surface freshening of the Canada Basin, 2003–2007: River runoff versus sea ice meltwater, J. Geophys. Res., 114, C00A05, https://doi.org/10.1029/2008JC005000, 2009.

Yashayaev, I. and Loder, J. W.: Further intensification of deep convection in the Labrador Sea in 2016, Geophys. Res. Lett., 44, 1429–1438, https://doi.org/10.1002/2016GL071668, 2017.

Yasunaka, S., Murata, A., Watanabe, E., Chierici, M., Fransson, A., van Heuven, S., Hoppema, M., Ishii, M., Johannessen, T., Kosugi, N., Lauvset, S. K., Mathis, J. T., Nishino, S., Omar, A. M., Olsen, A., Sasano, D., Takahashi, T., and Wanninkhof, R.: Mapping of the air–sea CO2 flux in the Arctic Ocean and its adjacent seas: Basin-wide distribution and seasonal to interannual variability, Polar Sci., 10, 323–334, https://doi.org/10.1016/j.polar.2016.03.006, 2016.

Yasunaka, S., Siswanto, E., Olsen, A., Hoppema, M., Watanabe, E., Fransson, A., Chierici, M., Murata, A., Lauvset, S. K., Wanninkhof, R., Takahashi, T., Kosugi, N., Omar, A. M., Van Heuven, S., and Mathis, J. T.: Arctic Ocean CO2 uptake: An improved multiyear estimate of the air-sea CO2 flux incorporating chlorophyll a concentrations, Biogeosciences, 15, 1643–1661, https://doi.org/10.5194/bg-15-1643-2018, 2018.

Young, I. R. and Ribal, A.: Multiplatform evaluation of global trends in wind speed and wave height, Science, 364, 548–552, https://doi.org/10.1126/science.aav9527, 2019.

Yu, J., Wang, X., Fan, H., and Zhang, R. H.: Impacts of Physical and Biological Processes on Spatial and Temporal Variability of Particulate Organic Carbon in the North Pacific Ocean during 2003–2017, Sci. Rep., 9, 1–15, https://doi.org/10.1038/s41598-019-53025-4, 2019.

Zheng, C. W., Pan, J., and Li, C. Y.: Global oceanic wind speed trends, Ocean Coast. Manag., 129, 15–24, https://doi.org/10.1016/j.ocecoaman.2016.05.001, 2016.

Zheng, Z., Luo, X., Wei, H., Zhao, W., and Qi, D.: Analysis of the Seasonal and Interannual Variations of Air-Sea CO2 Flux in the Chukchi Sea Using a Coupled Ocean-Sea Ice-Biogeochemical Model, J. Geophys. Res. Oceans, 126, 1–18, https://doi.org/10.1029/2021JC017550, 2021.

Zhong, G., Li, X., Song, J., Qu, B., Wang, F., and Wang, Y.: Reconstruction of global surface ocean p CO 2 using region-specific predictors based on a stepwise FFNN regression algorithm, Biogeosciences, 19, 845–859, https://doi.org/10.5194/bg-19-845-2022, 2022.

Appendix A. Supplemental material for Chapter 2

Contents of this Appendix

Table A.1

Table A.1 Comparison of reported air-sea CO_2 flux densities in Canada's adjacent ocean basins including details about oceanographic region, methods used, and the spatial and temporal resolution and range. Abbreviations are as follows: Self Organizing Map (SOM), Feed Forward Network (FFN), Regional Ocean Modeling System (ROMS), Nucleus for European Modelling of the Ocean (NEMO), Pelagic Interactions Scheme for Carbon and Ecosystem Studies (PISCES), Multiple Linear Regression (MLR), Massachusetts Institute of Technology General Circulation Model (MITgcm).

Estimate location	**CO_2 flux (mol C m^{-2} yr^{-1})[a]**	**Estimate type**	**Resolution (time step, time range, latitude x longitude)**	**Reference**	**Figure 2 legend**
Pacific					
NE Pacific open ocean	-0.7	Local observations	August 1973 to July 1978, Ocean Observing Station PAPA, location: 50°N 145°W	(Wong and Chan, 1991)	1
NE Pacific open ocean	-0.97	Local mooring	3-hours, 2007-2014, Ocean Observing Station PAPA, location: 50°N 145°W	(Sutton et al., 2017)	2
NE Pacific open ocean	-1.86±0.44	Local observations	Spring 2010	(Palevsky et al., 2013)	3
NE Pacific open ocean	-0.6	Local observations	Monthly, 2000-2001	(Chierici et al., 2006)	4
NE Pacific open ocean	-1.7 to 0	Local averaged observations	Monthly, year 2000 climatology, 4°x5°	(Takahashi et al., 2009)	5
NE Pacific open ocean	-1.5±0.33	Local observations	Fall 2008	(Lockwood et al., 2012)	6

NE Pacific open ocean	-1.34	Global, SOM-FFN interpolation	Monthly, 1982-2019, 1°x1°	(Landschützer et al., 2020b)	7
NE Pacific open ocean	-1.46	Local, multiple linear regression interpolation	Monthly, climatology, 1/10°x1/5°	(Evans and Mathis, 2013)	8
NE Pacific open ocean	-1.27	Global, ensemble based FFN interpolation	Monthly, 1985-2020, 1°x1°	(Global Ocean Surface Carbon, E.U. Copernicus Marine Service Information MULTIOBS_GLO_BIO_CARBON_SURFACE_REP_015_008)	9
NE Pacific open ocean	-0.67	Global, mixed-layer scheme	Daily, 1957-2020, 2°x2.5°	(Rödenbeck et al., 2013)	10
NE Pacific open ocean	-1.46	Local, ROMS model	Idealized 2009, 3/100°	(Pilcher et al., 2018)	11
NE Pacific open ocean	-1.14±0.55	*Mean and standard deviation of estimates*			
NE Pacific coastal ocean	-1.61	Global, averaged observations	Monthly, climatology, 1/2°x1/2°	(Laruelle et al., 2014)	12
NE Pacific coastal ocean	-1.8	Integration of multiple studies	2009	(Chen and Borges, 2009)	13
NE Pacific coastal ocean	-1.59	Global, SOM-FFN interpolation	Monthly, climatology, 1/4°x1/4°	(Roobaert et al., 2019)	14
NE Pacific coastal ocean	-2.29	Global, NEMO-PISCES model	Monthly, 1993–2012, 1/5° to 1/2°	(Bourgeois et al., 2016)	15

NE Pacific coastal ocean	-1.82±0.33	*Mean and standard deviation of estimates*			
Canadian Pacific Shelf	-0.4	Global, averaged observations	Monthly, climatology, 1°x1°	(Chavez et al., 2007)	16
Canadian Pacific Shelf	-2.19	Local observations	Separate fall, winter, and summer cruises over 2008-2010	(Evans et al., 2012)	17
Canadian Pacific Shelf	-1.2	Integration of multiple studies	2005	(Borges et al., 2005)	18
Canadian Pacific Shelf	-0.50	Local, mass balance model	Idealized 1990, horizontal shelf, slope, and offshore regions	(Ianson and Allen, 2002)	19
	-2.91 to -1.67 -1.83 to +0.67 -2.00 to +1.25		Idealized year under varying upwelling regimes (weak, moderate, strong)	(Ianson et al., 2009)	20
Canadian Pacific Shelf	-0.8 to -1.46	Local, quasi 2-D ROMS model	Idealized summer season, 3/200°x1/100°	(Bianucci et al., 2011)	21
Canadian Pacific Shelf	-10.07±2.45 -5.51±1.83 -1.02±1.35	Local observations	Summer 2008, primary production hotspot, transition zone, offshore	(Ribalet et al., 2010)	
Canadian Pacific Shelf	-1.09±1.20	*Mean and standard deviation of estimates (excluding* Ribalet *et al.* (2010))			
Salish Sea	+2.8 -0.17	Local observations	Separate fall and summer cruises over 2008-2010, main exchange region,	(Evans et al., 2012)	22

			freshwater influence region		
Salish Sea	+0.69	Local, NEMO model	Up to 2 seconds, idealized year, 500 m	(Jarníková et al., 2022b)	23
Salish Sea	+1.11±1.53	*Mean and standard deviation of estimates*			
Gulf of Alaska	-0.16	Regional model, ROMS-COBALT	Monthly, 1993-2013, 4.5x4.5 km, greater than 50 km offshore	(Hauri et al., 2020)	24
Gulf of Alaska coastal ocean	+0.84	Regional model, ROMS-COBALT	Monthly, 1993-2013, 4.5x4.5 km, within 50 km from the coast	(Hauri et al., 2020)	25
Gulf of Alaska coastal ocean	-1.8	Integration of multiple studies	2009	(Chen and Borges, 2009)	26
Gulf of Alaska coastal ocean	-5.37±0.88	Local observations	Spring 2010	(Palevsky et al., 2013)	27
Gulf of Alaska coastal ocean	-0.91	Local, MLR interpolation	Monthly, climatology, 1/10°x1/5°	(Evans and Mathis, 2013)	8
Gulf of Alaska coastal ocean	-0.84	Local, ROMS model	Idealized 2009, 3/100°	(Pilcher et al., 2018)	11
Gulf of Alaska coastal ocean	-1.62±2.31	*Mean and standard deviation of estimates*			
Estimate location	**CO_2 flux (mol C m^{-2} yr^{-1})[a]**	**Estimate type**	**Resolution (time step, time range, latitude x longitude)**	**Reference**	**Figure 2 legend**
Atlantic					
Newfoundland Shelf	-1.25	Global, SOM-FFN interpolation	Monthly, 1982-2019, 1°x1°	(Landschützer et al., 2020b)	7

Newfoundland Shelf	-1	Global, SOM-FFN interpolation	Monthly, 1°x1°	(Landschützer et al., 2013)	28
Newfoundland Shelf	-1.13±0.18	*Mean and standard deviation of estimates*			
Scotian shelf	+1.4	Local mooring	2007-2008, high temporal resolution, location: 44.3°N 63.3°W	(Shadwick et al., 2011)	29
Scotian shelf	+1.7±0.2	Regional, ROMS model	3-day average forcing, 10 km horizontal resolution	(Rutherford et al., 2021)	30
Scotian shelf	-1.21	Local observations	Ship of Opportunity Program tracks	(Signorini et al., 2013)	31
Scotian shelf	-0.42	Regional, MLR interpolation	Monthly, 1978–2010, 0.15°x0.15°	(Signorini et al., 2013)	31
Scotian shelf	+0.37±1.41	*Mean and standard deviation of estimates*			
Gulf of Maine	+0.04	Local observations	Ship of Opportunity Program tracks	(Signorini et al., 2013)	31
Gulf of Maine	+0.37	Local observations	Ship of Opportunity Program tracks	(Vandemark et al., 2011)	32
Gulf of Maine	+0.01	Regional, MLR interpolation	Monthly, 1978–2010, 0.15°x0.15°	(Signorini et al., 2013)	31
Gulf of Maine	-0.5±0.2	Regional ROMS model	3-day average forcing, 10 km horizontal resolution	(Rutherford et al., 2021)	30
Gulf of Maine	-0.02±0.36	*Mean and standard deviation of estimates*			
Scotian Shelf and Gulf of Maine	-0.7	Integration of multiple studies	2006	(Cai et al., 2006)	
Grand Banks	-1.3±0.3	Regional ROMS model	3-day average forcing, 10 km horizontal resolution	(Rutherford et al., 2021)	30

Gulf of St. Lawrence	+0.36 to +0.74	Local observations (calculated from carbonate state variables)	Seasonal (spring/ summer cruises), 2003-2016, 1/2°x1/2°	(Dinauer and Mucci, 2017)	33
Bay of Fundy	+1.4	Local mooring	2015-2016, high temporal resolution, location: 44.3°N 66.3°W	(Horwitz et al., 2019)	34
Coastal Labrador Sea	-1.72	Global, averaged observations	Monthly, climatology, 1/2°x1/2°	(Laruelle et al., 2014)	12
Coastal Labrador Sea	-1.88	Global, SOM-FFN interpolation	Monthly, climatology, 1/4°x1/4°	(Roobaert et al., 2019)	14
Coastal Labrador Sea	-1.27	Global, NEMO-PISCES model	Monthly, 1993–2012, 1/5° to 1/2°	(Bourgeois et al., 2016)	15
Coastal Labrador Sea	-1.62±0.32	*Mean and standard deviation of estimates*			
NW Atlantic coastal ocean	-1.0	Integration of multiple studies	2009	(Chen and Borges, 2009)	
Central Labrador Sea	-3.2 to -1.9	Local mooring (SeaCycler)	2016-2017, high temporal resolution, location: 56.82°N 52.22°W	(Atamanchuk et al., 2020)	35
Central Labrador Sea	-2.7	Local mooring (K1)	2004 - 2005, high temporal resolution, location: 56.50°N 52.60°W	(Koertzinger et al., 2008)	36
Central Labrador Sea	-4.6	Local mooring	2000 - 2001, high temporal resolution,	(DeGrandpre et al., 2006)	37

			location: 56.54°N 52.64°W		
Central Labrador Sea	-3.1	Local mooring	2004 - High temporal resolution, location: 53.00°N 49.00°W	(Martz et al., 2009)	38
Central Labrador Sea	-3	Global, SOM-FFN interpolation	Monthly, 1998-2007, 1°x1°	(Landschützer et al., 2013)	28
Central Labrador Sea	-2.2	Global, SOM-FFN interpolation	Monthly, 1982-2019, 1°x1°	(Landschützer et al., 2020b)	7
Central Labrador Sea	-2.96±0.87	*Mean and standard deviation of estimates*			
Estimate location	**CO_2 flux (mol C m^{-2} yr^{-1})[a]**	**Estimate type**	**Resolution (time step, time range, latitude x longitude)**	**Reference**	**Figure 2 legend**
Arctic					
Barents Sea	-4.05	Local, MLR interpolation	Multiple cruises over all seasons from 2005-2007	(Lauvset et al., 2013)	
Barents Sea	-3.83±1.50	Local observations	9 cruises over all seasons from 1992-2001	(Nakaoka et al., 2006)	
Barents Sea	-4.25±0.70	Regional, MLR interpolation	5 cruises over spring, summer, and fall from 1995-2002	(Omar et al., 2007)	
Barents Sea	-3.67±0.80	Local, mass balance model	Summer 1996	(Fransson et al., 2001)	
Barents Sea	-2.42±0.90	Local, mass balance model	Summer 1999	(Kaltin et al., 2002)	
Barents Sea	-1.46	Local averaged observations	Monthly, year 2000 climatology, 4°x5°	(Takahashi et al., 2009)	

Barents Sea	-2.58	Regional, numerical model with sea ice carbon system	~1/4° horizontal resolution, 1m vertical resolution at surface; 1980-2015 run	(Mortenson et al., 2020)	
Barents Sea	-1.46	Regional, coupled ocean-sea ice-biogeochemical model, MITgcm	Average over 1996–2007	(Manizza et al., 2013)	
Barents Sea	-0.73±0.36	Local observations	Based on (Takahashi et al., 2009) modified to 2008-2009	(Land et al., 2013)	
Barents Sea	-3.65±1.46	Regional, SOM interpolation	Monthly, 1997-2013, 1°x1°	(Yasunaka et al., 2016)	
Barents Sea	-3.65±1.10	Regional, SOM interpolation	Monthly, 1997-2014, 1°x1°	(Yasunaka et al., 2018)	
Chukchi Sea	-5.11±0.73	Local observations	Winter/spring 2002, summer 2004	(Bates et al., 2006)	39
Chukchi Sea	-1.41	Local observations	3 summer cruises from 1998–2000	(Murata and Takizawa, 2003)	40
Chukchi Sea	-1.46±0.73	Local observations	SOCAT data from 2003-2014	(Evans et al., 2015b)	41
Chukchi Sea	-2.81±0.69	Local observations	Early winter 2018	(Murata et al., 2018)	42
Chukchi Sea	-1.46±1.46	Regional, SOM interpolation	Monthly, 1997-2013, 1°x1°	(Yasunaka et al., 2016)	43
Chukchi Sea	-1.83±1.10	Regional, SOM interpolation	Monthly, 1997-2014, 1°x1°	(Yasunaka et al., 2018)	44
Chukchi Sea	-1.36	Regional, coupled ocean-	Average over 1998-2015	(Zheng et al., 2021)	45

		sea ice-biogeochemical model			
Chukchi Sea	-7.17±1.80	Local, mass balance model	Summer 1996	(Anderson and Kaltin, 2001)	46
Chukchi Sea	-2.83±2.17	*Mean and standard deviation of estimates*			
Amundsen Gulf	-0.3±0.2	Local observations	Annual from fall 2007-summer 2008	(Else et al., 2013)	47
Baffin Bay	-7 to -0.4	Local observations (calculated from carbonate state variables).	Separate spring/summer 1998, and fall 1999 cruises	(Miller et al., 2002)	48
Canadian Archipelago	-1.02	Global, averaged observations	Monthly, climatology, 1/2°x1/2°	(Laruelle et al., 2014)	12
Canadian Archipelago	-0.40	Global, SOM-FFN interpolation	Monthly, climatology, 1/4°x1/4°	(Roobaert et al., 2019)	14
Canadian Archipelago	-1.09	Regional, MLR interpolation	2010-2016	(Ahmed and Else, 2019)	49
Canadian Archipelago	-0.52	Global, NEMO-PISCES model	Monthly, 1993–2012, 1/5° to 1/2°	(Bourgeois et al., 2016)	15
Canadian Archipelago	-1.17	Regional, numerical model with sea ice carbon system	~1/4° horizontal resolution, 1m vertical resolution at surface; 1980-2015 run	(Mortenson et al., 2020)	50
Canadian Archipelago	-0.84±0.35	*Mean and standard deviation of estimates*			

Hudson Strait	-1.57	Local observations	Spring/summer 2018, open water	(Ahmed et al., 2021)	51
Hudson Bay	+0.72	Regional, MLR interpolation	Fall 2005	(Else et al., 2008b)	53
Hudson Bay	+0.31	Global, NEMO-PISCES model	Monthly, 1993–2012, 1/5° to 1/2°	(Bourgeois et al., 2016)	15
Hudson Bay	-1.86	Local observations	Spring/summer 2018, open water	(Ahmed et al., 2021)	51
Hudson Bay	-0.27	Local observations	Fall 2005	(Else et al., 2008a)	52
Hudson Bay	-1.38	Global, SOM-FFN interpolation	Monthly, climatology, 1/4°x1/4°	(Roobaert et al., 2019)	14
Hudson Bay	-0.50±1.10	*Mean and standard deviation of estimates*			
Beaufort Sea	-1.41	Local observations	3 summer cruises from 1998–2000	(Murata and Takizawa, 2003)	40
Beaufort Shelf Beaufort Basin	-0.42 -0.42	Regional, numerical model with sea ice carbon system	~1/4° horizontal resolution, 1m vertical resolution at surface; 1980-2015 run	(Mortenson et al., 2020)	50
Canada Basin	-1.75 to -0.91	Local observations	Fall 2012	(Islam et al., 2016)	
Kara Sea	-0.08	Local, mass balance model	Summer 1996	(Fransson et al., 2001)	
Kara Sea	-11.97 to -6.68	Local observations	3 cruises over summer/fall 2006, 2007, and 2009	(Pipko et al., 2017)	

Kara Sea	-0.31 to -0.15	Local observations	Based on (Takahashi et al., 2009) modified to 2008-2009	(Land et al., 2013)	
Laptev Sea	-5.73 to -0.29	Local observations	3 cruises over summer/fall 2006, 2007, and 2009	(Pipko et al., 2017)	
Laptev Sea	-0.2	Local, mass balance model	Summer 1994	(Nitishinsky et al., 2007)	
Laptev Sea	-0.25	Regional, numerical model with sea ice carbon system	~1/4° horizontal resolution, 1m vertical resolution at surface; 1980-2015 run	(Mortenson et al., 2020)	
East Siberian Sea	+0.29 to +4.2	Local observations	3 cruises fall 2003, 2004, and 2008	(Pipko et al., 2011)	
East Siberian Sea	-3.98 to -0.37	Local observations	Multiple cruises over all seasons from 1996-2005	(Semiletov et al., 2007)	
East Siberian Sea	+0.1	Local, mass balance model	Summer 1994	(Nitishinsky et al., 2007)	
Central Arctic Basin	-1 to -0.3	Local observations	Winter/spring 2002, summer 2004	(Bates et al., 2006)	
Greenland/Norwegian Sea	-2.08	Regional, numerical model with sea ice carbon system	~1/4° horizontal resolution, 1m vertical resolution at surface; 1980-2015 run	(Mortenson et al., 2020)	
Greenland/Norwegian Sea	-4±1	Regional, SOM interpolation	Monthly, 1997-2013, 1°x1°	(Yasunaka et al., 2016)	

Greenland/Norwegian Sea	-2.92±1.00	Local observations	Based on Takahashi *et al.* (2009) modified to 2008-2009	(Land et al., 2013)	
Greenland/Norwegian Sea	-4.38±1.82	Local observations	9 cruises over all seasons from 1992-2001	(Nakaoka et al., 2006)	
Greenland/Norwegian Sea	-4.38±0.37	Local observations	Multiple cruises over all seasons from 1993-1998	(Anderson et al., 2000)	
Greenland/Norwegian Sea	-3.29	Regional, MLR interpolation	Daily, 9 km, 1998–2003	(Arrigo et al., 2010)	
Greenland/Norwegian Sea	-0.73	Regional, coupled ocean-sea ice-biogeochemical model, MITgcm	Average over 1996–2007	(Manizza et al., 2013)	
Greenland/Norwegian Sea	-2.50±0.68	Regional, SOM interpolation	Monthly, 1997-2013, 1°x1°	(Yasunaka et al., 2016)	
Greenland/Norwegian Sea	-3.29±1.10	Regional, SOM interpolation	Monthly, 1997-2014, 1°x1°	(Yasunaka et al., 2018)	
Arctic Ocean	-1.46±1.46	Regional, SOM interpolation	Monthly, 1997-2013, 1°x1°	(Yasunaka et al., 2016)	
Arctic Ocean	-1.83±1.10	Regional, SOM interpolation	Monthly, 1997-2014, 1°x1°	(Yasunaka et al., 2018)	
Arctic Ocean	-1.53 to -0.62	Integration of multiple studies	2009	(Bates and Mathis, 2009)	
Arctic Shelf Seas	-2.2	Integration of multiple studies	2009	(Chen and Borges, 2009)	

[a]Negative flux (blue) indicates oceanic sink, positive flux (red) indicates oceanic outgassing.

Appendix B. Supplemental material for Chapter 3

Contents of this Appendix

Text B.1

The reported fCO_2 estimates were converted to pCO_2 using the equation S1 (Körtzinger, 1999):

$$pCO_2 = fCO_2 \times \exp[P_{atm}^{surf} \frac{B+(2\delta)}{RT}]^{-1}, \quad \text{(S1)}$$

where P_{atm}^{surf} is the total atmospheric surface pressure, B and δ are viral coefficients (Weiss, 1974), R is the gas constant and T is the absolute temperature. National Centers for Environmental Prediction (NCEP) monthly mean sea level pressure was used for P_{atm}^{surf} (Kalnay et al., 1996).

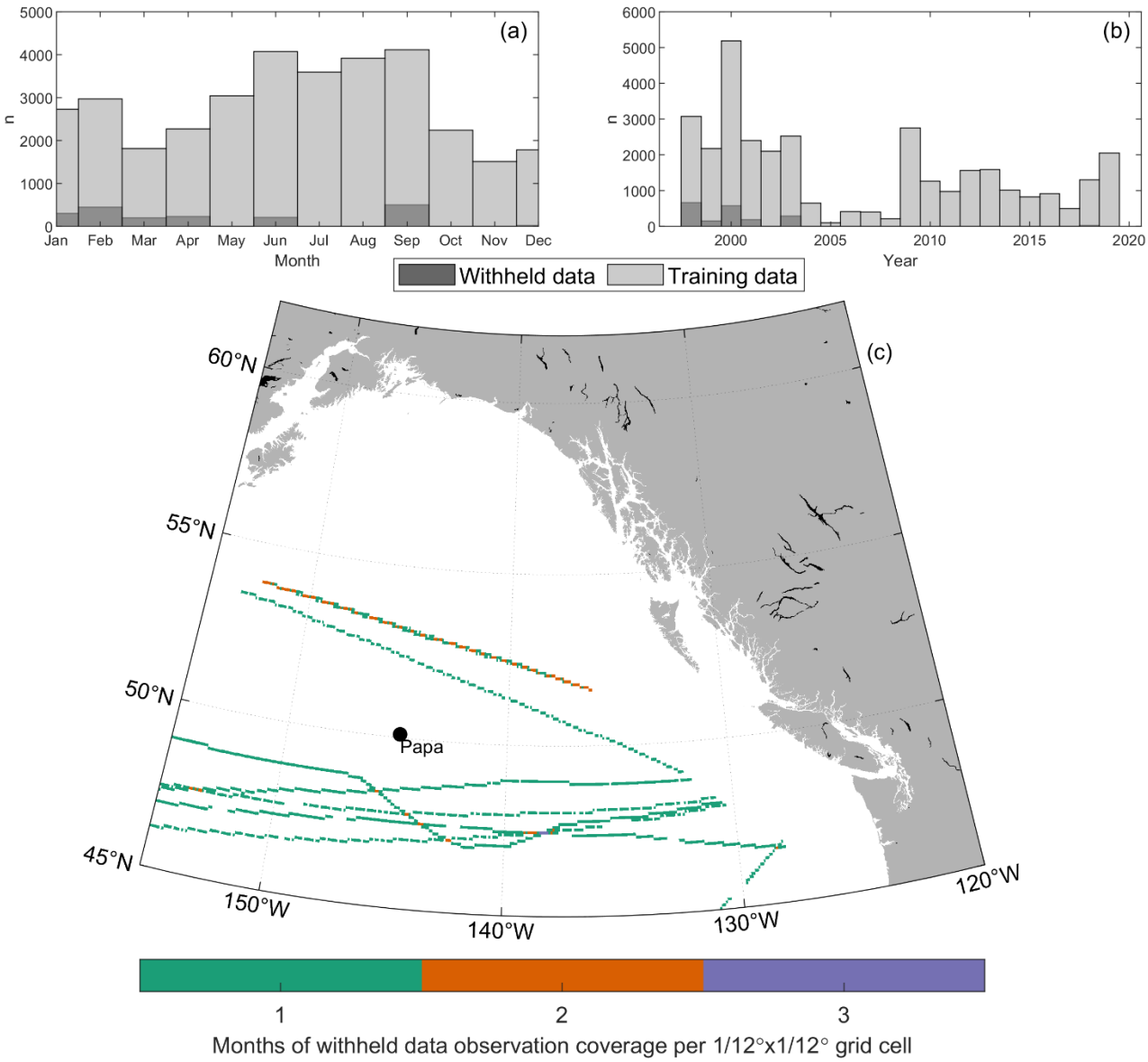

Figure B.1 Withheld data (dark grey) distribution in (a) months, and (b) years relative to training data (light grey), and (c) geographically as the number of months of observational coverage per 1/12 °x1/12 ° grid cell. Ocean Station Papa is shown for reference.

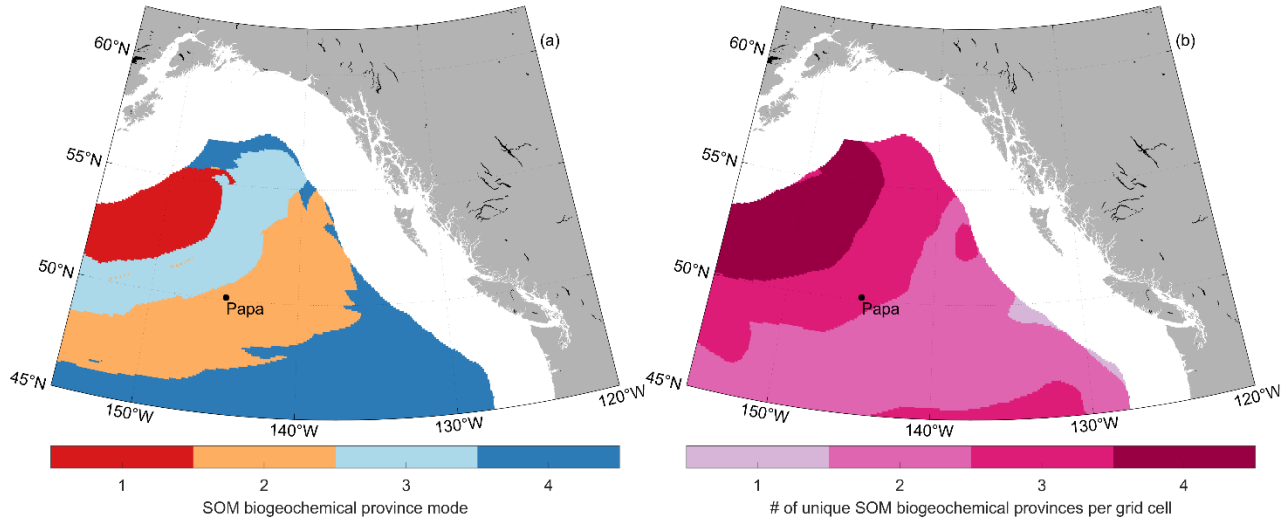

Figure B.2 Mapped (a) mode of SOM biogeochemical provinces (i.e., most frequent occurrence), and (b) the number of unique SOM biogeochemical provinces each grid cell belongs to for each month from January 1998 to December 2019.

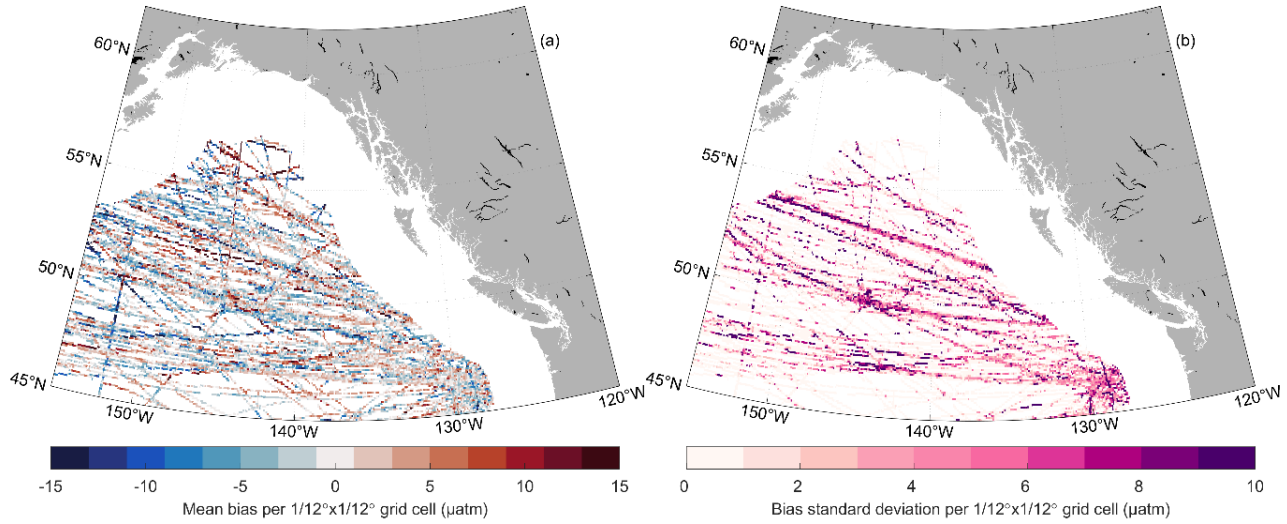

Figure B.3 Mapped mean bias and standard deviation in residuals between ANN-NEP pCO_2 estimate and 1/12°x1/12° gridded SOCAT data.

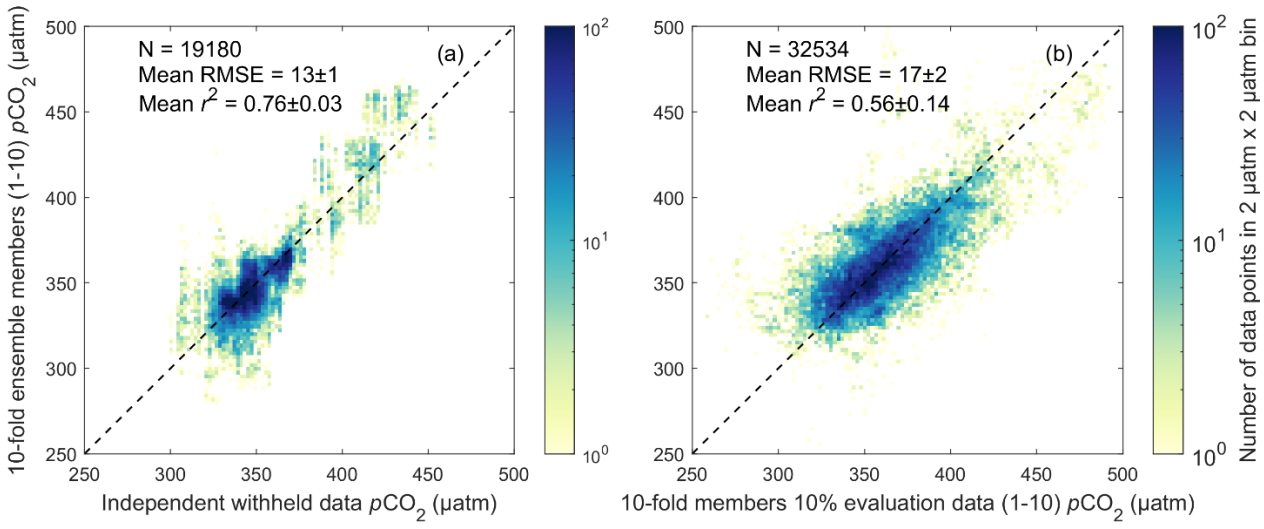

Figure B.4 10-fold cross-evaluation (Section 3.3.5) individual ensemble member estimated pCO_2 against the (a) independent withheld data, and (b) 10% 10-fold evaluation data specific to that ensemble member. Mean root mean squared error (RMSE) and coefficient of determination (r^2) are across all individual ensemble members. Data is binned into 2 µatm by 2 µatm bins. The dashed black line represents a perfect fit of slope (c_1) = 1 and intercept = 0.

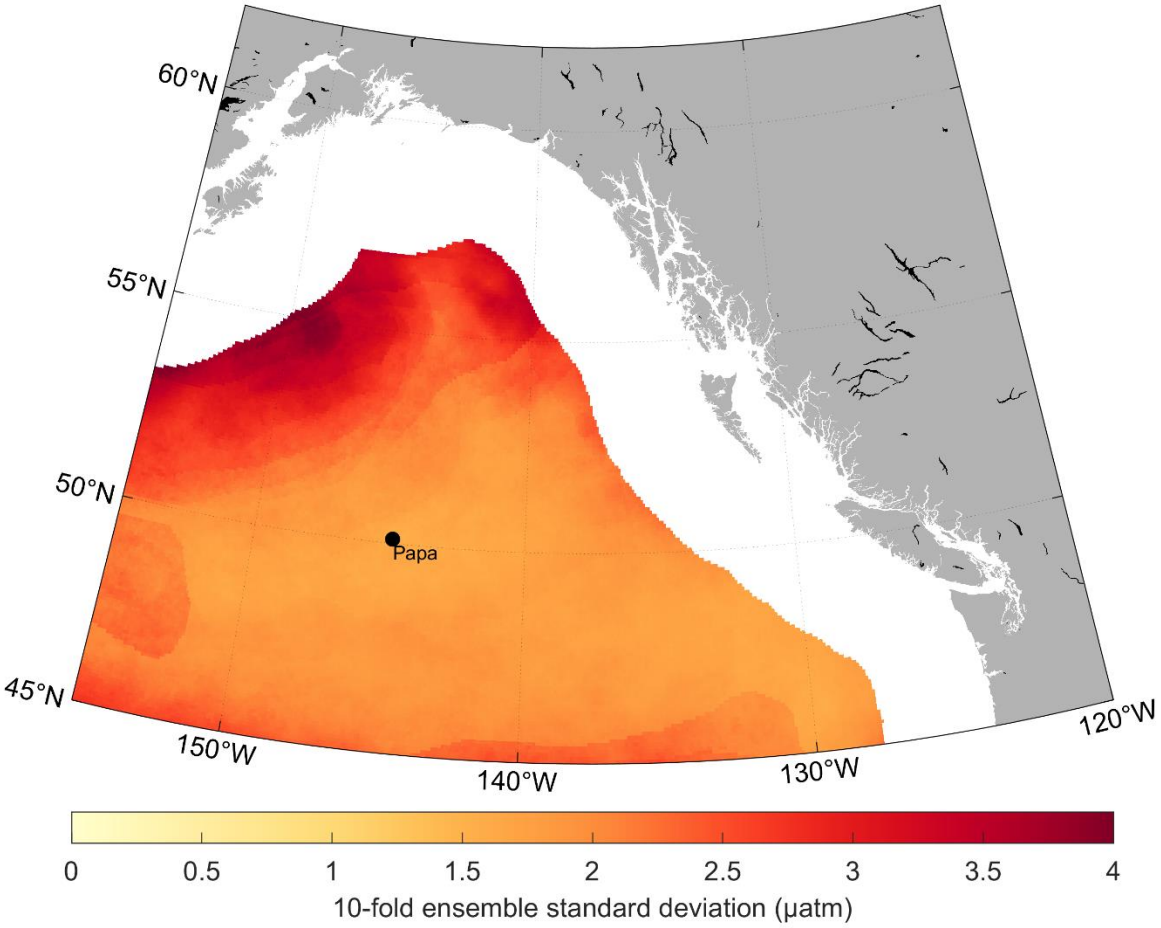

Figure B.5 Mean pCO_2 standard deviation between ANN-NEP 10-fold ensemble members. Ocean Station Papa is shown for reference.

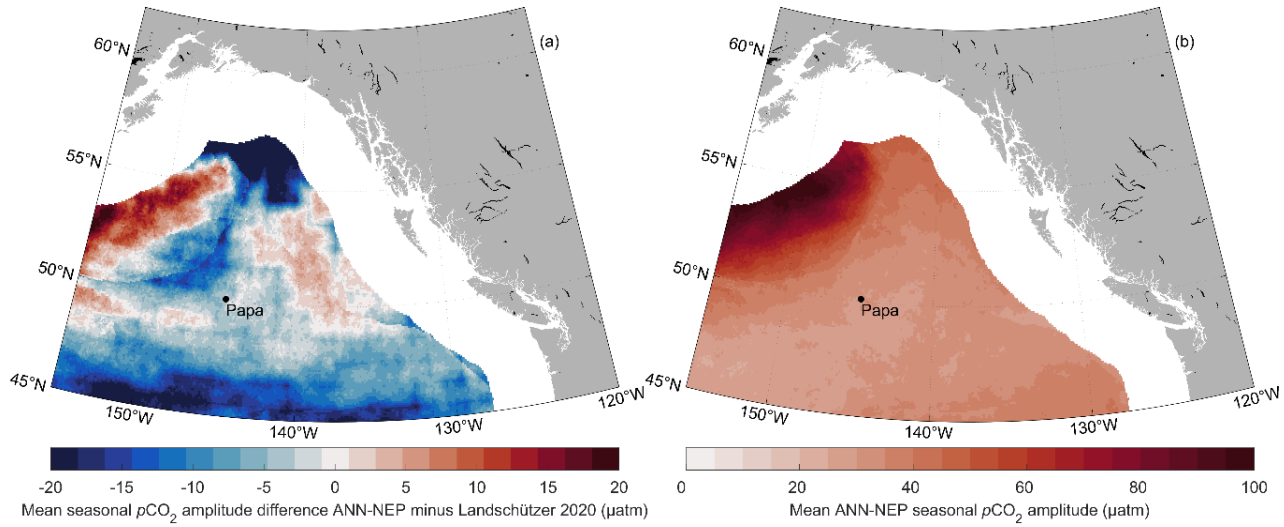

Figure B.6 (a) Mean difference in the surface ocean pCO_2 seasonal amplitude in µatm between the ANN-NEP estimate (this study) and the Landschützer et al. (2020) global product. Positive (negative) differences indicate higher pCO_2 seasonal amplitude for the ANN-NEP (Landschützer et al. (2020)) estimate. The Landschützer et al. (2020) estimates were interpolated to the 1/12 °x1/12 ° grid of this study. (b) Mean ANN-NEP seasonal surface ocean pCO_2 seasonal amplitude in µatm. Ocean Station Papa is shown for reference.

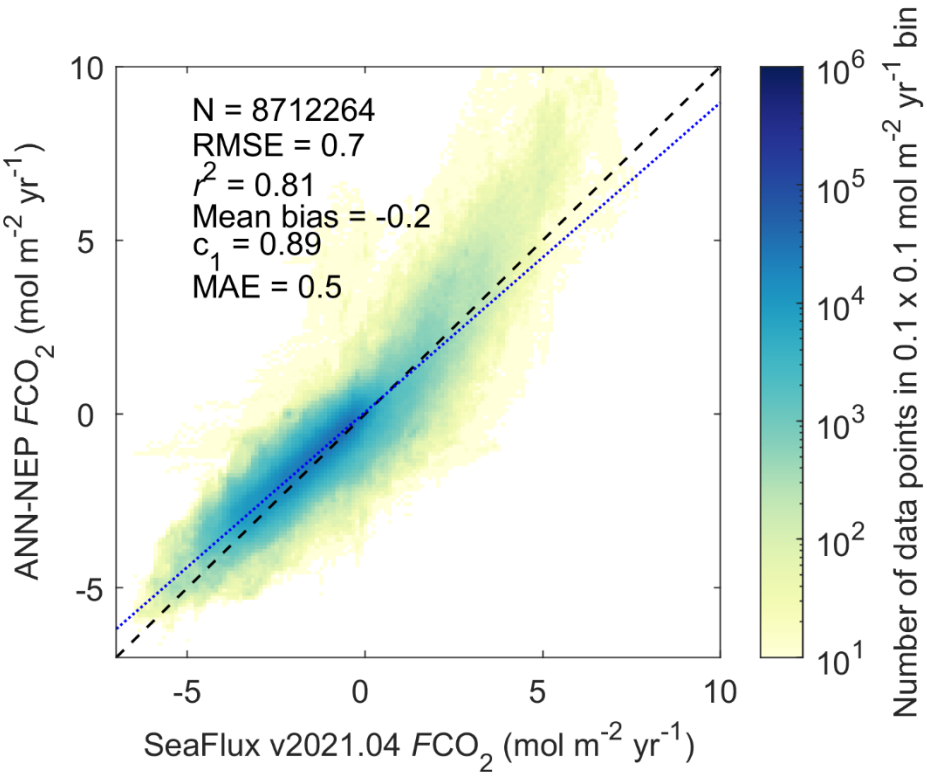

Figure B.7 Property to property plot of air-sea CO_2 flux density values calculated from ANN-NEP and from SeaFlux v2021.04 (Fay et al., 2021). The SeaFlux estimates were interpolated to the 1/12 °x1/12 ° grid of this study. Number of overlapping grid cells withing the study area (N), root mean squared error (RMSE), coefficient of determination

(r^2), mean absolute error (MAE), mean bias (calculated as the mean residual), and the slope of the linear regression (c_1). The observed linear relationship is represented by the dotted blue line. Data is binned into 0.1 by 0.1 mol m^{-2} yr^{-1} bins. The dashed black line represents a perfect fit of slope (c_1) = 1 and intercept = 0. Colorbar shows data density on a log scale.

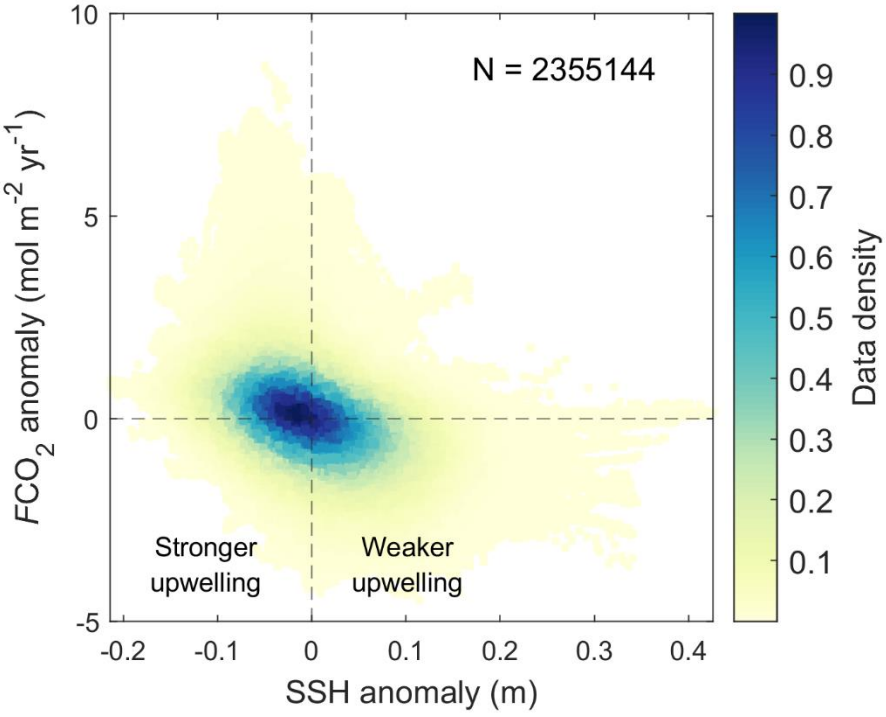

Figure B.8 Property to property plot of air-sea CO_2 flux density anomalies and sea surface height (SSH) anomalies (grid cell by grid cell) in the subpolar Alaskan Gyre region of our study area (latitudes north of 52 °N). Stronger (weaker) upwelling label relates to gyre upwelling strength driven by winds enhancing (damping) Ekman pumping and depressing (elevating) SSH.

Table B.1 Regional high-resolution artificial neural network Northeast Pacific (ANN-NEP) pCO_2 product performance against all SOCAT pCO_2 observation data grouped by year and month. Number of observations (N), root mean squared error (RMSE), coefficient of determination (r^2), and mean bias (calculated as the mean residual).

	N	**RMSE**	r^2	**Mean bias**
Year				
1998	3085	8.1	0.73	-1.4
1999	2184	7.5	0.91	1.4
2000	5195	8.1	0.93	0.0
2001	2404	5.7	0.96	1.2
2002	2110	7.1	0.91	1.0
2003	2526	5.2	0.84	-1.3
2004	652	4.5	0.94	1.2
2005	110	6.8	0.69	-3.6
2006	413	3.3	0.93	-2.6
2007	405	6.4	0.87	-2.8
2008	217	4.0	0.95	-1.3
2009	2751	5.0	0.94	-0.4
2010	1267	6.5	0.96	1.9
2011	980	9.1	0.87	-1.0
2012	1567	6.1	0.93	1.3
2013	1593	4.3	0.99	0.9
2014	1017	5.1	0.95	-1.5
2015	836	9.1	0.95	1.5
2016	919	6.3	0.91	-0.4
2017	511	4.7	0.89	1.0
2018	1303	5.7	0.94	1.2
2019	2051	8.1	0.93	-0.6
Month				
January	2731	5.2	0.97	0.7
February	2971	5.8	0.98	-0.7
March	1816	6.8	0.96	-1.0
April	2277	4.3	0.97	0.3

May	3041	5.6	0.94	0.1
June	4077	9.0	0.92	-1.1
July	3601	9.6	0.86	-0.1
August	3922	7.5	0.94	1.0
September	4121	6.6	0.93	0.2
October	2240	4.9	0.91	1.2
November	1511	3.9	0.97	-0.4
December	1788	4.4	0.97	0.8

Table B.2 Regional artificial neural network Northeast Pacific pCO_2 product performance at varying resolutions against training and independent withheld SOCAT pCO_2 observations. Mean and standard deviation between lower 10^{th} percentile (5 of 50 runs) of overfitting metric values for each resolution with varying internal data division ratios between the pCO_2 training data used by the ANN to train and internally evaluate. Number of observations (N), root mean squared error (RMSE), coefficient of determination (r^2), mean absolute error (MAE), mean bias (calculated as the mean residual), and the slope of the linear regression (c_1). Courser resolution product uncertainties are also included where overall pCO_2 product uncertainty (θ_{pCO2}) is calculated from the square root of the sum of the three squared errors: observational uncertainty (θ_{obs}), gridding uncertainty (θ_{grid}), and ANN interpolation uncertainty (θ_{map}). The 10-fold ensemble approach was not run for the courser resolution products, likely leading to a slight underestimate of overall uncertainty as ANN run randomness uncertainty (θ_{run}) was excluded.

	Training data					
Resolution	**N**	**RMSE**	**r^2**	**Mean Bias**	**c_1**	**MAE**
1°	2547	11.8±0.6	0.79±0.02	-0.1±0.1	0.73±0.02	8.8±0.5
1/2°	5569	10.9±0.7	0.83±0.02	0.1±0.2	0.77±0.02	7.9±0.6
1/4°	11253	11.3±0.9	0.82±0.03	0.0±0.1	0.77±0.03	8.2±0.7
1/8°	21869	12.2±1.0	0.79±0.03	0.0±0.2	0.74±0.03	8.8±0.8
1/12°	31392	10.5±1.0	0.84±0.03	0.0±0.2	0.79±0.03	7.4±0.8
	Independent withheld data					
1°	155	11.7±0.3	0.76±0.01	-0.7±0.5	0.88±0.01	8.4±0.1
1/2°	350	11.5±0.6	0.78±0.02	0.1±0.7	0.93±0.03	8.3±0. 5
1/4°	716	11.5±0.8	0.79±0.03	0.1±0.6	0.98±0.02	8.6±0. 7
1/8°	1387	12.5±0.6	0.76±0.01	-0.1±1.2	0.93±0.04	9.2±0. 5
1/12°	1857	11.4±0.5	0.79±0.01	2.1±0.6	0.92±0.03	8.4±0. 5
	pCO_2 product uncertainty					
	θ_{obs}	θ_{grid}	θ_{map}	θ_{pCO2}		
1°	3.1	3.7	11.7	12.6		
1/2°	3.1	2.8	11.5	12.3		
1/4°	3.1	2.0	11.5	12.2		
1/8°	3.1	2.0	12.5	13.0		

Appendix C. Supplemental material for Chapter 4

Contents of this Appendix

Text C.1

The reported fCO_2 estimates were converted to pCO_2 via (Körtzinger, 1999):

$$pCO_2 = fCO_2 \times \exp[P_{atm}^{surf} \frac{B+(2\delta)}{RT}]^{-1}, \quad \text{(C.1)}$$

where P_{atm}^{surf} is the total atmospheric surface pressure, B and δ are viral coefficients (Weiss, 1974), R is the gas constant, and T is the absolute temperature. National Centers for Environmental Prediction (NCEP) monthly mean sea level pressure was used for P_{atm}^{surf} (Kalnay et al., 1996).

Text C.2

We find that correcting pCO_2 observations to an estimated temperature at the mass boundary layer (i.e., where gas exchange with the atmosphere occurs in the top ~100 μm; Goddijn-Murphy et al., 2015; Woolf et al., 2016) would introduce significant error in our coastal study area. Shipboard underway and mooring pCO_2 observations are collected at varying, platform-dependant depths in the surface ocean mixed layer (typically ~5 m depth by ship). Recent work has shown that this measured *in situ* SST at times is not representative of the mass boundary layer. Correcting observed *in situ* pCO_2 to the mass boundary layer SST strongly impacts global air-sea CO_2 fluxes (Watson et al., 2020). Two techniques have been developed to make this correction. One estimates boundary layer SST from monthly, collocated satellite measurements (Shutler et al., 2016; Woolf et al., 2016). The other proposes a latitudinally varying SST correction derived from drifting buoy data (Dong et al., 2022). Both techniques then correct *in situ* pCO_2 at *in situ* SST to their respective mass boundary layer SST using the pCO_2 solubility relationship (Text C.5).

Both approaches to correcting *in situ* pCO_2 are not applicable in the coastal ocean due to its highly dynamic nature. We evaluate the satellite SST approach collocating monthly, 1/12°x1/12° gridded satellite SST with individual *in situ* pCO_2 measurements. Over the full study area, the approach leads to large (20% of corrections > 20 μatm) absolute differences between observed *in situ* pCO_2 and satellite SST corrected pCO_2 (Figure C.10a&C.11a). A cruise track from August 2011 highlights these large discrepancies (Figure C.10b&c). For example, in the nearshore off the west coast of Washington State, SST differences between *in situ* and satellite data often exceed 4 °C, as *in situ* observations reflect the cool temperatures from the Columbia River freshwater plume or upwelled waters from depth (e.g., Hales et al., 2005) that are not captured by the collocated monthly satellite SST. These differences are largest closest to the coast (Figure C.10b). Likely, satellite SST is biased by monthly averaging and gridding, or

retrieval issues (e.g., cloud masking, impact of aerosols, diurnal variability, uncertainty estimation, and validation) in coastal and highly dynamic regions (O'Carroll et al., 2019). We did not evaluate the Dong et al. (2022) correction derived from drifting buoys, because we were unsure how the drivers of their global open ocean latitudinally varying correction would translate to the coastal zone. Correcting *in situ* pCO_2 to mass boundary layer SST in the coastal ocean (at monthly temporal resolution) results in large, aphysical offsets that would likely introduce additional uncertainty.

Text C.3

Sea surface temperature (SST) and chlorophyll-*a* (Chl) concentration came from the satellite-based European Space Agency Climate Change Initiative (Merchant et al., 2019). We did not interpolate Chl to fill gaps in coverage due to cloud cover, low retrieval angles, or terrestrial contamination (in contrast to other studies; e.g., Yasunaka et al., 2018; Roobaert et al., 2023). Where no Chl satellite data were available, the ANN was run again with the remaining physical predictors, and output was merged to fill empty grid cells (Landschützer et al., 2014). Gaps accounted for 23% of total coverage, occurring mostly during winter months north of 52 °N latitude, or in the nearshore (Figure C.1). Chl was log10-transformed to produce a distribution of values closer to normal before the FFN step.

Sea surface salinity (SSS) and sea surface height (SSH) were obtained from Copernicus Marine Environment Monitoring Service global ocean eddy-resolving reanalysis (Jean-Michel et al., 2021). Jointly assimilated observations include satellite altimeter data and *in situ* vertical profiles of salinity (Table 4.1). The ocean general circulation model is based on the Nucleus for European Modelling of the Ocean (NEMO) platform, driven at the surface by the European Centre for Medium-Range Weather Forecasts ERA-Interim winds (Jean-Michel et al., 2021). Atmospheric pCO_2 in µatm was downloaded from Landschützer, Gruber, et al. (2020), derived from the National Oceanic and Atmospheric Administration (NOAA) Earth System Research Global Monitoring Laboratory (https://gml.noaa.gov/ccgg/globalview/) atmospheric mole fraction of CO_2 (χCO_2) and SST (Reynolds et al., 2002) as well as sea level pressure (Kalnay et al., 1996) following Dickson et al. (2007).

Wind speed came from the Regional Deterministic Reforecast System (RDRS-v2.1; Gasset et al., 2021), based on a limited-area (i.e., North America) forecast system configuration of the Global Environmental Multiscale model (Côté et al., 1998) with a 10-km grid spacing initialized with the Global Deterministic Prediction System model (Bélair et al., 2009).

Text C.4

Overall, individual ensemble members showed relatively little deviation (RMSE < 25 μatm) from the ensemble mean (Figure 4.2c). Each individual ensemble member also performed relatively well compared to the 10% subsample of corresponding 10-fold evaluation data (mean RMSE = 67±12 μatm; Figure C.6). The mean standard deviation across all grid cells within the 10-fold ensemble is 7±5 μatm, with a pronounced increase closer to shore (mapped in Figure C.7).

Text C.5

pCO_2 can be decomposed into a thermal and biophysical component (Takahashi et al., 1993, 2002):

$$pCO_{2\,(T)} = pCO_{2\,(am)} \times \exp\left[0.0423\left(T_{(mm)} - T_{(am)}\right)\right], \quad \text{(C.2)}$$

$$pCO_{2\,(BP)} = pCO_{2\,(mm)} \times \exp\left[0.0423\left(T_{(am)} - T_{(mm)}\right)\right], \quad \text{(C.3)}$$

$$R_{(T\,BP^{-1})} = \frac{\max\left(pCO_{2\,(T)}\right) - \min\left(pCO_{2\,(T)}\right)}{\max\left(pCO_{2\,(BP)}\right) - \min\left(pCO_{2\,(BP)}\right)}, \quad \text{(C.4)}$$

Here the subscripts T and BP represent thermal and biophysical effects, respectively, while subscripts am and mm represent annual mean and monthly mean values, respectively. Eq. C.2 imposes the empirical temperature dependency on the annual mean pCO_2 value providing an estimate of seasonal temperature control (Sarmiento and Gruber, 2006; Takahashi et al., 2002). Eq. C.3 removes the temperature dependency from the monthly mean pCO_2 values providing an estimate of the residual, biophysical controls on pCO_2 including circulation, mixing, gas exchange, and biology. The ratio of the seasonal amplitudes of the two components (Eq. C.4; $R_{(T\,BP^{-1})}$) can differentiate the dominant process, where a value greater (less) than one indicates that thermal (biophysical) processes dominate.

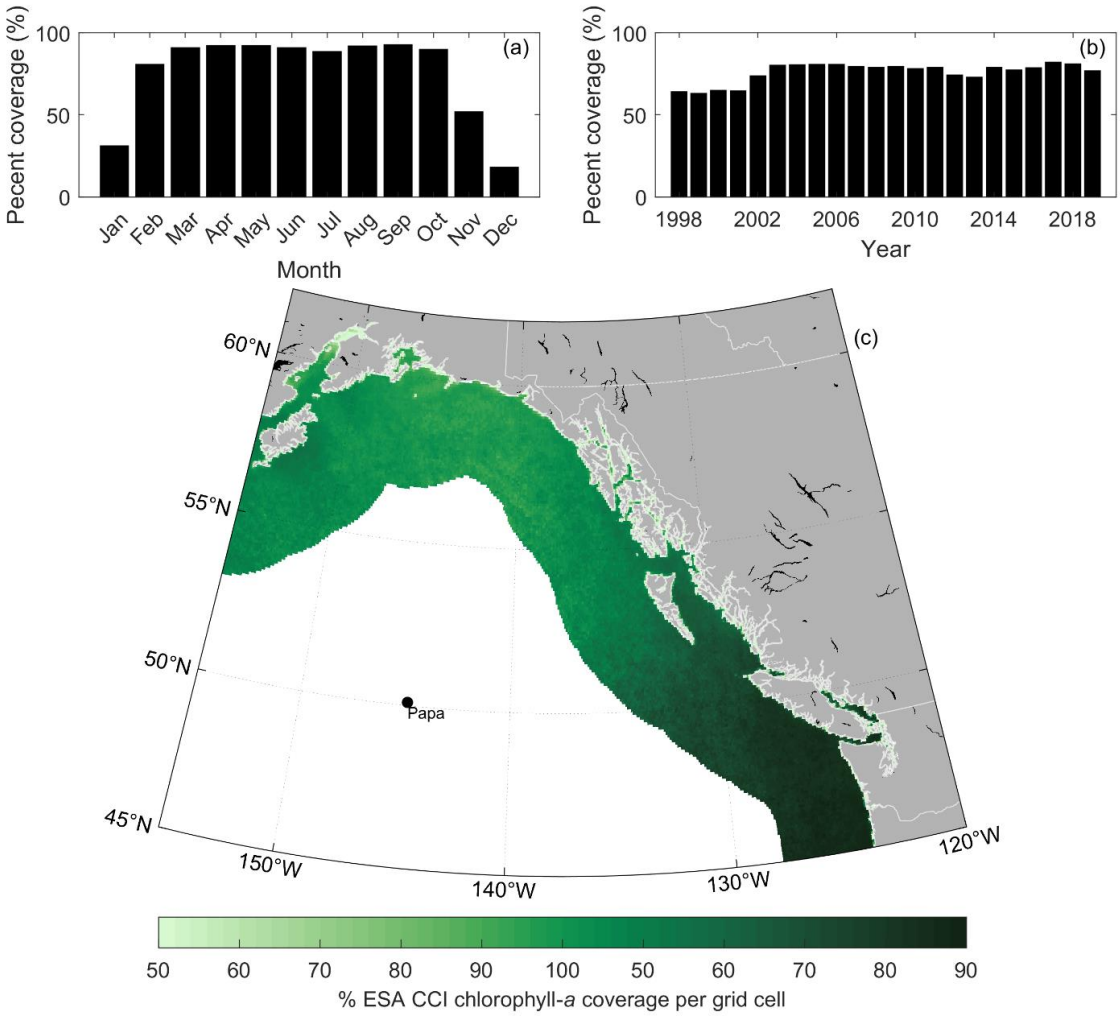

Figure C.1 (a) Monthly and (b) yearly distribution of satellite-based European Space Agency Climate Change Initiative chlorophyll-a concentration data product (ESA Ocean Colour Climate Change Initiative (Ocean_Colour_cci): Global chlorophyll-a data products gridded on a geographic projection, Version 5.0). (c) Mapped percent observational coverage per grid cell over 264 months (1998–2019).

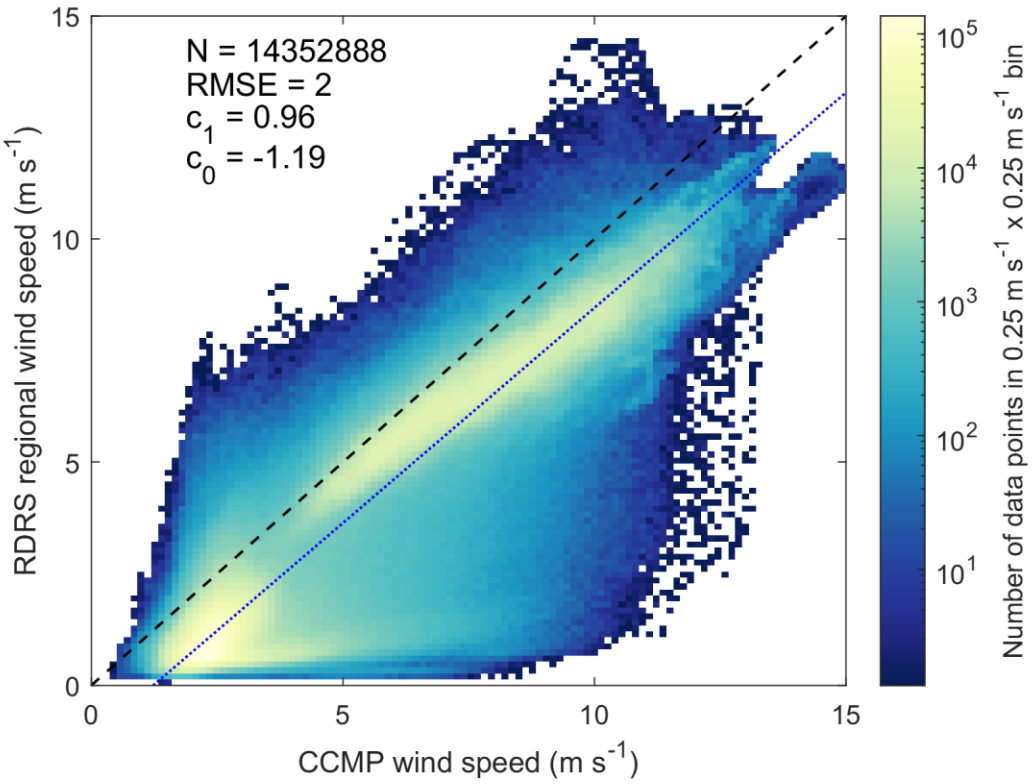

Figure C.2 RDRS regional high-resolution wind speeds (Gasset et al., 2021) against CCMP global wind speed product (Mears et al., 2019) over the entire study area from 1998-2019 (grid cell by grid cell). CCMP windspeed estimates are higher (approximately 1 m s^{-1}) across the study area compared to RDRS. Both products have been interpolated to the 1/12 °x 1/12 ° grid of this study. Number of overlapping grid cells within the study area (N), root mean squared error (RMSE), and the slope (c_1) and intercept (c_0) of the linear regression. The observed linear relationship is represented by the dotted blue line. Data are binned into 0.25 by 0.25 m s^{-1} bins. The dashed black line represents a perfect fit of slope (c_1) = 1 and intercept = 0. Colorbar shows data density on a log scale.

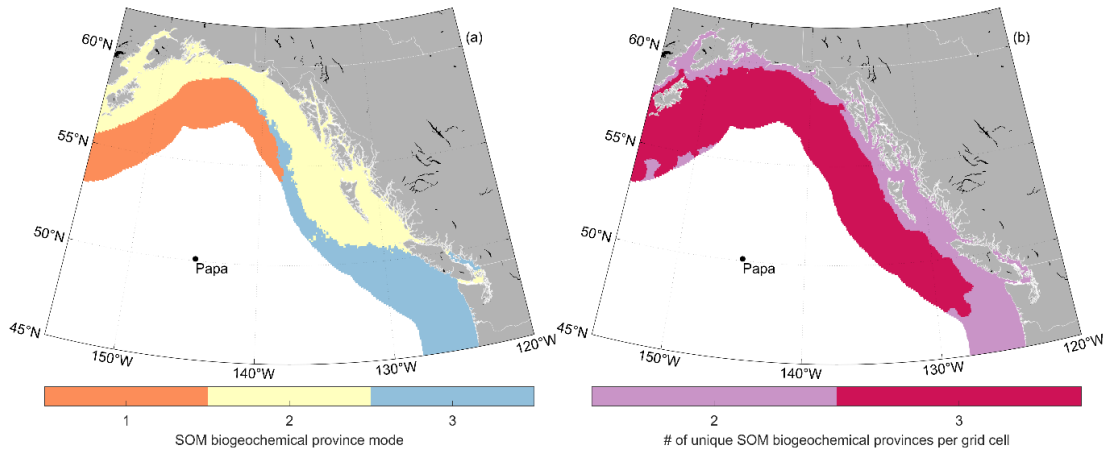

Figure C.3 Mapped (a) mode of SOM biogeochemical provinces (i.e., most frequent occurrence), and (b) the number of unique SOM clusters each grid cell belongs to for each month from January 1998 to December 2019. All grid cells belong to more than one SOM biogeochemical province.

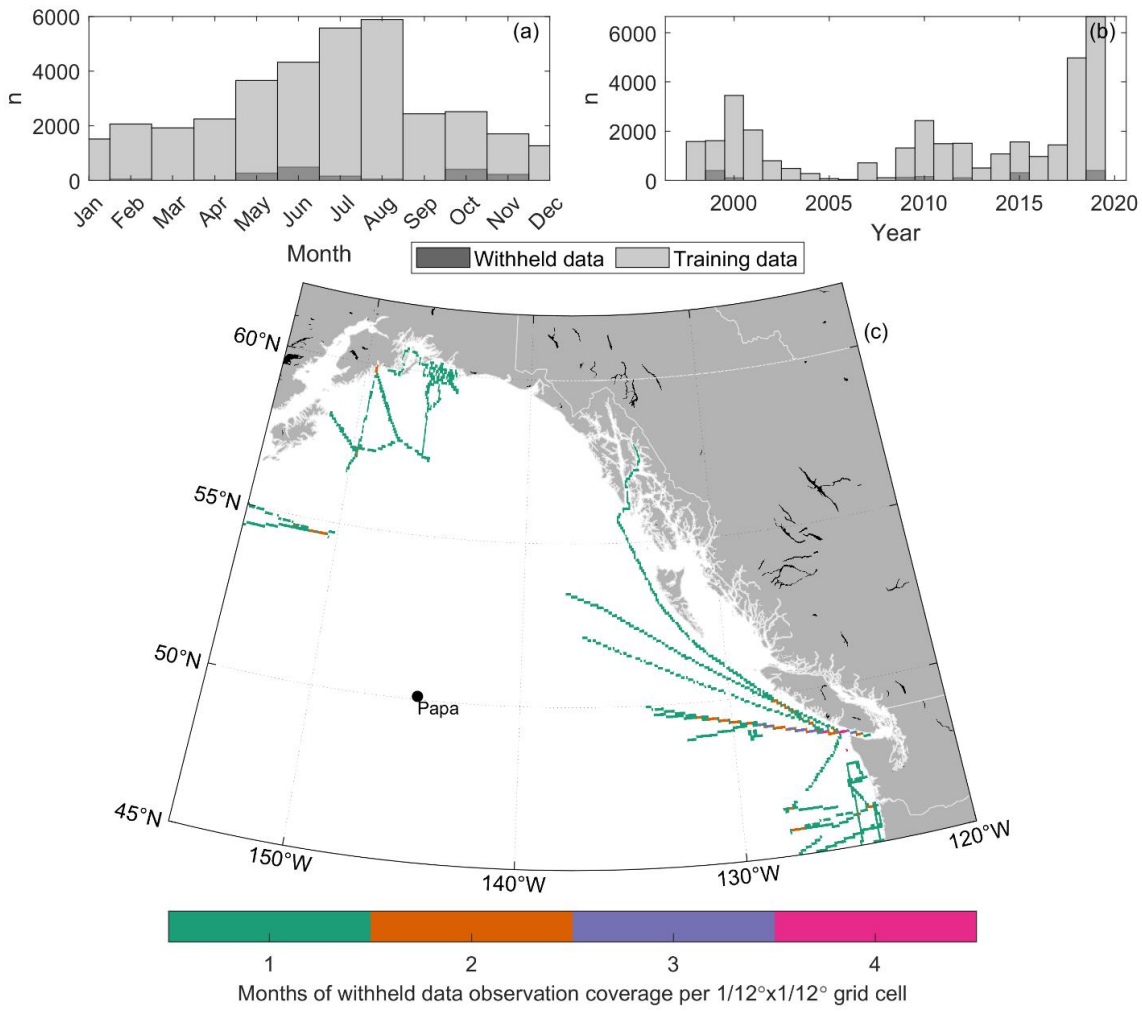

Figure C.4 Independent withheld data (dark grey) distribution in (a) months, and (b) years relative to training data (light grey), and (c) geographically as the number of months of observational coverage per 1/12 °x1/12 ° grid cell.

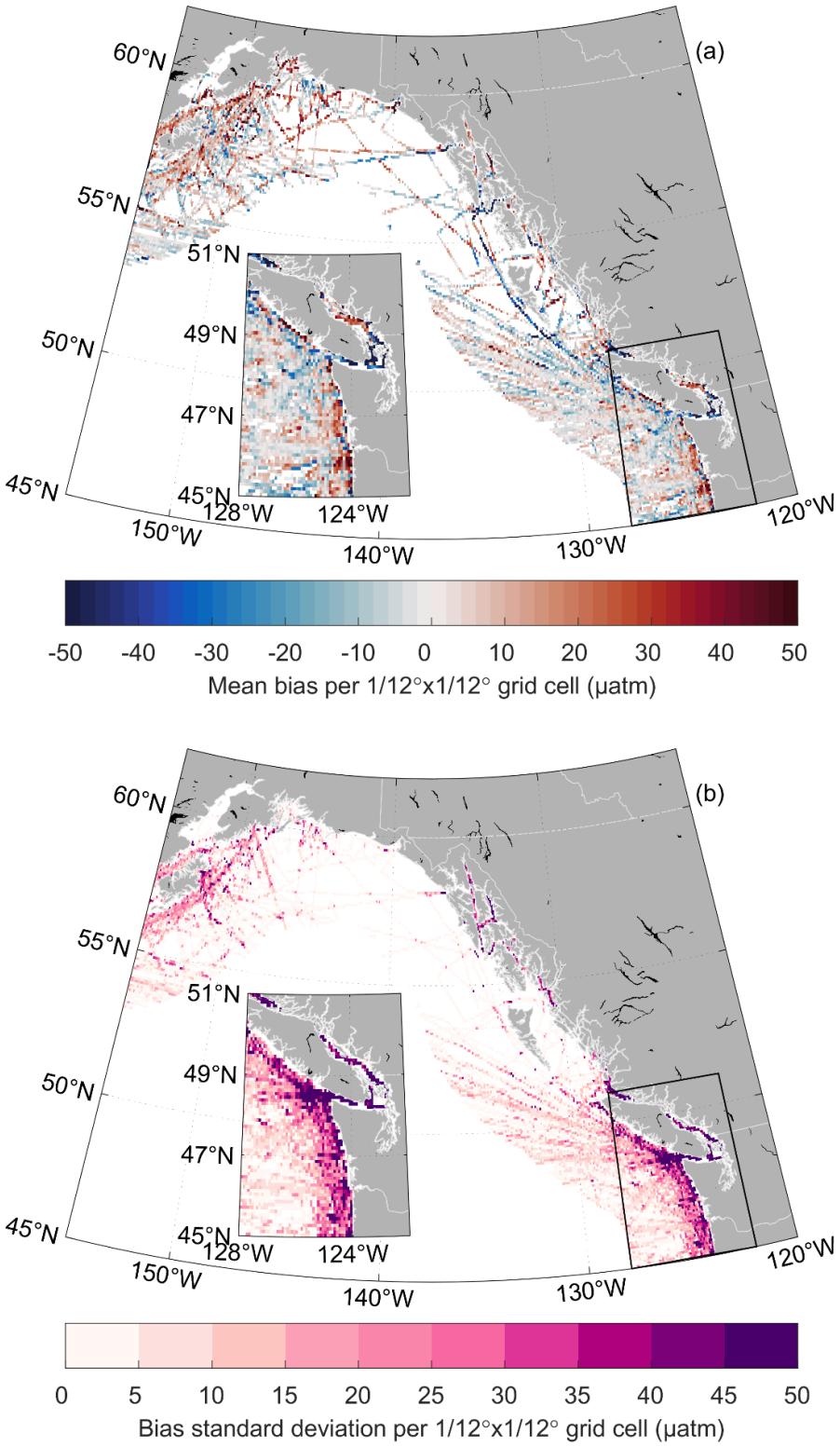

Figure C.5 Mapped (a) mean bias and (b) standard deviation in residuals between our ensemble mean pCO_2 estimate (ANN-NEPc) and 1/12°x1/12° gridded observational data.

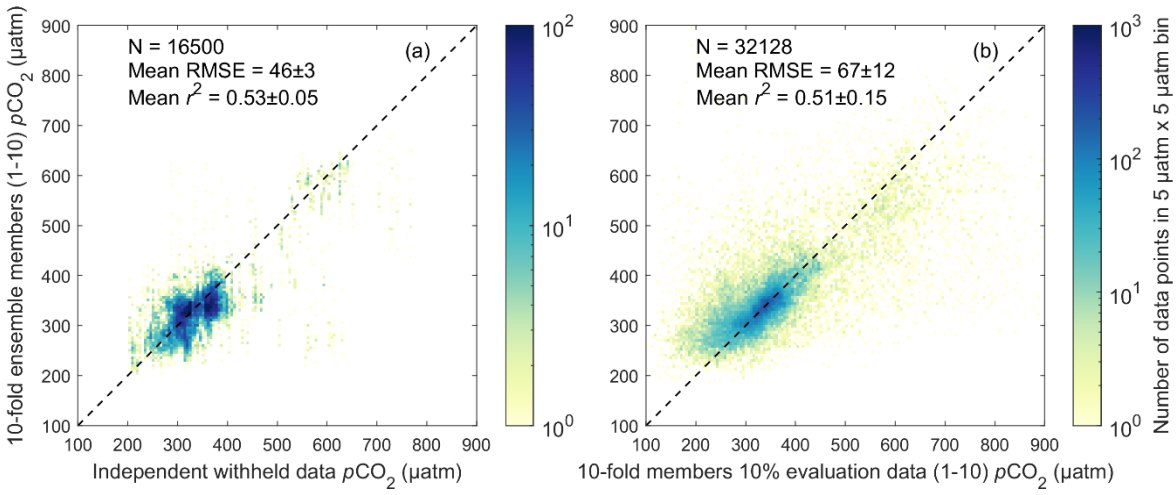

Figure C.6 10-fold (Section 4.3.3) individual ensemble member estimated pCO_2 against the (a) independently withheld data, and (b) 10% 10-fold internal evaluation data specific to that ensemble member. Mean root mean squared error (RMSE) and coefficient of determination (r^2) are across all individual ensemble members. Data is binned into 5 µatm by 5 µatm bins with data density shown in the colorbar on a log scale. The dashed black line represents a perfect fit of slope (c_1) = 1 and intercept = 0.

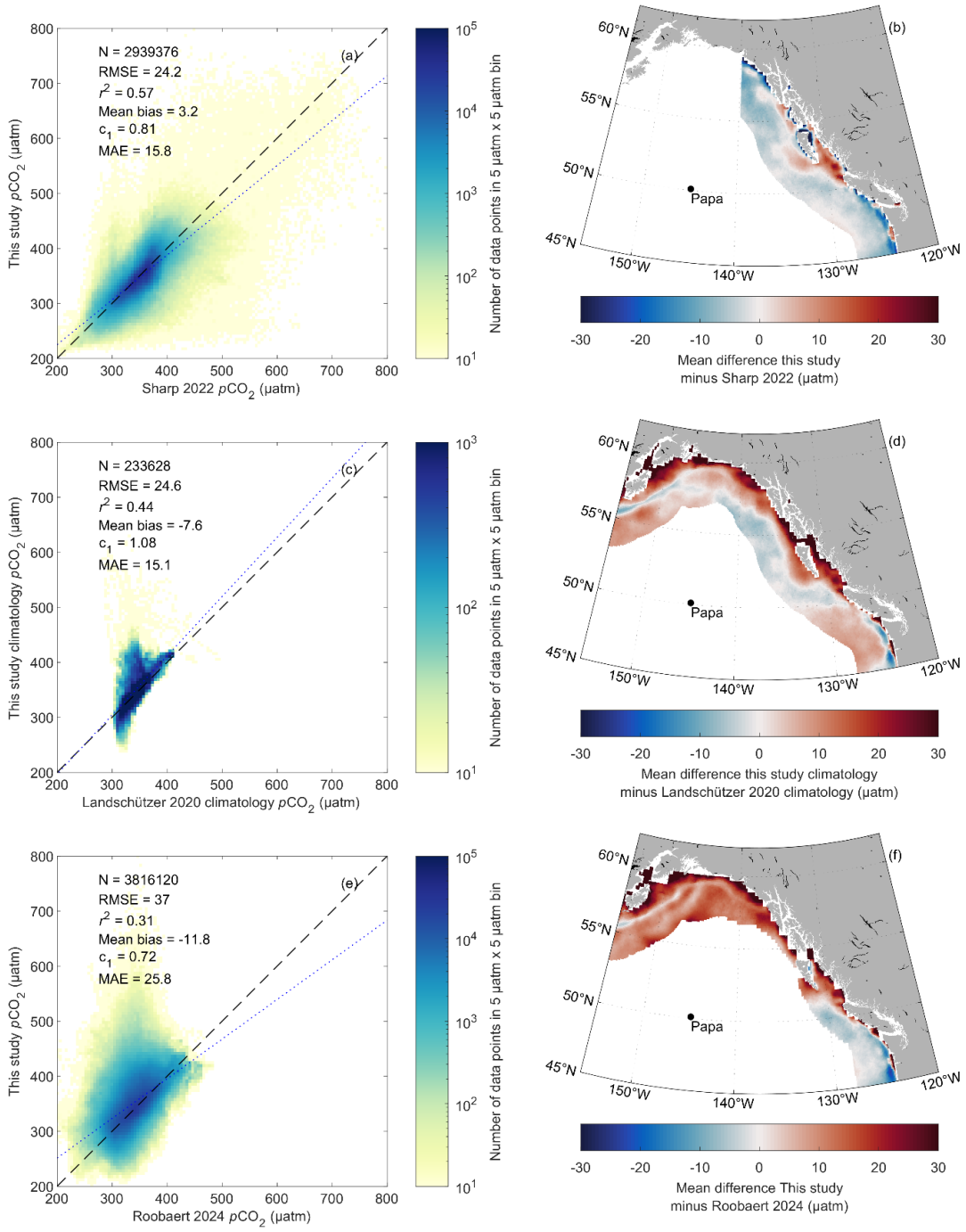

Figure C.7 This study's pCO_2 product compared against (a)&(b) Sharp et al. (2022), (c)&(d) Landschützer, Laruelle, et al. (2020), and (e)&(f) Roobaert et al. (2024) in overlapping domains. Lefthand panels show our product vs. others (grid cell by grid cell). Number of observations (N), root mean squared error (RMSE), coefficient of determination (r^2), mean absolute error (MAE), mean bias (calculated as the mean residual), and the slope of the linear regression (c_1). Dashed black line is the 1:1. Dotted blue line is the least squares best fit. Righthand panels show mapped mean difference between this study and others.

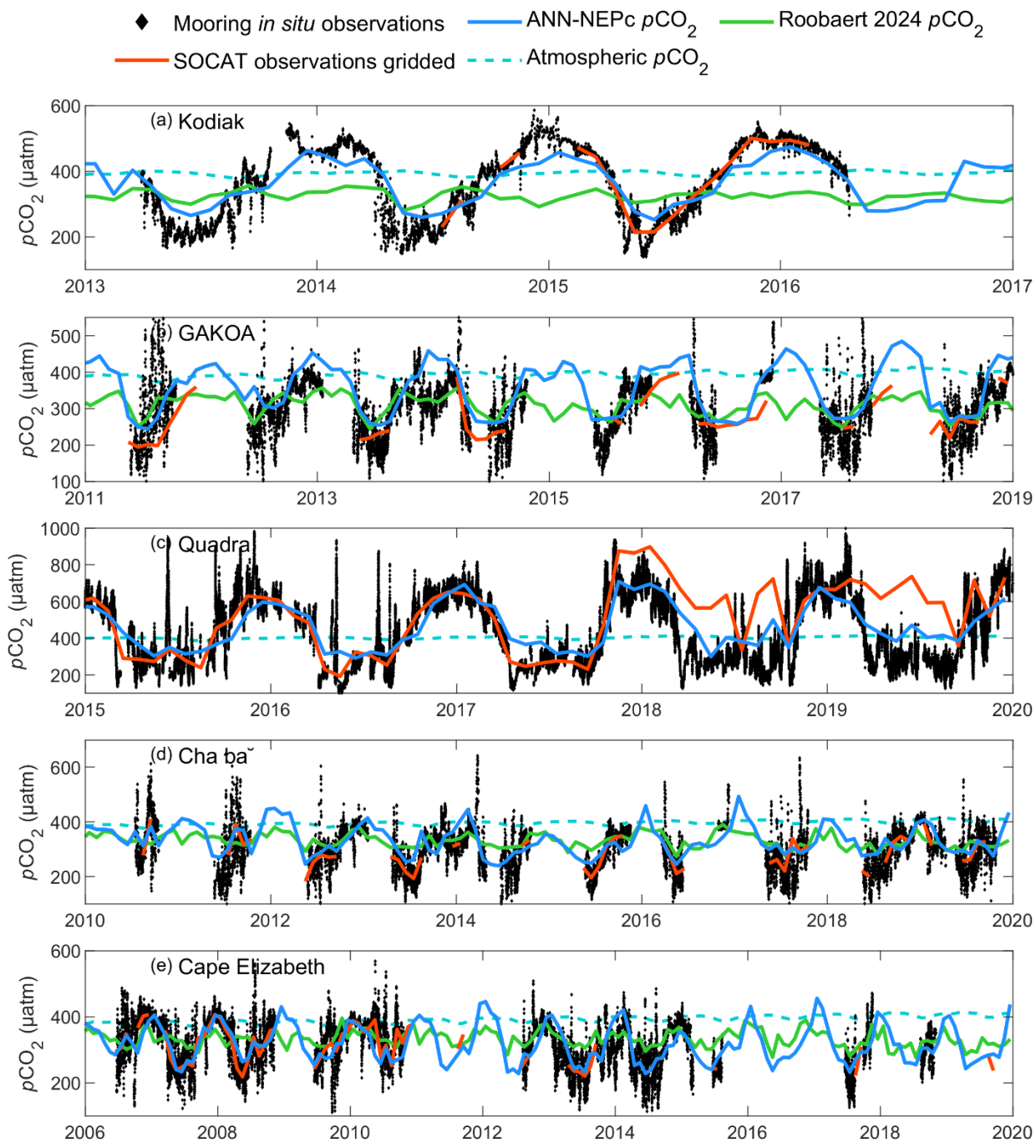

Figure C.8 Complete mooring deployment comparison for (a) Kodiak (b) Gulf of Alaska Ocean Acidification (GAKOA), (c) Quadra, (d) Chá bă, and (e) Cape Elizabeth moorings. In situ pCO_2 data (black diamonds; not all included in SOCATv2021) plotted with co-located gridded SOCATv2021 (orange solid line), our estimated pCO_2 (ANN-NEPc, blue solid line), Roobaert et al. (2024) pCO_2 (green solid line; no nearshore coverage with Quadra), and atmospheric pCO_2 (light blue dashed line).

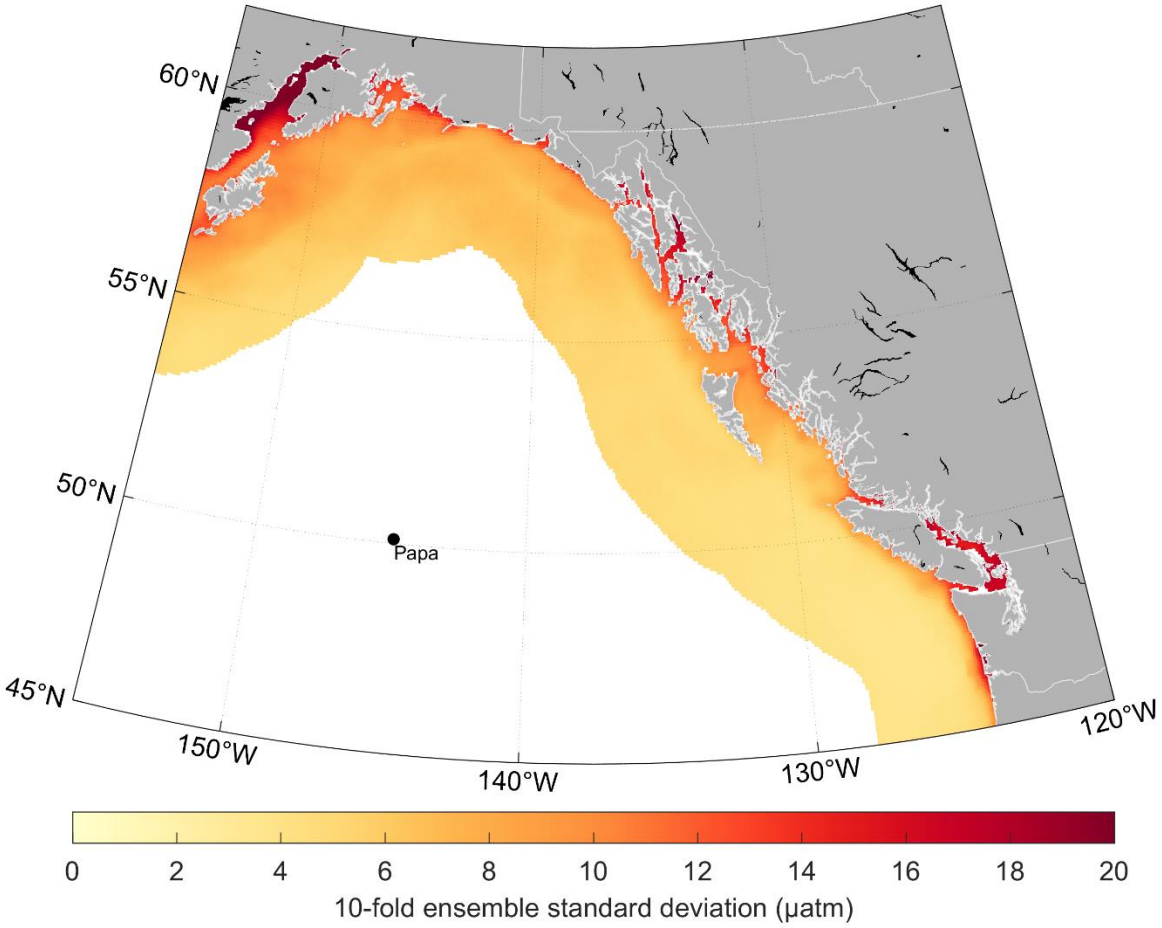

Figure C.9 Mapped mean pCO_2 standard deviation among 10-fold ensemble members.

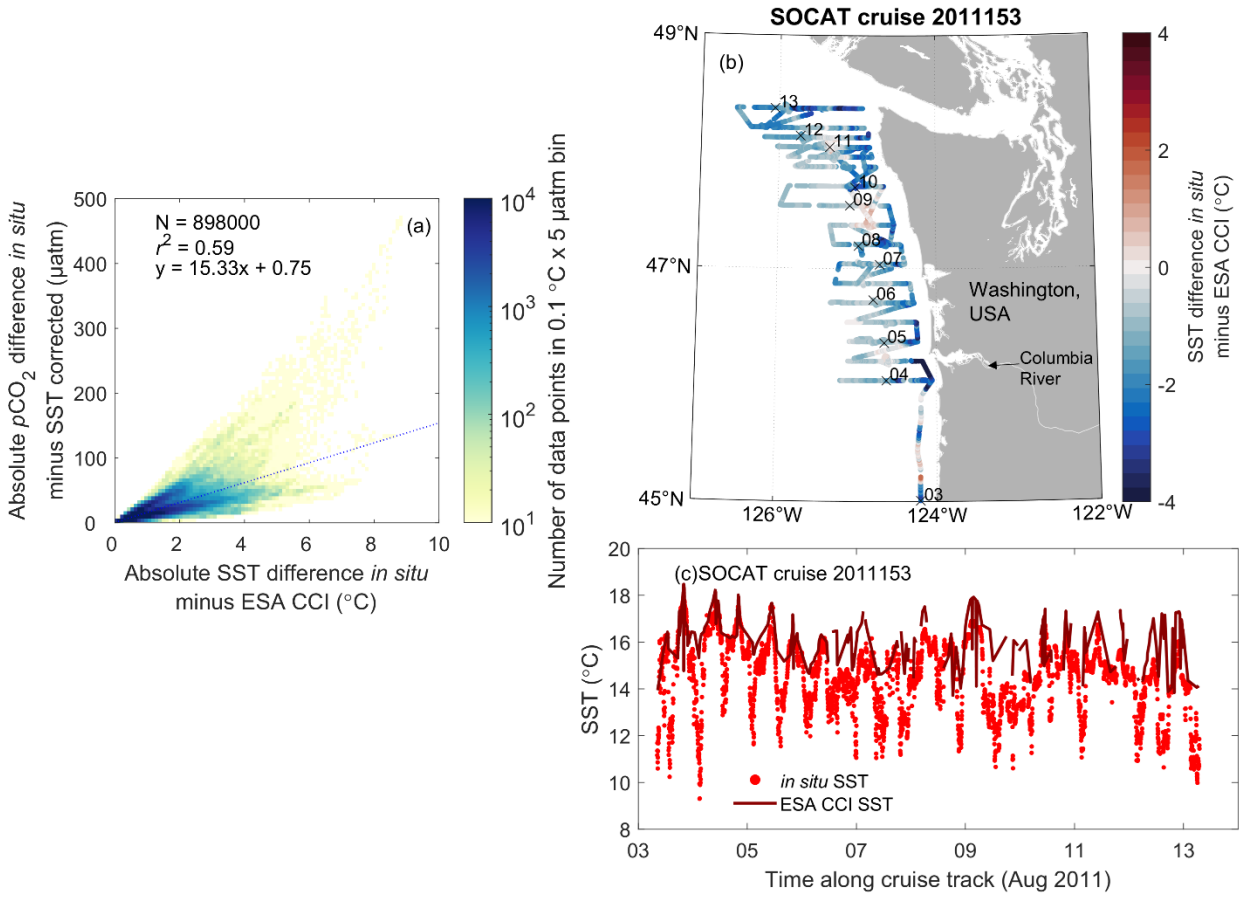

Figure C.10 (a) Absolute pCO_2 difference between in situ and pCO_2 corrected to mass boundary layer SST (i.e., using co-located European Space Agency Climate Change Initiative (ESA CCI) satellite-based SST) vs. absolute difference between in situ SST and mass boundary layer SST for all available SOCAT and additional pCO_2 data (Section 4.3.1). Number of in situ observations within the study area (N), coefficient of determination (r^2), and least squares best fit ($y = c_1x + c_0$; where c_1 is the slope and c_0 is the intercept of the fit; also shown in the dotted blue line). Data are binned into 0.1 ℃ by 5 µatm bins with data density shown in the colorbar on a log scale. (b) Difference between in situ SST and mass boundary layer SST along a west coast cruise track (cruise 2011153) from 3 Aug 2011 to 13 Aug 2011. Dates along cruise track are marked with an X followed by the day of Aug 2011. (c) Underway in situ SST (red dots) and co-located mass boundary layer SST (dark red solid line) against time along same cruise track (cruise 2011153) from 3 Aug 2011 to 13 Aug 2011.

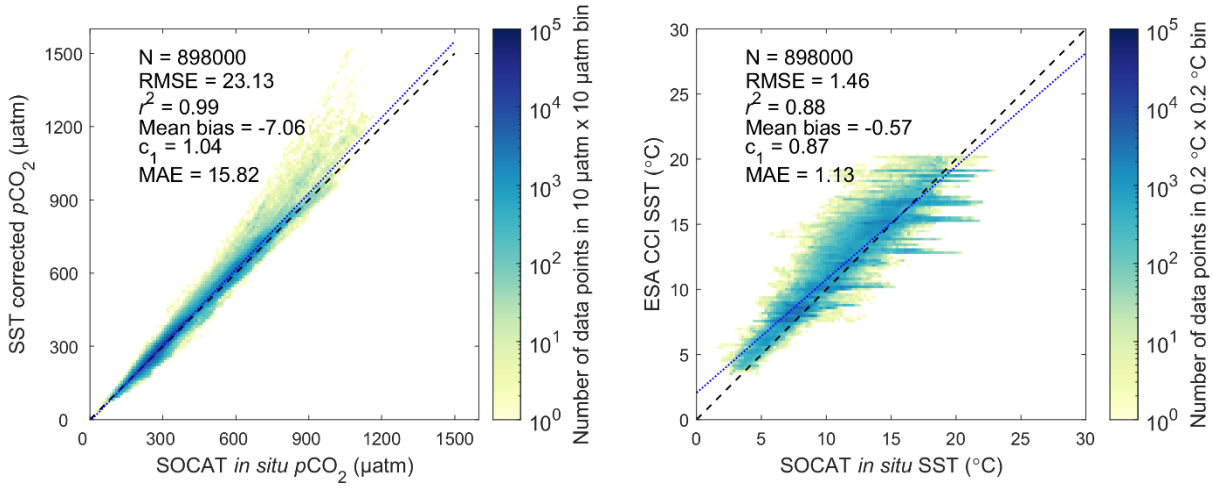

Figure C.11 (a) pCO_2 corrected to mass boundary layer SST (i.e., using co-located monthly satellite-based SST) vs. in situ pCO_2. (b) Mass boundary layer SST as estimated from monthly ESA CCI satellite data vs. in situ SST. Data are binned into (a) 10 µatm by 10 µatm or (b) 0.2 ℃ by 0.2 ℃ bins with data density shown in the colorbar on a log scale. Dashed black line is the 1:1. Dotted blue line is the least squares best fit. Also shown are number of observations (N), root mean squared error (RMSE), coefficient of determination (r^2), mean absolute error (MAE), mean bias (calculated as the mean residual), and the slope of the linear regression (c_1).

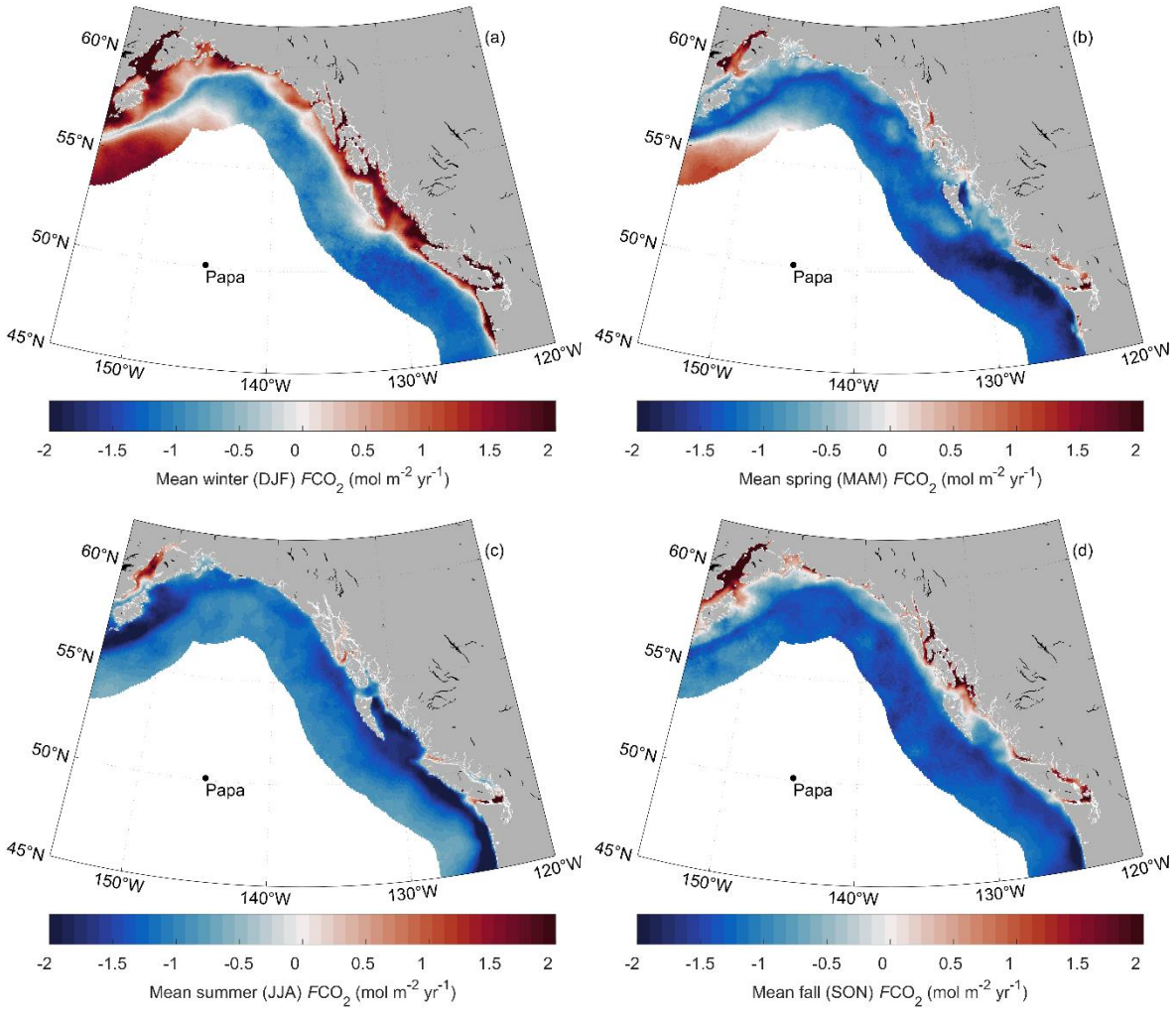

Figure C.12 Mean seasonal air–sea CO_2 flux (1998-2019) in mol m^{-2} yr^{-1}. Negative flux values indicate CO_2 uptake by the ocean. Seasonal groupings are (a) winter (December, January, February), (b) spring (March, April, May), (c) summer (June, July, August), and (d) fall (September, October, November).

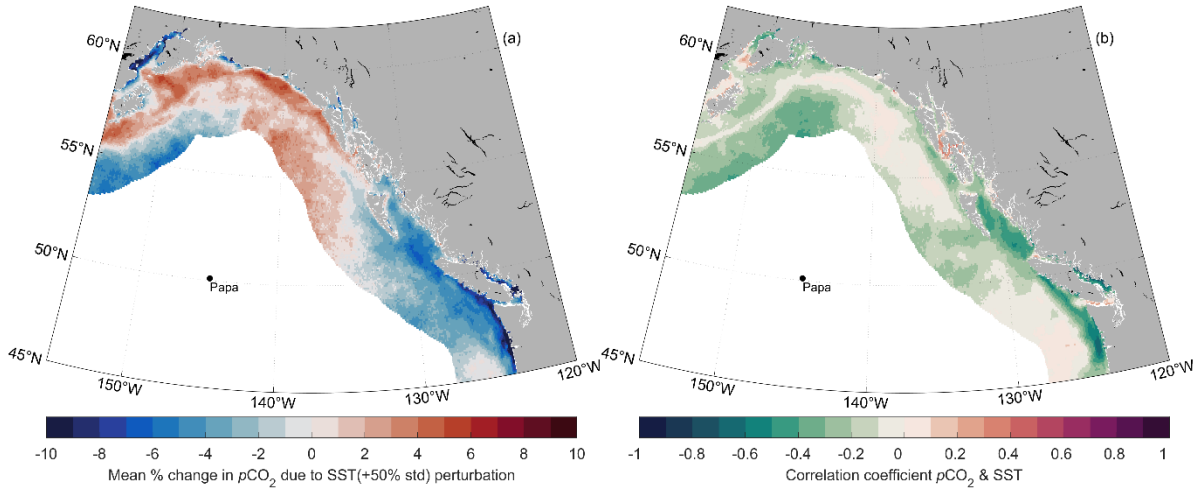

Figure C.13 (a) Mean pCO_2 difference from baseline run during SST perturbation-based spatial sensitivity analysis (Section 4.3.5). (b) Correlation coefficient between SST and baseline run.

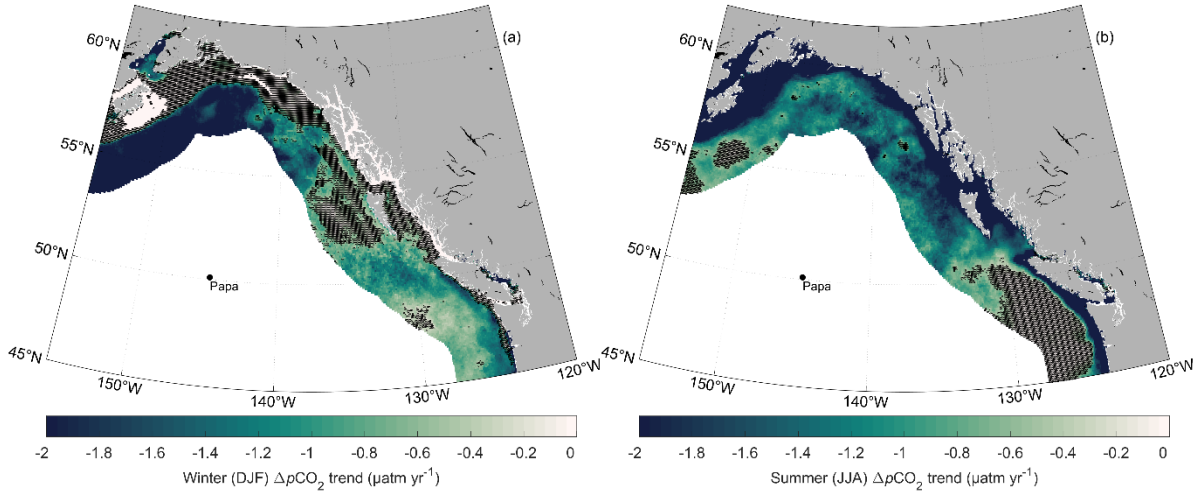

Figure C.14 1998-2019 trend in (a) winter (December, January, February) and (b) summer (June, July, August) ΔpCO_2 (air-sea) anomaly (i.e., deseasonalized; trends calculated from monthly values) where more negative (darker) values indicate an increase in air-sea pCO_2 disequilibria with time. Black crosshatches show grid cells with an insignificant calculated trend (outside the 95% confidence level; $p \geq 0.05$).

Table C.1 Our pCO_2 product (ANN-NEPc) performance against all pCO_2 observation data (training and withheld; Section 4.3.1) grouped by year and month. Number of observations (N), root mean squared error (RMSE), coefficient of determination (r^2), and mean bias (calculated as the mean residual).

	N	**RMSE**	r^2	**Mean bias**
Year				
1998	1541	18.8	0.89	-3.8
1999	1601	22.0	0.83	-0.9

2000	3423	22.8	0.91	0.1
2001	2028	26.9	0.9	0.2
2002	794	22.4	0.92	1.9
2003	471	24.1	0.87	-1.4
2004	270	10.7	0.85	1.1
2005	77	9.6	0.58	-4.0
2006	33	15.2	0.48	4.8
2007	647	38.8	0.88	1.4
2008	106	15.5	0.69	3.2
2009	1323	37.4	0.86	2.5
2010	2302	36.2	0.87	3.7
2011	1478	42.0	0.88	-2.7
2012	1481	29.1	0.93	-0.9
2013	510	24.2	0.87	-1.2
2014	1053	19.1	0.92	-1.1
2015	1537	32.2	0.8	7.5
2016	940	30.0	0.91	2.1
2017	1190	43.1	0.95	3.4
2018	3958	44.2	0.89	-2.3
2019	5797	40.7	0.87	-0.2
Month				
January	1391	23.5	0.95	2.9
February	1873	22.4	0.95	3.5
March	1657	33.6	0.89	-1.3
April	1991	33.1	0.84	-6.8
May	3371	36.9	0.85	-5.2
June	3961	36.2	0.85	-2.6
July	5340	31.3	0.86	-2.8
August	5607	35.3	0.87	-1.5
September	2277	39.5	0.81	5.1
October	2391	36.8	0.87	10.4

November	1570	32.8	0.94	9.8
December	1131	36.1	0.94	9.6

Table C.2 Regional freshwater drainage for the Northeast Pacific coastal ocean from (Morrison et al., 2012; Wang et al., 2004) between latitudes 45°N and 62°N and longitudes 120°W and 155°W.

Drainage region	**Mean annual runoff ($km^3\ y^{-1}$)**	**Total glacier contribution to regional runoff ($km^3\ y^{-1}$)**	**Percent of regional runoff from glacier area (%)**
Southeast Alaska	370	99	27
Central Coast Alaska	200	170	85
Copper River	65	45	69
Prince William Sound	95	57	60
Knik Arm/Kenai	36	17	47
Susitna River	46	10	22
West Cook Inlet/Kodiak	54	7	14
North coast BC	245.2		
Central coast BC	125.7		
Continental Salish Sea (including Fraser River)	213.6	7	3
Vancouver Island	89.7		
Haida Gwaii	38.6		
Washington State	55.5		
Columbia River	211.4		
Total	**1845.7**	**412**	**22**

Appendix D. Supplemental material for Chapter 5

Contents of this Appendix

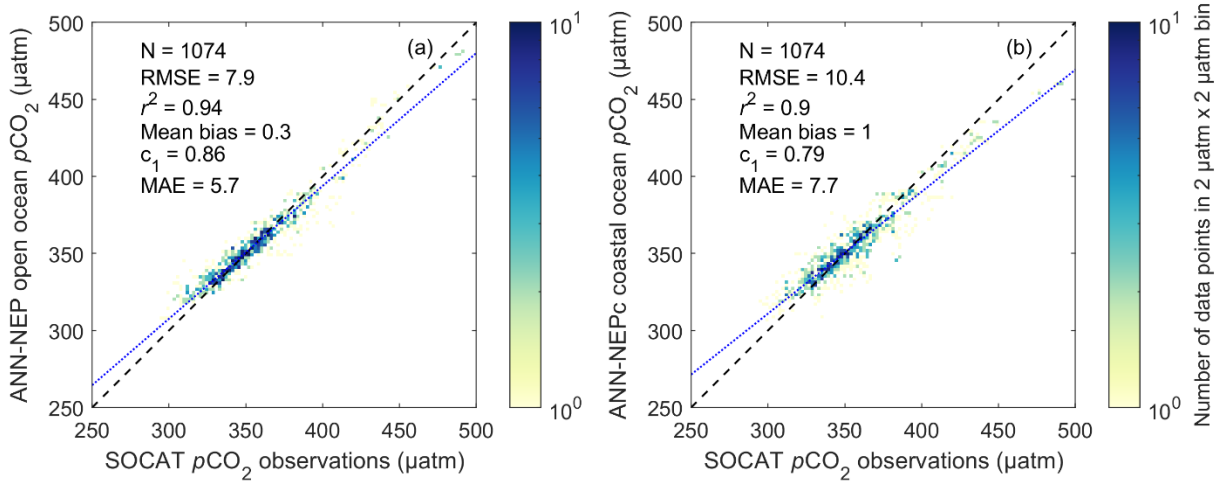

Figure D.1 (a) Open ocean pCO_2 estimate (ANN-NEP) and (b) coastal pCO_2 estimate (ANN-NEPc) against gridded Surface Ocean CO_2 Atlas (SOCAT) v2021 (Bakker et al., 2016) pCO_2 observations within the overlapping domain (grid cell by grid cell; Figure 5.2). Data are binned into 2 µatm by 2 µatm bins with data density shown in the colorbar on a log scale. Dashed black line is the 1:1. Dotted blue line is the least squares best fit. Also shown are number of overlapping grid cells in space and time (N), root mean squared error (RMSE), coefficient of determination (r^2), mean bias (calculated as the mean residual), the slope of the linear regression (c_1), and the mean absolute error (MAE).

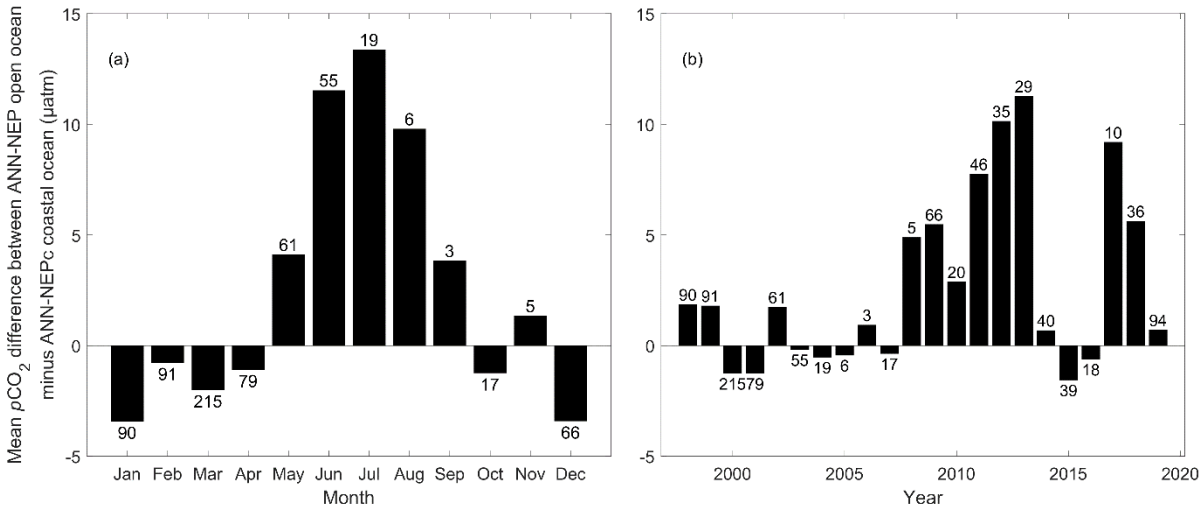

Figure D.2 Mean difference between the open ocean pCO_2 estimate (ANN-NEP) and the coastal pCO_2 estimate (ANN-NEPc) within the overlapping domain grouped by (a) months across all calendar years, and (b) years. Numbers above each bar indicate the number of gridded Surface Ocean CO_2 Atlas (SOCAT) v2021 (Bakker et al., 2016) pCO_2 observations within each grouping. Months and years where there are a high number of observations the difference between products tends to be closer to zero.

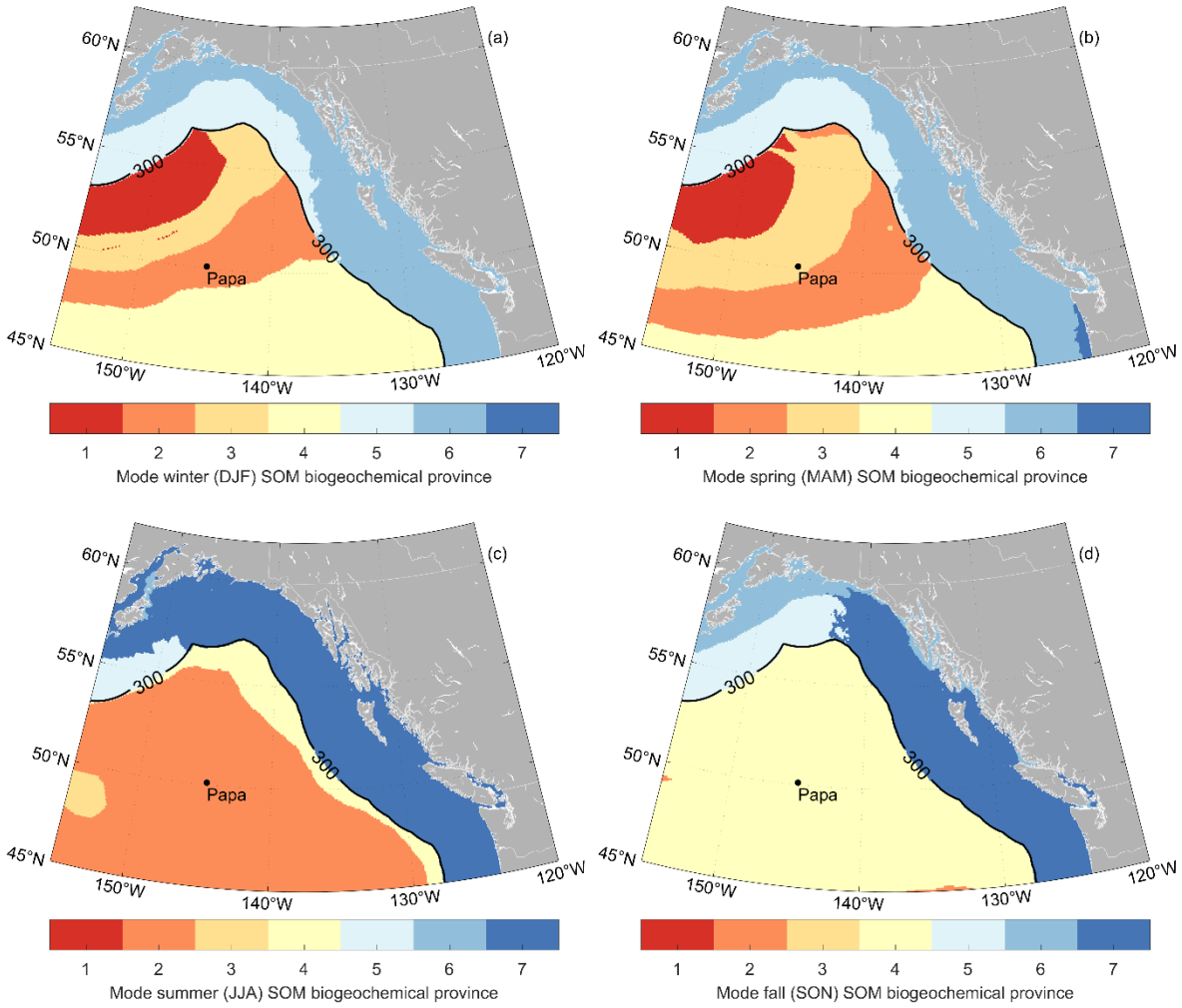

Figure D.3 Mapped mode of SOM biogeochemical provinces (i.e., most frequent occurrence) from January 1998 to December 2019 group by season for both the open ocean pCO2 estimate (ANN-NEP) and the coastal pCO2 estimate (ANN-NEPc). Seasonal groupings are (a) winter (December, January, February), (b) spring (March, April, May), (c) summer (June, July, August), and (d) fall (September, October, November). 300 km offshore line shown for coastal–open-oceanic boundary used in this study (solid black line labelled '300').